DRY GRANULATION VIA ROLLER COMPACTION:

INVESTIGATION ON SCALE UP STRATEGIES INTEGRATING PROCESS PARAMETERS AND CRITICAL MATERIAL ATTRIBUTES

DISSERTATION

ZUR ERLANGUNG DES DOKTORGRADES (DR. RER. NAT.)

DER MATHEMATISCH-NATURWISSENSCHAFTLICHEN FAKULTÄT

DER RHEINISCHEN FRIEDRICH-WILHELMS-UNIVERSITÄT BONN

vorgelegt von

Robert Schmidtke

aus Düsseldorf

Dezember 2017

Angefertigt mit Genehmigung der Mathematisch-Naturwissenschaftlichen Fakultät der Rheinischen Friedrich-Wilhelms-Universität Bonn

Auszüge aus der Arbeit wurden an folgender Stelle vorab veröffentlicht:

Schmidtke R., Schröder D., Braun M., Wagner K.G.:
Dry granulation: Scale-up of roller compaction processes based on quality attributes of ribbons and tablets
Poster, APV World Meeting 2016 Glasgow

Schmidtke R., Schröder D., Menth J., Staab A., Braun M., Wagner K.G:
Prediction of solid fraction from powder mixtures based on single component compression analysis
International Journal of Pharmaceutics, Volume 523, Issue 1, 15 May 2017, Pages 366-375, ISSN 0378-5173, http://doi.org/10.1016/j.ijpharm.2017.03.054

Schmidtke R., Schröder D., Braun M., Wagner K.G.:
Dry granulation: Scale - up of a roller compaction process - Adapted process settings to achieve same product quality at different scales
Poster, APV World Meeting 2018 Granada

Für meine Familie

Danksagung

TABLE OF CONTENTS

IV

ABBREVIATIONS AND SYMBOLS

Abbreviation	Definition
API	Active pharmaceutical ingredient
CARB	Sodium carboxymethylcellulose (AcDiSol®)
CPP	Critical process parameters
DL	Drug load
GeoPyc	GeoPycnometer
LAC	α−Lactosemonohydrate (Tablettose 80®)
MacroPactor	M1075-GMP-Polygran
MCC	Microcrystalline cellulose (Avicel® PH102)
MET	Metformin hydrochloride
MGST	Magnesiumstearate (LIGAMED®)
NIR	Near infrared reflectance
PCA	Principal component analysis
PLS	Partial least square regression
PSD	Particle size distribution
RSD	Relative standard deviation %
SD	Standard deviation of mean
SF	Solid fraction
TS	Tensile strength
USP	United States Pharmacopeial

Symbol	Definition
ε	Porosity
$x_{Excipient}$	Weight fraction of excipient in mixture [% w/w]
σ_t	Tensile strength [N/mm²]
σ_{tmax}	Maximal tensile strength [N/mm²]
π	Pi
A	Heckel - Intercept
a	Kawakita constant
b	Kawakita constant
C	Degree of volume reduction
c_r	Curvature radius
D	Diamter [cm]
d_{50}	Median particle dimension [µm]
d,f,g	Exponential constants
d_{rolls}	Diamter rolls [cm]

F	Force [N]
h	Height [cm]
h_c	Heigth calotte [cm]
k	Heckel slope
m	Mass [g]
p_c	Critical concentration or percolation treshold (percolation theory)
P	Pressure [MPa]
P_y	Heckel Yield pressure
q	Critical exponent or compressibility exponent (percolation theory)
r	Radius
R^2	Correlation coefficient
S	Proportional constant (percolation theory)
SF_{max}	Maximal solid fraction
t	Production time [min]
$TS_{granule}$	Tensile strength tablets of granules [N/mm²]
TS_{powder}	Tensile strength tablets of powder [N/mm²]
V_0	Initial volume [cm³]
V_{min}	Minimal achievable volume [cm³]
V_P	Volume of tablet at applied pressure [cm³]
v_{rolls}	Velocity rolls [rpm]
W	Central cylinder thickness [cm]
w_{rolls}	Width rolls [cm]
x_p	Compression pressure [MPa]
y	Surface tension
θ	Contact angle [°]
ρ_{APP}	Apparent density [g/cm³]
ρ_{TRUE}	True density [g/cm³]
X	System property (percolation theory)
p	Site occupation or bond probability (percolation theory)
π	Pi
y	Surface tension liquid [dyn/cm]
θ	Angle [°]

1.   INTRODUCTION

Granulation processes for solid oral dosage forms have been widely used as an intermediate process step in the pharmaceutical industry. The advantages of a granulation process are improved granule attributes such as flowability, compressibility, tabletability and less segregation of the active pharmaceutical ingredient (API) and excipients, which contributes to a better accuracy of metering, content uniformity and followed by a higher final product quality [1]. The purpose of this technique is to agglomerate excipients with the API and to obtain a desired product quality of e.g. tablets or capsules. Whenever this method is applied, the quality of the final product is controlled by resulting attributes of granules, which are influenced by the process parameters of the granulation technique. Wet and dry granulation techniques represent the main techniques. During wet granulation, using binder solution to build liquid bridges based on capillary and viscous force between particles, causes agglomeration. In contrast, dry granulation is characterised by using mechanical force to facilitate interparticulate bond formation. In comparison to wet granulation, dry granulation provides the following advantages:

- suitable for water- or heat-sensitive APIs,
- simple to operate due to integrated process control mechanism [2],
- minimal energy consumption,
- increased bulk density of the product,
- feasible for implementation in a continuous manufacturing process [1,3].

Most commonly applied dry granulation method is roller compaction. The granulation unit is equipped with two counter-rotating rolls, whereby a screw system (auger) conveys powder into a compaction zone between these rolls. By applying a specific compaction force, a compact is formed. An integrated mill afterwards grinds the formed ribbon, to obtain granules for downstream processing, e.g. tableting. The main disadvantage of roller compaction is the loss of tensile strength of tablets that are produced based on the granules in comparison to tablets based on unprocessed material, caused by previously consumed plasticity (work hardening phenomena), particle size enlargement of the granules and lubrication effects by added lubricant [4–10]. Furthermore, in the pharmaceutical industry the change from small development batches to commercial batches requires a transfer from a small scale to a larger scale (scale up) to satisfy market demands. However, scaling up roller compaction processes is still not fully understood, identifying the factors that finally determine reproducible tablet quality remains to be accomplished. Investigating these factors, comprising material attributes

and the impact of the scale on the final drug product quality will be shown in the course of this thesis.

2.   OBJECTIVES

The objective of this thesis was to investigate the effect of different roller compactor scales over the whole process chain on the quality attributes of intermediate- and final products, i.e. tablets, in order to develop a reliable scale up strategy.

At first two commonly used formulations for a roller compaction process with different properties, containing different fractions of Microcrystalline cellulose (MCC) and pre-agglomerated α–Lactosemonohydrate (LAC), will be characterised to understand their impact on the quality attributes for downstream processing (i.e. tableting). Furthermore, a comparison of analytical techniques for the critical quality attribute solid fraction of a ribbon was performed to find an appropriate method for this thesis. Based on these experiments, both formulations were compacted, using equal process parameters at both scales to identify and separate differences caused by material attributes (formulation) and scale. This was expected to result in a profound new view on the scalability of a roller compaction process. Afterwards a scale approach was proposed balancing the difference between various scales to achieve the same quality attributes of a tablet, whereby the controversially discussed topic of the impact of the solid fraction of ribbons, particle size distribution and porosity of granules on tablet's quality attributes was assessed. In this aspect, the influence of the solid fraction of the ribbon was investigated in a more detailed view between scales using a newly developed near infrared spectroscopy method. Moreover, solid fraction was an important impact factor, which reinforced the development of theoretical models to predict the solid fraction for powder mixtures based on single component compression analysis.

Table 1   Overview objectives

Chapter	Objective	Summary
4.1	Characterisation of material attributes and method evaluation for the measurement of the solid fraction of ribbons	
4.2	Investigation of the impact of formulation attributes and different scales on intermediate products ribbon, granules and tablets at different scales at same process settings	4.2.5
4.3	Scale Model approach to balance observed differences between scales at adapted process settings	4.3.4
4.4	Determination of the solid fraction distribution of ribbons along the roll width between two scales via near infrared reflectance	4.4.5
4.5	Prediction of the solid fraction of tablets from powder mixtures based on single component compression analysis	4.5.3

This thesis is structured in five chapters. The first three chapters (chapter: 4.1, 4.2, 4.3) contain the impact of material attributes of two formulations and correlated differences caused by the scale of the roller compactor. Three main quality attributes will be investigated: (1) solid fraction of ribbons, (2) attributes of granules and (3) tablets. Finally, the solid fraction between scale will be determined more detailed (4.4), followed by comparing three theoretical models (4.5) to predict the solid fraction of mixtures for tablets.

3. THEORETICAL ASPECTS AND MODEL DEVELOPMENT

3.1 ROLLER COMPACTION

Three main process areas can be distinguished for a roller compactor (see Figure 1):

1. Conveying system -> Powder
2. Compaction zone -> Ribbon
3. Milling system -> Granules

A powder blend is conveyed by an agitator, feed auger and tamp auger (force-feed system) between counter-rotating rolls into the compaction zone. Depending on the manufacturer, various orientations of the conveying system are used [3].
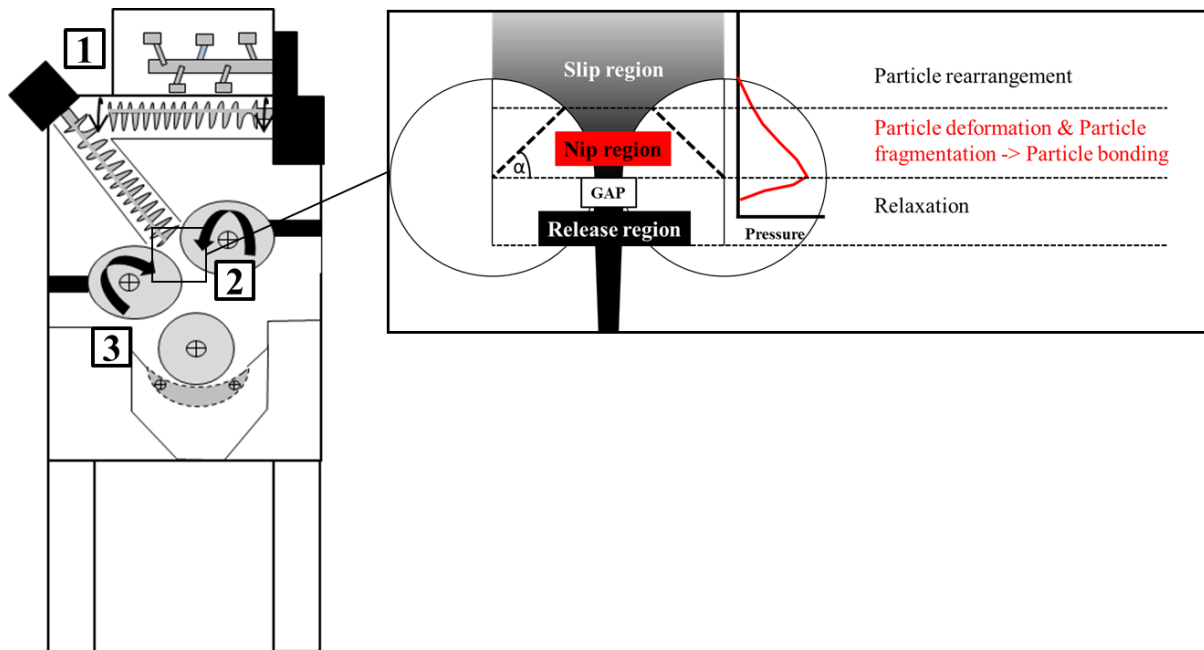
Figure 1   Schematic drawing – Roller compactor

The compaction zone is divided into a slip, nip region and release region [1]. Initially, in the slip region particle rearrangement and de-aeration occurs, followed by an increasing specific compaction force in the course along the nip region, where the velocity of the particles becomes equal to the rotating rolls [11,12]. Different surfaces of the rolls (e.g. knurled, smooth) improve the friction between rolls and powder, which ease the dragging of powder into the nip region. Powder densification occurs in this region. Particle deformation (plastic deformation) and particle fragmentation takes place, whereby new bonds occur between particles, caused by more contact points and newly formed surfaces. Maximum pressure is achieved on the powder right before the minimal gap between the two rolls [1]. A seal system (cheek plates or rim rolls) encloses the compaction zone to prevent side seal leakage of the

powder. A ribbon is being released from the compaction zone to the milling system. Here, the released ribbon is sheared and sliced against a sieve mesh by an oscillating granulator to obtain granule particles.

Two roller compactors were used for this thesis: A MiniPactor® and a M1075-GMP-Polygran®. Both machines are products of the company Gerteis (Gerteis Machinen + Processengineering AG, Switzerland). The roller compactors are characterised by an inclined conveying system with a feed auger and tamp auger (see Figure 1). These machines provide an automatic gap control system, whereby the feed of the augers is automatically adjusted if the gap exceeds the defined value, which results in a constant powder supply and thus to a low fluctuation of the gap. The ratio of the feed/tamp auger can be set as process parameter. Samples of the ribbons are taken after achieving steady state conditions for the gap. Both machines were equipped with cheek plates as side seal system. Details of the used process parameter for each experiment are provided in 6.1.1. Figure 2 gives an overview of all design aspects and process parameters for a roller compaction process.

Design aspects
Orientation conveying system
Agitator
Feeding auger
Tamping auger
Roll diameter
Roll surface
Roll width
Seal system: Cheek plates
            Rim rolls

Roller compaction

Ribbon

Granulator type
Mesh size [μm]
Mesh type

Milling

Granules

Process parameters
Speed [rpm]:
 - Agitator
 - Feeding auger/ Tamping auger
 - Roll
Gap width [mm]
Specific compaction force [kN/cm]

Gap control:
Ratio feed/tamp auger 160%

Speed granulator [rpm]
Angle oscillating granulator [°]

Figure 2   Design aspects and process parameters of a roller compactor

All construction aspects between both machines are equal, except for the roll width. The MiniPactor® (small scale) has a roll width of 25 mm, in contrast to the M1075-GMP-Polygran® (large scale), which has a roll width of 50 mm and thus increases the throughput. M1075-GMP-Polygran® will be referred to as MacroPactor® in this thesis.

3.2 POWDER COMPACTION AND SOLID FRACTION THEORY

3.2.1 Powder compaction - Definitions

Single solid dosage forms are mostly prepared by compressing powder to tablets. Applying pressure on powder causes a volume reduction, whereby bondings are formed by plastic deformation, particle fragmentation, resulting in new available surfaces for bondings, and a formed compact is obtained (e.g. ribbon, tablet). The compact can be characterised measuring their tensile strength (TS) and solid fraction (SF).

Solid fraction (SF) is the possible volume reduction related to its true density (lowest possible volume), and represents how dense a compact is compressed.

$$Solid\ fraction = \frac{\rho_{Apparent\ density}}{\rho_{True\ density}} = \frac{\frac{m}{V_P}}{\frac{m}{V_{min}}} \qquad \text{Eq. (1)}$$

m = mass of powder/tablet [g]; V_P = volume at applied pressure [cm³]; V_{min} = minimal volume [cm³]

Solid fraction is a quality attribute of ribbons manufactured by a roller compaction (see 3.2.2) and tablets. The solid fraction of a tablet is a critical quality attribute (CQA) as it correlates to disintegration and dissolution [13–15] (i.e. faster dissolution and disintegration with lower solid fraction). The reason is that a low SF combined with a high porosity facilitates liquid penetration into tablets (Porosity (ε) = 1- solid fraction).

The second attribute of a compact is the tensile strength (TS), which is determined by measuring the required radial force to break the compact, whereby the geometry of the compact is considered for calculation (generalised breaking force) [16]. TS as parameter of mechanical strength of tablets has a major relevance for tablets during downstream processing due to mechanical impact during coating, transportation and packaging [17].
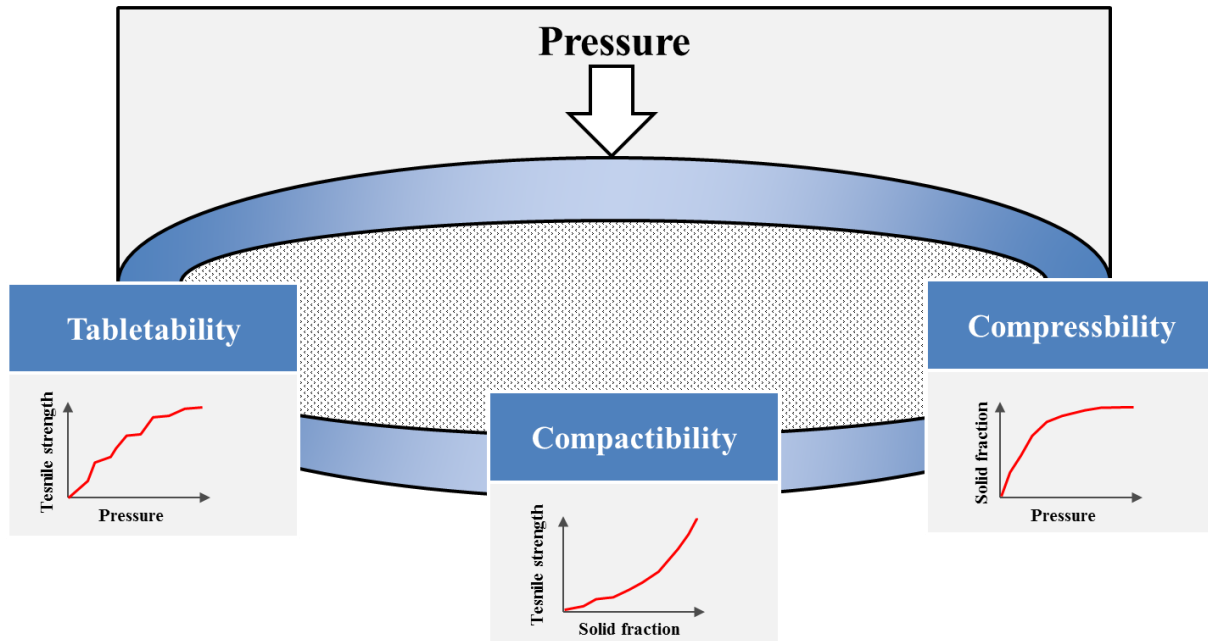
Figure 3   Definitions – Tabletability, Compressibility and Compactibility

Measurements of the tensile strength and solid fraction allow characterising materials and granules with regard to their tabletability, compressibility and compactibility (see Figure 3). Compressibility plots enable a view on the consolidation process of the material under pressure. Mathematical equations can be applied for compressibility plots to get a deeper insight into the physical behaviour of the densification process (e.g. Heckel, Kawakita, see 6.2.1.5). Tabletability shows the mechanical strength dependent on pressure, and compactibility is a combination of both values as the tensile strength is depicted on a certain degree of densification.

3.2.2   Solid fraction of the ribbon as critical quality attribute for roller compaction

In respect to the regulatory guidance of the ICH Q8 (R2) Pharmaceutical development [18] application of Quality-by-Design (QbD) approach means to understand the process in depth, which enables to "built in" quality into the product by a process design space. Based on this, intermediate critical material attributes (iCMA), critical process parameters (CPP) and critical quality attributes (CQA) are examined during the development of a drug product. These three aspects define the control strategy of a drug product. For roller compaction the solid fraction of ribbon is a key intermediate critical quality attribute [5,8], as it shows an impact on particle size distribution (PSD) [5,19–24], porosity of granules [25] and the tensile strength of tablets [5–7,9,26]. Different process parameters like the speed of the conveying system, roll speed, gap width and specific compaction force have an impact on these quality attributes [20].

As an example, a short dwell time of the ribbon is caused by a low speed of the rolls or conveying system and results to a low solid fraction [21,27–29]. In contrast, a high solid fraction is obtained by an increased specific compaction force or a lower gap width [5]. A control strategy for a roller compaction process contains these process parameters, but the resulting solid fraction of a ribbon reflects a combination of all process parameters together. Hence, it is not surprising that various authors have investigated the solid fraction in depth. Studies reported determining the solid fraction comprise different analytical techniques:

- X-ray µCT [30],
- ultra sonics [31],
- geometrical method [32],
- modified geometrical method [27,33],
- throughput [5,26,27,34]
- GeoPycnometer [8,17,35],
- mercury porosimetry [22],
- light transmission [36],
- oil absorption [22,37],
- throughput method [5,26,27,34],
- buoyancy method [33],
- near infrared reflectance [32,38],
- near infrared reflectance – chemical imaging [21,22]

It was demonstrated that a non-uniform solid fraction distribution of the ribbon along the roll width occurs [21,30,31,36]. Two design aspects of the roller compactor are identified to cause this effect: Conveying and side seal system. A periodical sinusoidal solid fraction distribution is obtained due to the feeding pressure of the last flight of the tamp auger [39]. Different side seal systems are used: cheek plates and rim rolls. Rim rolls led to a higher solid fraction at the edges [27], whereby a higher solid fraction at the centre was obtained using cheek plates [40], which can be diminished by internal powder lubrication [41].

In contrast, only a few authors measured and investigated the effect of different scales on the solid fraction. Unfortunately, the few reports on scale were controversial. Alleso et al. (2016) [37] stated that the scale has no impact on the solid fraction of the ribbon. In contrast to that, Shi et al. (2016) [42] and Ana Pérez Gago et al. (2017) [43] recognized a scale dependent influence. Unfortunately, neither the solid fraction distribution nor a potentially resulting impact on the granule and tablet quality were discussed or published.

3.2.3 Reduced tabletability caused by particle size enlargement effect, lubricant, porosity and work hardening effect

Potential reasons are described in literature, explaining the main disadvantage of roller compaction process, namely the loss of tensile strength (tabletability), comprise four main reasons:

- work hardening phenomena,
- particle size enlargement effect,
- porosity of granules,
- added amount of Magnesium stearate to the granules,

The term of work-hardening was first introduced by Malkowska et al. (1983) [44] who compressed excipients, milled and re-tableted the obtained granules. They observed a loss of tensile strength compared to the unprocessed excipients. It was stated that work-hardening means "resistance to deformation" of material, which can be described as a partial loss of their ability to build a new network of bonds. The probability of building bonds increases with a higher contact area between particles, which is dependent on the specific surface of particles and thus to the particle size distribution (PSD) [45]. As a coarser granule size occurs after roller compaction, which has a reduced specific surface, various authors tried to distinguish if the work-hardening or the particle size enlargement would affect the loss of tensile strength after roller compaction.

Sun et al. (2006) [46] tableted a small and a coarse lubricated sieve fraction of Microcrystalline cellulose (MCC) after multiple compaction cycles and observed within one sieve fraction a decrease of the specific surface area, whereby the coarser sieve fraction provided always a lower tensile strength. They concluded that the particle size enlargement effect caused the loss of tensile strength. In contrast, Herting et al. (2008) [47] used unlubricated sieve cuts of MCC and stated that the loss of tensile strength is impacted due to an effect of both work-hardening and particle size enlargement. Wu et al. (2007) [48] determined that the particle size enlargement effect can be considered as negligible by using brittle components, as these components consolidate under an extensive fracturing during tableting into smaller particles with a higher specific surface. Compared to brittle components, He et al. (2007) [49] showed that MCC (plastic consolidation) is more sensitive towards addition of Magnesium stearate (MGST) regarding loss of tensile strength. Mosig et al. (2015) [10] tried to investigate these effects: particle size enlargement, work hardening and added lubricant for a plastic (MCC) and brittle (α – Lactosemonohydrate = LAC) components. They confirmed the study of He et al. (2007) [49] as they detected that the loss

of tensile strength after roller compaction of MCC was enhanced due to lubrication. Additionally, an effect of work-hardening and particle size enlargement was verified. Furthermore, no loss of tensile strength for LAC could be observed either by lubrication, particle size enlargement or after roller compaction, due to the brittle fracturing behaviour, which results into smaller particles with new unlubricated surfaces. Nordstrom et al. (2015) [25] proposed an interesting new aspect. Highly porous granules disintegrate into their primary particles during tableting, which diminishes the impact of the granule size on the loss of tensile strength. Thus, the granule porosity is an important factor, which has an impact on granules' attributes. Recently, Sun et al. (2016) [50] published a mini review on this topic, where they concluded that all factors have to be considered for a roller compaction process.

3.3 PREDICTION OF SOLID FRACTION BASED ON COMPRESSION ANALYSIS FOR TABLETS

The solid fraction is commonly understood as an important aspect of formulation design as it directly influences tensile strength, disintegration of tablets, dissolution time of tablets, drug product stability [13,14,51,52] and serves as scale up characteristic [53]. Thereby, it can be considered as critical quality attribute (CQA) [15].

Hence, predicting of the solid fraction based on single compression analysis of commonly used excipients would be highly beneficial for development purposes. The prediction may serve as a systematic guidance for the formulator to select appropriate excipients depending on the active pharmaceutical ingredient to build quality into the drug product according to the Quality by Design approach.

Compression analysis of pharmaceutical powders has been reported by various authors [54–60]. The most frequently used compression models are Heckel [61] and Kawakita [62], which provide a physical interpretation of the volume reduction process of powders dependent on the applied pressure. The Heckel model for pharmaceutical powders is derived from compression experiments of metal powders and assumes that the consolidation (plastic deformation) follows first-order kinetics, which results in the Heckel equation Eq. (2), where ε is the porosity of the compact and k the reciprocate of the Yield pressure.

$$-\ln(\varepsilon) = k * P + A \hspace{4cm} \text{Eq. (2)}$$

ε = porosity; k = slope Heckel; P = compression pressure; A = intercept

A linear course of the Heckel plot at increasing pressure indicates plastic deformation. However, in contrast to metal powders, pharmaceutical powders display additionally to plastic deformability, particle rearrangement and/or elastic deformation, which leads to deviations from the linear course of plastic deformation behaviour (see 6.2.1.5.1). In this context the Heckel plot shows a curvature in the lower pressure region [54]. Duberg et al. (1986) decided to divide the Heckel plot into 3 phases for pharmaceutical powders to reach a better applicability of the Heckel equation: particle rearrangement or fracturing, elastic or plastic deformation and decompression. Consequently, no single Heckel equation will be able to describe the compressibility of pharmaceutical powders appropriately for the entire range of the applied compression pressure. As for implementing, a prediction model for solid fraction for the widest possible range of compression pressure requires a model, which parameters describe the compression behaviour of the respective pressure range, the Heckel equation was excluded for this study. In contrast to the Heckel model, the Kawakita Eq. (3) equation

assumes that particles under compression pressure (P) are in an equilibrium and the product of the pressure term and volume term is constant [57].

$$\frac{P}{C} = \frac{P}{a} + \frac{1}{ab}$$ Eq. (3)

C = degree of volume reduction; P = compression pressure [MPa]; a = Kawakita constant; b = Kawakita constant

Consequently, a linear course is obtained when plotting P/C vs. compression pressure, where C is the degree of volume reduction. The Kawakita parameters a and b^{-1} are determined by linear regression and likely to deliver appropriate results over the whole compression pressure. Promising results were found using the Kawakita equation to predict the compressibility of a tablet successfully [58,64,65]. Another potential model is the percolation model. Usually employed to elucidate the governing property of a material in a powder mixture dependent on its volume fraction, it can also be applied to describe a property, dependent on the fracture or extent of a process parameter. In this case, the tablet property of interest would be the solid fraction while the process parameter would be the compression pressure. A successful implementation of this concept has been demonstrated by various authors [66–70]. A sudden property change of a tablet will only be observed if the particle rearrangement is completed and an infinite cluster can be formed [66]. This sudden change (percolation threshold) is not considered by the simplification of the compressibility by the Kawakita equation. Therefore, percolation theory was applied for predicting the solid fraction as a function of the compression pressure. This adapted model has the potential to improve predictions for the solid fraction of a ternary mixture compared to Kawakita.

3.3.1 Theoretical considerations Percolation, Kawakita and exponential model - Mathematical model development

Two theoretical models Percolation and Kawakita will be evaluated for model application. An exponential model is added to elucidate whether the two-parametrised models with theoretical background are superior in terms of predictability of solid fraction compared to a model without parametrised variables.

3.3.1.1 Percolation

In the course of the percolation theory Eq. (4), tableting of powder is considered as forming site- and bond clusters in a lattice [66]. After particle rearrangement an infinite cluster is formed throughout the whole tablet, and the particles cannot disintegrate into their primary particles again [66]. Before this percolation threshold is reached, the voids of the powder bed

are filled by particle rearrangement. The percolation threshold is typically between the tapped density and the bulk density, where a first compact is formed and the interparticulate bonding starts, so that isolated clusters (finite clusters) are combined to form an infinite cluster throughout the tablet, which corresponds to a massive property change in the system.

Basic formula of percolation phenomena:

$$X = S * (p - p_c)^q \text{ [66]} \qquad \text{Eq. (4)}$$

Percolation formula for tensile strength:

$$\frac{\sigma_t}{\sigma_{tmax}} = S * (p - p_c)^q \text{ [69]} \qquad \text{Eq. (5)}$$

X = system property; S = proportional constant or scaling factor; p = site occupation or bond probability; p_c = critical concentration or percolation threshold; q = critical exponent; σ_t = tensile strength [N/mm²]; σ_{tmax} = maximal tensile strength [N/mm²]

In theory, the basic power law is only valid near the percolation threshold in a lattice [66]. Kuentz & Leuenberger found that it is possible to use the percolation theory for a broader range regarding modified Young's modulus and tensile strength [68,69,71] . Different authors evaluated the applicability of the percolation theory for tensile strength by considering the system property X as tensile strength, p as relative density (or solid fraction), and q as fractural exponent of the tablet [66–69]. They defined the percolation threshold (p_c) as a minimum of solid fraction which leads to a mechanical strength or as a "critical volume fraction in a continuum percolation" [69]. The value found for the percolation threshold was between the relative bulk density and the tapped density for the excipients [69]. The theoretical value of the critical exponent q can be calculated by applying the Bethe lattice approximation or mean field theory. For mechanical strength it is defined as constant with a value of 2.7 [67]. Some authors found that q can differ from theoretical values for tensile strength in a binary system [67–69]. Related to this knowledge, q was defined as variable parameter to predict the solid fraction referring to it as compressibility exponent *(q)* throughout the manuscript. The solid fraction (*SF*) is normalised by the highest detected value for *SF* (SF_{max}), which leads to:

$$\frac{SF}{SF_{max}} = S * \left(x_p - p_c\right)^q \qquad \text{Eq. (6)}$$

SF = solid fraction; SF_{max} = measured maximal solid fraction; S = scaling factor; x_p = compression pressure [MPa]; p_c = Percolation threshold; q = compressibility exponent

Eq. (6) was used for fitting the model variables S, p_c and q using the measured *SF* and SF_{max} values.

3.3.1.2   Kawakita

The Kawakita equation [72] Eq. (7) is based on the volume reduction of powder (C) under compression pressure. C is defined as the degree of volume reduction (engineering strain) at applied pressure P. V_0 is the initial in-die volume of the powder, and V_P is the volume of the powder at applied pressure.

$$C = \frac{V_0 - V_P}{V_0} = \frac{a*b*P}{1+b*P} \qquad \text{Eq. (7)}$$

a and b are Kawakita compression parameters which can be determined by linear regression using the linearized form of Eq. (8) [73,74],

$$\frac{P}{C} = \frac{P}{a} + \frac{1}{ab} \qquad \text{Eq. (8)}$$

a represents the maximal strain or degree of compression at maximal pressure (C_{max}). The inverted b^{-1} ($1/b$) describes the pressure to reach $a/2$, which can be correlated to the plasticity (Yield pressure, Heckel) and initial compressibility of single ductile granules [74] or can be seen more simplified as deformation capacity [75]. The parameters a and b were determined by applying linear regression on a plot of *P/SF* vs. *P*. Kawakita's a is equal to 1/slope and b^{-1} is equal to slope multiplied with y-intercept. Considering the determination of C and therefore the initial volume (V_0) can have an important influence on the results [76,77]. There are three methods described for the determination of V_0. The first is to measure V_0 between 1-2 MPa [77] or at the lowest measurable pressure. The second is to define V_0 based on bulk density which delivers better results compared to the first method [78]. The third is to determine initial density using nonlinear regression with three parameters [77,79]. These estimate are highly dependent on the method of determination (process and user) and hence, prone to errors. Thus, the resulting Kawakita parameters are difficult to compare between various research laboratories.

Therefore, a modified approach to determine V_0 was chosen, where V_0 should only be material-dependent and particle size dependence is negligible. Similarly, to the Heckel approach, the reference volume was the lowest possible volume, i.e. the volume at maximum density or true density. Subsequently, C was related to solid fraction and V_0 changed to V_{min}, which was measured by Helium-pycnometry, an easy and reliable determination method. The values of V_{min} and V_P are defined in Eq. (9) and Eq. (10) :

$$\rho_{TRUE} = \frac{m}{V_{min}}; \; V_{min} = \frac{m}{\rho_{TRUE}} \qquad\qquad\text{Eq. (9)}$$

$$\rho_{APP} = \frac{m}{V_P}; \; V_P = \frac{m}{\rho_{APP}} \qquad\qquad\text{Eq. (10)}$$

ρ_{TRUE} = true density [g/cm³]; ρ_{APP} = apparent density [g/cm³]; m = mass of tablet [g]

where V_P represents the volume of the powder at applied pressure, and ρ_{APP} is the corresponding apparent density in Eq. (10). As V_{min} is always smaller than V_P, C is derived as:

$$C = \frac{V_{min}}{V_P} \qquad\qquad\text{Eq. (11)}$$

If Eq. (9) is combined with Eq. (10):

$$\frac{V_{min}}{V_P} = \frac{\frac{m}{\rho_{TRUE}}}{\frac{m}{\rho_{APP}}} \quad \text{or} \quad \frac{V_{min}}{V_P} = \frac{\rho_{APP}}{\rho_{TRUE}} \qquad\qquad\text{Eq. (12)}$$

Considering Eq. (12) and Eq. (1) leads to:

$$C = SF = \frac{\rho_{APP}}{\rho_{TRUE}} = \frac{a*b*P}{1+b*P} \qquad\qquad\text{Eq. (13)}$$

Where SF is the solid fraction.

Thus, the modified Kawakita parameter a can be considered as the maximum solid fraction at an examined compression pressure range that is achievable for an excipient by tableting. Therefore, the following modified Kawakita formula is proposed and used:

$$\frac{P}{SF} = \frac{P}{a} + \frac{1}{ab} \qquad\qquad\text{Eq. (14)}$$

3.3.1.3 Exponential

In addition to the prediction of solid fraction by the modified Kawakita model and the Percolation model, a simple exponential function Eq. (15) was used to predict the solid fraction without a mechanistic model behind it, i.e. the variable d, f and g are adapted, non-parametrised variables.

$$SF = d + f * e^{(g*P)} \qquad\qquad\text{Eq. (15)}$$

The variables d, f and g were fitted by linear regression using a compressibility plot (solid fraction vs. compression pressure [MPa]).

3.3.1.4 Additive rule

Ramaswamy et al. (1970) demonstrated that the volume of a mixture follows an additive rule of the volume of single components, under the condition that the single components have the same particle size [80].

$$Solid\ fraction_{Mixture} = x_{MCC} * (Model) + x_{LAC} * (Model) + x_{CARB} * (Model) \quad \text{Eq. (16)}$$

$x_{Excipient}$ = weight fraction (% w/w) of excipient in mixture

This hypothesis was applied by various authors to predict the porosity, percolation threshold, or tensile strength of mixtures [75,79,81–83] and was shown to be adequate for excipients with different particle size. This approach was applied for all three models to predict the solid fraction, where $x_{Excipient}$ is the weight fraction (% w/w) of the respective single excipient of the mixture. Magnesium stearate was not included in the calculations as it was used as lubricant at a constant level for both, the single excipients and the mixtures. It was necessary to determine the true densities of the materials to apply the calculation of the solid fraction according to Eq. (1) and to calculate the true densities of the mixtures   Eq. (17).

For the mixtures the true density was calculated by the weight fraction of MCC, LAC and Sodium carboxymethylcellulose(CARB) divided by 99.5, as described by Gupta et al. (2005) [84], to reduce the number of input parameters for the models.

$$\rho_{TRUE\ Mixture} = \frac{x_{MCC}}{99.5} * (\rho_{TRUE\ MCC}) + \frac{x_{LAC}}{99.5} * (\rho_{TRUE\ LAC}) + \frac{x_{CARB}}{99.5} * (\rho_{TRUE\ CARB}) \quad \text{Eq. (17)}$$

ρ_{TRUE}= true density [g/cm³]; $x_{Excipient}$ = weight fraction (% w/w) of excipient in mixture

4. RESULTS & DISCUSSION

4.1 MATERIAL ATTRIBUTES AND METHOD COMPARISON FOR SOLID FRACTION MEASUREMENTS OF RIBBONS

4.1.1 Material attributes of raw materials and blends

In order to understand the results of a roller compaction process, it is necessary to characterise the excipients and blends with respect to their attributes (see 4.1.1.1) and compression behaviour (compressibility, tabletability and compactibility, see 3.2.1).

4.1.1.1 Raw material properties

Table 2   Material attributes - Raw materials and blends

Composition	True density [g/cm³]	Bulk density [g/ml³]	Tapped density [g/ml]	Hausner ratio (2500 taps)	Particle size distribution d_{50}
Microcrystalline cellulose	1.5565	0.21	0.27	1.32	87
α–Lactose-monohydrate	1.5417	0.63	0.79	1.27	157
Sodium carboxymethylcellulose	1.5934	0.50	0.71	1.38	61
MCC 2:1 LAC	1.5472	0.48	0.58	1.23	103
MCC 1:1 LAC	1.5447	0.52	0.63	1.23	110
Metformin hydrochloride	1.3559	-	-	-	-
MET 21	1.5066	0.50	0.62	1.23	98

MCC = Microcrystalline cellulose; LAC = α − Lactosemonohydrate; MET 21 = Metformin with drug load 21 %

For all excipients and blends (MCC 2:1 LAC, MCC 1:1 LAC) their true density, bulk/tapped density, particle size distribution (d_{50}) were characterised. In Table 2, an overview of the material attributes is provided.

4.1.1.2 Compression analysis

In literature, there are a several methods described for the analysis of the powder densification process to define the properties of the material [60–63,85–88]. Compressibility, tabletability and compactibility plots were considered in this thesis (see 3.2.1). All single components (LAC, MCC, CARB) and blends (MCC 2:1 LAC, MCC 1:1 LAC) were tableted by a single punch tablet press (FlexiTab). Despite the knowledge that MGST can influence the compression behaviour [89], 0.5 % MGST was added to the excipients to guarantee same process conditions compared to the lubricated blends processed by a roller compactor.

4.1.1.2.1 Compressibility

An incremental displacement transducer system traced the displacement of the punches during compression in order to obtain force displacement data in the range of 0 – 235 MPa.
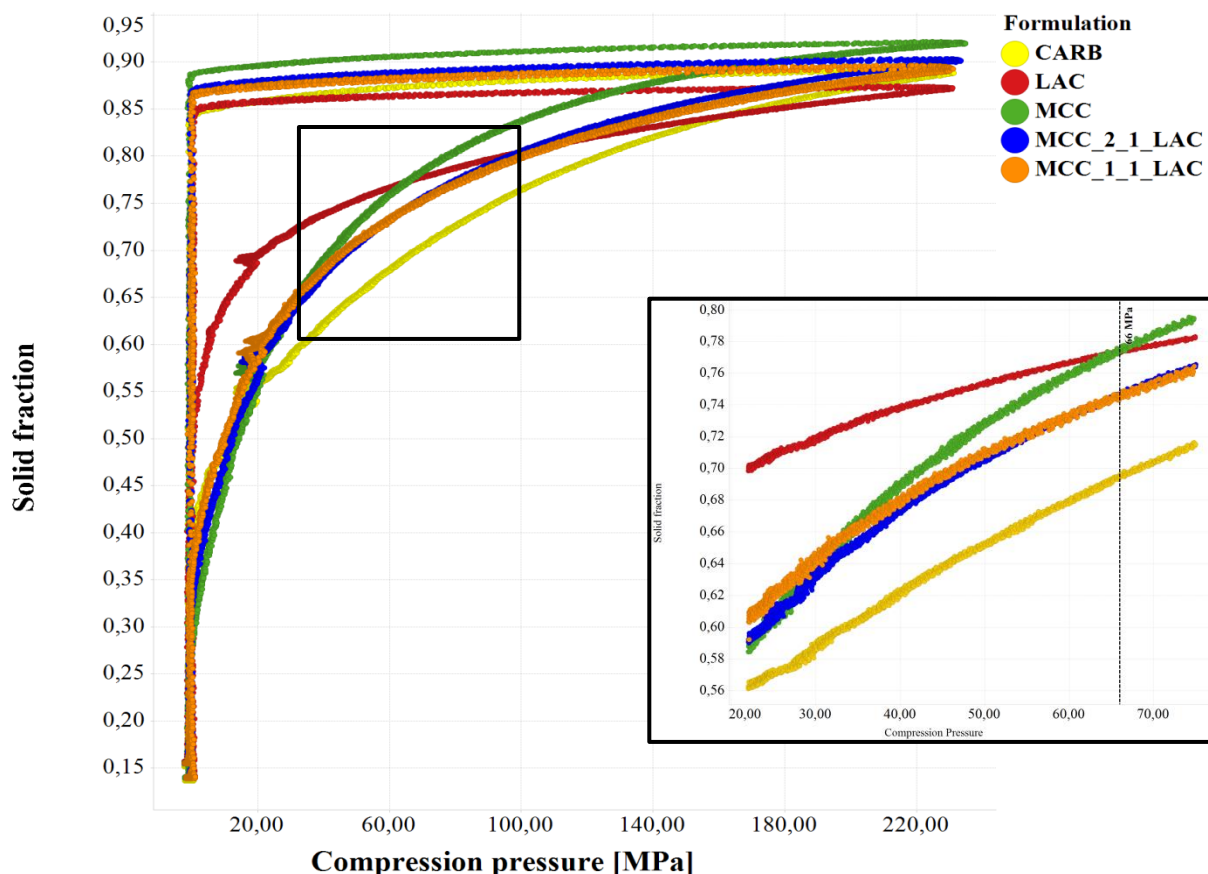

Figure 4   Compressibility – "In- die" measurement excipients and blends,

CARB = Sodium carboxymethylcellulose,

LAC = α – Lactosemonohydrate, MCC = Microcrystalline cellulose –

Image section: Compression pressure 20 – 70 MPa, Exceedance of

LAC's solid fraction by MCC's solid fraction at 66 MPa

Consequently, the solid fraction of the tablet was plotted against the compression pressure (see Figure 4). LAC achieved a higher solid fraction at a low compression pressure compared to MCC. LAC consisted of spherically pre-agglomerated particles and had a higher bulk density of 0.63 g/cm³ (working/starting density) compared to the density of 0.21 g/cm³ of MCC. The compression behaviour between LAC and MCC is different. LAC has a brittle compression behaviour [90,91]. In contrast, MCC consolidates by plastic deformation under pressure [60], explaining the steeper slope of the compressibility plot and exceeded LAC's solid fraction at around 0.77 ($\approx$ 66 MPa). CARB also undergoes plastic consolidation, but compared to MCC to a lower extent. The short decrease of compression pressure at 22 MPa (1.7 kN) was attributed to the switching threshold from pneumatic to hydraulic pressure of the FlexiTab. Considering the compressibility of both blends, MCC 1:1 LAC had a higher solid fraction at lower compression pressure compared to MCC 2:1 LAC, which is attributed to the high fraction of LAC. At around 0.74 SF ($\approx$ 66 MPa) MCC 2:1 LAC exceeded the solid fraction of MCC 1:1 LAC, indicating a higher impact of the plastic consolidation of MCC. The course of the solid fraction plot versus compression pressure of all mixtures was in agreement with the sum of the properties of the single components in relation to their fraction within the mixture. This finding is consistent with results published by various authors [58,80,92,93] who have shown that the volume reduction of a blend (eq. solid fraction) follows an additive rule of the volume reduction of single excipients in a blend (see 3.3.1.4).

4.1.1.2.1.1 Compressibility equation – Heckel

Yield pressure (Heckel) determination was done in a pressure range between 20 MPa – 120 MPa for unprocessed material as this range corresponds to a solid fraction of the blends between 0.60 – 0.80, which represents an expected range for a solid fraction of a ribbon at dry granulation [17]. A low Yield pressure illustrates a good plastic consolidation, which is defined as a low resistance against material deformation.

LAC showed the highest Yield pressure of 188.68 MPa compared to all other investigated excipients and blends. This was attributed to the brittle deformation behaviour of LAC [90,91]. In contrast, MCC showed the lowest Yield pressure of 86.21 MPa, which was caused by the good plastic consolidation. The Yield pressure of the blends (107.53 MPa MCC 2:1 LAC, 119.05 MPa MCC 1:1 LAC) increased with a higher fraction of the brittle LAC [56,93]. Determined values are consistent with literature [54,56], knowing the limitation that Heckel plots are difficult to compare between various research laboratories [54]. All correlation coefficients were above 0.98. Assuming that particle rearrangement is not fully completed at

20 MPa and that normal operating range for a Heckel plot is ≥ 50 MPa [63,93,94], the fitting result were adequate.
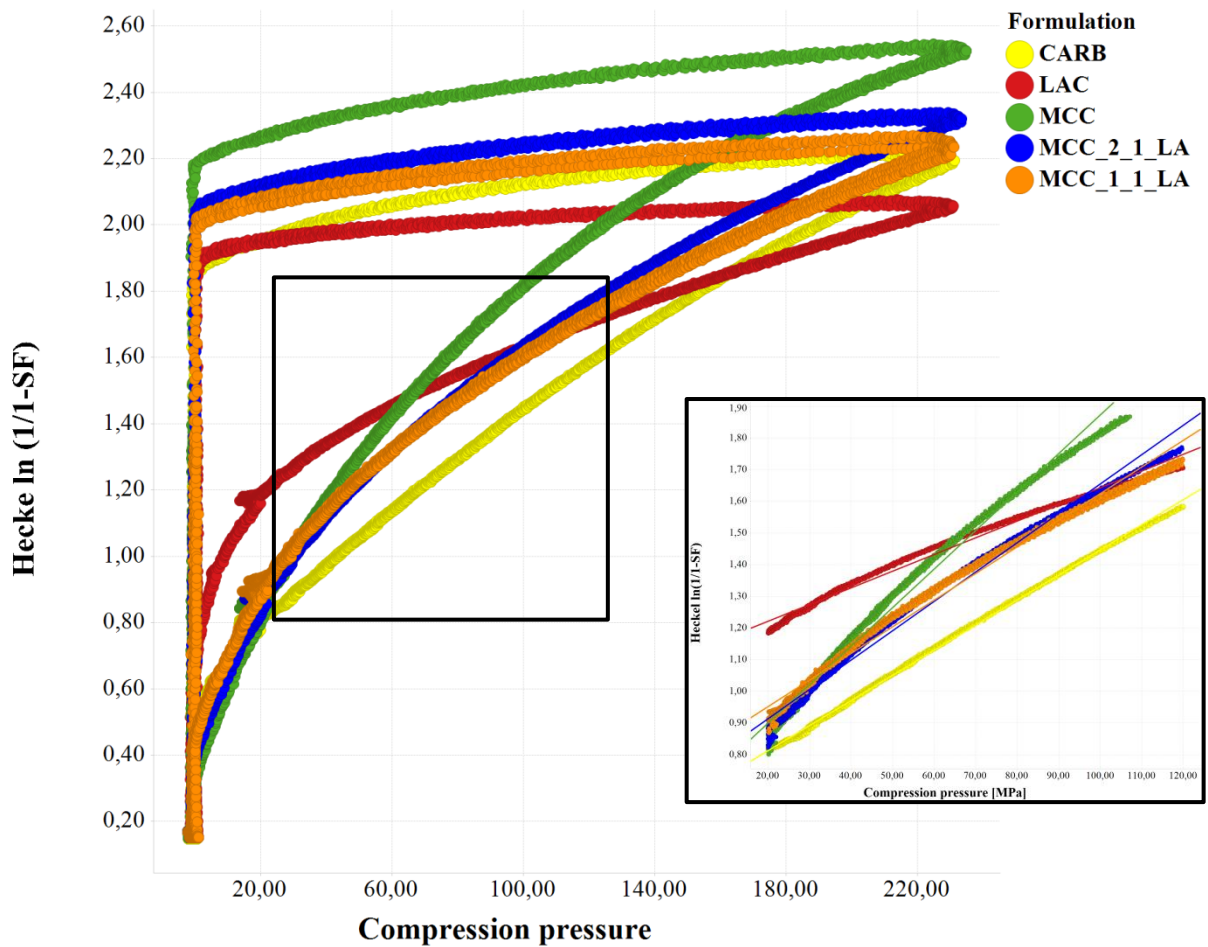
Figure 5   Heckel plot – "In-die" measurement excipients and blends, CARB = Sodium carboxymethylcellulose , LAC = α − Lactosemonohydrate, MCC = Microcrystalline cellulose - Image section: Pressure range for Yield pressure determination (linear regression)

Table 3   Results Heckel – Excipients and blends

	MCC	LAC	CARB	MCC 2:1 LAC	MCC 1:1 LAC
Slope	0.0116	0.0053	0.0079	0.0093	0.0084
P_y (1/slope)	86.21	188.68	126.58	107.53	119.05
R²	0.9863	0.9855	0.9988	0.9877	0.9867

P_y = Yield pressure Heckel; R^2 = coefficient of correlation; MCC = Microcrystalline cellulose;

LAC = α − Lactosemonohydrate; CARB = Sodium carboxymethylcellulose

4.1.1.2.2   Tabletability

In Figure 6 the course of the tensile strength depending on compression pressure for each excipient and blend is shown. The tensile strength increased with rising compression pressure. At low compression pressure, determination of the tensile strength of LAC was not possible using an automatic tablet tester because the resulting tablets were too fragile.
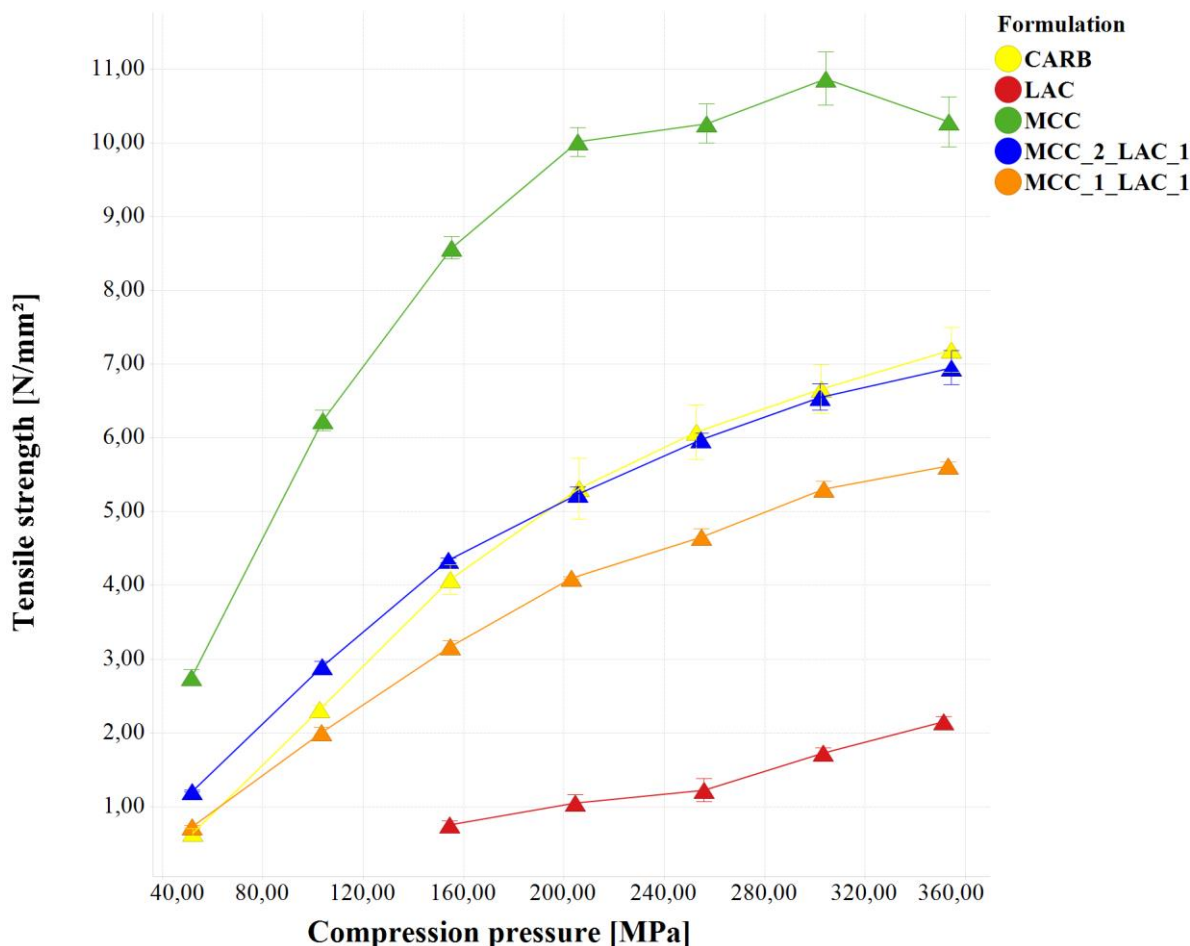
Figure 6   Tabletability – Excipients and blends, mean (n = 6), error bars
                           (standard deviation of mean), CARB = Sodium
                           carboxymethylcellulose, LAC = α − Lactosemonohydrate,
                           MCC = Microcrystalline cellulose

The maximal of tensile strength decreased in the order MCC > CARB > LAC, which was a result of the compression behaviour of good plastic consolidation (MCC, CARB) and brittle fracturing (LAC) during compression. The plastic flow of MCC and CARB resulted in strong bonds and consequently led to a higher tensile strength. LAC showed a nearly linear increase of the tensile strength [95], however at overall a low tensile strength level. Considering the

blends, tensile strength decreased with a higher fraction of LAC. These differences were persistent over the whole range of compression pressure.

4.1.1.2.3   Compactibility

A good compactibility represents a high tensile strength at a low degree of solid fraction. MCC achieved the highest tensile strength at a comparable solid fraction (≈ 0.90) followed by MCC 2:1 LAC > MCC 1:1 LAC > LAC. CARB achieved only a maximal solid fraction of about 0.83, which however was sufficient to achieve a good tensile strength (see Figure 7).
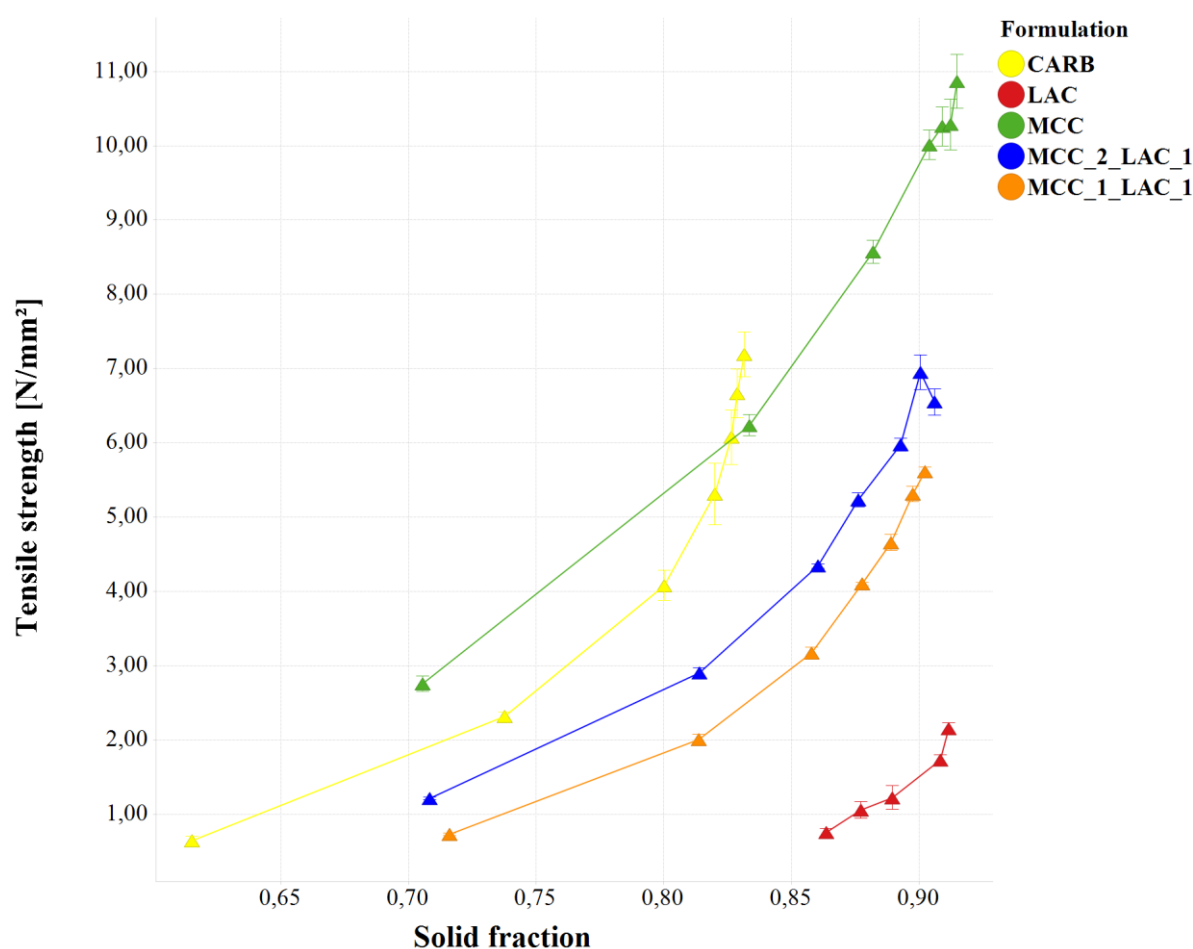
Figure 7   Compactibility – Excipients and blends, mean (n = 6), error bars
                   (standard deviation of mean), CARB = Sodium
                   carboxymethylcellulose, LAC = α − Lactosemonohydrate,
                   MCC = Microcrystalline cellulose

Considering the course of the blends, it is obvious that MCC 2:1 LAC always showed a higher tensile strength at a similar solid fraction compared to MCC 1:1 LAC. In other words MCC 2:1 LAC needed less pressure (eq. solid fraction) to reach a higher tensile strength [96] because of the higher proportion of MCC and its good plastic consolidation under pressure.

4.1.1.2.4   Summary

In summary, a high plastic deformation under pressure resulted in a good tabletability and high compactibility. MCC showed the highest values over the whole range of investigated compression pressures. A higher fraction of LAC in a mixture resulted in a lower tabletability and compactibility. Considering the compressibility plot, LAC reached a higher solid fraction than MCC at a low compression pressure. Heckel Yield pressure results confirmed the course of the compressibility plots.

Table 4   Summary - Compression analysis excipients and blends – Descending order of maximal achievable tabletability and compactibility

Composition	P_y	Tabletability	Compactibility
Microcrystalline cellulose	86.21		
Sodium carboxymethylcellulose	126.58		
MCC 2:1 LAC	107.53		
MCC 1:1 LAC	119.05		
$\alpha-$Lactose-monohydrate	188.68		

P_y = Yield pressure Heckel; MCC = Microcrystalline cellulose; LAC = $\alpha -$ Lactosemonohydrate

4.1.2 Comparison of throughput, mercury porosimetry and GeoPycnometry method to determine the solid fraction of ribbons

As a first step, it is important to identify an appropriate method to analyse the ribbons. Different methods have been described by authors for the determination of solid fraction for a ribbon (see 3.2.2). A few techniques were compared. These methods can be distinguished by the determination of the "in-gap" solid fraction within the gap during compaction, (three throughput methods) and "out of gap" solid fraction, after the ribbon is released (throughput + height measurement, GeoPycnometry, mercury porosimetry) (see 6.2.2). All samples were produced within one roller compactor (MacroPactor) at 2, 4, 6 and 8 kN/cm (MCC 2:1 LAC).
In gap methods - Three "in-gap" methods [5,26,27] were compared. As depicted in Figure 8, solid fraction increased up to 6 kN/cm. Comparing the "in-gap" methods of Herting et al. (2007) [26], Gamble et al. (2010) [5] and Peter (2010) [27] differences could not be noticed (see Figure 8).
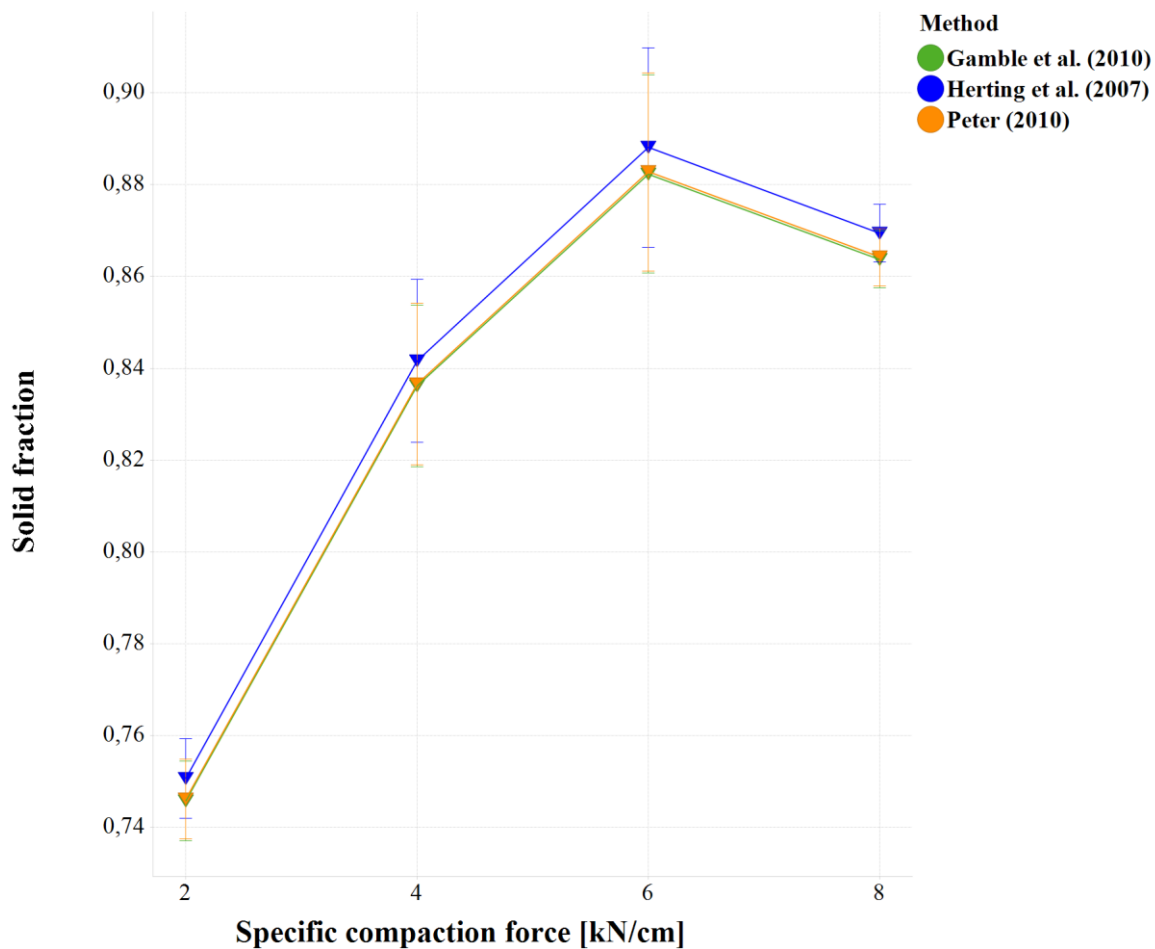
Figure 8   "In-gap" solid fraction ribbon – Mean (n = 5), error bars (standard deviation of mean) – Comparison of three approaches to calculate the solid fraction of ribbons by weighing the granule throughput

The volume calculation of the ribbon was based on the equation of Herting et al. (2007) [26]. An extension of this equation was done by Gamble et al. (2010) [5] who took the voids of the knurled surface of the rolls also into account. Peter (2010) [27] did a correction by multiplying the circumference by half of the gap. Considering these three equations (see 6.2.2.1) the calculated volume was fixed and defined by the geometry of roller compactor and process settings (gap width). Thus, only the produced mass of granules per minute (g/min) could have an impact on the results. Small relative standard deviations for the solid fraction between 0.72 – 2.44 % were obtained. Higher specific compaction forces result in higher solid fraction and higher tensile strength of the ribbons [17,23]. As a result, the ribbons require more time to get milled by the granulator [97,98]. Throughput per minute dropped, and therefore the calculated solid fraction was reduced, too (Figure 8, see equations 6.2.2.1). This effect was most pronounced for the specific compaction force of 8 kN/cm.

Out of gap methods - The "out of gap" porosity was measured by the proposed approach of
Nkansah et al. (2008) [34], by GeoPycnometry and mercury porosimetry. Three methods were
compared. In order to consider the elastic relaxation of the ribbons, measurements were done
48h following compaction. For Nkansah et al. (2008) [34] mean height of the ribbons was
measured five times by a micrometer screw. In the range of 2-4 kN/cm, differences could not
be identified between these methods. At 6 kN/cm the solid fraction of Nkansah et al. (2008)
[34] was lower than the others. The difference increased to 0.08 for ribbons at 8 kN/cm (see
Figure 9).
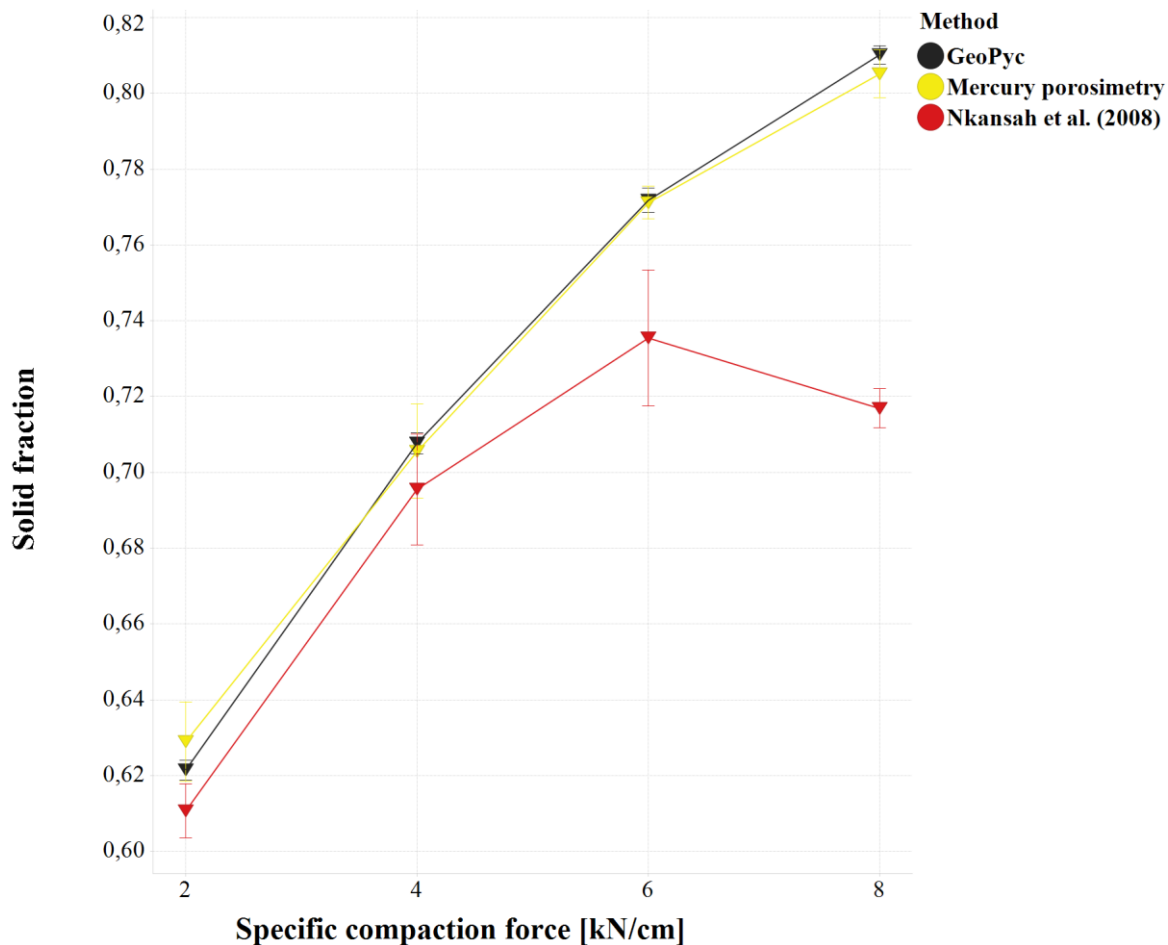
Figure 9   "Out of gap" solid fraction ribbon – Mean, error bars (standard
                  deviation of mean), methods: GeoPycnometer (n = 5), Mercury
                  porosimetry (n = 3), Nkansah et al. (2008) [34] (n = 5)

A higher residence time of the ribbons in the granulator caused a decrease in solid fraction for
the obtained ribbons. The observed maximal relative standard deviation were smaller for
mercury porosimetry (0.78 – 1.75 %) and for the GeoPycnometry (0.29 – 0.42 %) compared
to Nkansah's approach (0.72 – 2.44 %). The differences between the GeoPycnometry and
mercury porosimetry were in a range between -0.61 and 1.21 %. A significant difference

(p ≤ 0.05) between both methods was not observed (see APPENDIX 8.2.1 T-Test). Hence, there is neither a systematic nor significant deviation between GeoPycnometry and mercury porosimetry. In summary the "in-gap" solid fraction did not include the elastic recovery as only the gap setting of the roller compactor is a variable for the calculation (see 6.2.2.1). Therefore, higher values were delivered for the solid fraction compared to the "out of gap" solid fraction (see Figure 10). The throughput methods ("in-gap" & "out of gap") delivered reasonable results at lower specific compaction force, but they were prone to errors at higher specific compaction forces.
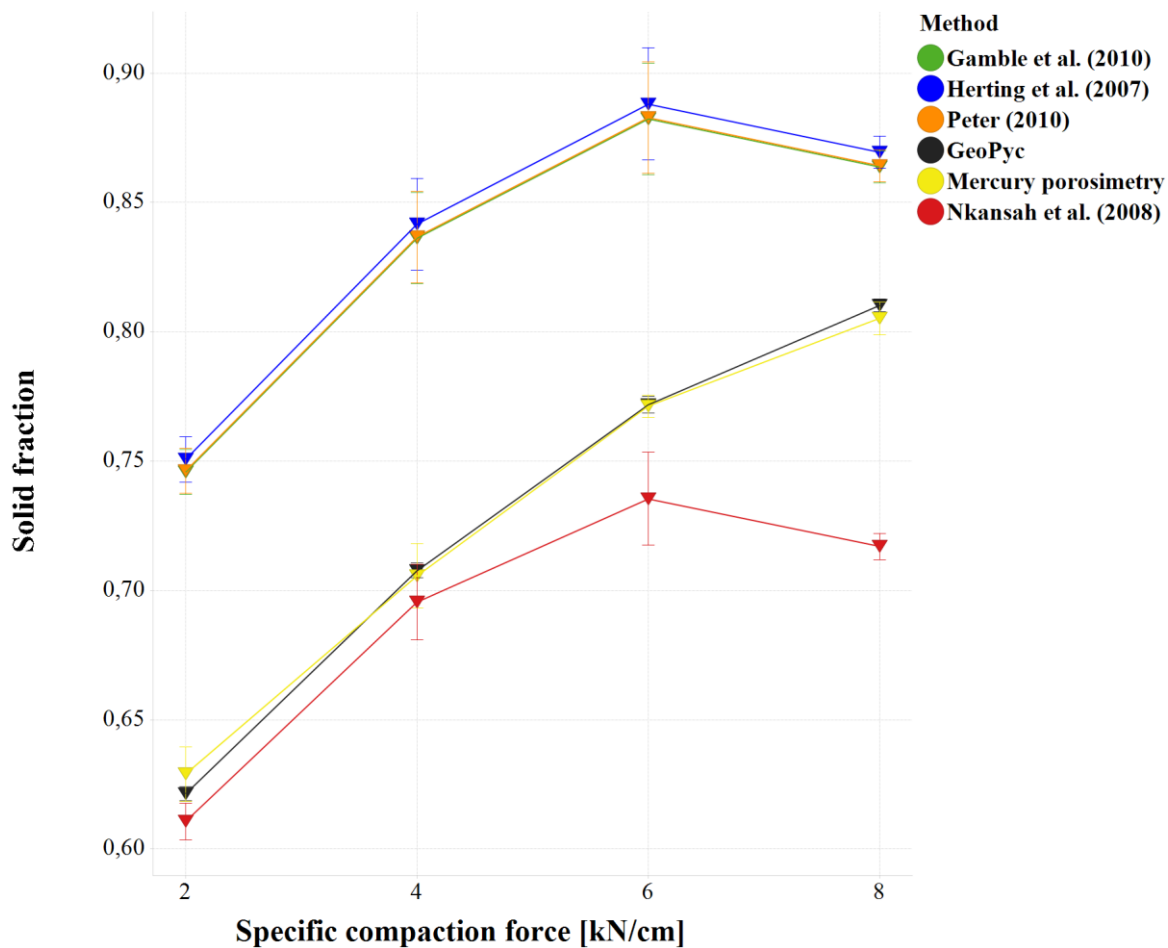
Figure 10   MacroPactor – Comparison of analytical methods for solid fraction of ribbon, mean, error bars (standard deviation of mean)

Due to the low maximal relative standard deviation and robustness of the measurement, the mercury porosimetry and GeoPycnometry are the analytical methods of choice. Considering sample preparation, only small pieces (2* 25 mm * 10 mm) can be analysed by mercury porosimetry, because of the small volume of sample chamber of the Dilatometer compared to the GeoPycnometry (6 * 25 mm * 30 mm), which will give a more representative result. Analysis time is around 1 h for mercury porosimetry compared to 15 - 20 min of the

GeoPycnometry. Hence, for both reasons the GeoPycnometry was the analytical method for determination of ribbon's solid fraction in this thesis.

**4.2   COMPARISON OF TWO ROLLER COMPACTORS OF DIFFERENT
SCALE AT SAME PROCESS SETTINGS**

Two formulations MCC 2:1 LAC and MCC 1:1 LAC were compacted at four specific
compaction levels (2, 4, 6, 8 kN/cm) at different scales, while process parameters were kept
identical (see Table 13). The main difference between these roller compactors was the roll
width (25 mm MiniPactor, 50 mm MacroPactor). Solid fraction of the ribbons, attributes of
granules and tablets were examined in particular regarding following two aspects:

1. Impact of the formulation (MCC 2:1 LAC, MCC 1:1 LAC)

2. Influence of different scales (MacroPactor, MiniPactor)

4.2.1   Formulation impact on the solid fraction within one scale

MacroPactor - Solid fraction increased with increasing specific compaction force [99]. The
solid fraction range increased from 0.62 to 0.82 for applied force of 2 kN/cm to 8 kN/cm.
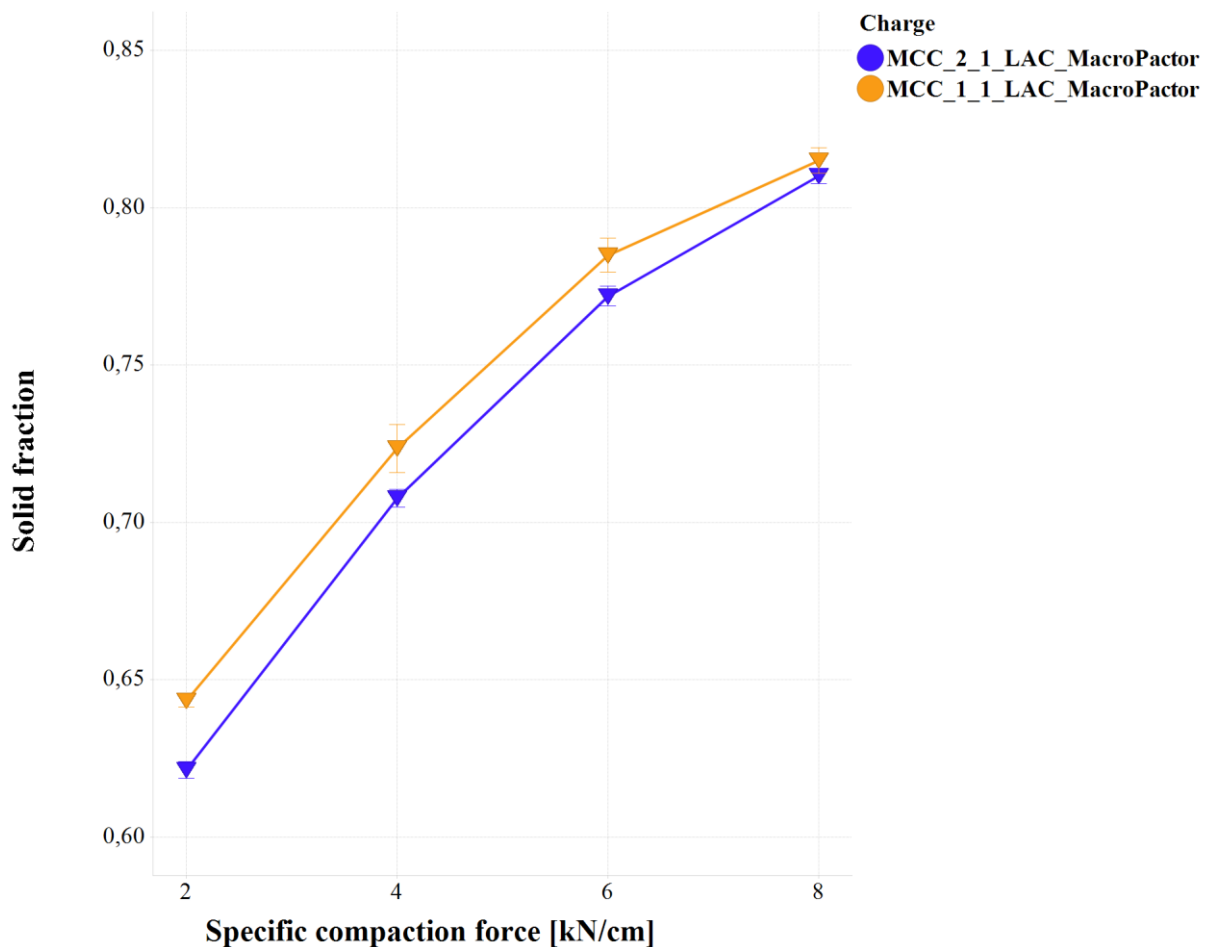
Figure 11   Solid fraction ribbon – MacroPactor, mean (n = 5), error bars
                (standard deviation of mean)

This solid fraction was in agreement with previously published normal operating range for a roller compaction process [17]. The relative standard deviation of means was small (0.30 % – 1.05 %, see Figure 11). A T-test indicated significant difference ($p \leq 0.05$) between these two formulations (see APPENDIX 8.2.2). A higher fraction of LAC led to a higher solid fraction of the ribbon, which was consistent with findings of various authors [4,23].

Compression behaviour of the spherically shaped pre-agglomerated LAC particles indicated a higher solid fraction. LAC had higher bulk and tapped density (0.63 g/ml³, 0.79 g/ml³) compared to MCC (0.21 g/ml³, 0.27 g/ml³). Additionally, LAC needed less pressure for particle rearrangement because of the brittle compression behaviour [90,91], which is characterised by the fracturing of pre-agglomerated primary particles under pressure. A higher fraction of LAC causes a consolidation to a higher solid fraction [4]. This behaviour was confirmed by "In-die" tableting measurements of single components previously (see 4.1.1.2, Figure 4). The compaction process of a tablet press and a roller compactor is not precisely comparable because the roller compactor has a longer dwell time according to Hilden et al. (2011) [100]. But a higher fraction of LAC caused the formulation of MCC 1:1 LAC to reach a higher solid fraction compared to MCC 2:1 LAC up to a compression pressure of 66 MPa for "In-die" tableting (see 4.1.1.2, Figure 4). Exceeding that pressure MCC 2:1 LAC will result in higher solid fractions. Initially, the solid fraction of LAC was higher at low compression pressure, which was reflected by a high bulk and tapped density. Considering the course of the profiles in Figure 11, the differences decreased from 0.022 to 0.005 between both formulations from low to high specific compaction force. A higher fraction of MCC induces a stronger increase of the solid fraction by plastic consolidation [101], which took place at higher specific compaction forces and compensated the initial lower solid fraction of formulation MCC 2:1 LAC. A comparable behaviour was observed for unprocessed blends by "In-die" tableting (see 4.1.1.2, Figure 4).

MiniPactor – MiniPactor showed similar results for the ribbons compared to the MacroPactor for both formulations. An equal impact of the formulation attributes on the resulting solid fraction of ribbons was observed (Figure 12). T-test indicated significant difference ($p \leq 0.05$) (see APPENDIX 8.2.2). Relative standard deviation 0.59 % - 3.90 % was higher compared to the MacroPactor. A explanation could be a lower steady state powder supply into the gap for the small scale, which led to a higher relative standard deviation. However, the relative standard deviation was still in an acceptable range. Difference between formulations decreased from 0.039 to 0.008 (2 kN/cm to 8 kN/cm).
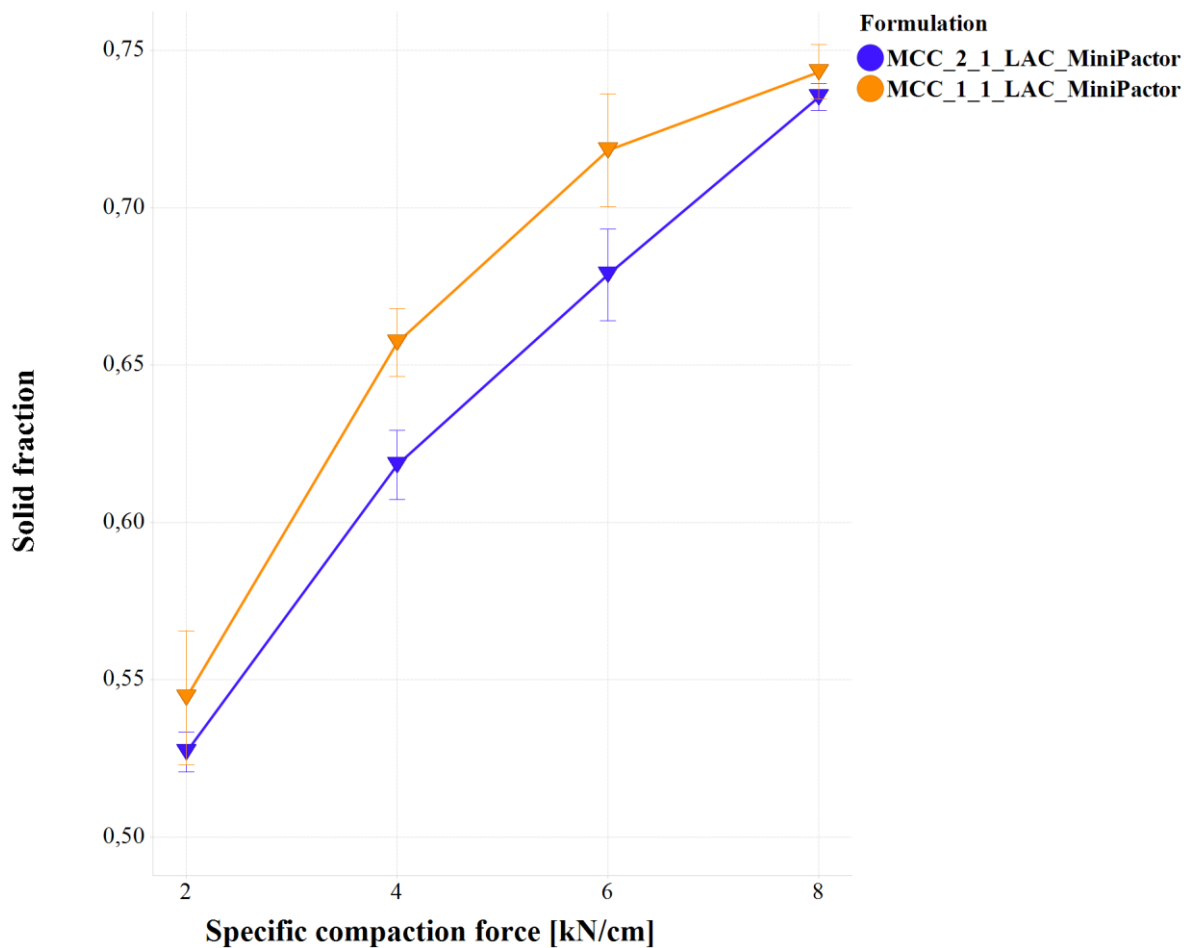
Figure 12   Solid fraction ribbon – MiniPactor, mean (n = 5), error bars (standard deviation of mean)

4.2.2   Comparison of the solid fraction between different scales

Comparing the solid fraction of ribbons at two different scales for each formulation, a
difference between both scales was observed, despite identical process parameters were
chosen (see Figure 13).
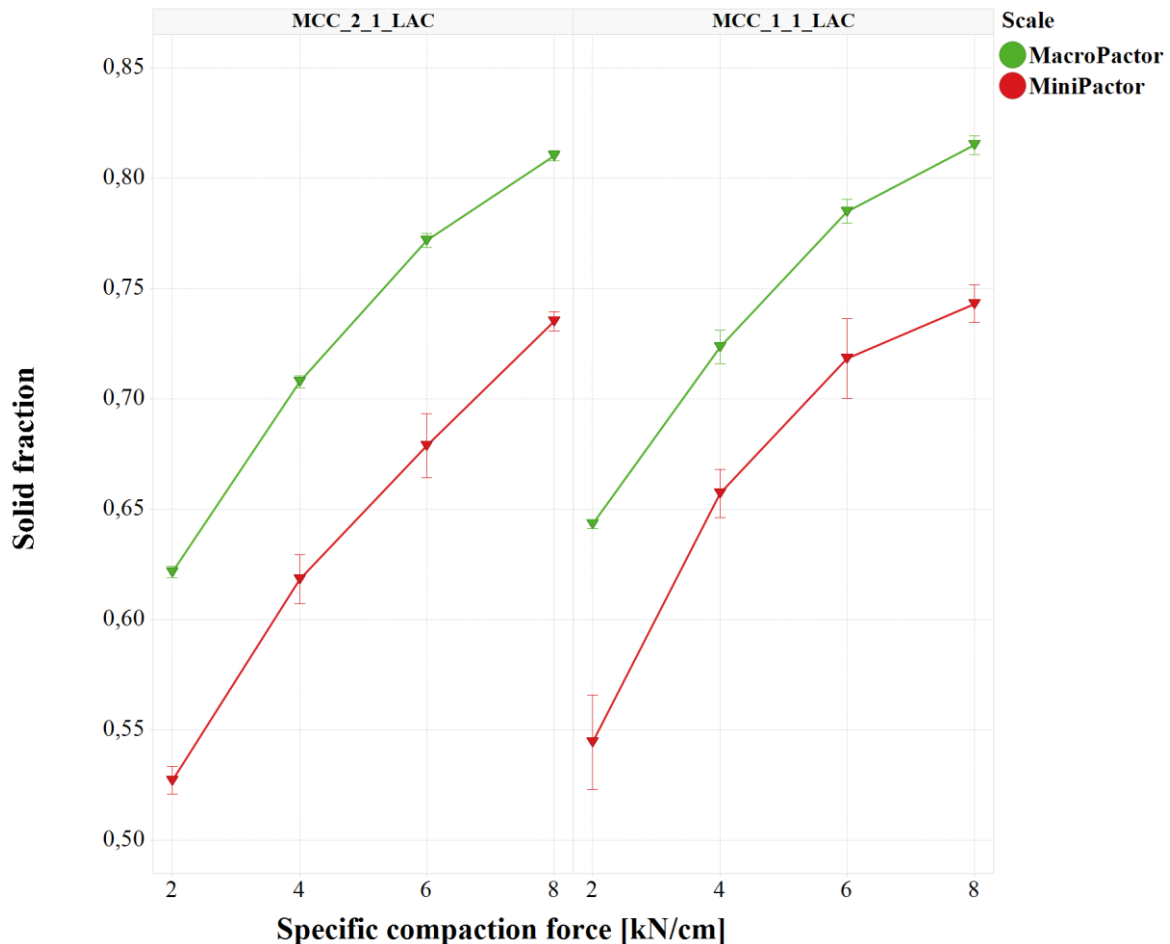
Figure 13   Comparison solid fraction ribbon - MacroPactor/MiniPactor –
                            MCC 2:1 LAC/MCC 1:1 LAC, mean (n = 5), error bars (standard
                            deviation of mean)

The deviation between the two scales was between 18.18 % to 9.27 %, the lowest difference
occurred at highest specific compaction force of 8 kN/cm. A T-Test confirmed a significant
difference ($p \leq 0.05$) of the solid fraction between both scales (see APPENDIX 8.2.2). In
literature, only limited information is available about direct comparisons of two different
scales with the same formulation at same process settings. Alleso et al. (2016) [37] used only
MCC and obtained no difference for four of five batches. They concluded that the solid
fraction of ribbons at different scales is equal. Shi et al. (2016) [42] recognized a higher solid
fraction for the ribbons that were produced at a larger scale, which is in accordance to Figure

13. Recently, Ana Pérez Gago et al. (2017) [43] published that dependent on the used formulation, a different scale can impact the solid fraction. A clear explanation for this difference was however, not provided. Thus, a contradictory picture exists in literature and no author has shown the effect of scale on granules and likewise on resulting tablets. In conclusion, a combined analysis of the granules (4.2.3) and tablets (4.2.4) is still missing to better understand the influence of the observed difference at different scales.

4.2.3   Particle size distribution of granules

4.2.3.1   Impact of formulation attributes on particle size distribution within one scale

MacroPactor - It is common understanding that an increased specific compaction force (eq. solid fraction) results in coarser granules [19–22]. Results of the d_{50} of the granules can be seen in Figure 14.

Figure 14 d_{50} granules – MacroPactor – MCC 2:1 LAC/MCC 1:1 LAC, mean
(n = 3), error bars (standard deviation of mean)

The d_{50} of MCC 2:1 LAC increased from 83 µm to 133 µm and the bulk density from 0.51 g/cm³ to 0.56 g/cm³ for specific compaction force of 2 kN/cm to 8 kN/cm, which reflected a densification of the formulation.

Considering Figure 15, the fraction of fine particles (≤ 63 µm) increased up to 6 kN/cm, compared to the unprocessed blend (0 kN/cm). Fracturing of pre-agglomerated particles of LAC under pressure causes smaller particles with a higher surface in respect to unprocessed LAC [19,23,102]. The higher surface can also be considered as an increased bonding capacity.
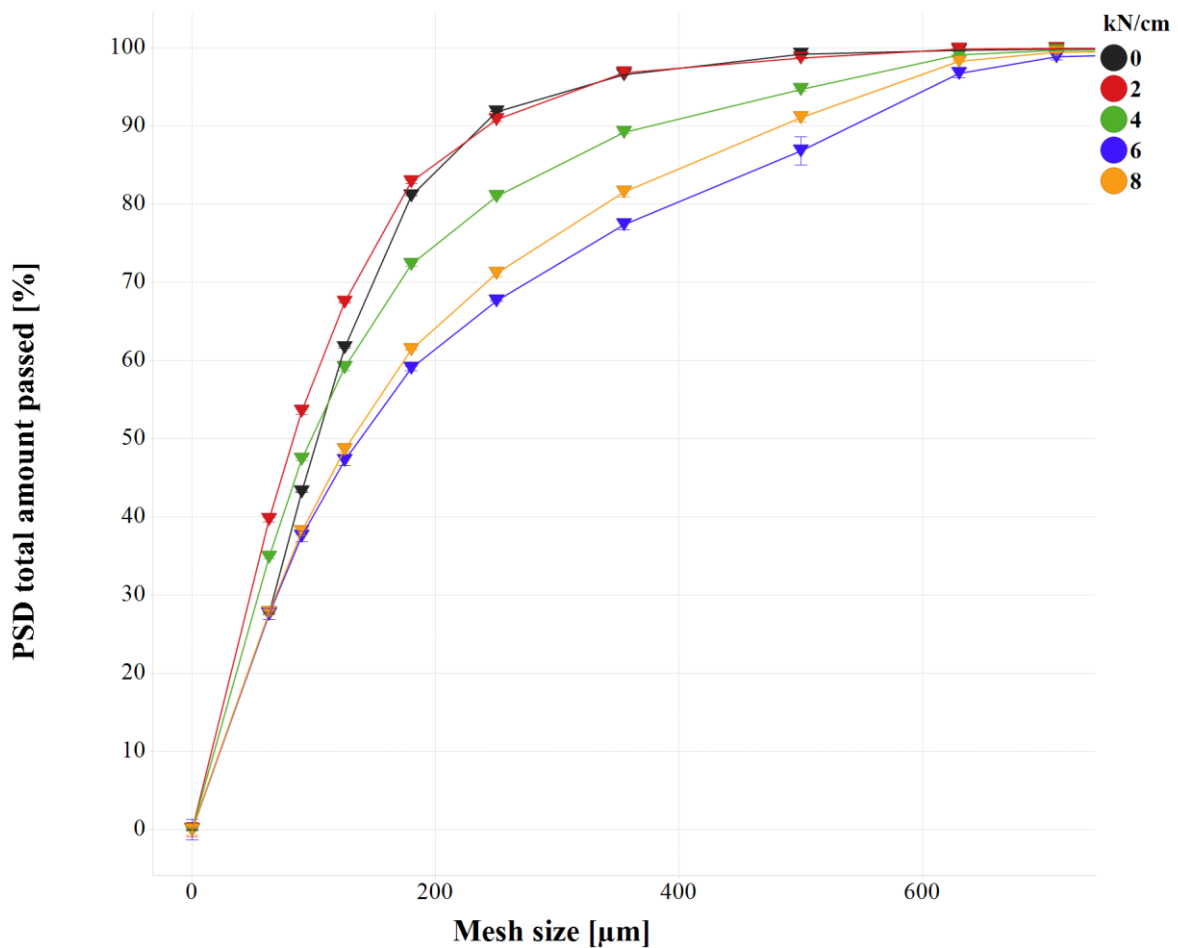
Figure 15   PSD granules – MacroPactor - MCC 2:1 LAC, triangle (mean, n = 3), error bars (standard deviation of mean), colour indicates different specific compaction forces [kN/cm]

The effect of disintegration into fine particles by pre-agglomerated particles and brittle fracturing was reduced at a higher solid fraction of the ribbon caused by an increased impact of the plastically consolidated MCC. LAC particles can fill the voids between fibrous MCC particles [4] to build a ribbon to resist the shear stress of the milling process of the granulator (see Figure 15).

The d_{50} of the particle size distribution (PSD) of the formulation MCC 1:1 LAC increased from 79 µm to 210 µm and the bulk density increased from 0.53 g/cm³ to 0.59 g/cm³. At a same specific compaction force, it would be expected, that the higher fraction of the MCC in formulation MCC 2:1 LAC would result in a stronger ribbon characterised by a higher tensile strength compared to MCC 1:1 LAC (see 4.1.1.2.2). Hence, a higher d_{50} occurs [23], but this was not be observed for 8 kN/cm (see Figure 14).

Figure 16   Side seal leakage of unprocessed material above cheek plates –
                   MacroPactor – MCC 2:1 LAC at 8 kN/cm

A leakage at the side seal system was observed for MCC 2:1 LAC at 8 kN/cm. Unprocessed, smaller material slipped above the compaction zone (see Figure 16). With a higher amount of smaller particles the d_{50} of MCC 2:1 LAC was reduced. This explained the lower d_{50} of 133 µm for MCC 2:1 LAC compared to 210 µm for formulation MCC 1:1 LAC at 8 kN/cm. Furthermore, no increase of the d_{50} could be observed between 6 kN/cm and 8 kN/cm (see Figure 14). Hence, MiniPactor results will be more representative for a reliable formulation comparison for PSD of granules within one scale as no side seal leakage was observed.

MiniPactor – An increased d_{50} of the granules was obtained at rising specific compaction force. MCC 2:1 LAC showed a strong increase of the d_{50} from 88 µm to 136 µm compared to MCC 1:1 LAC (70 µm to 105 µm, see Figure 17). Same process parameters resulted in a higher d_{50} for MCC 2:1 LAC. This was caused by the higher amount of MCC, which is correlated with a higher plastic deformation, resulting in a higher tensile strength (see Figure 6), to resist the destructive load of the milling process of the granulator. LAC needed a higher pressure (e.g. degree of consolidation) to gain the same level of tensile strength (see Figure 6). Therefore, a higher d_{50} was obtained for MCC 2:1 LAC at the same specific compaction force compared to MCC 1:1 LAC.
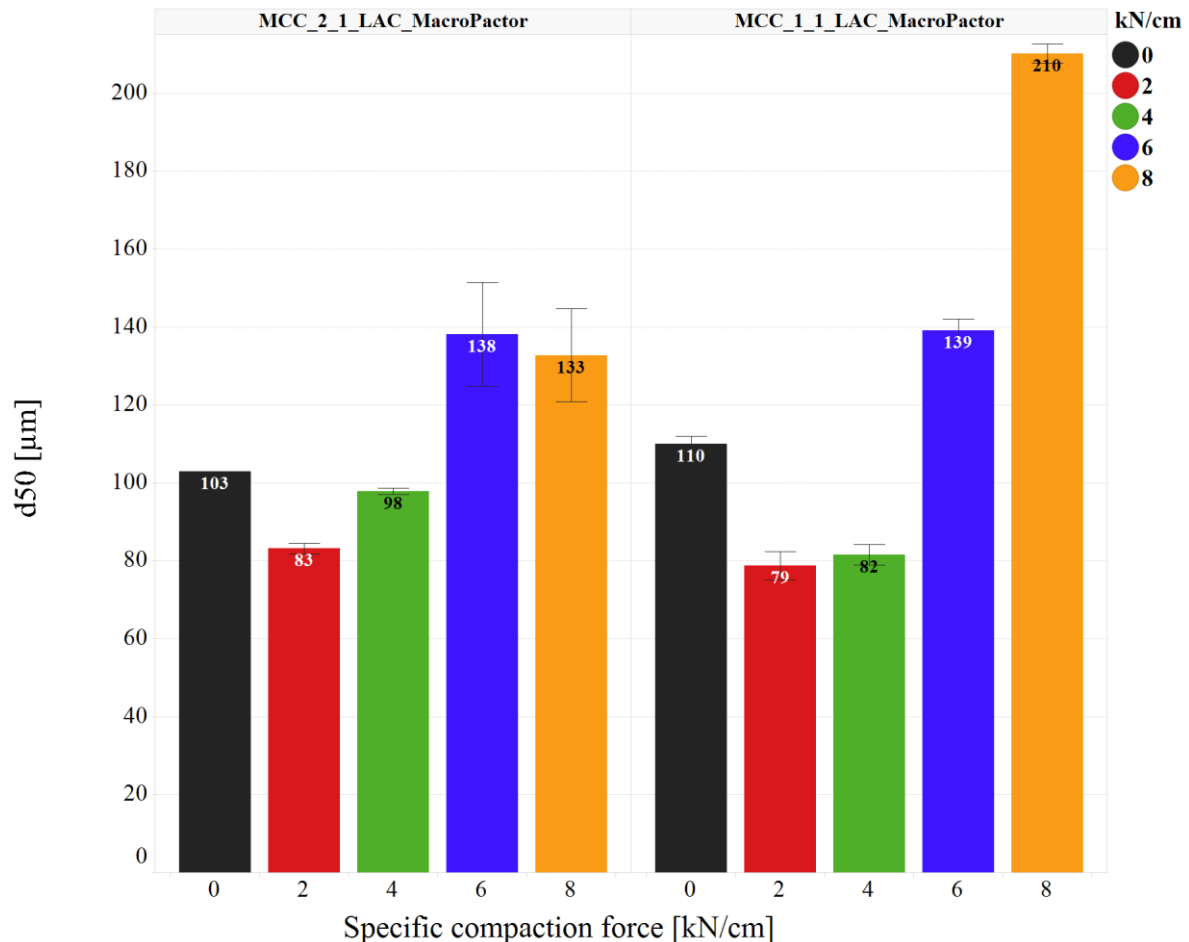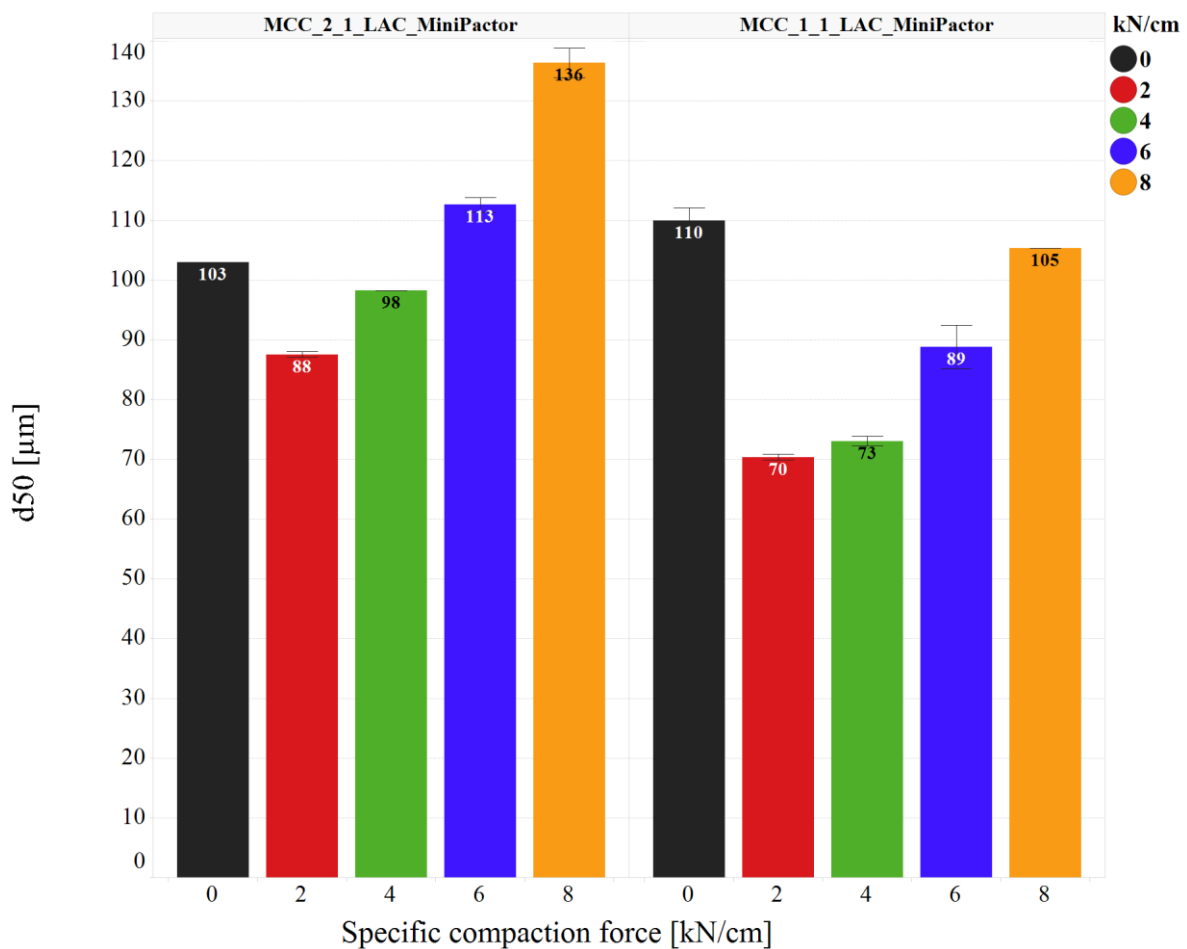

Figure 17 d_{50} granules – MiniPactor – MCC 2:1 LAC/MCC 1:1 LAC, mean (n = 3), error bars (standard deviation of mean)

Brittle behaviour and destruction of the fine pre-agglomerated LAC particles showed a lower d_{50} at low specific compaction force compared to unprocessed blends. The d_{50} of the unprocessed blends have been firstly exceeded after a specific compaction force of about 6 kN/cm (see Figure 17). Bulk density increased from 0.47 g/cm³ to 0.56 g/cm³ (2 kN/cm –

8 kN/cm, MCC 2:1 LAC) and from 0.50 g/cm³ to 0.60 g/cm³ (2 kN/cm – 8 kN/cm, MCC 1:1
LAC) with rising solid fraction, which indicated a densification of both formulations.

Comparing both formulations, a higher fraction of fine particles were found for MCC 1:1
LAC compared to MCC 2:1 LAC (see Figure 18, ≤ 63 µm). Although the formulation MCC
1:1 LAC reached a higher solid fraction of the ribbon within one scale (see Figure 13).
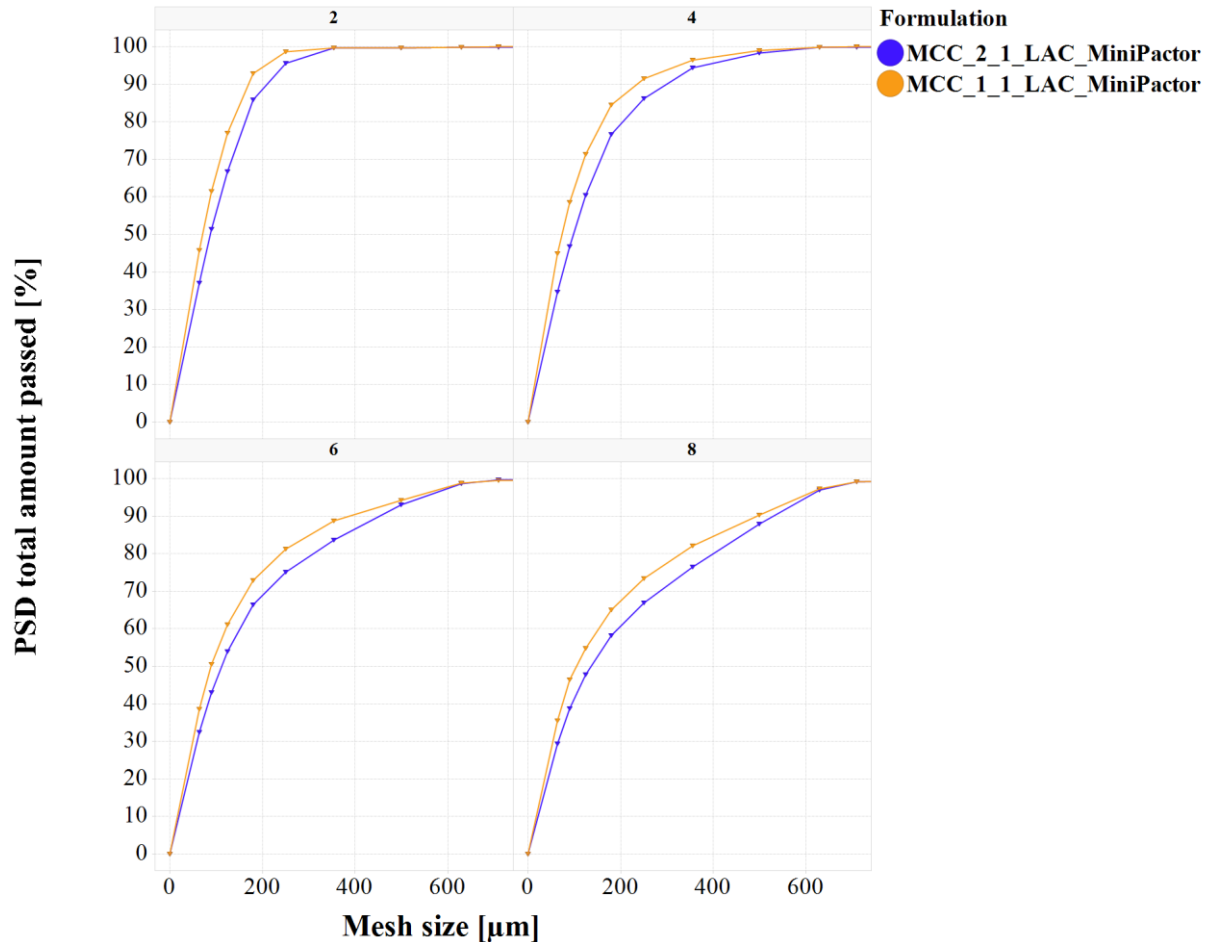
Figure 18   PSD granules– MiniPactor at 2, 4, 6 and 8 kN/cm –
                   MCC 2:1 LAC/MCC 1:1 LAC, triangle (mean, n = 3), error bars
                   (standard deviation of mean)

The formulation MCC 2:1 LAC had a higher ribbon compactibility (see 4.1.1.2.2), resulting
in a higher tensile strength of the ribbon [23], which enhanced the resistance against the shear
stress of the granulator, and resulted in a lower fraction of fine particles.

A higher solid fraction of the ribbon (MCC 1:1 LAC, see Figure 12) does not lead to a coarser
particle size if two different formulations are compared at identical process parameters within
one scale. Especially, if one contains a higher fraction of a brittle component (e.g. LAC). The
bonding strength between particles is essential for the PSD as it enhances the resistance
against the granulator and reduces the spall of small particles during granulation. MCC 1:1

LAC showed lower bonding strength (e.g. compactibility, see Figure 7), resulting in a higher amount of finer particles, compared to MCC 2:1 LAC.

4.2.3.2   Comparison of particle size distribution between different scales dependent on same formulation

MCC 2:1 LAC - PSD of granules at different scales showed only small differences. At low specific compaction forces (2 kN/cm, 4 kN/cm) a similar d_{50} was found, compared to 6 kN/cm or 8 kN/cm (see Figure 14, Figure 17), whereby 8 kN/cm can be excluded for evaluation, because a side seal leakage of fine particles was observed for the MacroPactor (see Figure 16). A detailed view on the PSD showed only a small difference between the small and the large scale (see Figure 19). A higher fraction of coarse granules was found at 6 kN/cm for the MacroPactor. A higher solid fraction of the ribbon at the MacroPactor resulted in a similar PSD of the granules at low solid fraction.
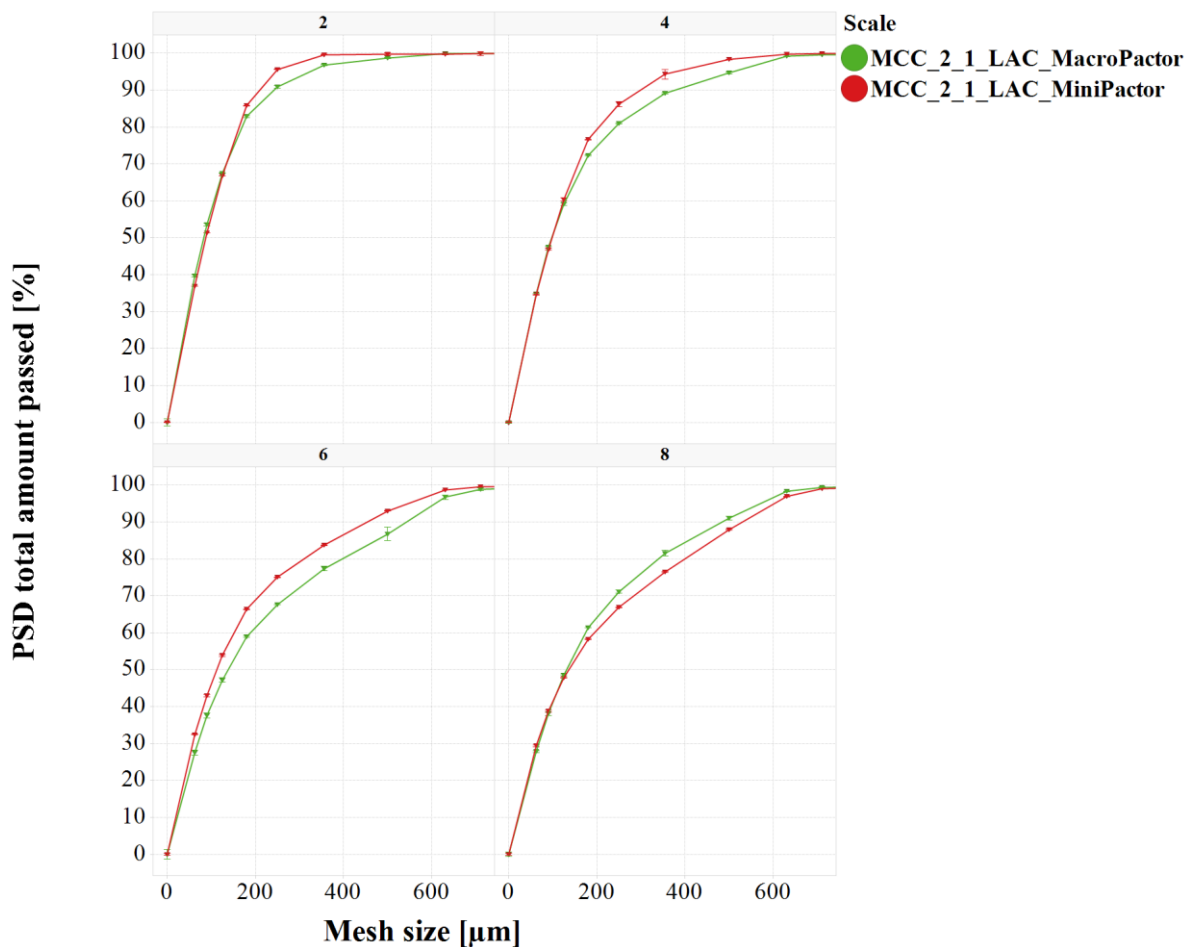
Figure 19   PSD granules - MacroPactor/MiniPactor at 2, 4, 6 and 8 kN/cm - MCC 2:1 LAC, mean (n = 3), error bars (standard deviation of mean)

MCC 1:1 LAC - Different results were found for the formulation MCC 1:1 LAC. Differences of the PSD at different scales were more distinctive at high specific compaction forces. The d_{50} was comparable (see Figure 14, Figure 17) at low specific compaction forces (2 kN/cm, 4 kN/cm). A higher d_{50} was achieved for the MacroPactor at 6 kN/cm and 8 kN/cm compared to the MiniPactor.
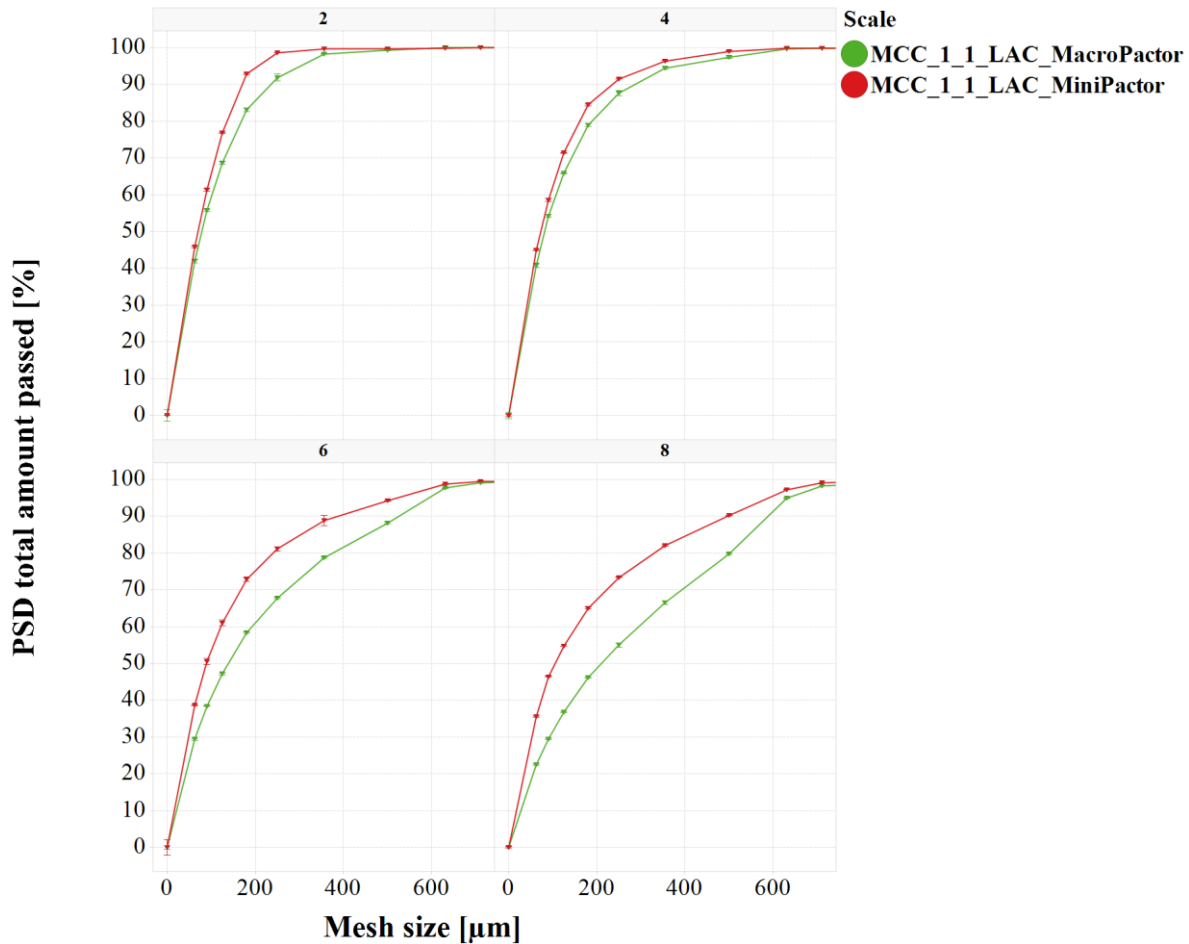
Figure 20   PSD granules – MacroPactor/MiniPactor at 2, 4, 6 and 8 kN/cm -
            MCC 1:1 LAC, triangle (mean, n = 3), error bars (standard deviation
            of mean)

A difference was noticeable for the fraction of fine particles between both scales (see Figure 20). The fraction of fine particles was smaller for the granules of the MacroPactor. This effect was more pronounced for formulation MCC 1:1 LAC compared to MCC 2:1 LAC (see Figure 19, Figure 20), because a lower fraction of MCC reduced the compactibility of the formulation to resist the shear stress of the granulator. This reduced compactibility was enhanced due to the increased amount of brittle LAC (see 4.1.1.2.3). The effect of a higher amount of LAC in the formulation, resulting in finer granules within one scale was previously mentioned (see 4.2.3.1). However, the impact of a higher solid fraction of the ribbon at a

larger scale (MacroPactor, see Figure 13) on the PSD was even more pronounced for a formulation with a lower compactibility (MCC 1:1 LAC). Thus, the higher solid fraction of the MacroPactor caused coarser granules compared to the MiniPactor.

4.2.3.3   Impact of the milling process at different scales

A comparison of the milling step at both scales was done to prove if the solid fraction of the ribbon would be the only impacting factor for the previously observed differences of PSD. Blends of both formulations were tableted at different target solid fractions (MCC 1:1 LAC 0.64, 0.79; MCC 2:1 LAC 0.62, 0.77; see Table 25) to compare the milling process between scales.
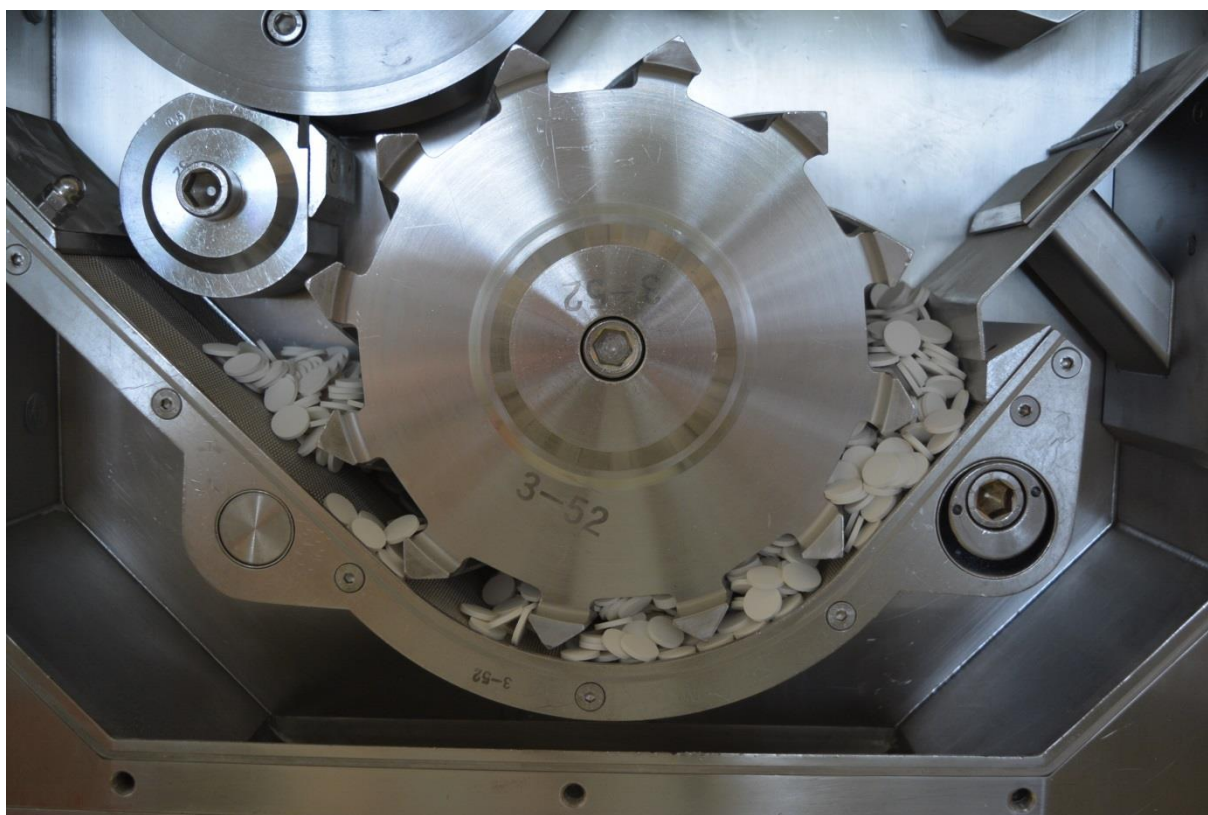
Figure 21   Comparison milling process scale – Granulator MacroPactor

One batch with the same solid fraction contained 2000 tablets, equally divided between the two roller compactors to be milled in the granulator. Eight granules were analysed. During tableting (FlexiTab®) the die wall was lubricated automatically by a press chamber coating system [103] after every ten tablets to reduce the friction between powder and die wall and to achieve a homogenous density distribution of the tablets [104]. The geometry of 20 tablets of each batch was determined by an automatic tablet tester to calculate the observed solid fraction (see APPENDIX 8.1.2).

Table 5 d_{50} milled tablets – MacroPactor/MiniPactor – MCC 2:1 LAC/MCC 1:1 LAC

Formulation	Target solid fraction	MacroPactor d_{50} [µm] ± SD	MiniPactor d_{50} [µm] ± SD
MCC 2:1 LAC	0.62	99 ± 5	100 ± 2
	0.77	163 ± 7	164 ± 10
MCC 1:1 LAC	0.64	86 ± 0	88 ± 2
	0.79	139 ± 7	146 ± 3

n = 3; d_{50} = Median particle dimension; SD = Standard deviation of mean

No significant differences of the d_{50} (p ≥ 0.05) between both scales were observed (see Table 5, see T-Test APPENDIX 8.2.2). A detailed examination of the PSD plot confirmed the impression. The milling process between the two scales had no significant impact on the particle size distribution of granules (see Figure 22).
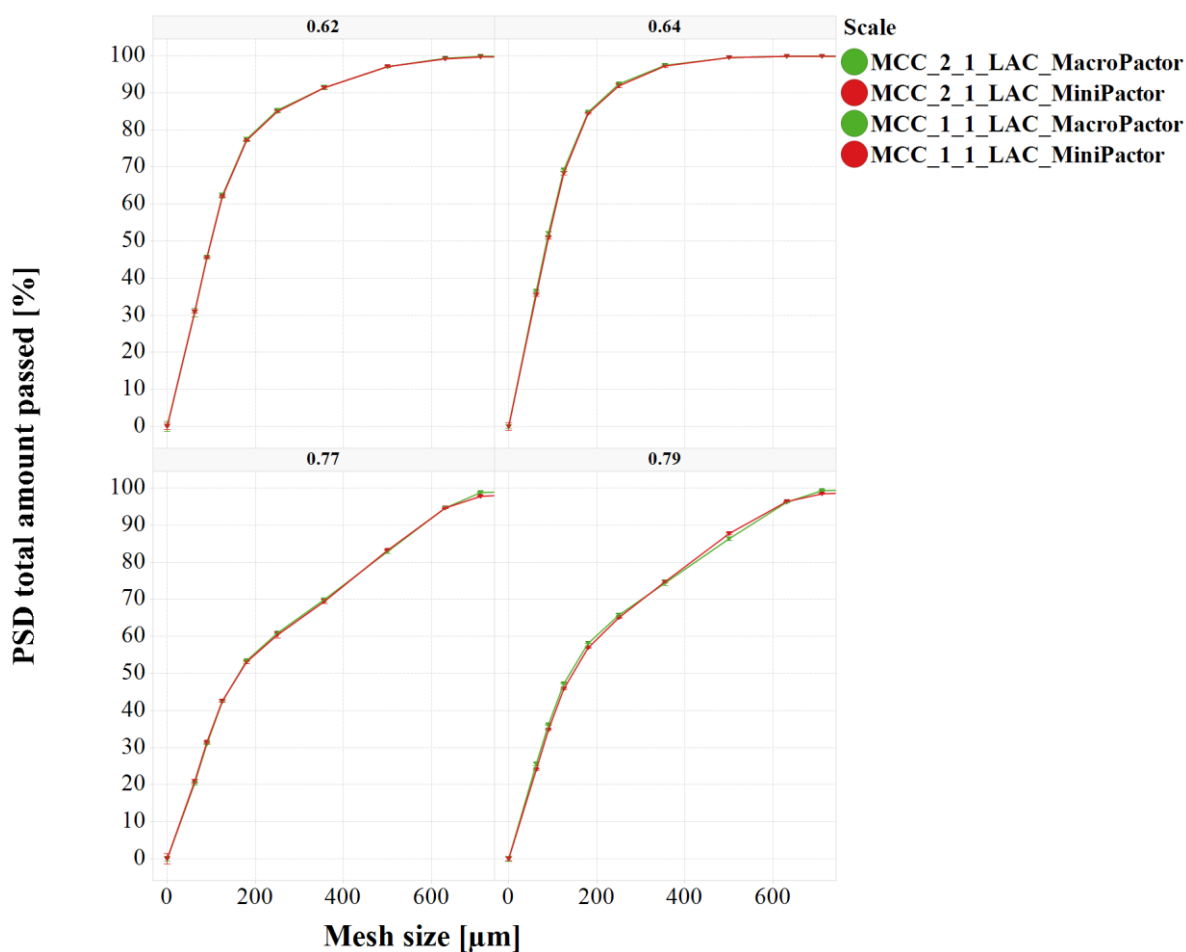
Figure 22   PSD milled tablets of 0.62, 0.64, 0.77 and 0.79 solid fraction - MiniPactor/MacroPactor – MCC 2:1 LAC/MCC 1:1 LAC, mean (n = 3), error bars (standard deviation of mean)

Thus, it can be concluded that milling a product (e.g. tablets) with the same solid fraction at different scale resulted in an equal PSD. Consequently, the previously demonstrated different PSD of the granules was the result of the diverse solid fraction of the ribbon at different scales (see Figure 19, Figure 20). This is in agreement with literature; authors have identified the solid fraction of the ribbon as key quality attribute for downstream processing [4,5,8,17,26,99]. Now, for the first time, differences of the PSD between two different scales applying identical process parameters were demonstrated.

In summary, it can be concluded that a high solid fraction (eq. specific compaction force) provided coarser granules (see Figure 14, Figure 17) in connection with a low amount of fine particles. A larger scale (MacroPactor) achieved a higher solid fraction compared to the smaller scale (MiniPactor) for both formulations at same process settings (Figure 13). Differences of the PSD of the granules between scales were more distinctive at high values (≥ 0.70) of the solid fractions. This was in particular seen for the formulation with a high amount of the brittle LAC, because formulation MCC 1:1 LAC had a lower compactibility than MCC 2:1 LAC (see 4.1.1.2.3). That enhanced the effect of a lower solid fraction of the ribbons on PSD for the smaller scale. In terms of the PSD of the resulting granules, MCC 1:1 LAC showed a higher susceptibility to different solid fraction caused by various roller compactors.

4.2.4   Influence of granules on tablet attributes

All granules and unprocessed blends were tableted with equal process parameters. In Figure
23 (MacroPactor) and Figure 24 (MiniPactor) the tensile strength of tablets vs. compression
pressure of each scales and for both formulations is plotted.

4.2.4.1   Tabletability of formulations within one scale
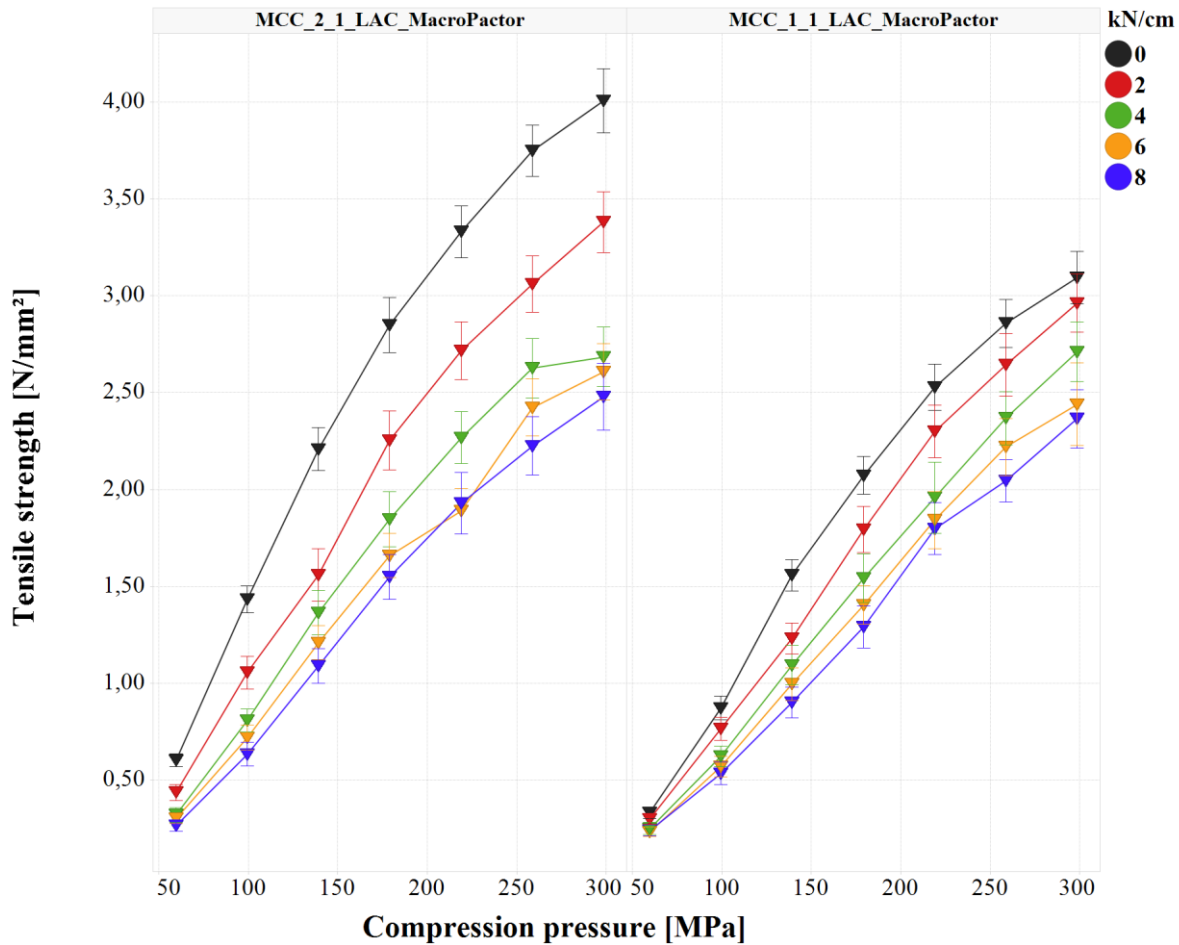
Figure 23   Tabletability – MacroPactor - MCC 2:1 LAC/MCC 1:1 LAC, mean
                        (n = 50), error bars (standard deviation of mean), colour indicates
                        different specific compaction force [kN/cm]

MacroPactor & MiniPactor - One way ANOVA with post hoc Bonferroni analyses was
performed to evaluate the impact of the specific compaction force on the tensile strength. A
significant difference ($p \leq 0.05$) was identified for all test samples.
(except 14 of 140 showed no difference; for details see APPENDIX 8.2.2). At an increasing
specific compaction force a decrease of the tensile strength could be found for all
formulations independent of scale. The observed loss of tabletability with increasing specific

compaction force after dry granulation is in agreement with various authors [4–7,9]. The loss
of tabletability is attributed to various reasons like work hardening [7,9,44,105,106], granule
size enlargement [46,47], an enhanced effect resulting from adding MGST to the granules
[48,49] and a different granule porosity [25]. Work hardening means that plastic deformable
excipients, which were loaded by pressure before, partially lost their ability to undergo plastic
deformation to build a network of bonds. In addition, building a coherent network like a tablet
is influenced by the ability to undergo bonds, which is correlated to the surface area of
individual particles [45]. This surface is affected by particle size and particle surface covered
by MGST on the particle. Brittle and porous excipients/granules tend to fracture during the
tableting process into smaller particles, creating new surfaces. These surfaces are not covered
by MGST and have larger specific surfaces (smaller particles) to build new contact points
[56], resulting in stronger bonds compared to unfractured coarse granules, which are covered
by a MGST layer.
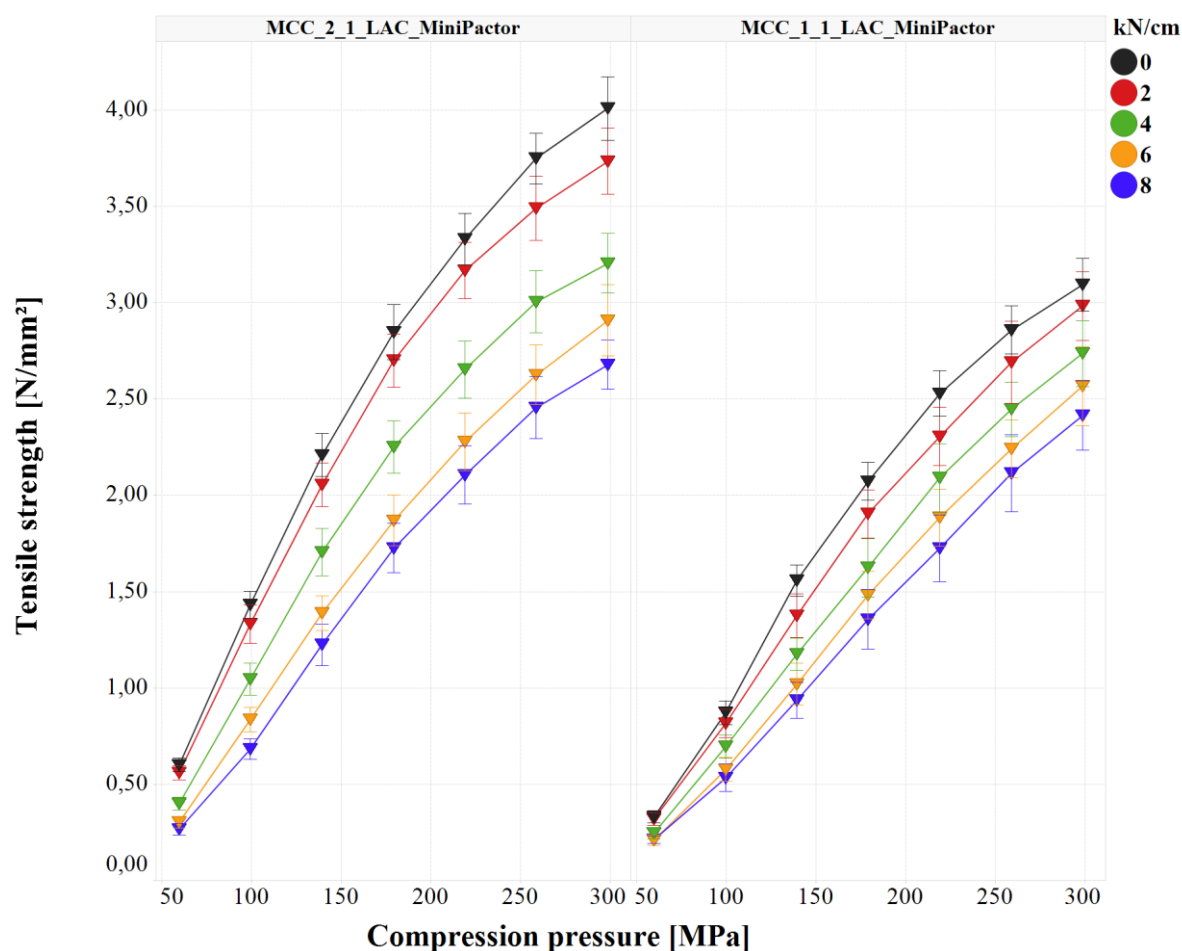
Figure 24   Tabletability – MiniPactor - MCC 2:1 LAC/MCC 1:1 LAC, mean (n =
50), error bars (standard deviation of mean), colour indicates different
specific compaction forces [kN/cm]

MCC 2:1 LAC reached a higher tensile strength in comparison to MCC 1:1 LAC at both scales (see Figure 23, Figure 24) because of the higher fraction of MCC, which showed a better tabletability and compactibility compared to LAC (see 4.1.1.2).

The loss of tabletability with increasing specific compaction force is more pronounced for MCC 2:1 LAC as the ability of MCC to undergo plastic deformation again, decreases with rising specific compaction force (work hardening) [44,46]. This effect enhances by internal lubrication, whereby the surfaces are covered with a layer of MGST [49]. Additionally, a filming or coating of the MCC particles by MGST can be observed, whereby the whole surfaces are covered by MGST, if high concentration of MGST and long blending duration were chosen. Filming or coating of the whole particles can be excluded for these results as only a total amount 1 % MGST and a low blending time was used (see Table 15, Table 21). In contrast, LAC shows insensitivity towards MGST [10] and only a negligible loss of tensile strength (low work hardening) compared to unprocessed LAC (0 kN/cm) after dry granulation, which is caused by the ability of fracturing into smaller particles with a higher specific surface [90,107].

Various authors [4,10,108,109] have shown a nearly linear increase of the tensile strength for LAC after roller compaction over a range of compression pressure. Only a minor influence of the specific compaction force of a roller compactor on the loss of tensile strength was found, which was independent of particle size enlargement (lower surface area). In other words, a high fraction of LAC (brittle) results in a higher reworkability of the formulation. MCC 1:1 LAC showed a linear course of the tensile strength at increased specific compaction forces compared to low specific compaction forces (see Figure 23, Figure 24), which can be correlated to a higher impact of the linear consolidation of the brittle LAC after dry granulation, because less plastic consolidation of the MCC was available (work hardening).

A good illustration of the reworkability of a formulation is the reworkability index, firstly introduced by Herting et al. (2007) [26]. He compared the achieved tensile strength of tablets of unprocessed material (0 kN/cm) with the tensile strength of granules at the same compression pressure after dry granulation. Based on a modification of this approach it is possible to compare the reworkability over the whole compression pressure range (see 6.2.3.1.1, Eq. (33)).

Figure 25   Reworkability index tablets –MacroPactor –

MCC 2:1 LAC/MCC 1:1 LAC, TS_{ratio} = tensile strength of tablets of compacted blend in proportion to unprocessed blend Eq. (33), mean (n = 350), error bars (standard deviation of mean)

The reworkability decreased with a higher specific compaction force for both formulations (see Figure 25). The differences of the reworkability between both formulations at the same specific compaction force increased from 11.7 % (2 kN/cm) to 14.0 % (8 kN/cm). 8 kN/cm has to be carefully considered because of the side leakage (see Figure 16). However, the TS_{ratio} showed that the formulation MCC 1:1 LAC had a higher reworkability within the same scale because of intense fracturing during tableting, insensitivity to MGST, lower susceptible

to the specific compaction force (work hardening) and insensitivity to the particle size enlargement effect. (MiniPactor results can be found in the APPENDIX 8.1.2)

4.2.4.2   Tabletability between different scales

MCC 2:1 LAC - Distinct differences of the tabletability between both scales were found. In Figure 26 and Figure 27 a comparison of the tabletability between both scales for the same specific compaction force is depicted (2 and 4 kN/cm, 6 and 8 kN/cm).

Figure 26   Tabletability – MacroPactor/MiniPactor at specific compaction force of 2 and 4 kN/cm – MCC 2:1 LAC, mean (n = 50), error bars (standard deviation of mean), scattered lines indicate ±10 % differences to the mean tensile strength of the MacroPactor

A pre-evaluation showed a relative standard deviation of tensile strength at a distinct compression pressure in the range of 6.72 % (298 MPa) up to 10.00 % (60 MPa) (see APPENDIX 8.2.2). This was attributed to the relative standard deviation of the compression pressure at the rotary tablet press (relative standard deviation (RSD) ≈ 5 %). Hence, it was defined that the mean tensile strength of different scales has to be in range of ±10 % of the

reference to achieve comparable tabletability. Statistical evaluation (T-test) showed significant differences ($p \leq 0.05$) between the tablets based on the MacroPactor and MiniPactor for all values within one specific compaction force except for compression pressure of 60 MPa at 6 kN/cm and 8 kN/cm (see APPENDIX 8.1.2). At 2, 4 and 6 kN/cm the MiniPactor's granules achieved a higher tensile strength compared to the MacroPactor exceeding the +10 % limit. A smaller difference between the two scales was found for the specific compaction force 8 kN/cm, but still near +10 %. This was caused by side leakage of unprocessed material, whereby smaller uncompacted material slipped above the side seal system, as mentioned at 4.2.3, and induced a higher tensile strength of the tablets for the MacroPactor.

Figure 27   Tabletability – MacroPactor/MiniPactor at specific compaction force of 6 and 8 kN/cm – MCC 2:1 LAC, mean (n = 50), error bars (standard deviation of mean), scattered lines indicate ±10 % differences to the mean tensile strength of the MacroPactor

Granules of a roller compaction process have a higher resistance against consolidation during tableting in comparison to unprocessed material [44]. To illustrate this, the Heckel plot is the

most commonly applied technique [106] (see Yield pressure 4.1.1.2.1.1). "In-die" tableting was performed to measure the Yield pressure of the granules.

Table 6   Heckel - Yield pressure granules - MiniPactor/MacroPactor - MCC 2:1 LAC

Yield pressure P_y (1/slope)		0 kN/cm	2 kN/cm	4 kN/cm	6 kN/cm	8 kN/cm
	MacroPactor	174.21	176.31	182.45	187.34	186.82
	MiniPactor	174.21	177.79	181.09	184.53	185.80
	Difference	0	-1.48	1.36	2.81	1.32

n = 3; P_y = Yield Pressure Heckel

Results showed that the Yield pressure increased with rising specific compaction force for both scales. Differences of the Yield pressure between scales were very small ($\approx 2\,\%$). It is well known that the determination of the Heckel plot is prone to errors in respect to PSD, surface of the particles and internal lubrication for granules. Granules had a different PSD and were lubricated using MGST. For these reasons, the results of the Heckel plot have to be considered carefully [106]. He et al. (2007) also recognized only a small increase of the Yield pressure for dry granulated MCC at increased specific compaction force because of internal lubrication, which can disguise the obviously effect of work hardening indicated by the Yield pressure. For these granules, analysis by Heckel plot is not the method of choice to investigate the work hardening effect.

TS_{ratio} gave better insights into the tabletability of both scales compared to Yield pressure. Reworkability was higher for the granules of the MiniPactor for all specific compaction forces and showed a higher reworkability. Differences decreased from 16.0 % (2 kN/cm) to 4.6 % (8 kN/cm) at higher specific compaction forces, which can be positive correlated with the observed decreased difference of the solid fraction of ribbons between both scales with rising specific compaction force (see 4.2.2, Figure 13).
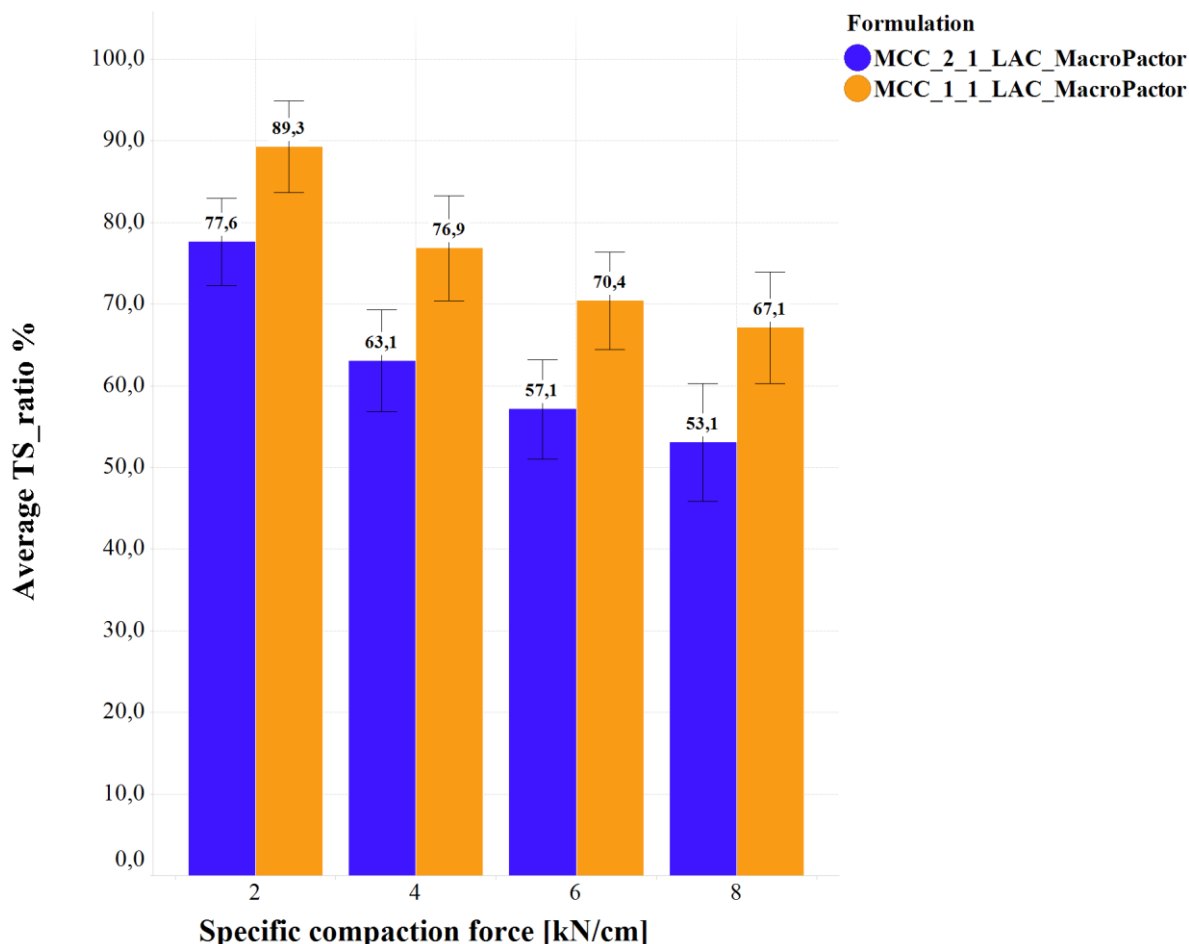

Figure 28   Reworkability index tablets - MiniPactor/MacroPactor – MCC 2:1 LAC, TS_{ratio} = tensile strength of tablets of compacted blend in proportion to unprocessed blend Eq. (33), mean (n = 350), error bars (standard deviation of mean)

Particle size distribution of the granules is one main factor, which can influence the tensile strength of tablets. Smaller particles have a greater specific surface to build more interparticle bonds which can result in a higher tensile strength [45,90]. The differences of particle size distribution between both scales at same specific compaction force were low (Figure 14, Figure 17). The d_{50} showed only small differences and the part of fine particles ($\leq 63\ \mu m$)

were similar. Thus, the influence of particle size distribution on the tensile strength was negligible.

The distinguished difference between these granules was the production scale, i.e. compactor size, which resulted in a different solid fraction of the ribbon. A higher solid fraction at the MacroPactor was obtained (> 10 %), followed by 10 % lower tensile strength of the tablets compared to the MiniPactor. A higher solid fraction reflects a higher consolidation and thus a higher consumption of plastic deformation, which will not be available for tableting (work hardening effect) again. Roller compaction of formulation MCC 2:1 LAC at different scales led to a different quality of the tablets although a comparable particle size distribution of the granules was achieved.

MCC 1:1 LAC - Different results were obtained for formulation MCC 1:1 LAC. In Figure 29 tensile strength vs. compression pressure is plotted for four different specific compaction forces. Considering Figure 29, a relevant difference of the tensile strength of the tablets between both scales could not be observed.
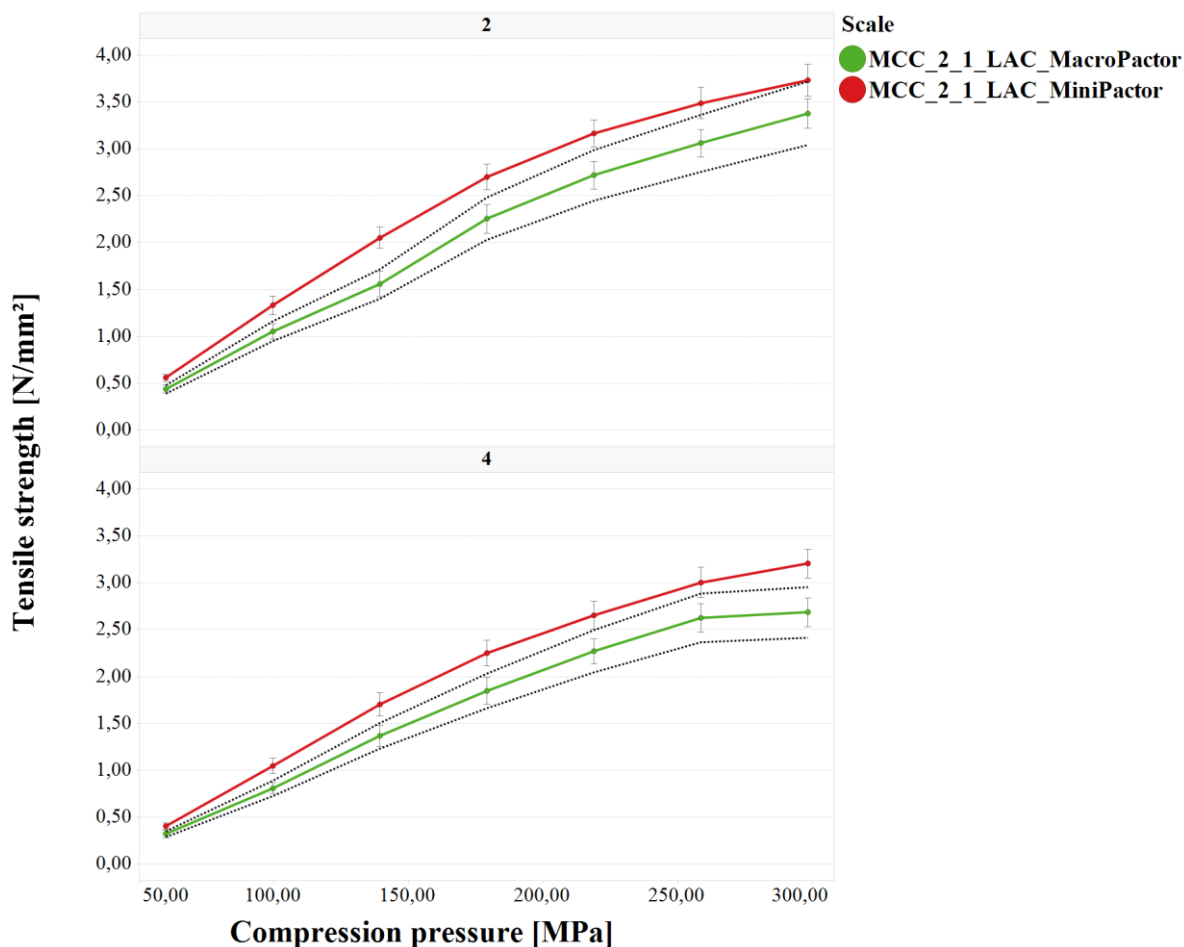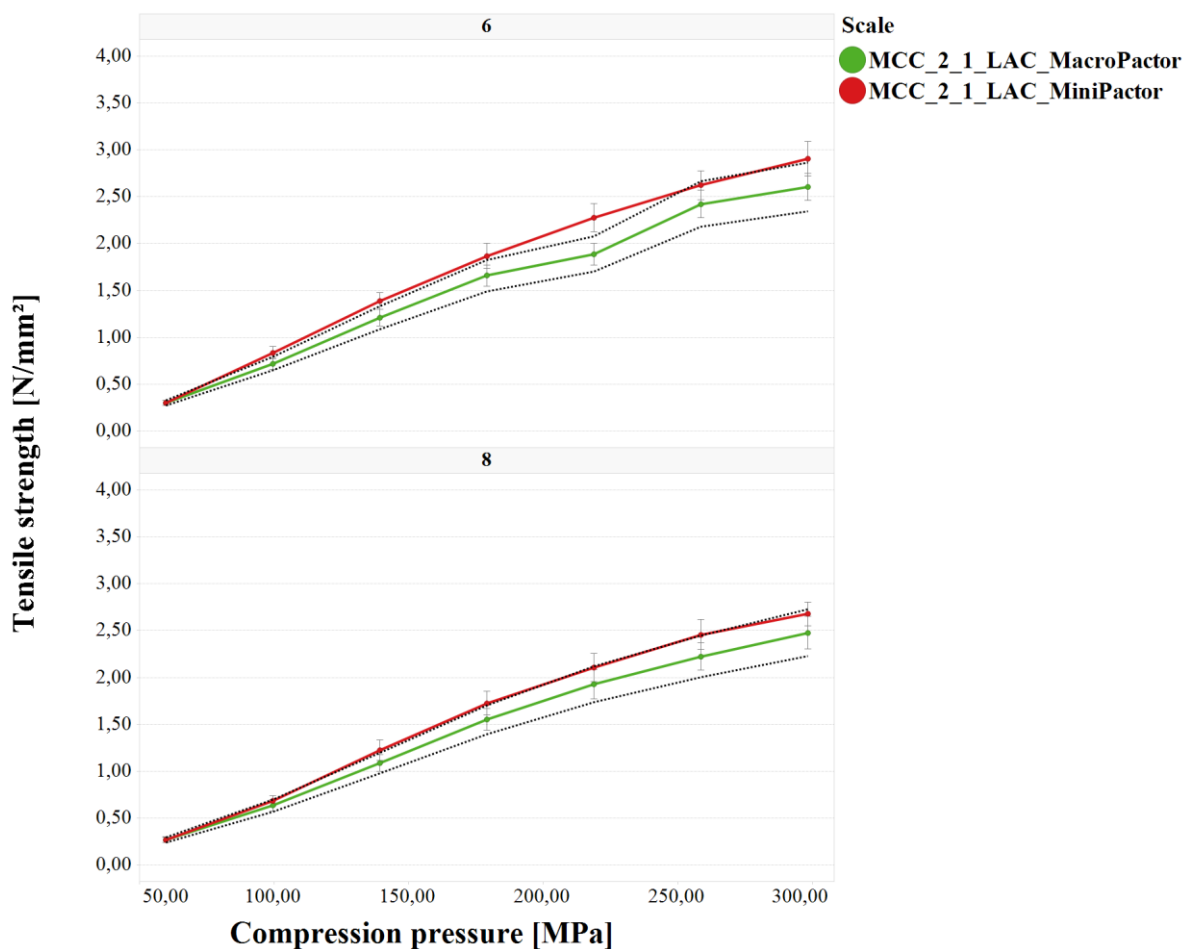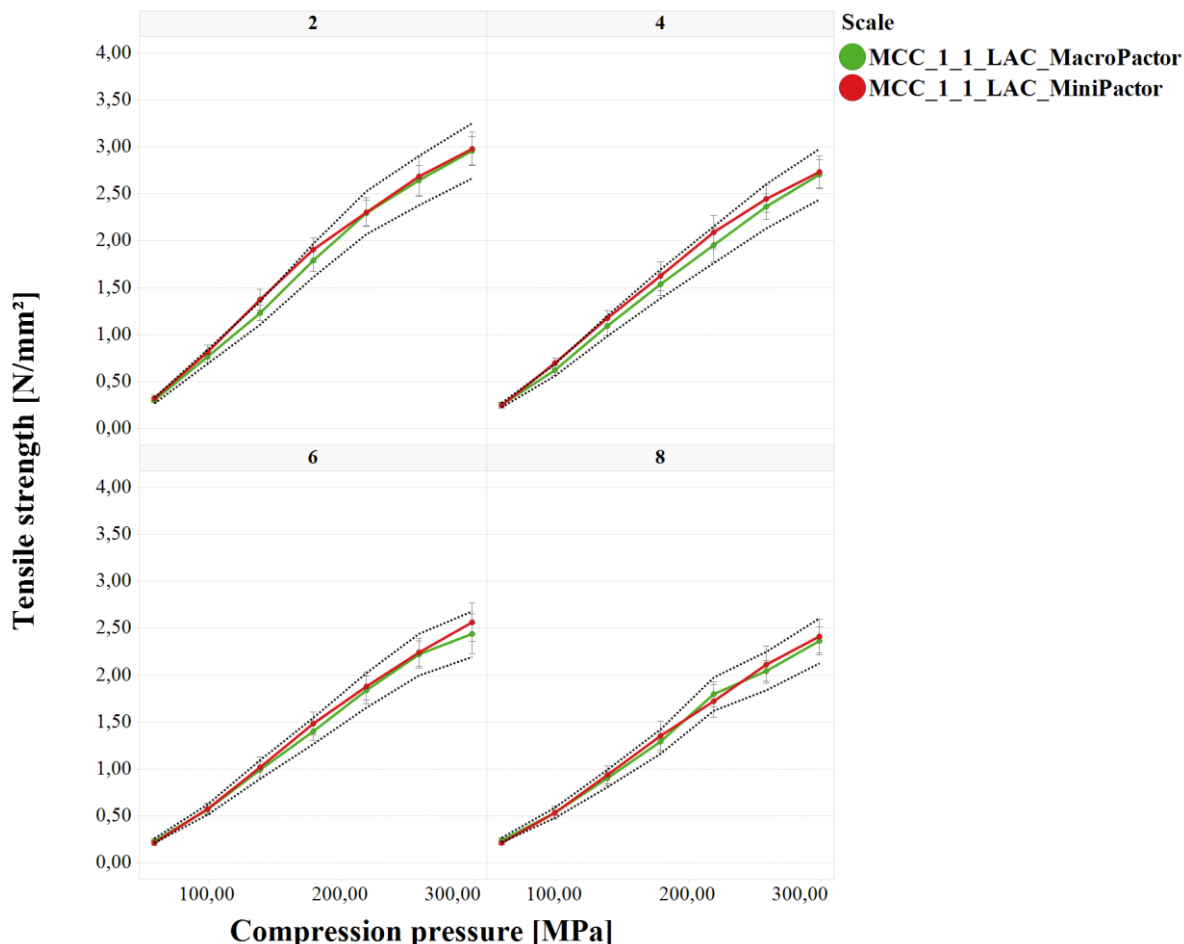

Figure 29   Tabletability – MacroPactor/MiniPactor at specific compaction force of 2, 4, 6 and 8 kN/cm – MCC 1:1 LAC, mean (n = 50), error bars (standard deviation of mean), scattered lines indicate ±10 % differences to the mean tensile strength of the MacroPactor

Statistical examination (T-Test) of the tensile strength of tablets at the same compression pressure between the two scales showed significant differences ($p \leq 0.05$) for 16 values of 28 (see APPENDIX 8.2.2). However, important to note is that T-Test will detect a significant difference between both scales when difference of only ± 5 % will be obtained, assuming a comparable variance for both samples and previously chosen sample size of n = 50. In particular, a high compression pressure resulted in a low RSD of the tensile strength (see exemplary power calculation for 5 % difference APPENDIX 8.2.2). As mentioned above, 10 % difference of tensile strength was defined as acceptable range, so that a relevant

difference for low compression pressure would be identified with a power of 0.94. Only two out of 28 values differed with more than 10 % from the reference i.e. MacroPactor (2 kN/cm 139 MPa, 4 kN/cm 100 MPa). Comparing Figure 26, Figure 27 (MCC 2:1 LAC) and Figure 29 (MCC 1:1 LAC), a more linear course of the tabletability plot was found for MCC 1:1 LAC, which can be correlated to the linear increase of the tabletability of the brittle LAC. LAC showed a higher impact on the consolidation behaviour with an increased amount in the formulation (MCC 1:1 LAC). Yield pressure measurements were done but did not allow any implication, as mentioned above (see APPENDIX 8.1.2).

TS_{ratio} of MCC 1:1 LAC showed only a small difference between both scales (max. 3.9 %, 2 kN/cm) compared to MCC 2:1 LAC (max. 16 %, 2 kN/cm, see Figure 28), which confirmed the impression based on the trend observed in the tabletability plots. The differences between both scales were low and decreased with rising specific compaction force.
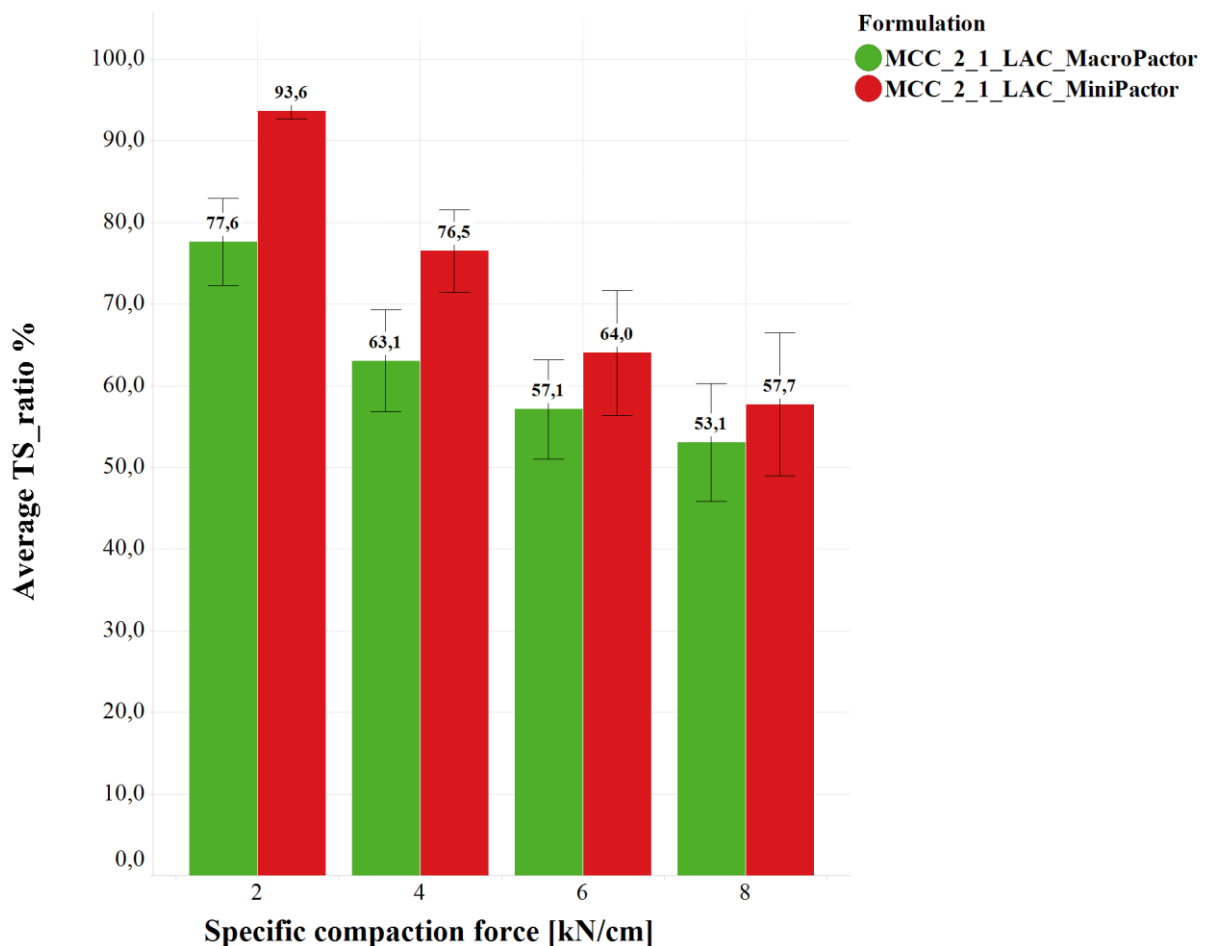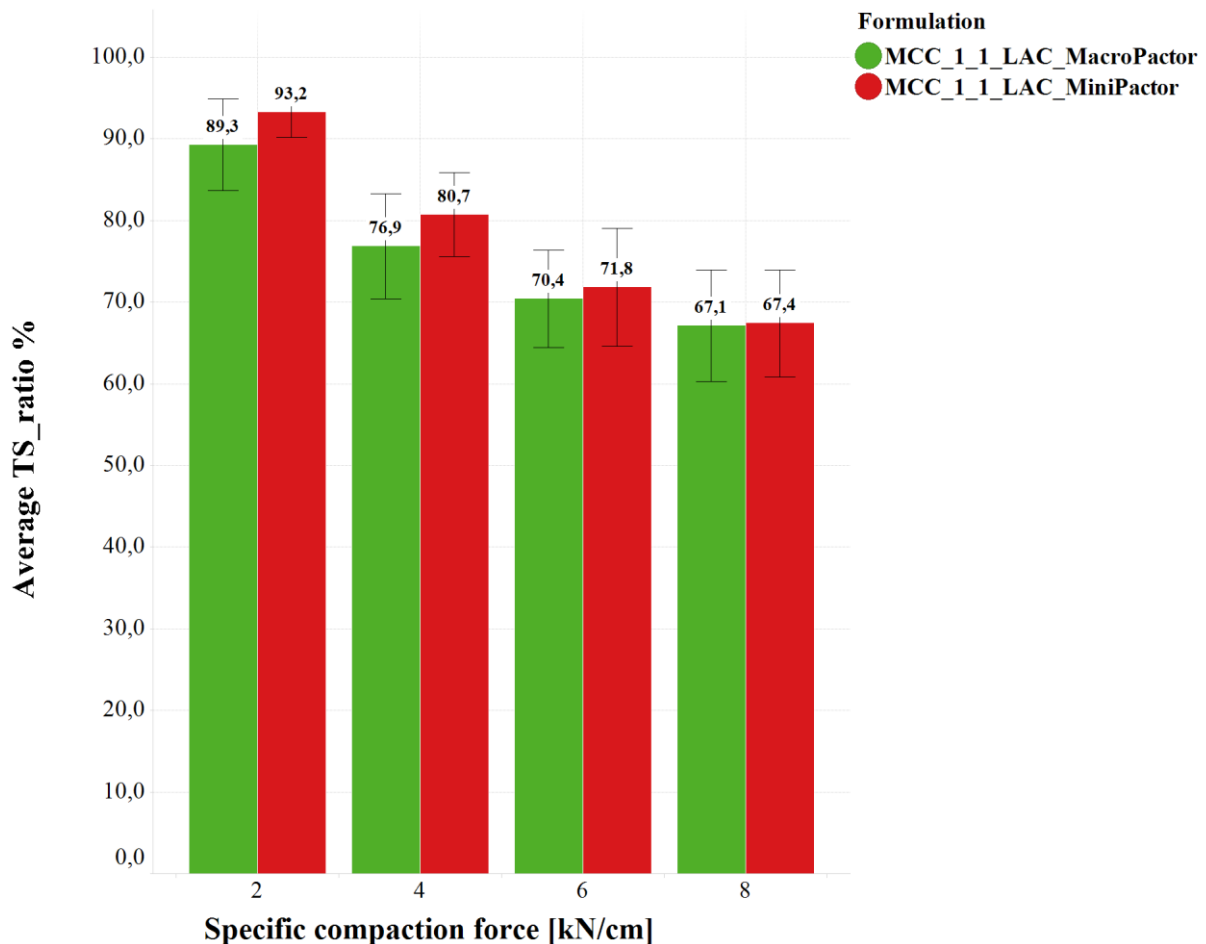

Figure 30   Reworkability index tablets - MacroPactor/MiniPactor–

MCC 1:1 LAC, TS_{ratio} = tensile strength of tablets of compacted blend in proportion to unprocessed blend Eq. (33), mean (n = 350), error bars (standard deviation of mean)

The tensile strength of the tablets of formulation MCC 1:1 LAC is comparable. Regarding the influence of the particle size on tensile strength, granules of the larger scale exhibited a similar d_{50} at low specific compaction forces and a higher d_{50} at 6 kN/cm and 8 kN/cm (see Figure 20). Usually it would be expected that the granules of the MiniPactor reaches a higher tensile strength caused by a smaller PSD, but the high fraction of brittle LAC decreases the influence of the particle size enlargement effect on tensile strength [107], because the granules will fracture into smaller particles or even primary particles. This effect was even more pronounced at higher specific compaction forces (see Figure 30), as the impact of the brittle LAC increased at high specific compaction forces compared to plastic MCC. Wu et al. (2007) dry granulated different single brittle excipients, tableted different sieve fraction of the granules and stated that the granule size had a negligible influence for the tabletability of brittle granules. A lower amount of MCC (MCC 1:1 LAC) reduced the effect of work hardening (lower reworkability), followed by a smaller decrease of the tensile strength (TS_{ratio} 67.1 %, at 8 kN/cm) caused by specific compaction force compared to MCC 2:1 LAC (TS_{ratio} 53.3 %, at 8 kN/cm, see Figure 25). This was enhanced as LAC shows less sensitivity towards MGST than MCC [49].

The obtained difference in solid fraction of ribbons at same process conditions for the large scale (> 9 %, see Figure 13) influenced the particle size distribution of granules for the formulation MCC 1:1 LAC. The expected particle size enlargement effect on tensile strength was levelled through fracturing of LAC and the lower fraction of MCC in an acceptable range of ±10 % tensile strength between scales. Tabletability of formulation MCC 1:1 LAC at both scales can be considered as equal. Despite a shift in PSD between Macro- and MiniPactor for formulation MCC 1:1 LAC, no difference in tabletability between the two scales could be observed. Obviously, the brittle character of LAC governs the consolidation and bonding properties under compression, making the formulation less susceptible towards work hardening and lubricant sensitivity

4.2.5 Summary

Two formulations (MCC 2:1 LAC, MCC 1:1 LAC) were dry granulated at two scales (50 mm roll width MacroPactor, 25 mm roll width MiniPactor) with equal process parameters. A higher solid fraction of the ribbons was obtained for both formulations at the MacroPactor. Solid fraction of the ribbons influenced the particle size of the granules in a different way. Same particle size distribution of granules was achieved for the predominantly plastic deforming formulation MCC 2:1 LAC, whereby coarser granules were the result for the predominantly brittle deforming formulation MCC 1:1 LAC at higher specific compaction force (MacroPactor, 6 kN/cm, 8 kN/cm). Granules of the MacroPactor resulted in a lower tensile strength of tablets compared to granules of the MiniPactor for formulation MCC 2:1 LAC.
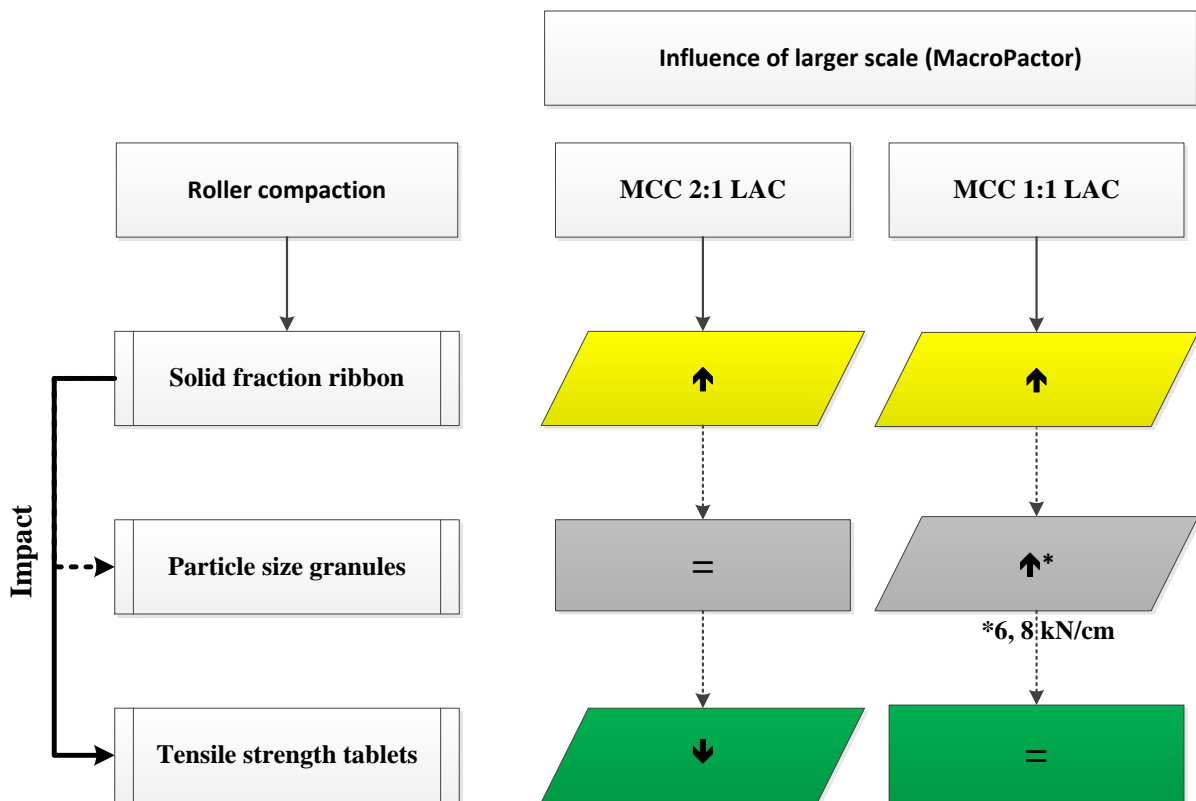
Figure 31   Summary - Impact of formulation and scale, obtained differences of intermediate products: solid fraction of ribbons, particle size of granules and tensile strength of tablets caused by larger scale (MacroPactor) compared to smaller scale (MiniPactor), equal sign = equal, arrow up/down = higher/lower, MCC = Microcrystalline cellulose, LAC = α - Lactosemonohydrate

Thus, the influence of the higher solid fraction corresponded directly to the tensile strength of the tablets, because of the high amount of MCC, which is mainly influenced by specific compaction force (work hardening) and sensitivity towards MGST. Only small differences of the tensile strength between both scales were observed for formulation MCC 1:1 LAC, although particle size distribution differed. This was driven by the impact of the brittle LAC, which resulted in negligible susceptibility towards specific compaction force (work hardening), MGST and particle size enlargement effect in respect to tensile strength of tablets. The second formulation MCC 1:1 LAC showed a higher robustness towards scalability. The impact of a different solid fraction at different scales on the tablet quality will be increased due to a higher amount of MCC in the formulation (work hardening effect).

Differences between the two scales in downstream processing (solid fraction, granules, tablets) have not been described before in literature. It can be concluded that using the same process settings for identically constructed roller compactors of different scale will not necessarily lead to the same quality of tablets, because the quality is formulation and scale dependent. The solid fraction of the ribbon was confirmed as an essential quality aspect in respect of a successful scale up. Differences of the solid fraction between scales were observed in this chapter and will be further investigated and explained in the following chapters.

4.3 ADAPTED PROCESS SETTINGS OF DIFFERENT SCALES TO ACHIEVE SIMILAR PRODUCT QUALITY

Formulation MCC 2:1 LAC was dry granulated using the MiniPactor at various specific compaction forces to achieve the target solid fractions of the MacroPactor, in order to reduce the difference between scales with respect to the tensile strength of tablets (see 4.2). Throughout this manuscript, the results of the adapted process parameter at the MiniPactor are called Scale Model.

4.3.1 Achieving the same solid fraction of ribbon by using adapted process parameter settings

Data of the previously measured solid fraction of the Macro- and MiniPactor at four specific compaction forces were used to determine the specific compaction forces (see Figure 13), which were required to achieve equal solid fraction for the MiniPactor. For this purpose, specific compaction forces were plotted versus solid fractions of the ribbons. Existing data of the solid fractions of the MiniPactor were fitted by a polynomial equation to obtain the required specific compaction forces (Scale Model).

Figure 32   Scale Model approach – Adapting specific compaction force of
MiniPactor to achieve target solid fraction of ribbon (MacroPactor) by
polynomic fitting, mean (n = 5), error bars (standard deviation of
mean)

Target solid fractions of the MacroPactor were set in this correlation function to predict the
required specific compaction force at the MiniPactor (4.1, 7.0, 9.6 and 11.4 kN/cm, see Figure
32). The predicted specific compaction forces were used for processing. Subsequently, the
solid fraction of the ribbons was measured to verify the proposed Scale Model. Adapted
specific compaction forces for the Scale Model are reported as 2, 4, 6 and 8 kN/cm.
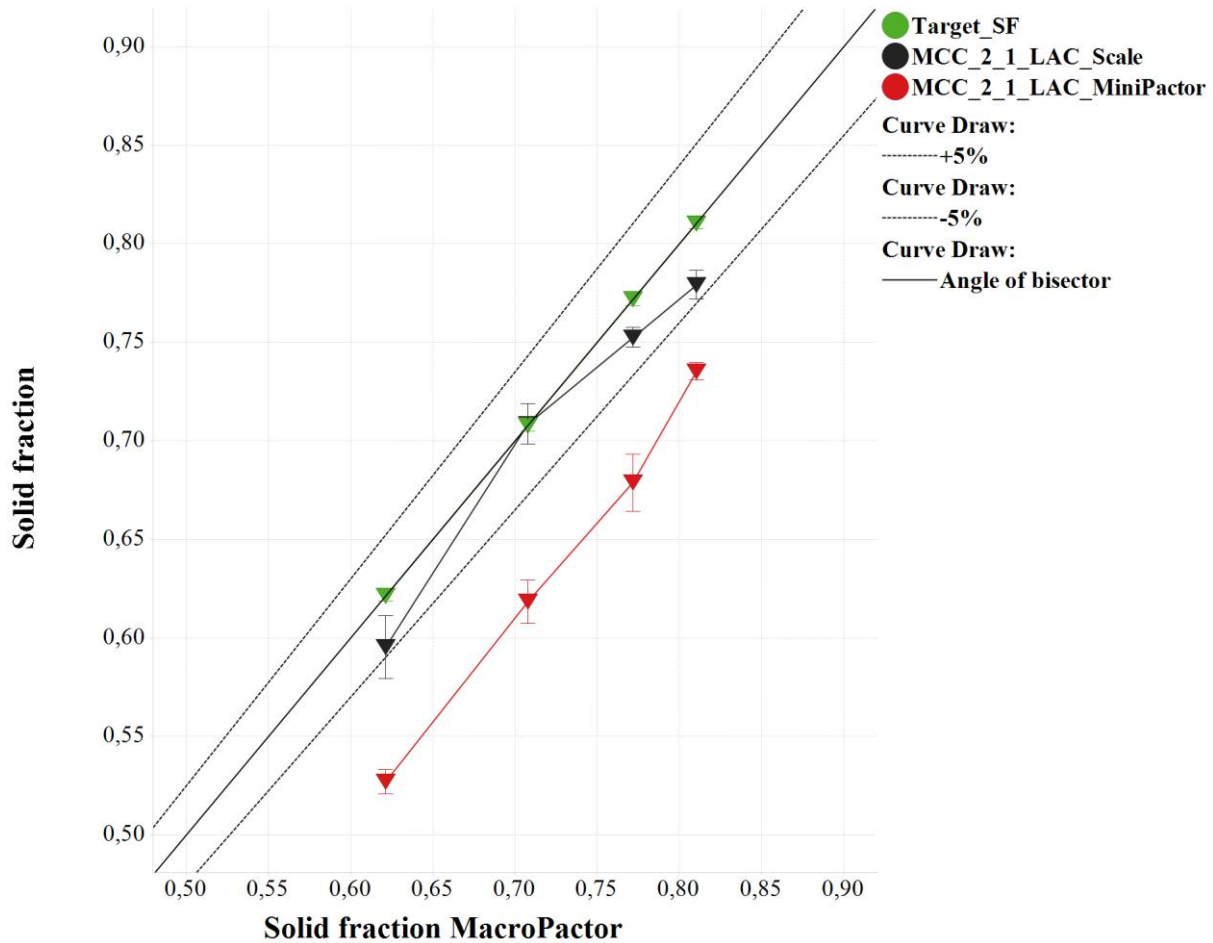
Figure 33 — Solid fraction ribbon – Results Scale Model (adapted process parameter settings) and MiniPactor (equal process parameters), mean (n = 5), error bars (standard deviation of mean), scattered lines indicate ± 5 % range to the target solid fraction (MacroPactor), SF = Solid fraction

Results of the solid fraction are depicted in Figure 33. T-test (p ≤ 0.05) results showed differences between three of four solid fractions between target solid fraction and the solid fraction of the Scale Model (see APPENDIX 8.2.3). Only the solid fraction for the specific compaction force of 7.0 kN/cm (0.7086 SF) showed no difference to the target solid fraction. However, the differences between both scales (applying adapted process parameter settings) were only -0.12 % to 4.39 %, compared to 10.20 % to 17.90 % by using equal process parameter settings (see Figure 13). All solid fractions of the ribbons were in a ± 5 % range to the target solid fraction. Results on downstream processing and an evaluation of this strategy for different scales will be discussed in the next sections. Based on previous findings, it can be assumed that the solid fraction is the most influential factor on downstream processing

(see 4.2) and therefore that a similar granule and tablet quality will be achieved at a comparable solid fraction of the ribbon at different scales.

4.3.2 Particle size distribution and porosity of granules

PSD - Application of the Scale Model resulted in a higher d_{50} for the whole range of investigated specific compaction forces (see Figure 34), which is in accordance to results in 4.2.3.2 where identical force settings resulted in a similar PSD at a lower SF for granules produced with the MiniPactor. T-test ($p \leq 0.05$) confirmed a difference between all granules at same solid fraction (see APPENDIX 8.2.3).
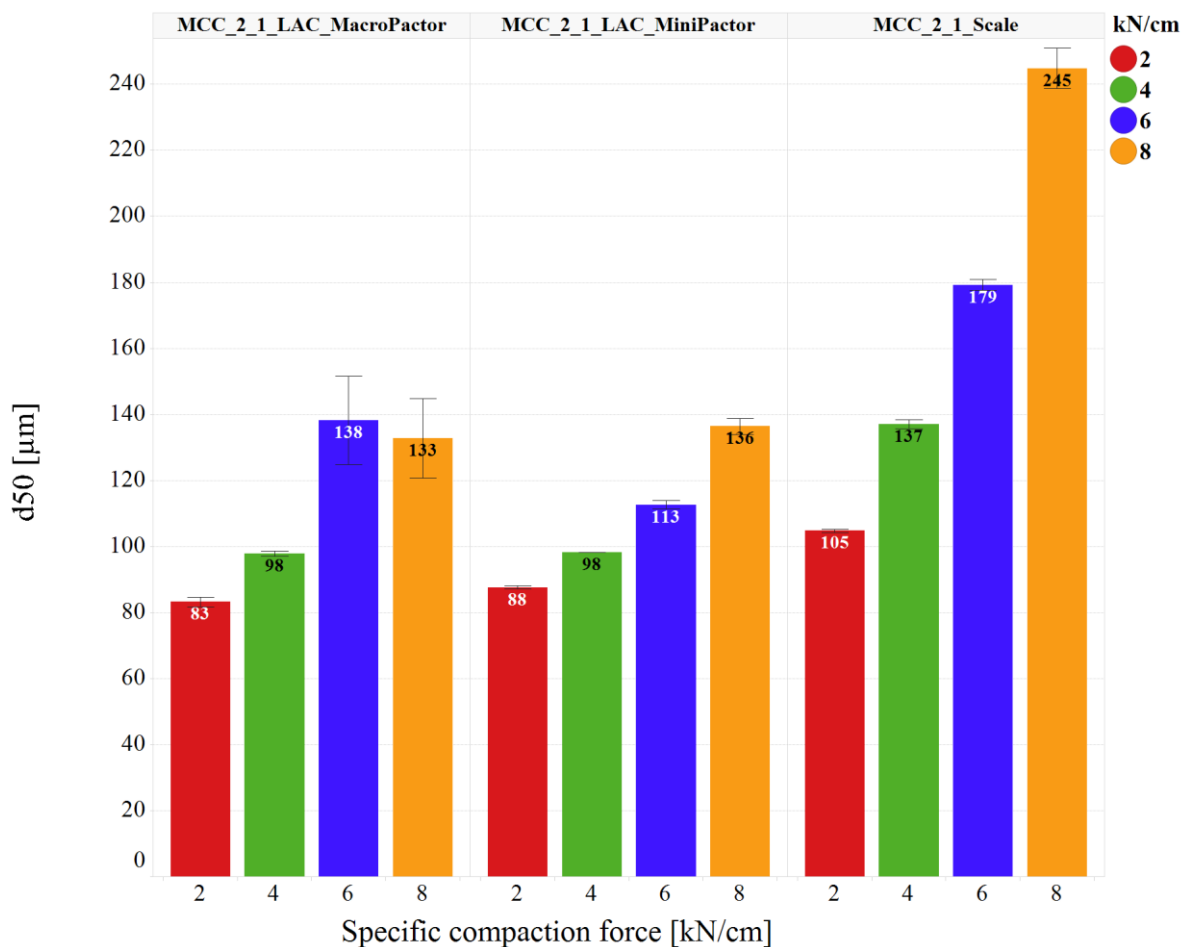
Figure 34 d_{50} granules - MacroPactor/MiniPactor/Scale Model, mean (n = 3), error bars (standard deviation of mean)

As mentioned above, higher specific compaction forces resulted in coarser granules at the same roller compactor. Analysing the PSD confirmed that coarser granules were obtained for the Scale Model (see Figure 35). Comparing all scales, a lower amount of fine particles was found for the Scale Model (see Figure 35). The impact of the milling process of the granulator on PSD between both scales could be demonstrated to be negligible (see 4.2.3.3). A potential

impact factor and explanation between scales can be the solid fraction distribution of the ribbon along the roll width, which will be discussed in the next section (see 4.4).
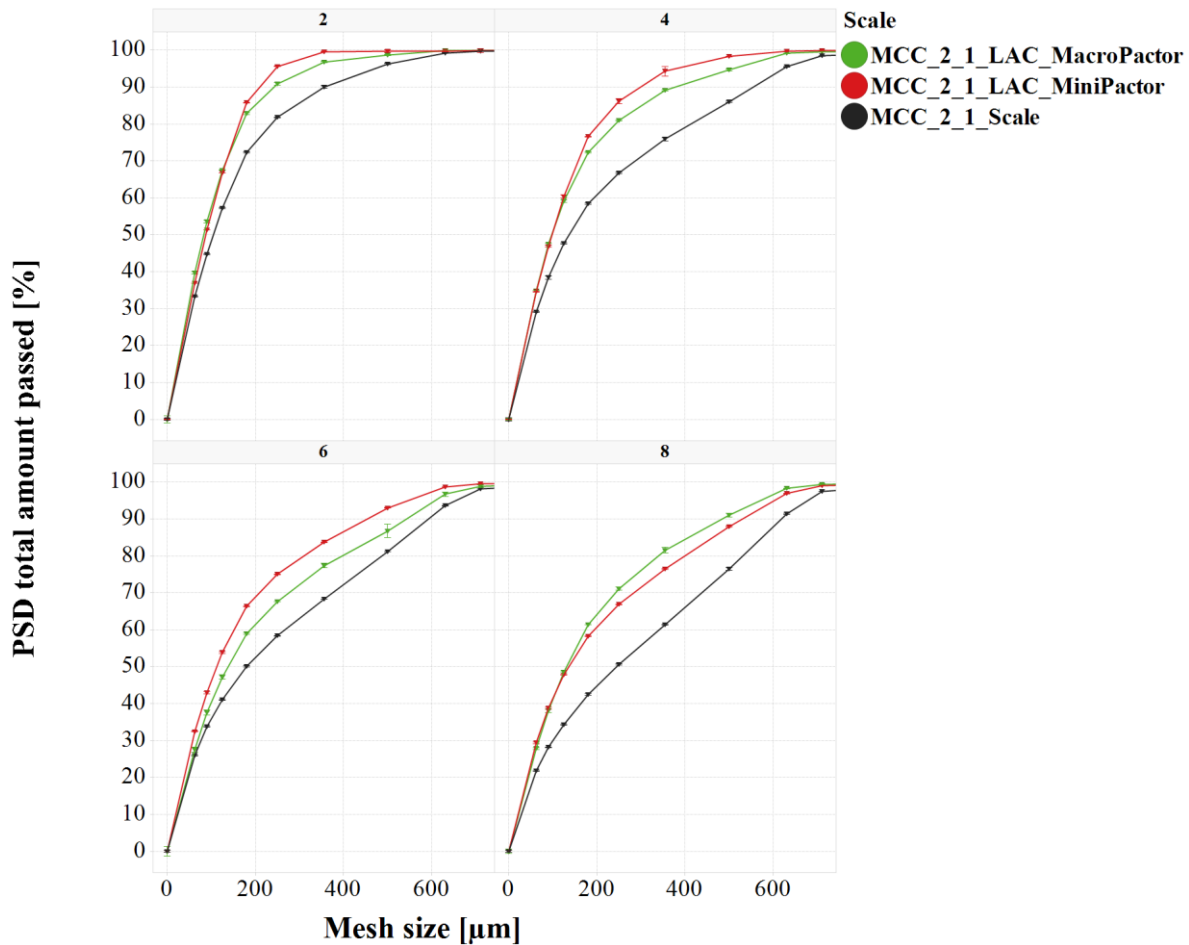
Figure 35   PSD granules– MacroPactor/MiniPactor/Scale Model at specific compaction force of 2, 4, 6 and 8 kN/cm, triangle (mean, n = 3), error bars (standard deviation of mean)

Porosity & Appearance – Measurements of the intragranular porosity by mercury porosimetry enable a deeper insight of differences between these granules. Other authors have shown that the particle size influences the measurement [110,111]. Therefore, sieve fractions of the granules were used (90, 180, 250 µm) in order to avoid measuring the interparticular voids (bimodal pore size distribution, see Figure 66), and to ensure a good comparability between granules of MacroPactor, MiniPactor and Scale Model. Unprocessed blend of MCC 2:1 LAC had a d_{50} of 103 µm. Sieve fractions of 180 µm and 250 µm will define agglomerated particles and 90 µm the fine particles. All granules were sieved and separated. Cumulative sum of the intruded mercury volume over a pore range of 0.4 – 1.8 µm (see 6.2.1.4) was used as porosity index. A linear decrease of the porosity was observed at increased solid fraction of the ribbons (see Figure 36, left plot). Solid fraction of ribbon

directly correlated with the porosity of granules in a linear coherence. Linear regression
showed a good correlation coefficient (R^2) of 0.8950. Granules generated by the MacroPactor
(SF = 0.8102, 8 kN/cm) were excluded for linear regression, due to the aforementioned side
seal leakage. For this reason unprocessed material slipped above the compaction zone (see
Figure 16), which resulted in a higher porosity (grey circles, left plot).
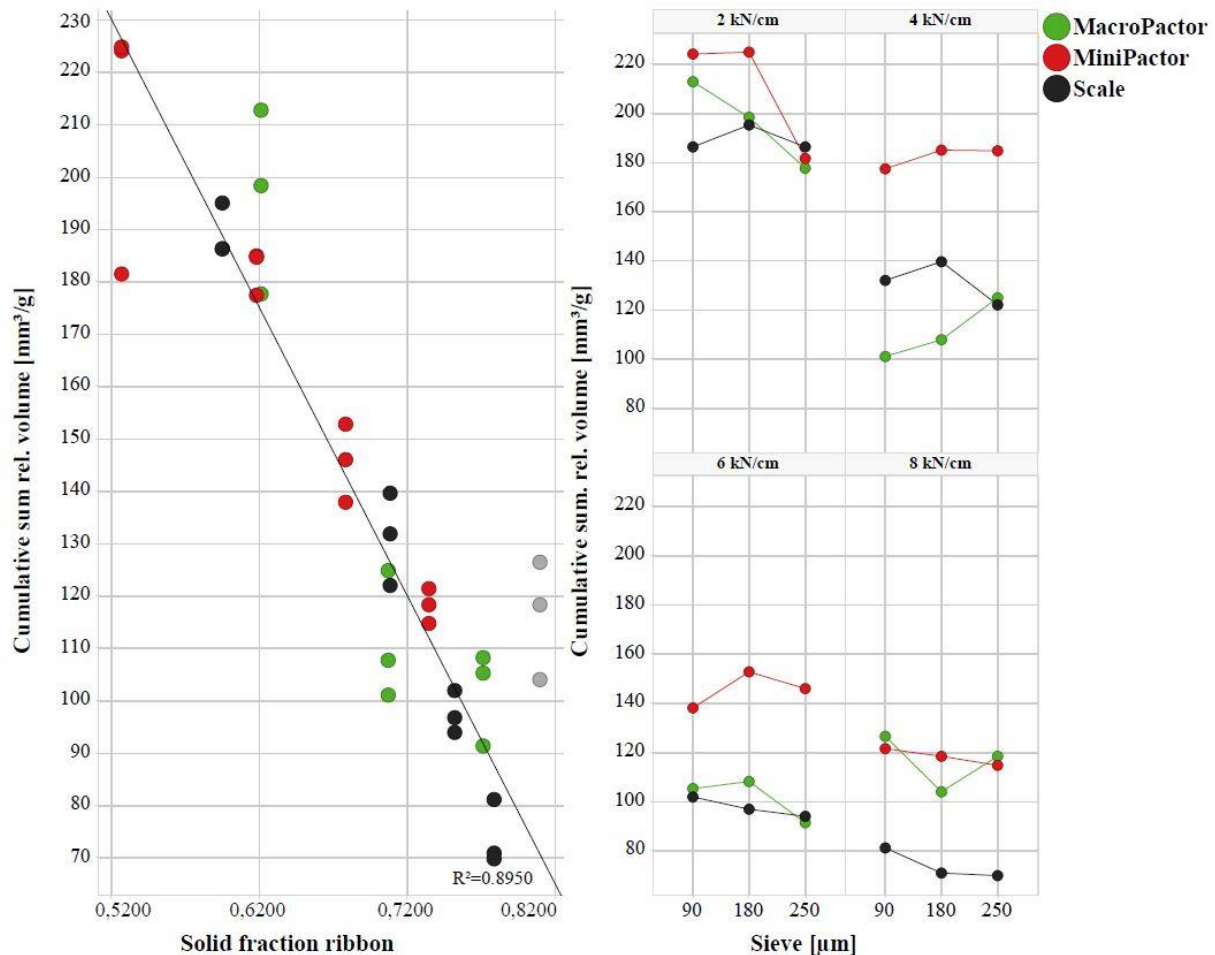
Figure 36   Granule porosity – MCC 2:1 LAC - Left plot: Cumulative sum
                     relative intruded mercury volume [mm³/g] (pore radius range 0.4 -
                     1.8 µm) vs. solid fraction ribbon – Right plot: Cumulative sum
                     relative intruded mercury volume [mm³/g] (pore radius range 0.4 -
                     1.8 µm) vs. sieve fraction of 90, 180, 250 µm, grey circles = excluded
                     for linear regression (MaroPactor at 8 kN/cm see 4.2.3.1)

Herting et al. (2008) have shown a decrease of the surface area of a dry granulated MCC sieve
fraction with increased specific compaction force, which was correlated to a lower porosity.
Nordstrom et al. (2015) have demonstrated a decrease of the porosity of re-tableted milled
tablets of MCC for a granule sieve fraction of 500 – 710 µm with increasing compression
pressure, but both did not evaluate the relation between the porosity of granules and the solid

fraction of ribbons. This evaluation of a decreasing porosity for granules with increasing solid fraction seems to be more appropriate for dry granulated granules, because a negative linear correlation was determined (see Figure 36, left plot). A high solid fraction correlated to a low porosity of granules. It was assumed that a coarser sieve fraction of 250 µm would be strained with a higher load of pressure at the same specific compaction force compared to a fine sieve fraction of 90 µm. The reason is that more particles were agglomerated under pressure and this results in a denser granule with lower porosity. Comparing the porosity of the sieve fraction 90, 180, 250 µm within the MacroPactor, MiniPactor or Scale Model at 2, 4, 6 or 8 kN/cm, no tendency of the porosity could be observed (see Figure 36, right plot). This can be attributed to the influence of the complex milling process by the granulator, whereby the particles are mainly sheared and sliced of the ribbons against the sieve mesh [112,113].
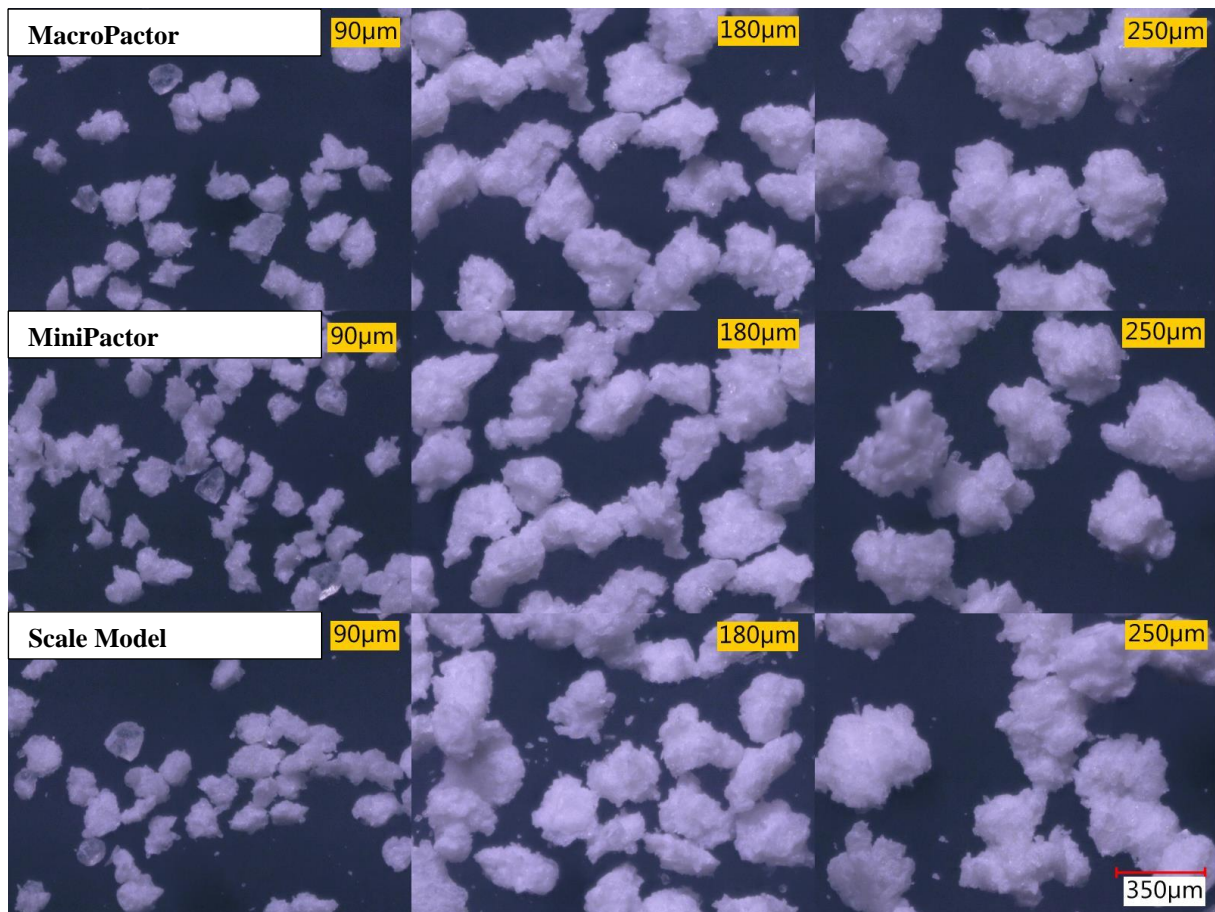
Figure 37   Appearance of particles at 4 kN/cm - Sieve fractions 90, 180, 250 µm of MacroPactor/MiniPactor/Scale Model

Particle morphology of the three sieve fractions within one specific compaction force and scale was visually inspected by microscopy (see Figure 37). The larger sieve fractions of 180 µm and 250 µm appeared rougher as they contained particles of a higher degree of agglomeration compared to the smaller sieve fraction of 90 µm. Considering the particle morphology, no differences between the MacroPactor, MiniPactor and Scale Model granules` sieve fractions were observed (see Figure 37).

A comparison of the porosity of the sieve fractions between different scales is depicted in Figure 38. For better illustration, the porosity of granules were normalized to the reference value (MacroPactor) for each sieve fraction; Porosities of the MiniPactor and Scale Model were subtracted from this reference value (see Figure 38). A positive value indicates a lower porosity and negative value a higher porosity compared to the MacroPactor.
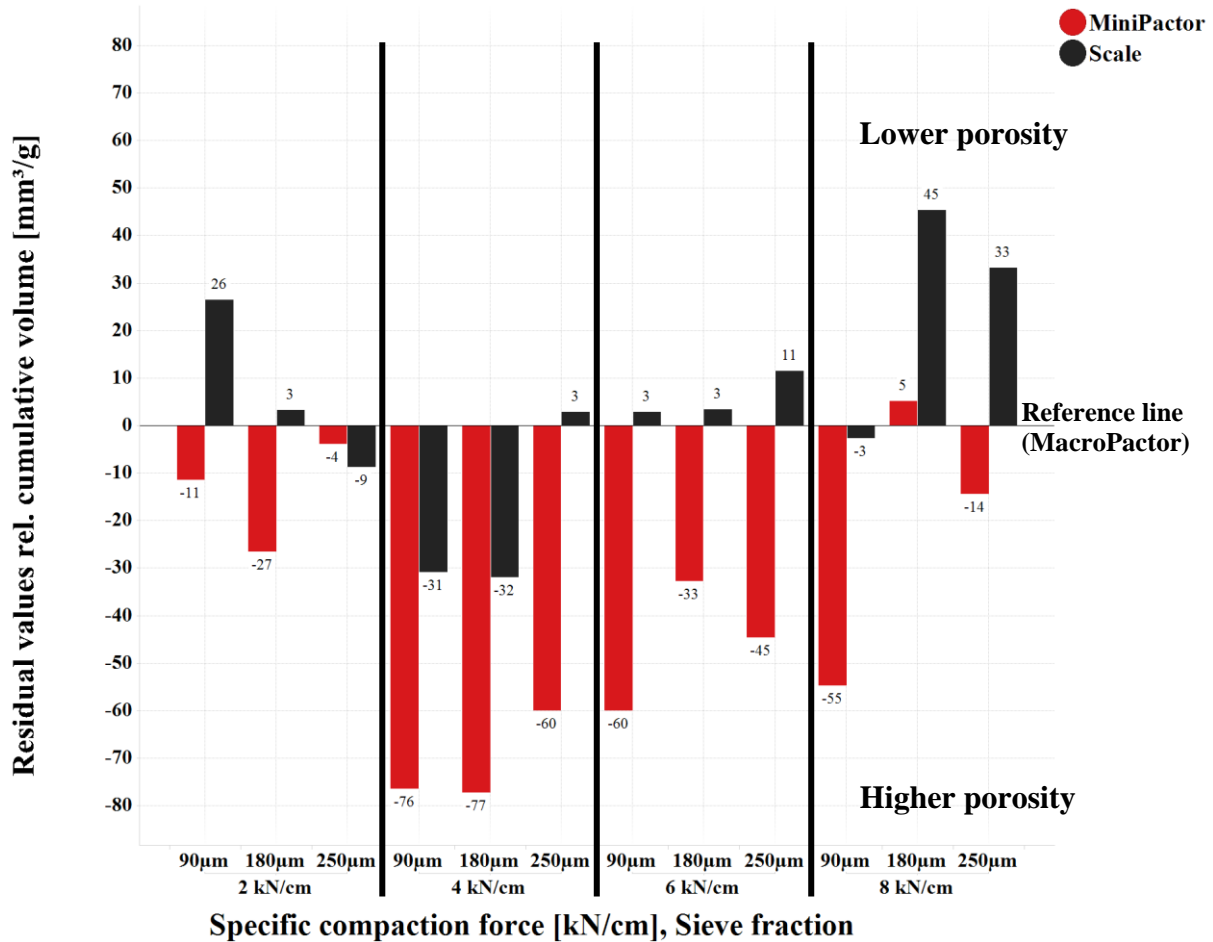
Figure 38   Granule porosity – Residual values cumulative sum relative intruded mercury volume [mm³/g] (pore radius range 0.4 -1.8 µm) to target granule porosity (MacroPactor) - Sieve fraction of 90, 180, 250 µm

Compared to the MacroPactor, the MiniPactor showed a lower solid fraction of the ribbon and the Scale Model achieved a similar solid fraction. The solid fraction of the ribbon can be correlated with the porosity of the granules. Granules of the MiniPactor led to higher porosities, in particular at the specific compaction force of 4 kN/cm and 6 kN/cm, whereby the porosities of the Scale Model were always closer to the reference value i.e. MacroPactor (see Figure 38). The specific compaction force at 2 kN/cm had a minor influence on the differences on the porosities of the granules, because the impact of the solid fraction of the ribbon was less. The first weak bonding between the particles occurred at a low solid fraction.

Considering all specific compaction forces, a small tendency of the granules of the Scale Model to lower porosities compared to the MacroPactor were observed. A different result was obtained for the 8 kN/cm, for which the Scale Model showed a difference to the reference value, while the MiniPactor had a similar porosity, which was caused by the slipped uncompacted material of the MacroPactor at 8 kN/cm (see 4.2.3.1). It can be concluded that a same solid fraction of the ribbon (MacroPactor & Scale Model) led to similar porosity of the granules. Therefore, the next step was to investigate how the different particle size distributions and a similar porosity will affect the tabletability and compressibility of the granules.

4.3.3 Tabletability and compressibility influenced by material attributes of granules and ribbons

Same process conditions were applied for tableting of the granules of the Scale Model compared to the granules of the MacroPactor and MiniPactor. No practical relevant difference between the tensile strength of MacroPactor and Scale Model was observed (< 10 %). T-Test between MacroPactor and Scale Model showed a significant difference (p ≤ 0.05) for most tablets (see APPENDIX 8.2.3). An example calculation for the power of the T-Test indicated that the T-Test would detect a ± 5 % difference of the tensile strength as significant with a power up to 0.97 (see APPENDIX 8.2.3).
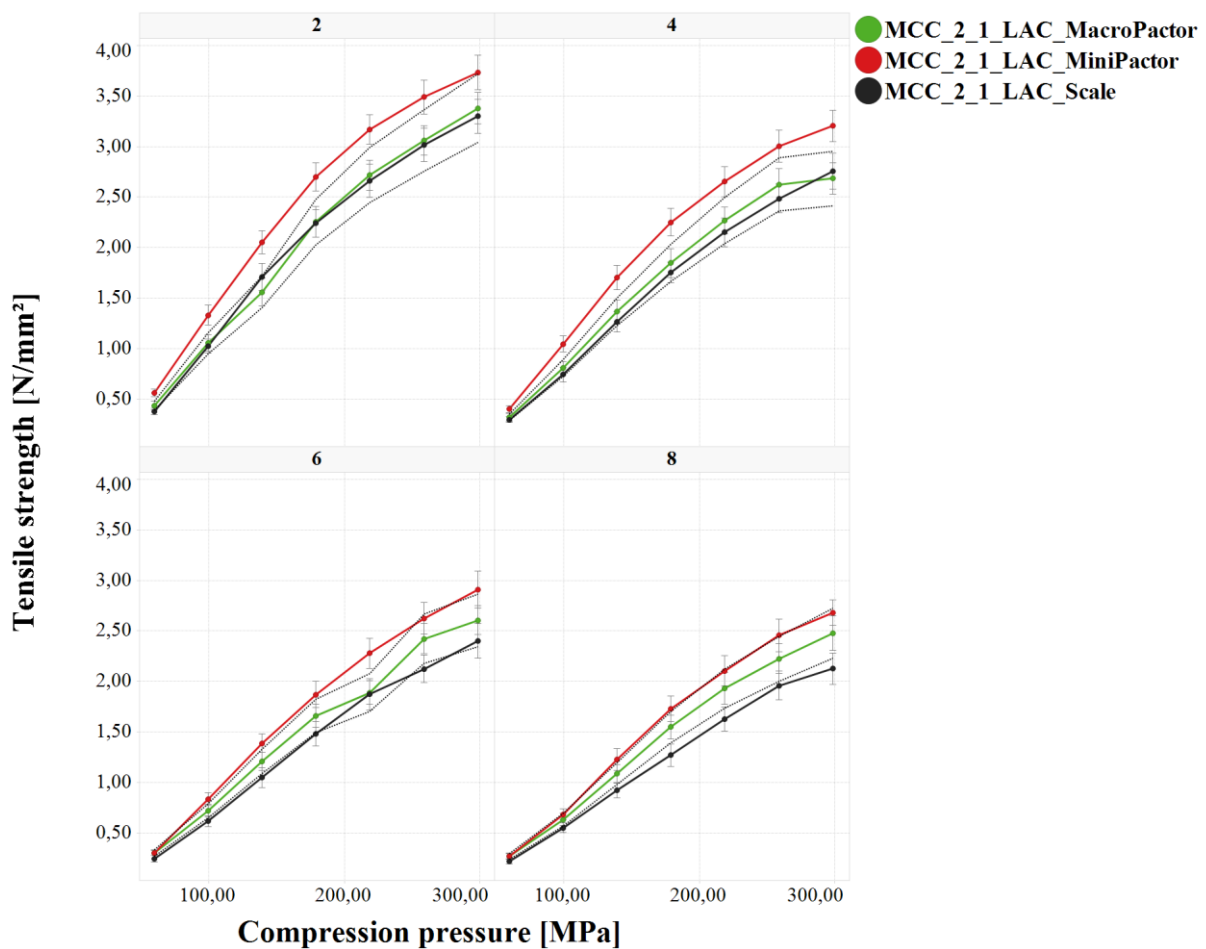
Figure 39   Tabletability –MacroPactor/MiniPactor/Scale Model at specific compaction force of 2, 4, 6 and 8 kN/cm, mean (n = 50), error bars (standard deviation of mean), scattered lines indicate ±10 % differences to the mean tensile strength of the MacroPactor

A pre-evaluation showed a relative standard deviation of 10 % for the tensile strength within one compression pressure for the same scale (see 4.2.4). Hence, a ± 10 % deviation of the

tensile strength is an acceptable range between two scales and the difference between MacroPactor and Scale Model is negligible. Considering the tabletability of granules of the Scale Model, these showed same tensile strength for the 2 kN/cm, 4 kN/cm and 6 kN/cm (see Figure 39). The resulting tensile strength was in a very good accordance and had a tensile strength lower than the desired acceptable deviation of $\pm$ 10 % to tablets of the MacroPactor (see 4.2.4). The achieved tensile strength of the applied 8 kN/cm was lower (see explanation 4.2.3 & 4.2.4).

Obviously, the coarser granules of the Scale Model (particle size enlargement effect) had a minor impact on the tensile strength and did not lead to a lower tensile strength of the tablets. The agglomerated particles i.e. granules collapsed into smaller particles during tableting.

The particle size enlargement effect caused by an initial coarser PSD of the Scale Model becomes negligible. The impact of coarser granules will only gain more influence if the granule strength is increased, which will prevent a fracturing of agglomerated particles [25,50]. Nordstrom et al. (2015) [25] have shown that the porosity of the dry granulated granules of MCC essentially influenced the tensile strength of tablets. Dry granulated granules with a high porosity will collapse into smaller particles during compression to tablets followed by a closer "intergranular void structure of a tablet" (e.g. solid fraction) [25] and an increased tensile strength. Additionally, the fracturing of granules into smaller particles can be enhanced if the mixture contains a brittle component [10,48] (see Figure 25). Effects like the porosity of granules and the more pronounced fracturing caused by the amount of brittle LAC in the formulation, diminished the effect of the coarser granules for the Scale Model. A confirmation of a low impact of the PSD on the tensile strength for this formulation (MCC 2:1 LAC) was observed for the MiniPactor granules. A similar PSD was found compared to the MacroPactor granules, which resulted in a higher tensile strength of the tablets for the MiniPactor (see Figure 39), reflecting the achieved lower solid fraction of the ribbon (see Figure 33) and the higher porosity of the granules i.e. fracturing tendency (see Figure 36).

The behaviour of the fracturing and densification process of granules can be evaluated by considering a compressibility plot. A different fracturing behaviour under pressure will result in a different microstructure (e.g. solid fraction) of the tablet at the same compression pressure level. Thereby, granules with a high fracturing or consolidation tendency will be more compressible. This will lead to a higher solid fraction at the same compression pressure compared to granules, which will be more "resistant to deformation of tableting" (work hardening) [50].
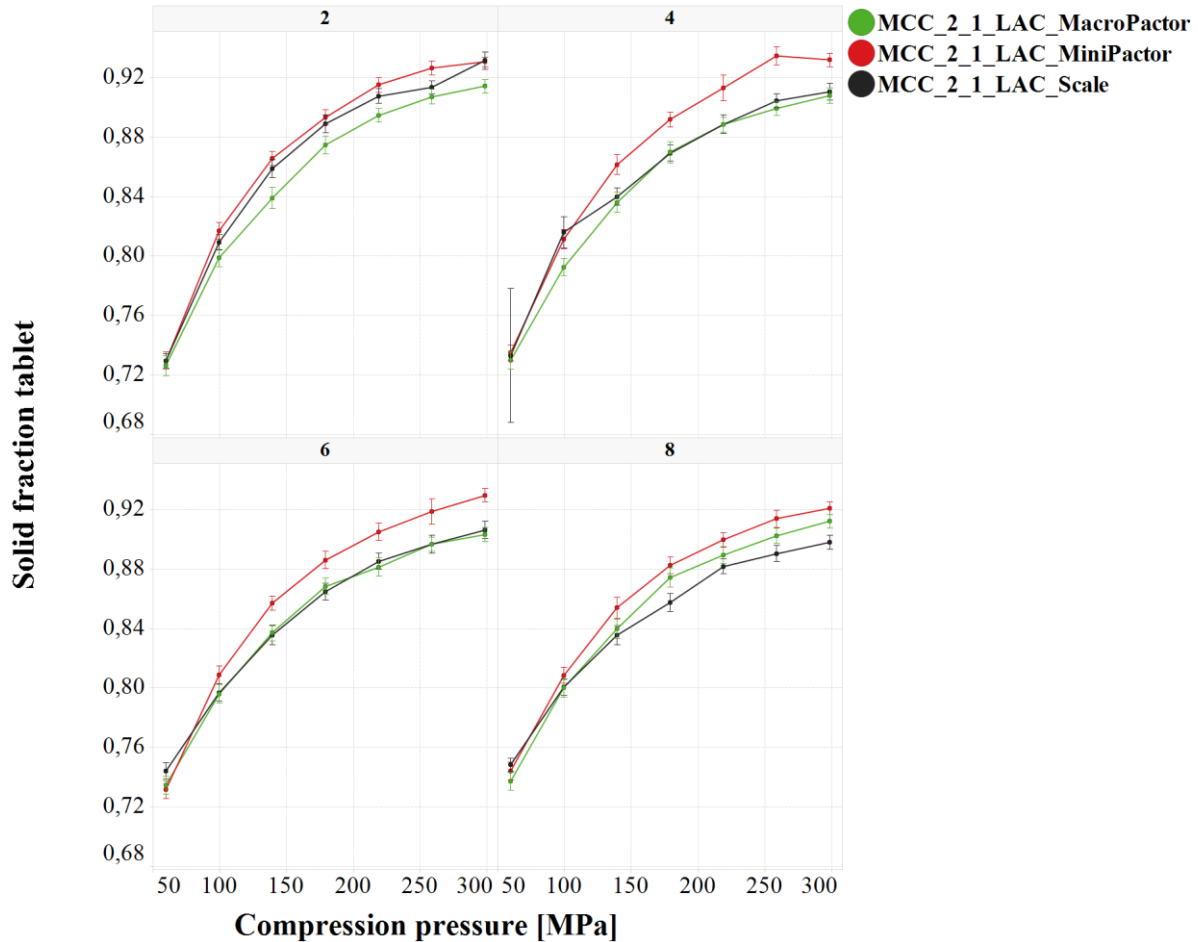
Figure 40   Compressibility –MacroPactor/MiniPactor/Scale Model at 2, 4, 6 and 8 kN/cm, mean (n = 50), error bars (standard deviation of mean)

The compressibility plot of the tablets indicated that the MiniPactor achieved a higher solid fraction for all investigated compression pressures (see Figure 40). This was caused by the higher porosity and fracturing tendency of the granules of the MiniPactor. The granules of the Scale Model demonstrated a similar compressibility compared to the MacroPactor. The compressibility plot confirmed that the initial coarser granules of the Scale Model had no influence on the compressibility and proved that the porosity of the granules levelled the granule size enlargement effect (lower bonding surface). The MacroPactor granules of

8 kN/cm confirmed this assumption as they gained a higher compressibility, which was caused due to a higher amount of unprocessed material with a higher porosity (see Figure 16).
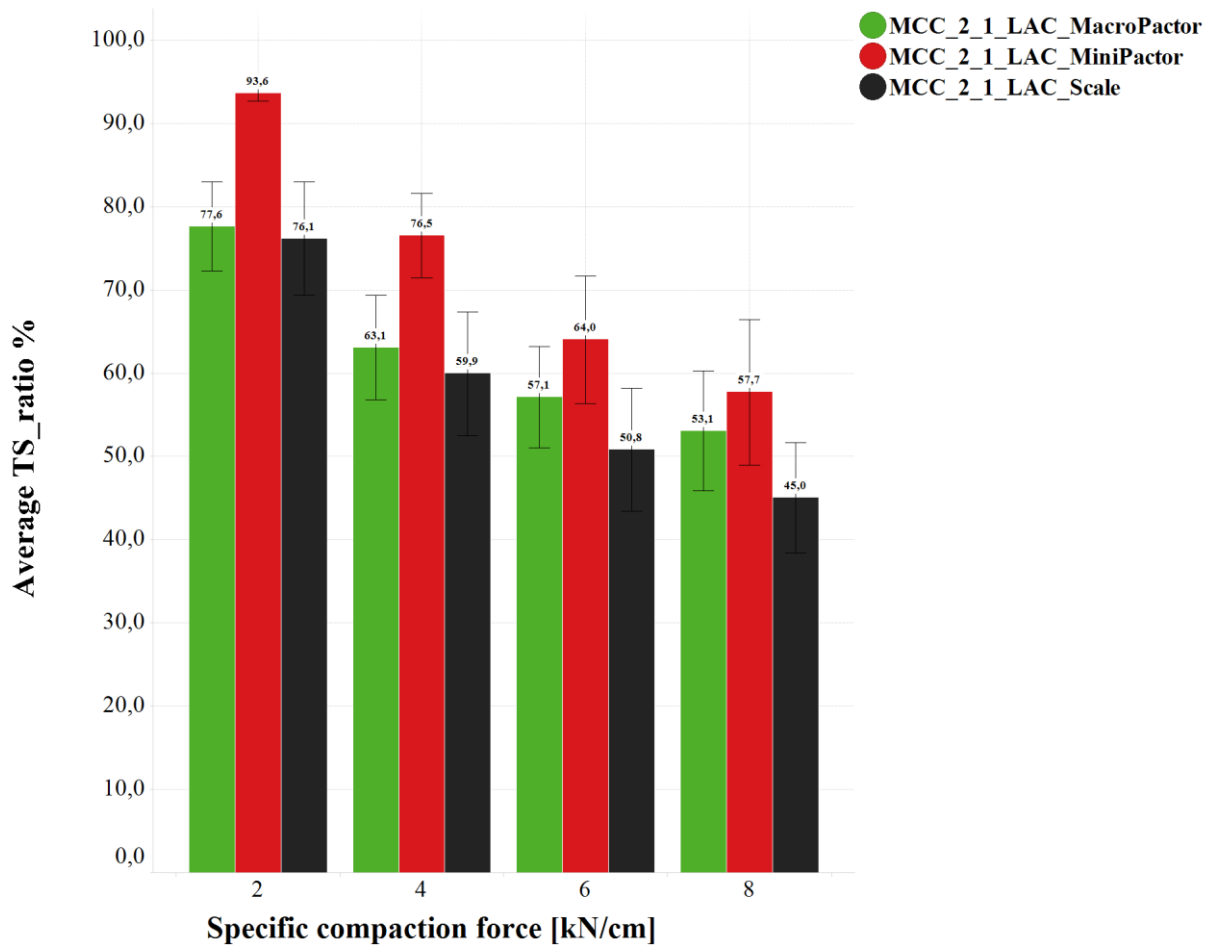
Figure 41   Reworkability index tablets –MiniPactor/MacroPactor/Scale Model, TS_{ratio} = tensile strength of tablets of compacted blend in proportion to unprocessed blend Eq. (33), mean (n = 350), error bars (standard deviation of mean)

Tensile strength of the tablets of the Scale Model was in good accordance with the tensile strength of the MacroPactor (see Figure 41). The proposed Scale Model resulted in a successful scale up regarding tabletability and compressibility. However, it needs to be further investigated why different ribbon solid fraction was obtained at identical process parameter at two scales (see 4.4).

4.3.4   Summary

It was demonstrated that same process settings at two different scales for a roller compaction process did not result in an equal tensile strength of the tablets. Therefore, a new approach was proposed (Scale Model) to first predict and then adapt the specific compaction force of the smaller scale (MiniPactor) to achieve the same target solid fraction of the ribbons of the larger scale (MacroPactor).

Ribbons were produced with the desired target solid fraction in a range of $\pm 5\%$ in comparison to ribbons produced with the MacroPactor.
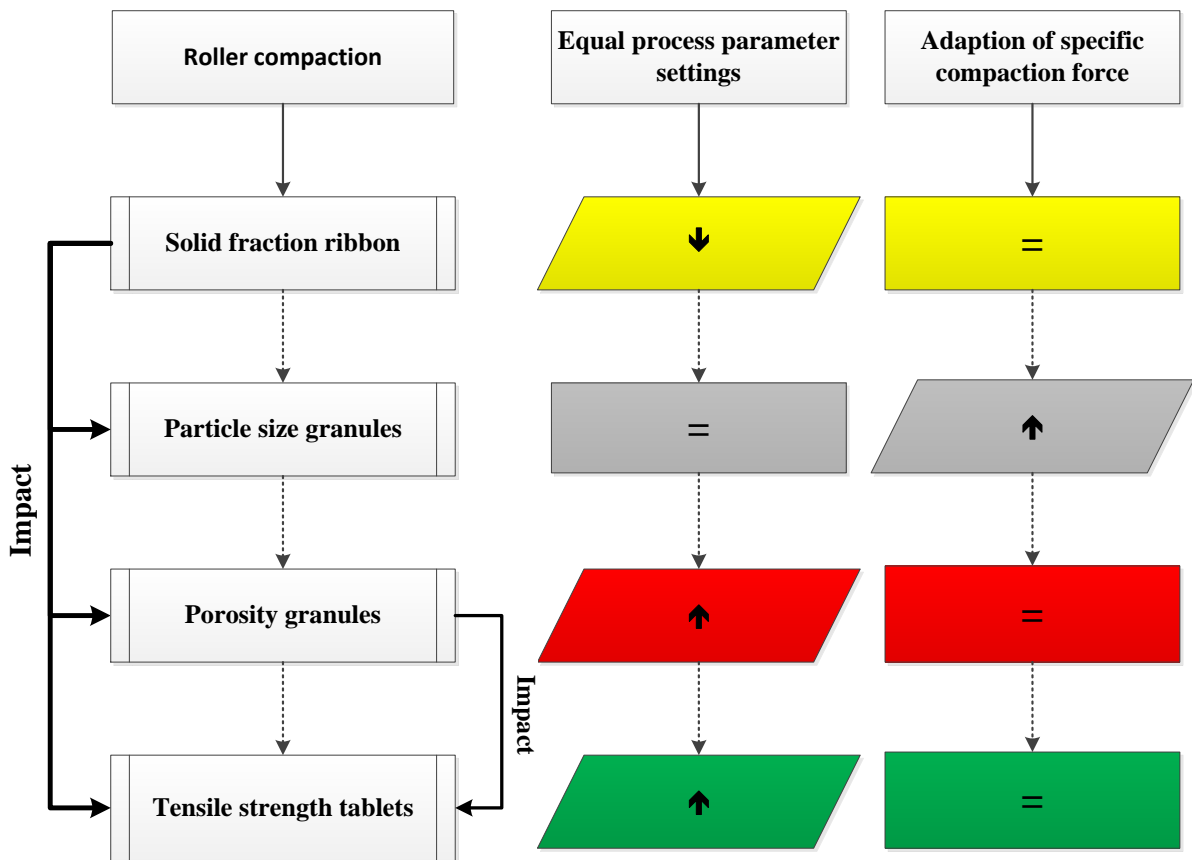
Figure 42   Summary – Impact of scale for formulation MCC 2:1 LAC (MCC = Microcrystalline cellulose, LAC = α –Lactosemonohydrate), differences of intermediate products: solid fraction of ribbons, particle size of granules, porosity of granules and tensile strength of tablets of the small scale (MiniPactor) at equal process parameters and adapted specific compaction force (Scale Model) compared to target intermediate quality attributes of the large scale (MacroPactor), equal sign = equal, arrow up/down = higher/lower

The resulting tensile strength of the tablets of the Scale Model was well in accordance with the target tensile strength of the tablets of the MacroPactor. The porosity of the granules demonstrated a negative linear correlation with increased solid fraction of the ribbon. Although the same solid fraction between both scales was achieved (MacroPactor, Scale Model), the resulting PSD distribution of the granules was different. The roll width is one impact factor, resulting in a different solid fraction distribution along the ribbon width, which will be investigated in the next section (see 4.4). However, the effect of granule size enlargement (lower bonding surface, Scale Model) was negligible as a similar granule porosity was achieved compared to the granules of the MacroPactor, which caused an equal "resistant to deformation of tableting" [50] (work hardening), a comparable fracturing behaviour (see Figure 40) and indicated a similar granule strength [25]. The impact of the fracturing tendency of the granules as an important factor for the tensile strength was proved in the previous chapter 4.2 for formulation MCC 1:1 LAC. It is common knowledge that a coarser granule size distribution (lower bonding surface, Scale Model) leads to a different compressibility and tensile strength, because of a lower surface area of the particles compared to finer particles. In contrast, this was not shown for this formulation (MCC 2:1 LAC) and process parameters as it was demonstrated that the resulted coarser particle size distribution of the adapted process parameters led to a similar tensile strength of the tablets.

A simplified summary of the effects and results for formulation MCC 2:1 LAC MiniPactor compared to the MacroPactor is provided in Figure 42. The Scale Model approach demonstrated a practicable solution to achieve a successful scale up during process development for a predominantly plastic deforming formulation. Nevertheless, a higher specific compaction force at the small scale (MiniPactor) was required to achieve the same solid fraction compared to the larger scale (MacroPactor). This aspect will be in investigated in the next chapter with a newly developed analysis method to better characterise the ribbons.

4.4 INVESTIGATION OF SOLID FRACTION DISTRIBUTION ALONG THE ROLL WIDTH BETWEEN DIFFERENT SCALES VIA NIR AT-LINE

In the previous chapters it was demonstrated that ribbons produced with either the MiniPactor or the MacroPactor applying identical process parameters showed different solid fraction. These obtained difference will be investigated with a near infrared reflectance method to characterise the solid fraction of ribbons along the roll width. Different authors have reported about a solid fraction distribution along the roll width within one scale [33,40,114–118]. This solid fraction distribution will be investigated with an NIR method between scales (MacroPactor, MiniPactor). NIR measurement allows measuring smaller parts of the ribbon in comparison to the GeoPycnometer method; this method was limited by the sample size (three pieces of 8 mm* 8 mm, see 6.2.2.3). Furthermore, applying the at-line NIR analysis results in a relevant time saving. Afterwards the previously proposed approach for a scale up will be evaluated by NIR in respect to the solid fraction. A formulation containing 21 % Metformin (w/w) with MCC 2:1 LAC will be used as model active pharmaceutical ingredient (API).

4.4.1 Method evaluation to determine solid fraction along the roll width by GeoPycnometer and NIR

As reference method for the NIR spectra (see Figure 43) the solid fraction was analysed using a GeoPycnometer. It was a prerequisite to measure small pieces of the ribbon with the reference method, because the NIR probe acquires a small area on the ribbon of about 0.5 cm².
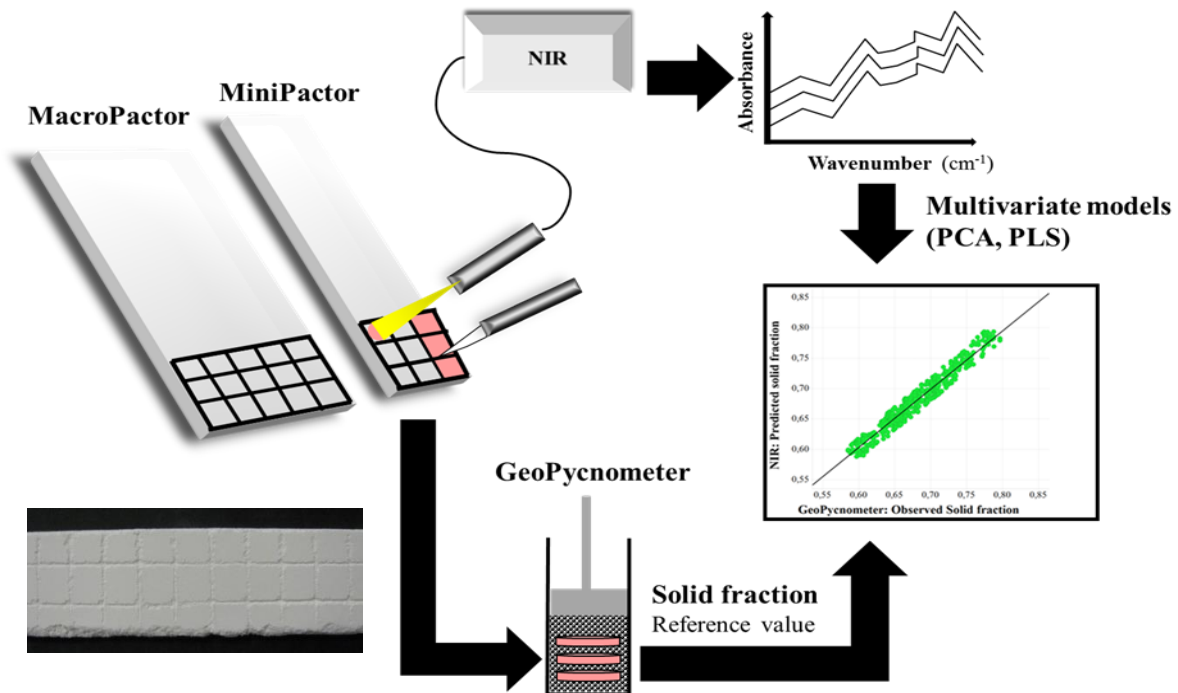
Figure 43   Schematic drawing - Process flow development NIR method

An appropriate and reproducible analytical method applying the GeoPycnometer will only be achieved if the sample size (ribbon) fills 20 % of the whole vessel volume (DryFlo® + ribbon volume). A pre-evaluation showed that a lower limit of the reference method was reached by analysing at least three cut pieces of 8 mm* 8 mm from the respective ribbon. Reference method for NIR was performed with a vessel of 12.7 mm diameter and a plunger force of 28 N. Sample volume in the vessel was always about 20 %. Ribbons were taken after gap settings reached steady state conditions (see 3.1). A small grid was scratched on the ribbon to identify the sample squares. Spectra of the squares were acquired by NIR. Afterwards, the ribbon was cut and separated into centre and edges (front, back) to also analyse the same ribbon with the GeoPycnometer. Spectra of three squares were correlated to one reference value for calibration purpose. A schematic flow process is depicted in Figure 43.

4.4.1.1   GeoPycnometer as reference method – Solid fraction along the roll width

A sample ribbon of 6 kN/cm (MiniPactor) was measured with the GeoPycnometer to evaluate whether differences occur along the roll width. A distance-weighted least square fitting was performed between measured samples of a ribbon (GeoPyc) in order to illustrate the difference between measured points.
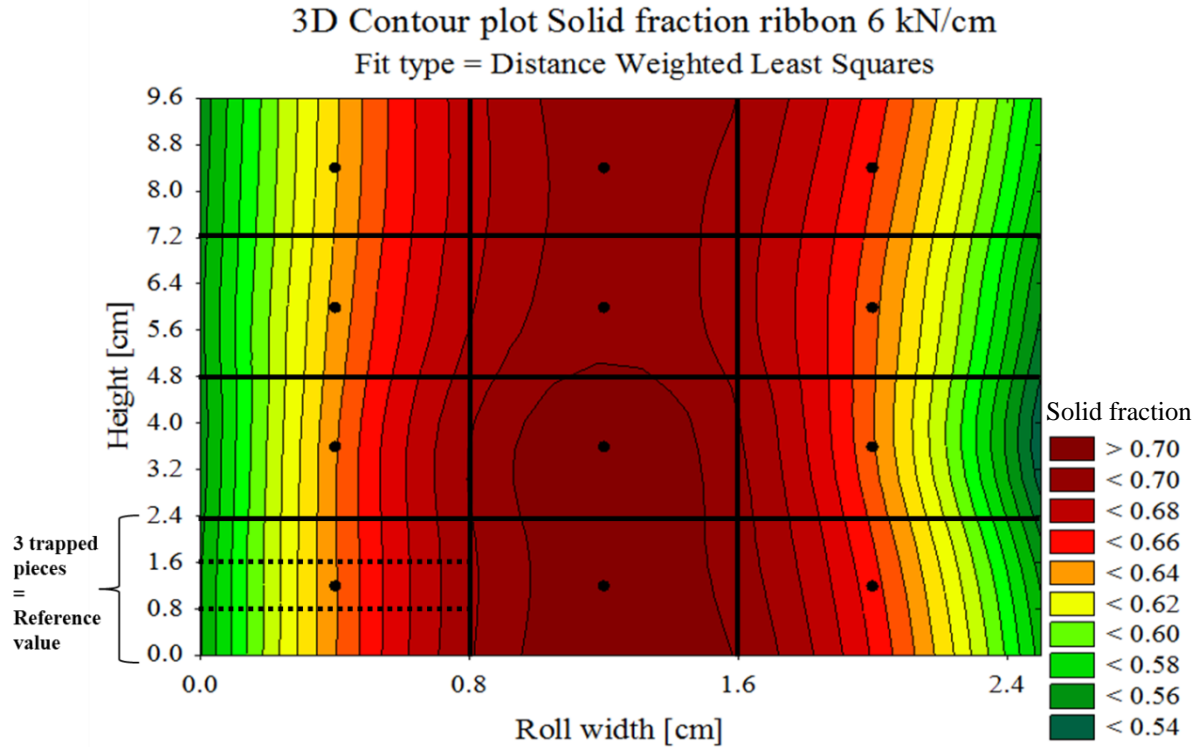
Figure 44   Evaluation solid fraction distribution of ribbon along roll width
                             measured by GeoPycnometer– Exemplary ribbon produced with
                             6 kN/cm, black circles = reference value by GeoPycnometer, colour
                             indicates different solid fractions

Figure 44 indicates a decrease of the solid fraction from the centre to the edges of the ribbon. This finding is in agreement with literature, as various authors have demonstrated a higher solid fraction at the centre of the ribbon for a cheek plate side seal system [21,30,31,36,40,41,115]. A non-uniform distribution of the solid fraction along the roll width is caused by the side seal system [33,115]. Using cheek plates will lead to friction force between powder and plates, whereby the powder entry into the gap is reduced at the edges. This side seal friction force counteracts the friction force between rolls and powder [116]. Therefore, a heterogeneous solid fraction can be observed. Reference method (GeoPycnometer) detected differences along the roll width and was appropriate for the purpose of an NIR method development.

4.4.1.2   NIR spectra of a ribbon along the roll width

Multiple exemplary NIR spectra of a ribbon compacted at 6 kN/cm are depicted in Figure 45. A difference between locations of the ribbon was detected by the NIR, which were indicated by a baseline shift of the spectra. This is consistent with the literature. Various authors observed a higher absorption of NIR spectra with an increased pressure for tablets (i.e. increased solid fraction) [119–121] and ribbons [32,38,122].
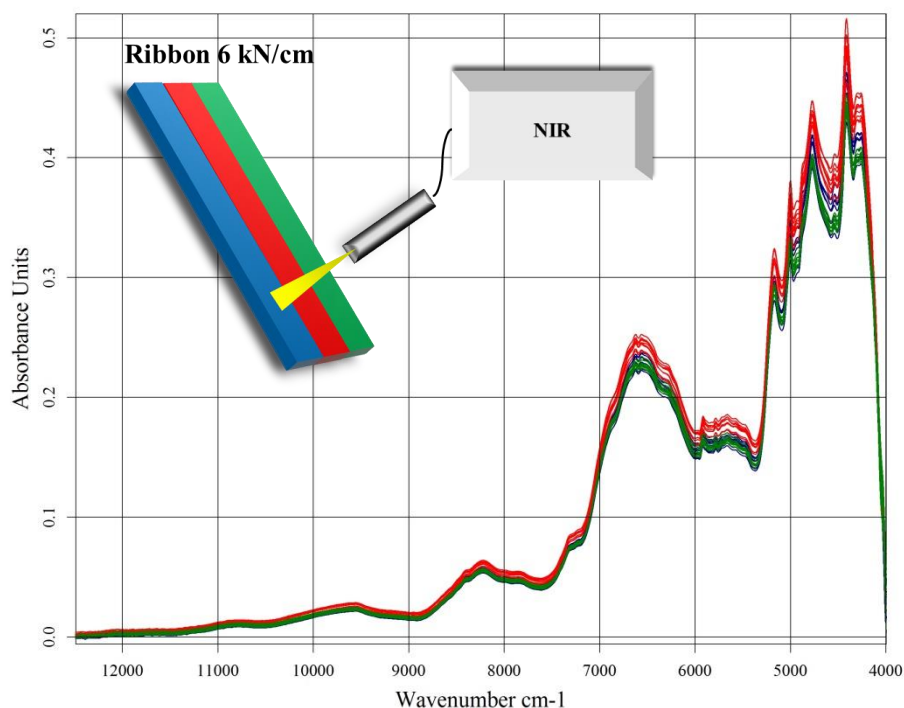
Figure 45   NIR spectra of a ribbon at 6 kN/cm – Front = blue, middle = red,
                      back = green

A higher absorption was positively correlated to a high solid fraction caused by less reflectance of the radiation in diffuse reflectance mode (see 6.2.2.4). Applying the above-mentioned NIR methodology differences along the roll width could be identified. Hence, this technique was considered as suitable technique to identify differences between scales.

4.4.1.2.1   Factors influencing the spectra of the ribbon

The overall target when developing a new analytical method is to ensure high accuracy, precision and robustness. It is essential to investigate different factors impacting these characteristics and how a proper measurement setup or data pre-process techniques reduce this interference [123]. Measurement setups were evaluated to ensure these characteristics. Different factors were considered and evaluated to find a reliable setup:

1. Sample condition (time after processing, damaged surface)
2. Measuring setup (distance probe to sample, angle probe to sample, light in the room)
3. Software setup (resolution of scans)

All measurements were done applying the NIR diffuse reflectance mode at a wavenumber range of 12.000 – 4.000 cm^{-1}.

4.4.1.2.1.1   Sample condition

All samples were stored for 48h at 0 – 65 % relative humidity and 19 - 25°C in respect to their elastic recovery after roller compaction. The smooth side of the ribbon was analysed as it was easier to scratch the grid on the ribbon. Surface of the ribbon can be irregular or damaged during processing, e.g. caused by powder adhesion on surface of the rolls or abrupt segmentations of the ribbon.
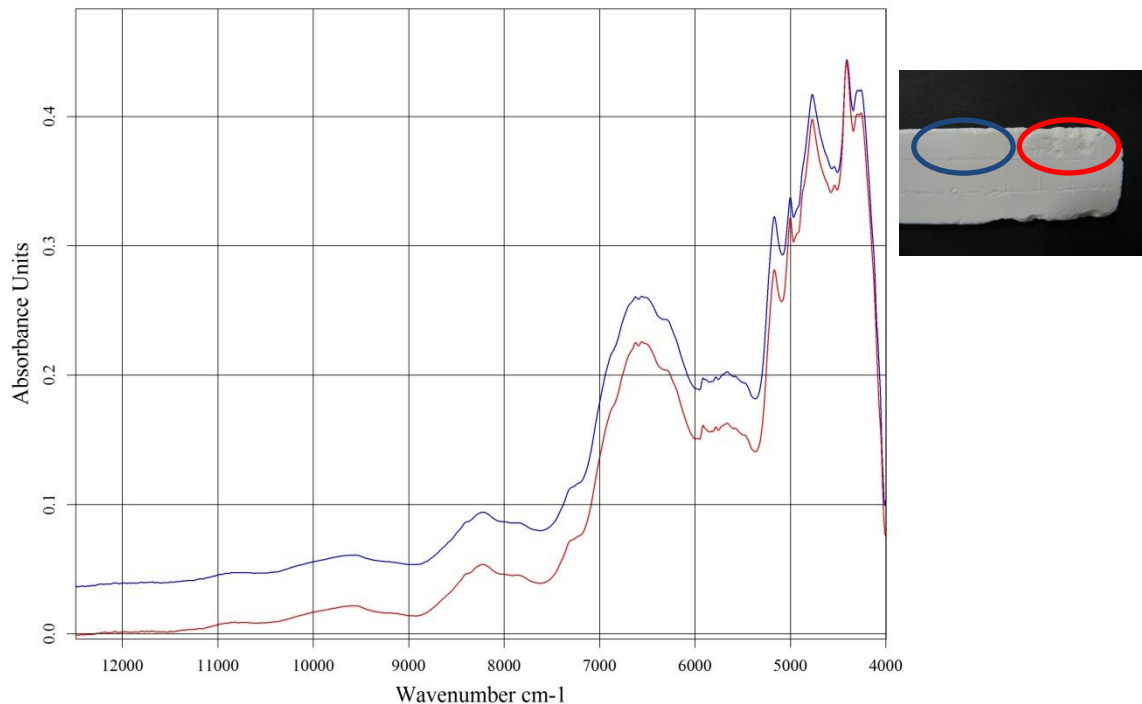
Figure 46   Absorption ribbon surface – Blue = damaged, red = normal

A ribbon sample was damaged for illustration by a knife to simulate a different surface. The square was measured before and after this manipulation. A higher absorption of the damaged surface could be observed because of the irregular shape of the surface, which enhanced the scattering [124], so that less radiation reached the detector and resulted in an offset (see Figure 46). Derogation of this offset can be obtained with data pre-processing techniques (see 6.2.2.4.2). First derivation levelled the observed baseline shift and will contribute to a reliable NIR-method (see Figure 47).
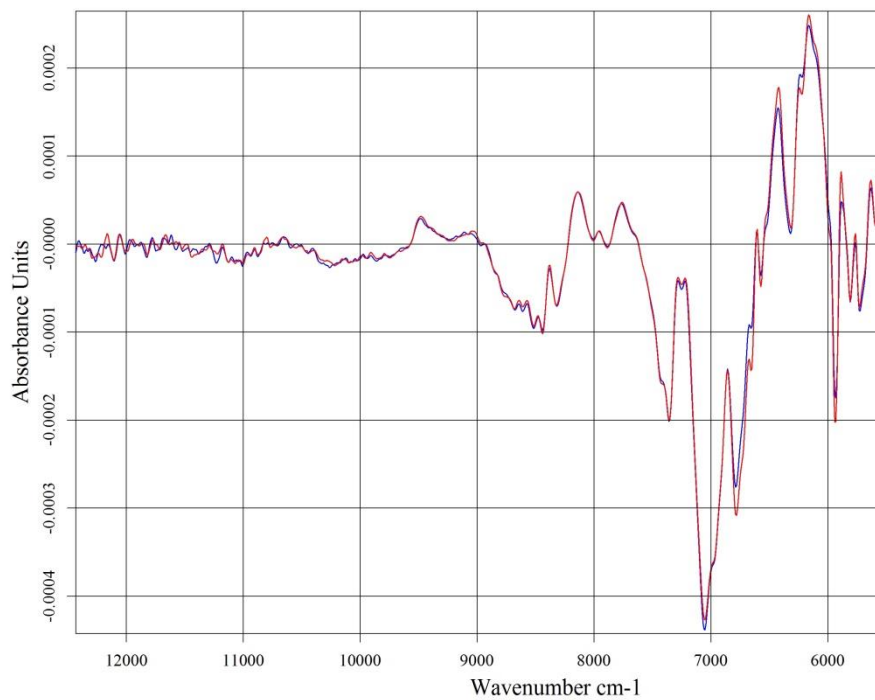
Figure 47   Surface: First derivation – Blue = damaged, red = normal

4.4.1.2.1.2   Measuring setup

Distance - Different distances of 0, 3, 6 and 12 mm from the probe to the sample were evaluated. Calibrated metal blocks clamped between the probe to adjust the position.
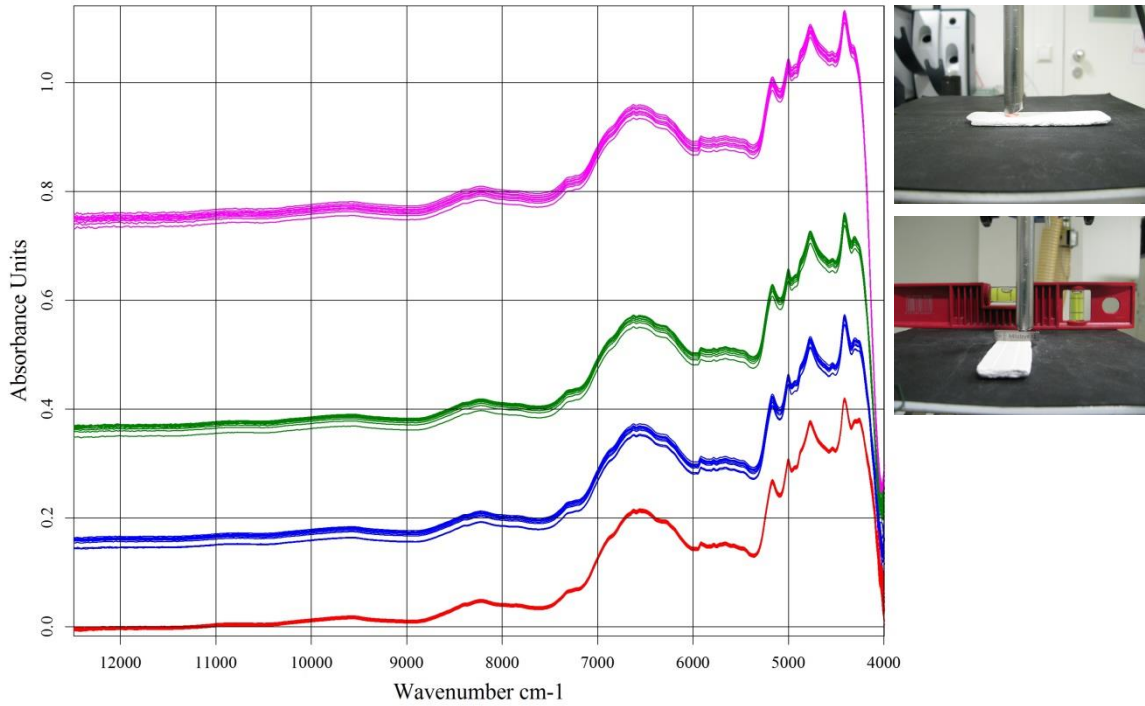
Figure 48   Distance probe to sample – Red = 0 mm, blue = 3 mm, green = 6 mm,
                             pink = 12 mm

Ten spectra of the same sample were acquired for each distance. A higher absorption with increased distance and a rising variation within the same distance between the 10 spectra were obtained (see Figure 48). A higher distance led to less detection of the radiation by the detector and resulted in a higher absorption.

Considering the first derivation of the spectra, a noisy signal could be observed with increased distance to the sample caused by a higher detection of stray light (see Figure 49). The distance of 0 mm was chosen as the best distance to the sample, which showed less variability between different spectra and a low noise signal. The zero position was defined as the longest part of the probe touching the sample.
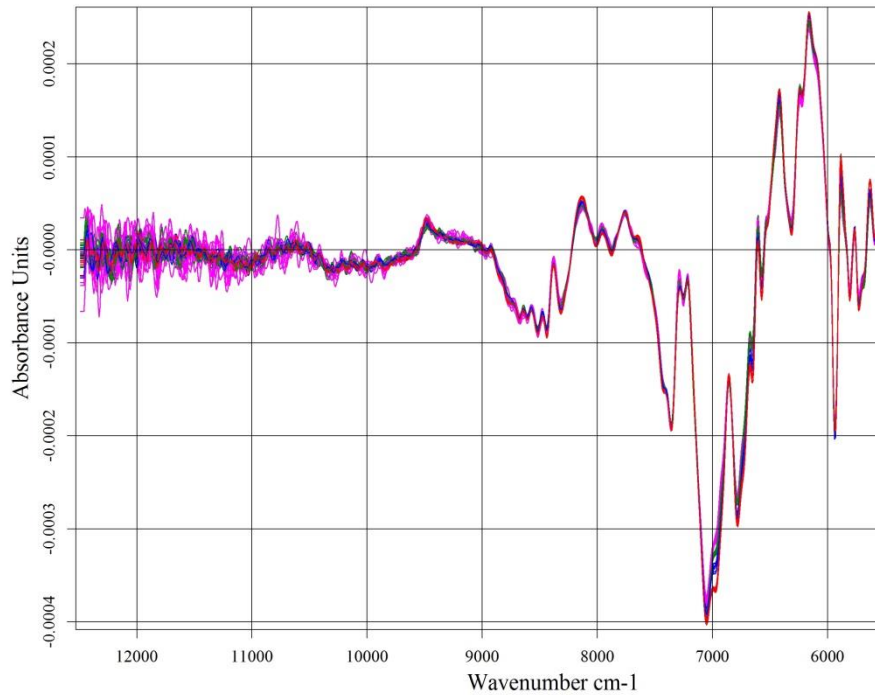
Figure 49   Distance probe to sample: First derivation - Red = 0 mm, blue = 3 mm, green = 6 mm, pink = 12 mm

Angle –Two angles of probe to the sample were evaluated. The probe had a bevel of 20°. Therefore, a 70° and 90° angle were examined. At 70° the whole surface of the probe was in contact with the sample. Ten re-adjustments of the zero position probe to sample within one angle were done. As depicted in Figure 50, an angle of 70° led to a higher variability within one setup. At an angle of 70° the laser beam of the probe was no longer apparent. This made it more difficult to adjust the position and find the same position on the sample square. Based on this a 90° angle was set as measuring setup.
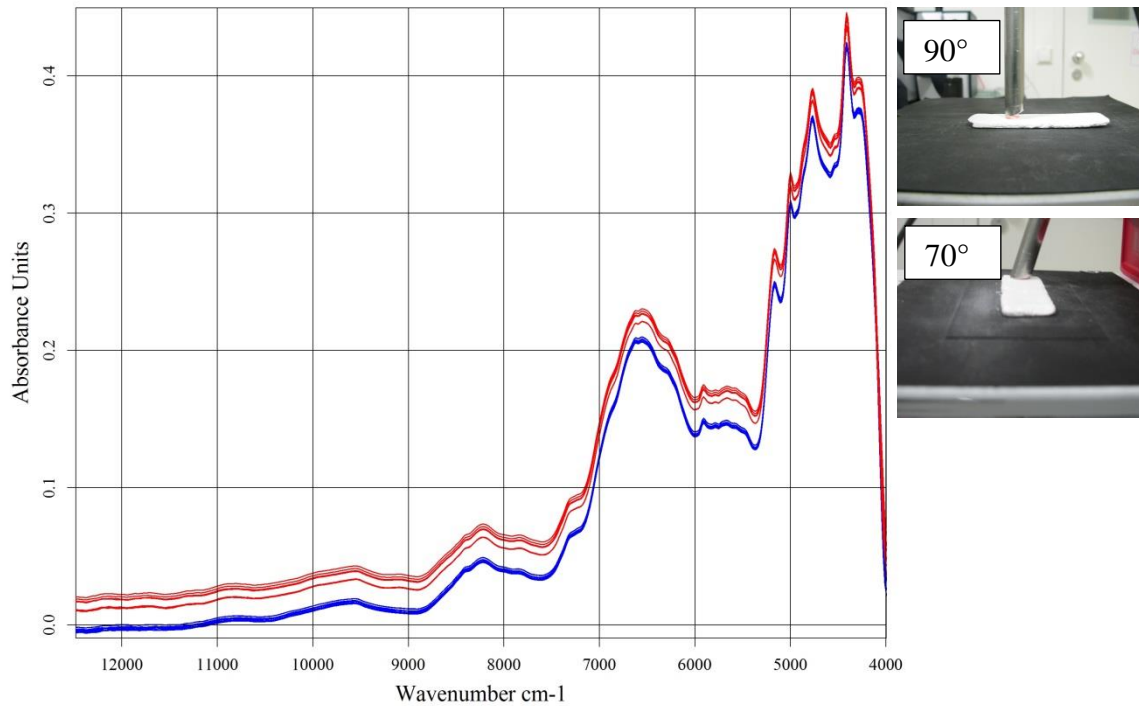
Figure 50   Angle probe to sample – Red = 70°, blue = 90°

Light – The light of the room may influence the absorption level. An evaluation with light and without light did not show any impact on the absorption. All spectra coincided. As it was easier to recognize the laser beam of the probe without light in the room and adjust the position on the ribbon, it was decided to use no light in the room. First derivation showed no difference between both (not shown).
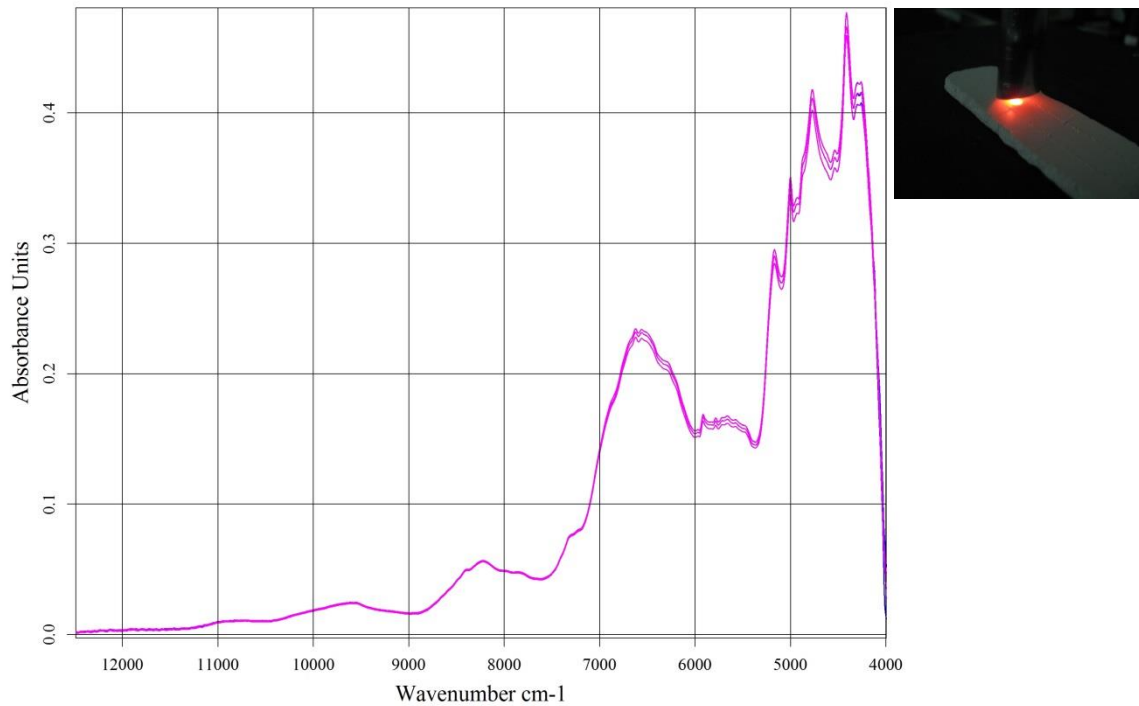
Figure 51   Light – Pink = off, blue = on

4.4.1.2.1.3   Software setup resolution

As a next step the software setup was evaluated. Different resolutions lead to a smoothing of the spectra over 8, 16 or 32 wavenumbers. Thus, a higher resolution indicates a higher smoothing and more information about the spectra gets lost. Figure 52 shows the first derivation of ten spectra for every resolution. A low resolution of 8 led to a noisy signal especially at higher wavenumbers. A resolution of 32 diminished too much spectral information. A resolution of 16 was chosen as software setup. The number of scans did not show any impact on the spectral information, a number of 64 scans was used.
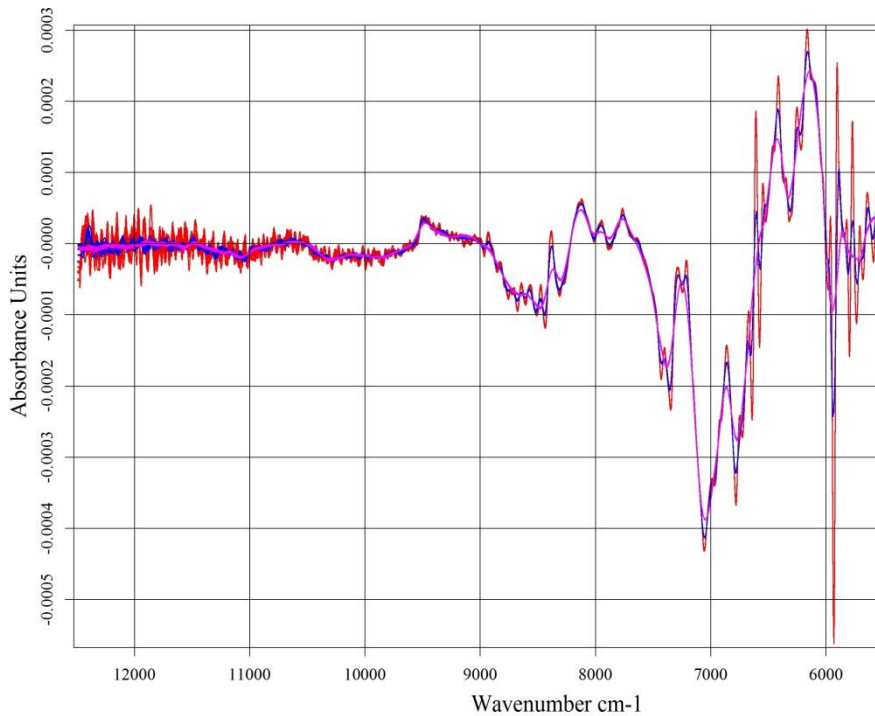
Figure 52   Resolution: First derivation - Red = 8, blue = 16, pink = 32

4.4.1.2.1.4   Specificity – Impact of composition on NIR spectra – Definition spectral range

NIR spectra can be used to derive chemical information. In particular by spectra peaks, which are representing characteristic chemical bonds of the used formulation (see 6.2.2.4). An adaption of the spectral range is necessary dependent on the formulation. It was a prerequisite for the measurement of the solid fraction (physical property) by NIR to diminish this impact in order to develop a reliable method, which is independent of the fraction of API or excipient. NIR spectra of the pure API, excipients and blend were acquired to evaluate an appropriate spectral range for the physical property of the ribbon.
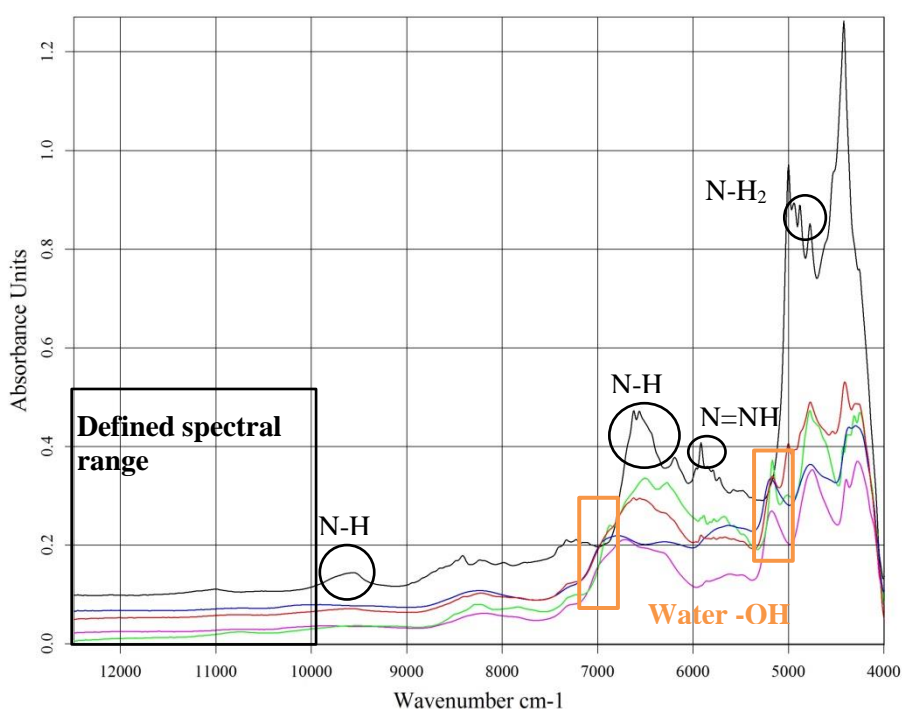
Figure 53   Spectra components and blend - Black = Metformin hydrochloride, green = α − Lactosemonohydrate, red = blend, blue = Sodium carboxymethylcellulose, pink = Microcrystalline cellulose

Different peaks occurred depending on the chemical structure of the components (see Figure 53). Specific peak maxima were observed for Metformin (combination band 5000 – 4000 cm^{-1}, first overtone band about 6570 cm^{-1}, second overtone band about 9596 cm^{-1}) [125] and water (combination band about 5200 cm^{-1}, overtone band about 7000 cm^{-1}) [126] (see APPENDIX 8.1.3). Based on these results, an appreciable spectral range above 9597 cm^{-1} will be evaluated for method development. At this spectral range, the impact of the composition showed less impact compared to a range of lower wavenumbers.

4.4.1.2.1.5   Summary

A summary of the evaluated NIR settings is depicted in Table 7. Using the first derivation of the spectra will reduce the impact of the measuring setup and sample condition.

Table 7   Summary - Evaluation NIR setup

Factor	Setup	Defined
Sample condition	Storage time	48 h (relative humidity 0-65 %, temperature 19-25°C)
	Ribbon surface	Smooth
Measuring setup	Distance probe to sample	0 mm
	Angle probe to sample	90°
	Ambient light	Off
Software setup	Resolution	16
	Scans	32
Spectral range	No influence of composition	above 9597 cm-1

4.4.2 Development of an at-line NIR method for solid fraction measurements of ribbons

4.4.2.1 Principal component analysis (PCA) – Verify spectral range

Multivariate data analysis was applied to describe the variance of the spectra over the range of wavenumbers (11941 cm^{-1} – 9665 cm^{-1}). Evaluation of an appropriate spectral range can be done by principal component analysis (PCA) (see 6.2.2.4.1). PCA verifies if the observed variance of the spectra can be distinguishing the solid fractions. A vast amount of data is compressed to principal components representing the variance of the spectra.
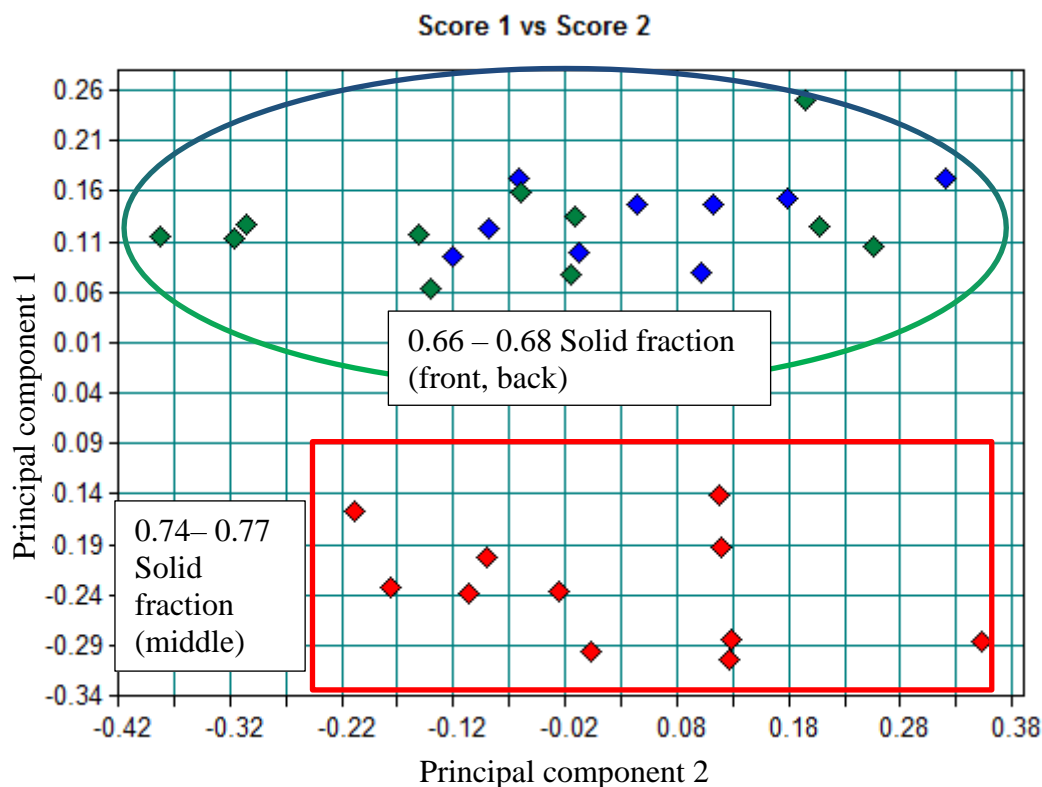
Figure 54   Principal component analysis – Ribbon at 6 kN/cm – Spectral range above 9597 cm^{-1}, location on the ribbon: front = blue, middle = red, back = green

Principal component 1 showed promising result as spectra were clustered by solid fraction. A distinction can be made by front, back and centre of the ribbon. The second principal component did not account for any difference between solid fractions. Principal component two was equally distributed over the spectra. Defined spectral range was appropriate to acquire a bigger sample size and to proceed with internal (cross validation) and external validation (test set).

4.4.2.2   Calibration data set – NIR method development

The calibration data set consisted of ribbons of the MiniPactor compacted at 4, 6, 8 and 10 kN/cm. In literature various authors correlated the slope of a linear regression over the whole spectral range [29,32,38,127] in order to determine the observed baseline shift (see 4.4.1.2) with increasing solid fraction. As investigated, various factors will have an impact on this baseline shift (e.g. distance probe to sample, see 4.4.1.2.1). First derivation allows to level these baseline shifts resulting in a higher accuracy, precision and robustness. Therefore, the first derivation was used for all spectra (see 4.4.1.2.1).

4.4.2.3   Results - Internal validation – Cross validation

Full cross validation of the calibration data set was performed by multivariate statistical method of partial least square analysis (PLS) (see 6.2.2.4.1). Each sample was removed from the full data set and predicted based on the regression results for the remaining samples (leave one out method).
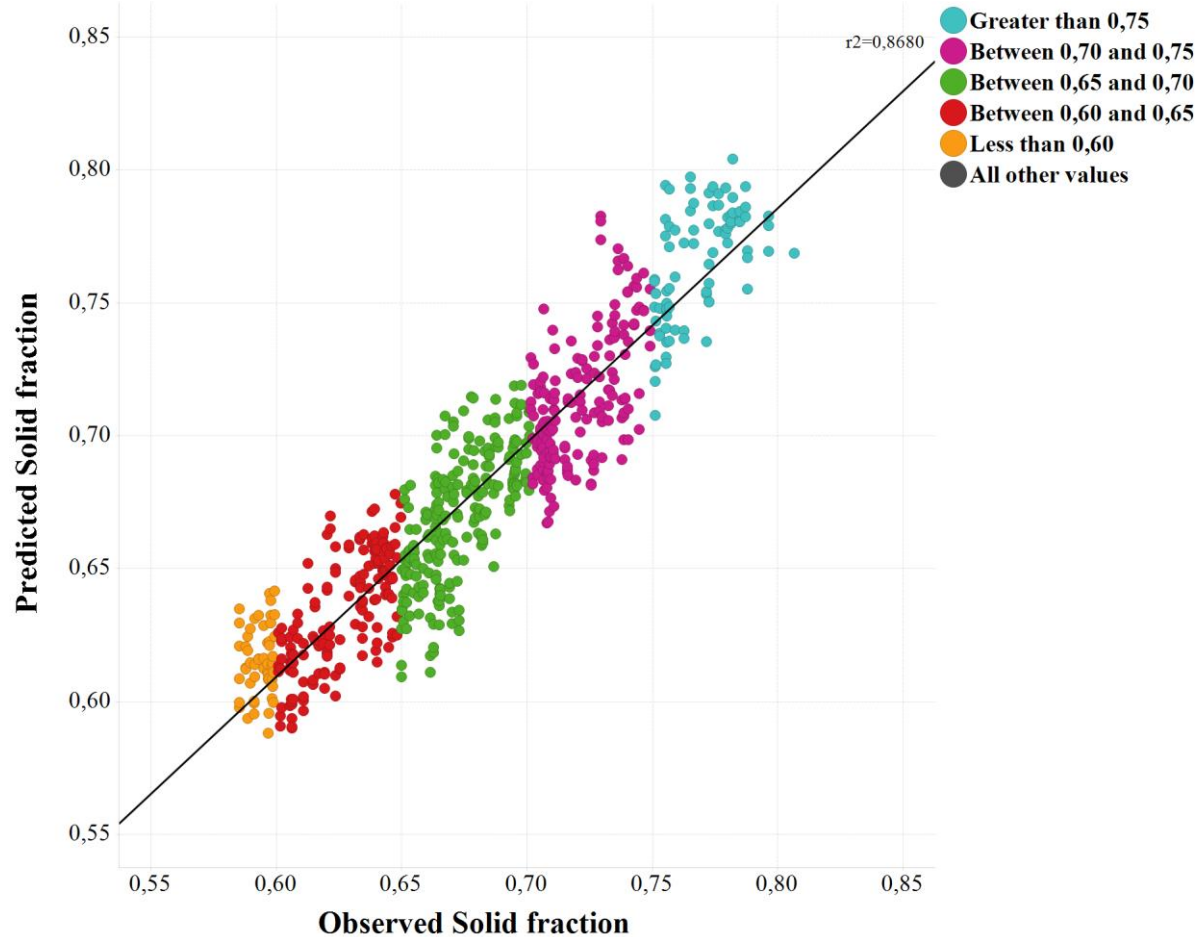
Figure 55   Results internal validation –

                            Predicted vs. observed solid fraction ribbon, colour indicates different

                            solid fraction ranges

A good correlation between predicted and observed values was found (see Figure 55). The correlation coefficient was 0.8680. Five principal components were necessary to reach this correlation coefficient (rank, PLS). Compared to the PCA, more principal components were necessary to describe this bigger data set. Furthermore, the root mean square error of cross validation and bias were low, which indicated a reliable model (see Table 8).

Table 8   Summary – Results internal validation

No. of calibration spectra included	699
Calibration range [Solid fraction]	0.5853 – 0.8066
Reference measurements [GeoPycnometer]	233
Data pre-processing technique	1st derivation
Selected wavenumber range	11941 cm^{-1} – 9658 cm^{-1}
Coefficient of correlation (R^2)	0.8680
Root mean square error of cross validation (RMSECV)	0.0188
Rank (PLS-factor)	5
Residual prediction deviation (RPD)	2.81
Bias	-0.0000366

4.4.2.4   Results - External validation – Test set validation

Unknown ribbon samples of 4, 6, 8 and 10 kN/cm were taken to evaluate the performance of
the developed method. Additionally, three drug loads (DL) of 15 %, 21 % (target drug load)
and 27 % were embedded in validation set to prove independence of the drug load.
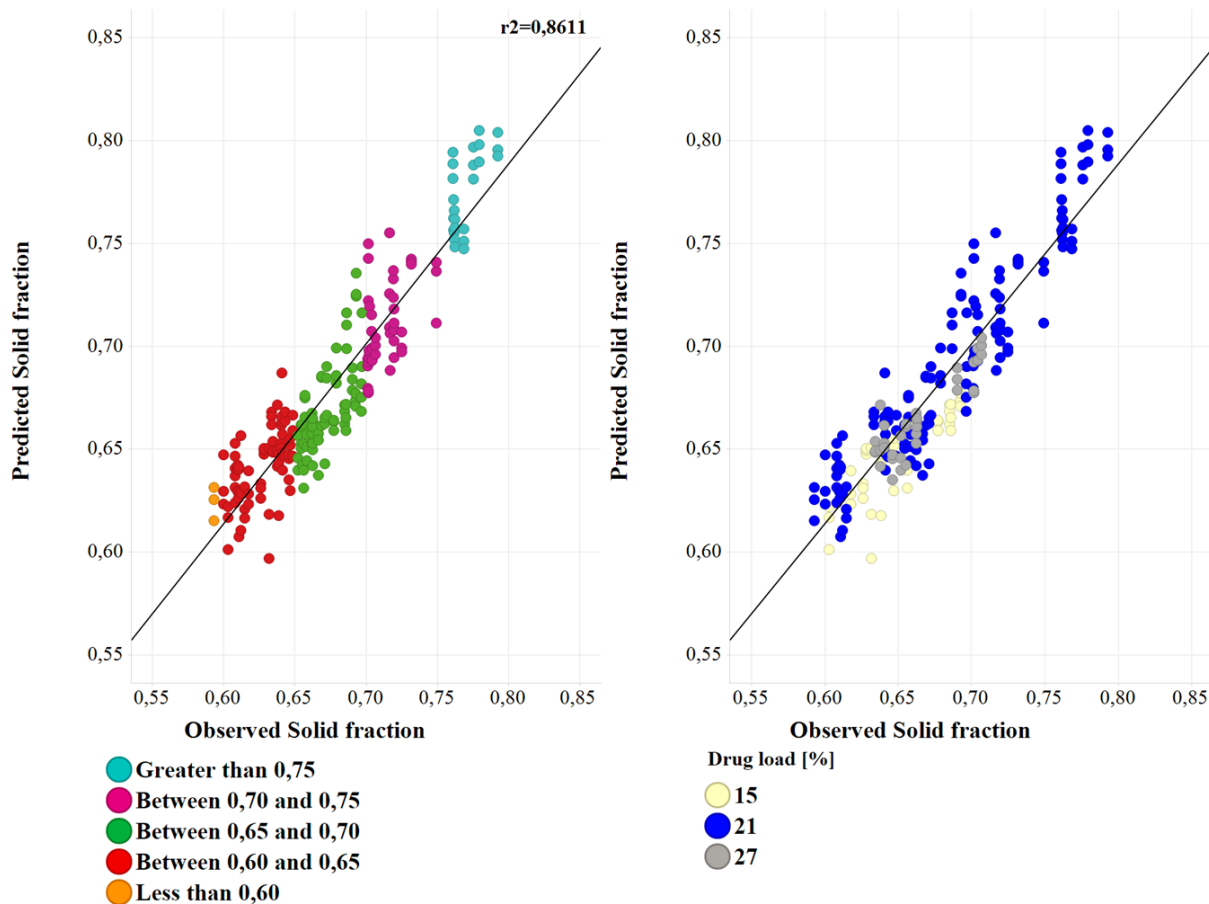
Figure 56   Results external validation – Left plot: Predicted vs. observed solid
                         fraction ribbon, colour indicates different solid fraction ranges of the
                         ribbon – Right plot: Predicted vs. observed solid fraction ribbon,
                         colour indicates different drug loads (%) for Metformin

Results of external validation were well in agreement with cross validation results. Similar
correlation coefficients (0.8611, 0.8680) and a low root mean square error of prediction and
bias could be found. (see Figure 56, left plot, Table 9). For the investigated drug loads of the
ribbon an impact on the accuracy of predicted solid fraction over the investigated range of
solid fractions was not found (see Figure 56, right plot). Predicted solid fractions were evenly
distributed around the observed solid fractions (GeoPycnometer). No trend in the residuals
could be identified for the different drug loads (see Figure 56, right plot). Validation results
confirmed that predictions of the solid fraction of unknown samples were successful. An

appropriate method was developed to further proceed with a scale up approach and to investigate the distribution of the solid fraction along roll width at different scales.

Table 9   Summary - Results external validation

No. of dosage strengths	21 %, 15 %, 27 %
No. of validation spectra included	216
Calibration range [Solid fraction]	0.5853 – 0.8066
Reference measurements [GeoPycnometer]	72
Data pre-processing technique	1st derivation
Seleceted wavenumber range	11941 cm^{-1} – 9658 cm^{-1}
Coefficient of correlation (R^2)	0.8611
Root mean square error of prediction (RMSEP)	0.0189
Rank (PLS-factor)	5
Residual prediction deviation (RPD)	2.68
Bias	-0.00425

4.4.3 Scale up approach – Comparison of solid fractions of ribbons of a Metformin formulation at two scales

The blend was compacted with the MiniPactor and MacroPactor at 4, 6, 8 and 10 kN/cm. Results of the solid fraction measurements are shown in Figure 57 (GeoPycnometer). Differences of the solid fraction of the ribbon were obtained between the two scales. MacroPactor achieved a higher solid fraction compared to the MiniPactor (Figure 57, left plot). These results were consistent with the results presented in previous chapters (see 4.2, 4.3).
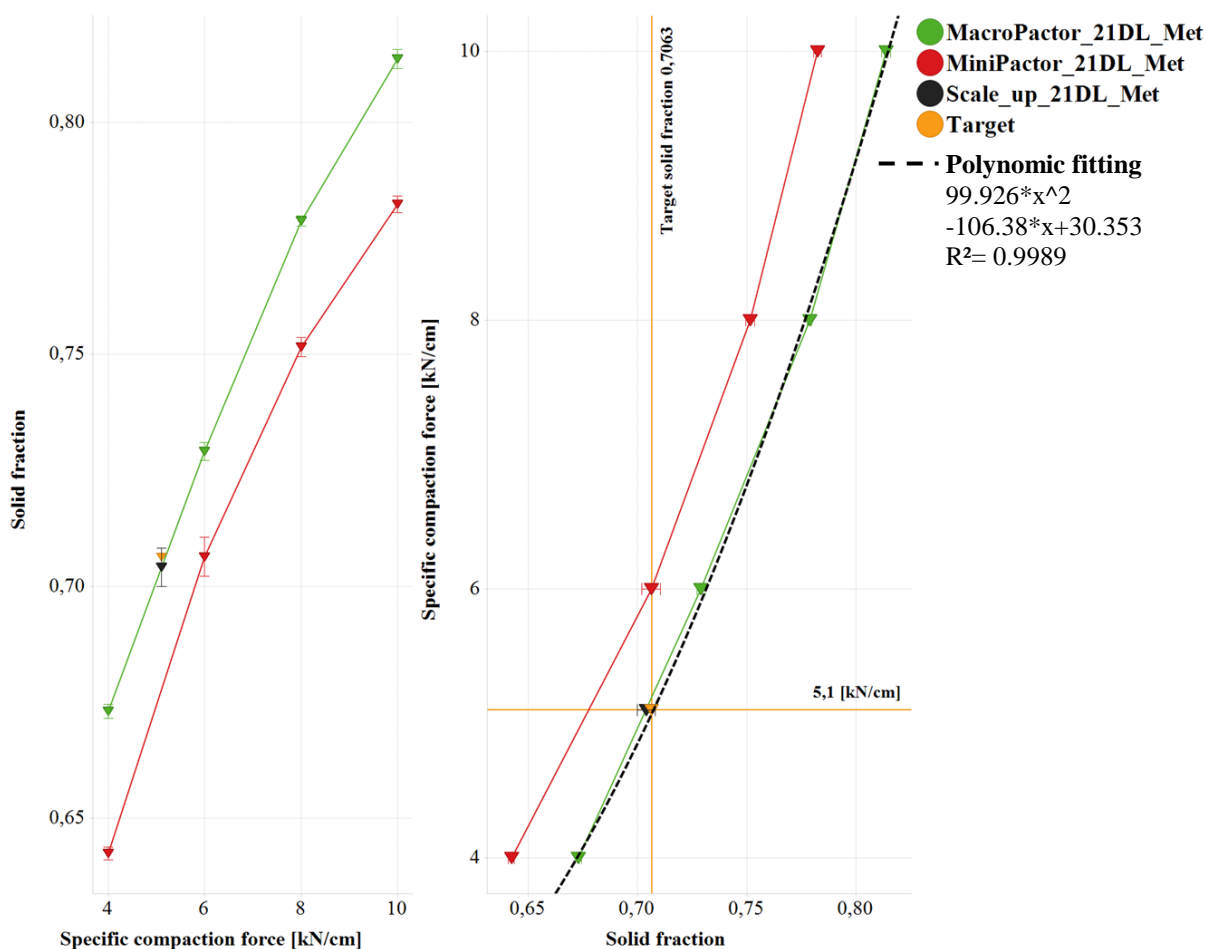
Figure 57   Comparison solid fraction ribbon MacroPactor/MiniPactor/Scale up - Left plot: solid fraction ribbon vs. specific compaction force - Right plot: specific compaction force vs. solid fraction ribbon, mean (n = 5), error bars (standard deviation of mean), DL = drug load, Met = Metformin

T-Test indicated differences (p ≤ 0.05) in SF between the MacroPactor and MiniPactor at all specific compaction forces (see APPENDIX 8.2.4). Solid fraction at 6 kN/cm of the

94

MiniPactor was defined as target solid fraction (0.7063) for a scale up (MacroPactor), which would be an appropriate value for the solid fraction of a ribbon to gain an acceptable product quality [17]. A polynomic fitting was done (see Figure 57, right plot), as previously described in chapter 4.3, to adapt the specific compaction force of the MacroPactor, and to achieve the target solid fraction of the MiniPactor. The polynomic equation allowed calculating the required specific compaction force at the MacroPactor by employing the target solid fraction of 0.7063 (MiniPactor, see Figure 57, right plot). Solid fraction of the adapted specific compaction force of 5.1 kN/cm (MacroPactor, black triangle) was 0.7040 and showed only a difference of -0.3 % to the target solid fraction. Ribbons were taken for NIR measurements.

4.4.4 Solid fraction distribution along the roll width between different scales by NIR

Independent samples of all specific compaction forces were analysed applying the NIR method. In Figure 58 the average solid fraction along the ribbon width for each scale at different specific compaction forces is shown. A polynomic fitting was done to illustrate the differences between the ribbons produced at two scales, where 0 cm represents the middle of the ribbon.
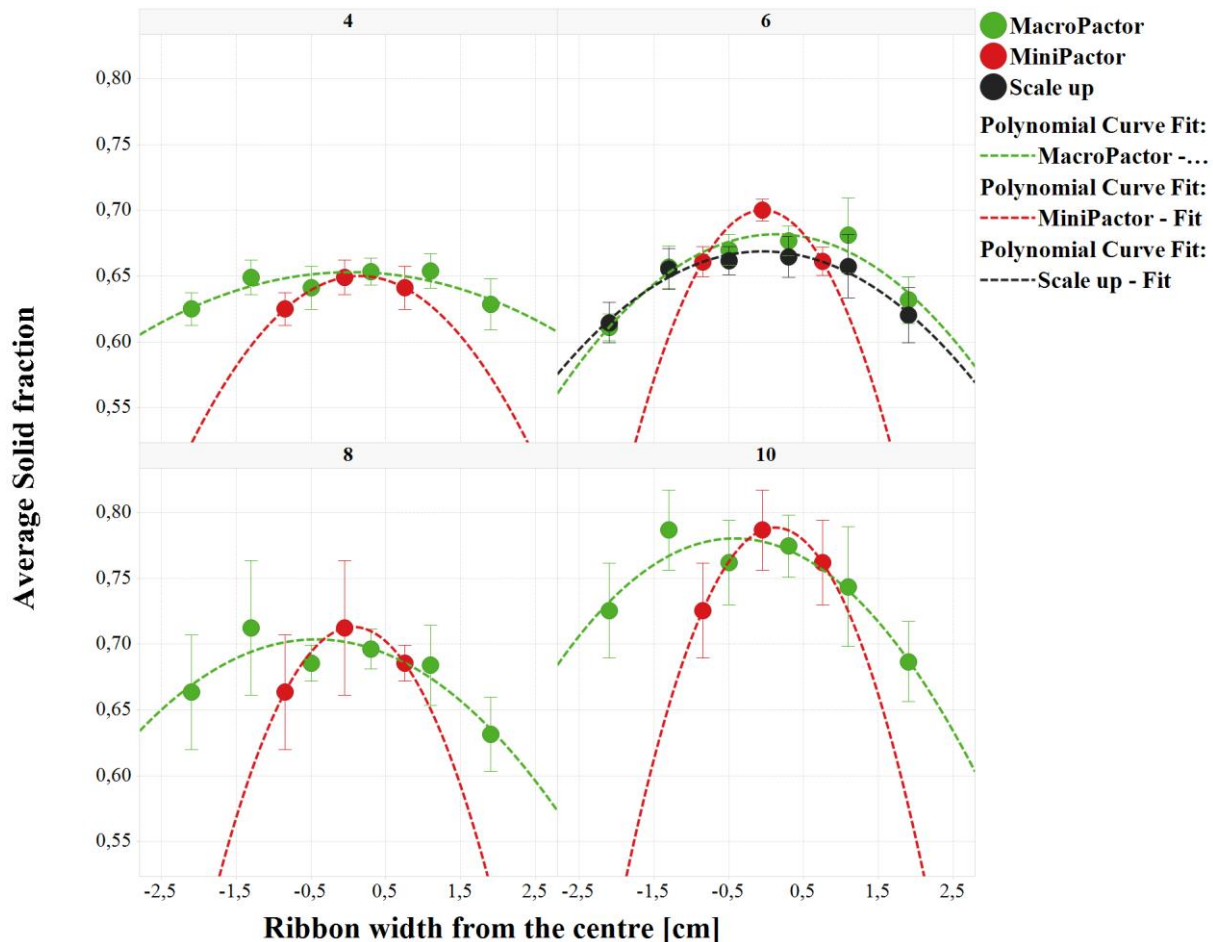
Figure 58   Mean solid fraction along ribbon width at compaction forces of 4, 6, 8 and 10 kN/cm, Scale up 5.1 kN/cm, mean (n = 12), error bars (standard deviation of mean), ribbon length 9.20 cm

Solid fraction increased from the edges to the centre from about 0.61 to 0.70 (+15 %) for both scales due to cheek plates effects (see 4.4.1.1) [21,30,31,36,40,41,115]. Ribbons of the MacroPactor obtained a narrow solid fraction distribution along the roll width because the impact of the cheek plates became lower with a larger distance to the edges (see 4.4.1.1). The ribbons produced with the MacroPactor had a larger area with a high solid fraction, which explains the higher "total" solid fraction measured by the GeoPycnometer for the ribbons of

the MacroPactor. This was previously observed with equal process parameters for both scales (see 4.2.2). For process development purposes, it is interesting to note that the standard deviation of the solid fraction increased with increasing specific compaction force (see Figure 58). At a higher specific compaction force, a higher amount of powder has to be dragged into the compaction zone by the tamp auger in order to reach steady state conditions at a gap of e.g. 3 mm. This can only be realized if the speed of the tamp auger is increased. Therefore, the impact of the periodical rotation by the tamp auger is enhanced, which is followed by a more diverse solid fraction along the ribbon length compared to lower specific compaction forces.
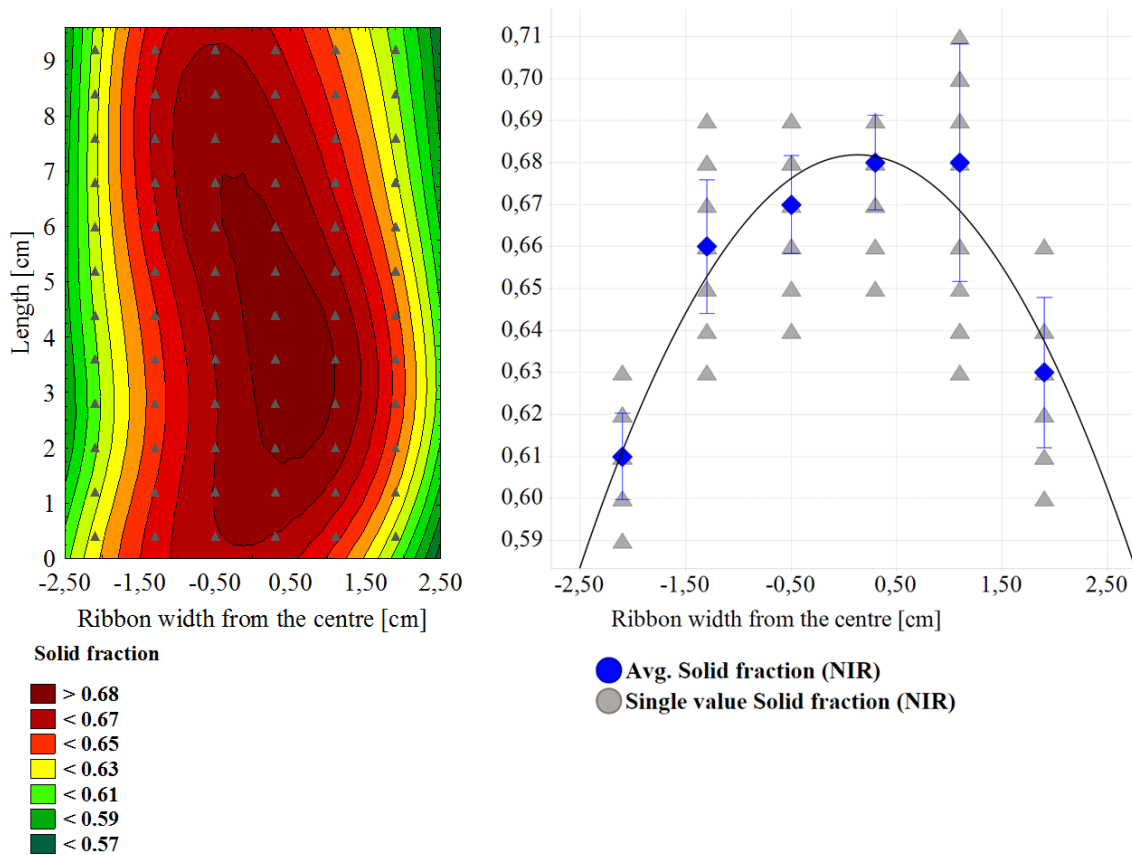
Figure 59   Solid fraction distribution ribbon (MacroPactor 6 kN/cm) -
     Left plot: solid fraction along ribbon length (contour plot, fit type
     = distance weighted least square), triangle measurement points of NIR
     - Right plot: solid fraction distribution of ribbon along ribbon width,
     triangle measurement points of NIR, circle (mean, n = 12), error bars
     (standard deviation of mean)

A sinusoidal periodical course of the solid fraction along the ribbon length, attributed to the periodically screw rotation of the tamp auger [29,36,39], could be exemplary shown for a ribbon of the MacroPactor (see Figure 59).

Additionally, the results of solid fraction distribution explained the lower observed tensile strength of tablets by the MacroPactor compared to the MiniPactor (see 4.2.4.2). A high solid fraction will lead to higher consumption of plastic deformation, lower porosity of granules and thus to a lower tensile strength of tablets (see 4.3.4). Considering the scale up approach, the sample showed an equal "total" solid fraction compared to the MiniPactor (see Figure 57). This comparable solid fraction will result in similar granule and tablet properties (see 4.3.2 & 4.3.3). A lower solid fraction can be obtained by adapting the specific compaction force (Scale up 5.1 kN/cm) to counteract the different solid fraction distribution along the roll width between two scales. Thus, adapting the specific compaction force by measurements of the "total" solid fraction (GeoPycnometer) is a suitable scale up strategy for a roller compaction process. A uniform distribution of the solid fraction at different scales would be preferable, but due to construction issues like roll width and side seal system, difficult to gain.

4.4.5   Summary

In previous chapters a different solid fraction of the ribbon at equal process parameters at different scales was obtained. A more efficient NIR method was developed to measure the solid fraction of ribbons along the roll width, as the GeoPycnometer method was limited by sample size. A new formulation with a model API Metformin was used. Various factors were investigated, which have a potential impact on the reliability of the NIR method. Sample conditions, measuring setup and API content. Afterwards internal validation and external validation was performed with independent samples, which illustrated a good correlation coefficient $R^2 \geq 0.86$ to the reference method. It was possible to predict the solid fraction of unknown samples by acquiring the NIR spectra comprising reduction of analysis time.

The developed NIR method allowed measuring the solid fraction distribution along the full roll width. A difference between the solid fraction of the ribbons based on different scales was found. MacroPactor showed a larger area with a high solid fraction along the roll width compared to the MiniPactor. The effect of the cheek plates (lower solid fraction at the edges), decreased with increased distance to the cheek plates (≈ 1 cm, see Figure 58), which was especially the case for the MacroPactor with a broader roll width. This leads to a higher "total" solid fraction of the ribbons produced by the large scale compared to a small scale at equal process parameters. These results explained different quality attributes of granules and tensile strength of the tablets impacted by the solid fraction of ribbons, which were observed in previous chapters at equal process parameters. The proposed scale up approach showed that the differences of resulting granules and tablets between scales can be balanced through adaption of the specific compaction force. Furthermore, this approach can be used in the pharmaceutical industry during process development from small development batches to commercial batches to satisfy market demands.

4.5 MODEL DEVELOPMENT – PREDICTING SOLID FRACTION OF A TABLET

Previous chapters have shown that compression behaviour of mixtures (solid fraction vs. compression) have an impact on roller compaction process. Thus, it would be beneficial to predict the compression behaviour of mixtures based on compression analysis of single excipients to support decision guidance for formulation development purposes.

The predictive power of the Percolation theory, the Kawakita model, and a simple exponential model were systematically evaluated for different direct compression formulations. Four mixtures were compressed over a wide pressure range at various fractions of microcrystalline cellulose (MCC) and pre-agglomerated lactose monohydrate (LAC). Formulations contained different amounts of MCC and LAC in range of 72 % to 24 % (see Table 17). First, all models were applied to single components and thereafter an additive rule was used (see 3.3.1.4), for predicting the solid fraction of the mixtures, reflecting the composition of the formulation. Finally, the prediction and the observed solid fractions of the compressed mixtures were compared to evaluate the suitability of the models (see Figure 60).
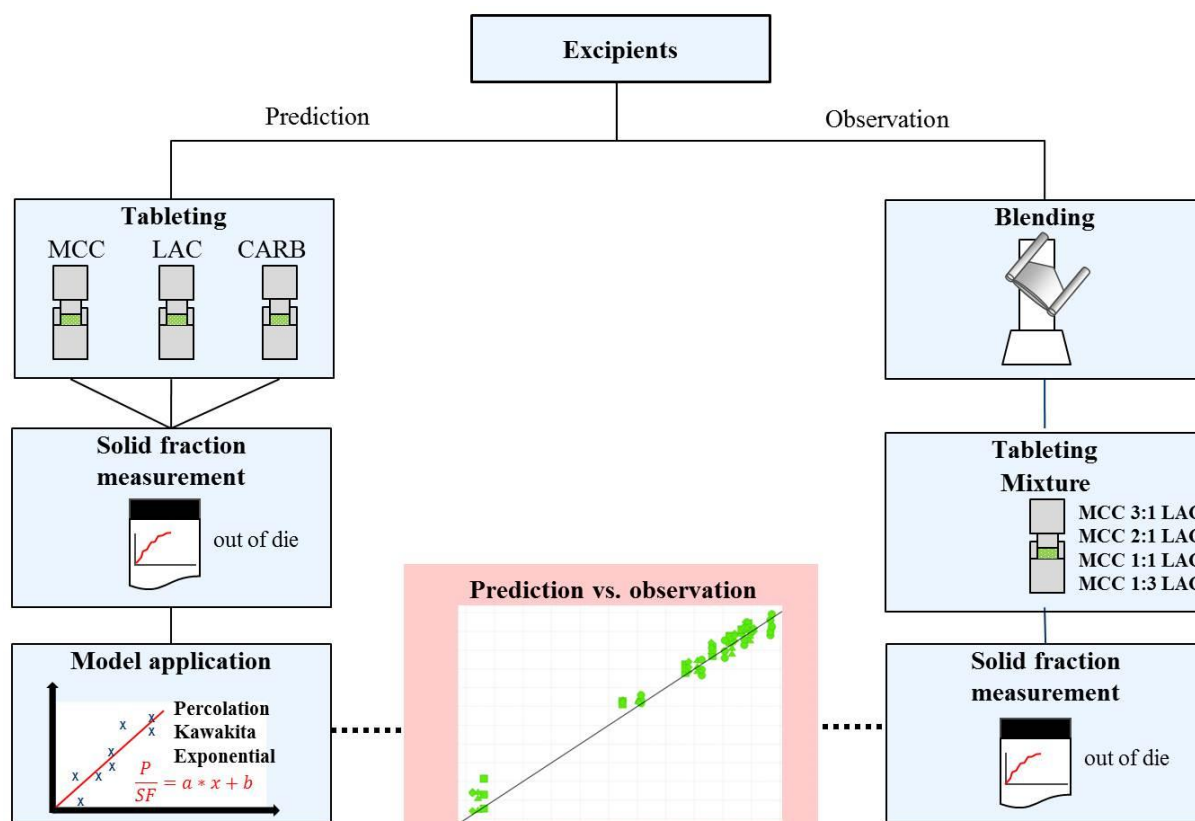
Figure 60   Process flow - Prediction solid fraction of tablets

4.5.1 Application of models – Excipients

4.5.1.1 Input data for model application

A low number of input values are a prerequisite to ease applicability of a model. Thus, solid fraction after compression and true density measurements (see Table 2) of MCC, LAC and CARB were used as input parameters. Forty-two tablets were compacted between 50 MPa – 350 MPa for each excipient. The tablets were weighed directly after ejection with an analytical balance. The diameter and the height of each tablet were determined by an automatic tablet tester to enable calculation of the solid fraction according to Eq. (34) and Eq. (35). Tablets only consisting of LAC compressed at a compression pressure of 50 MPa were too weak for being measured in the tablet tester. Results of the compressibility are depicted in Figure 61.
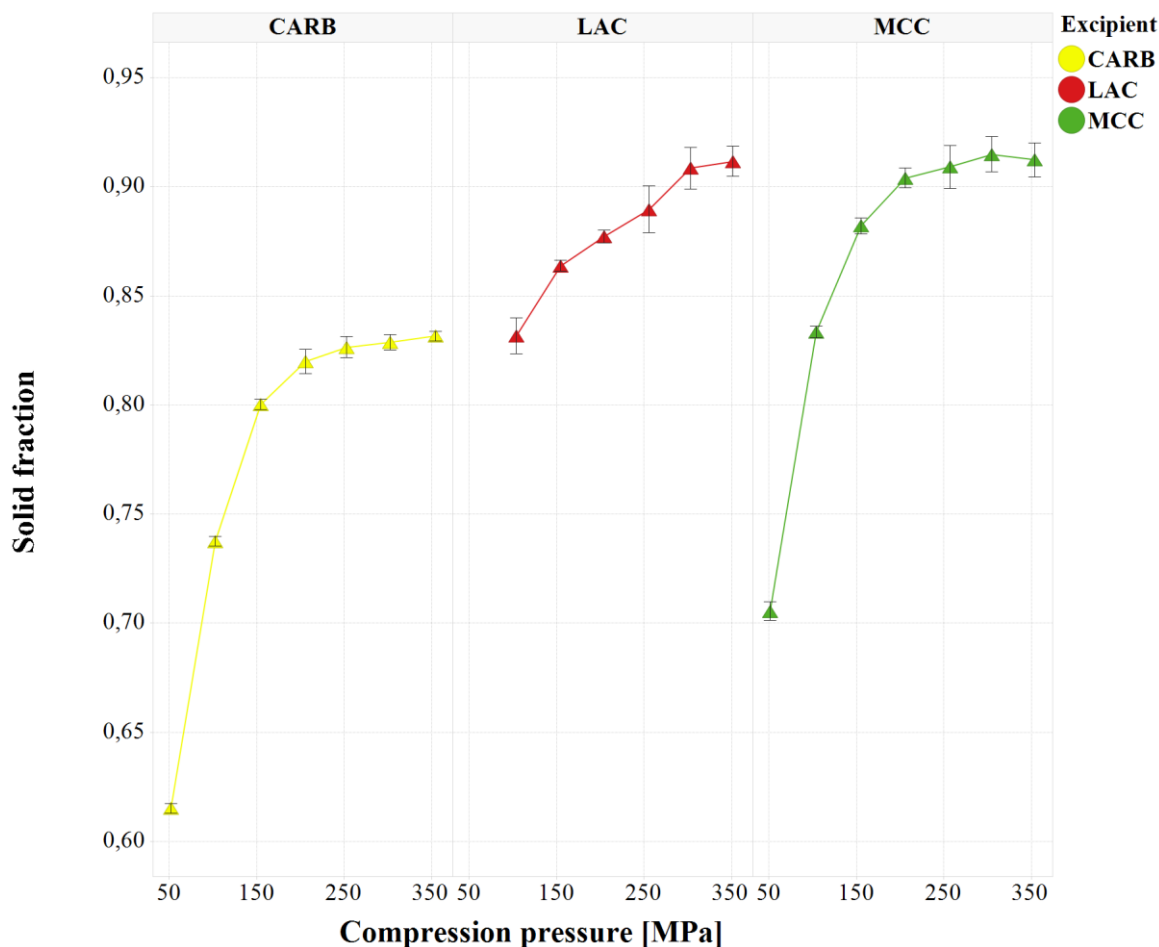
Figure 61   Excipients - Solid fraction vs. compression pressure [MPa], mean
                   (n= 6), error bars (standard deviation of mean)

True densities of mixtures were calculated according to   Eq. (17). Results can be seen in Table 10.

Table 10   Calculated true density mixtures

Mixture #1 MCC 3:1 LAC	Mixture #2 MCC 2:1 LAC	Mixture #3 MCC 1:1 LAC	Mixture #4 MCC 1:3 LAC
1.5540 [g/cm3]	1.5527 [g/cm3]	1.5504 [g/cm3]	1.5468 [g/cm3]

MCC = Microcrystalline cellulose; LAC = α − Lactosemonohydrate

4.5.1.2   Percolation

The different parameters in the model can be interpreted with regard to compressibility. The maximum achievable value of SF/SF_{max} is limited by the value of SF_{max} and cannot exceed the value of 1 (see Figure 62).
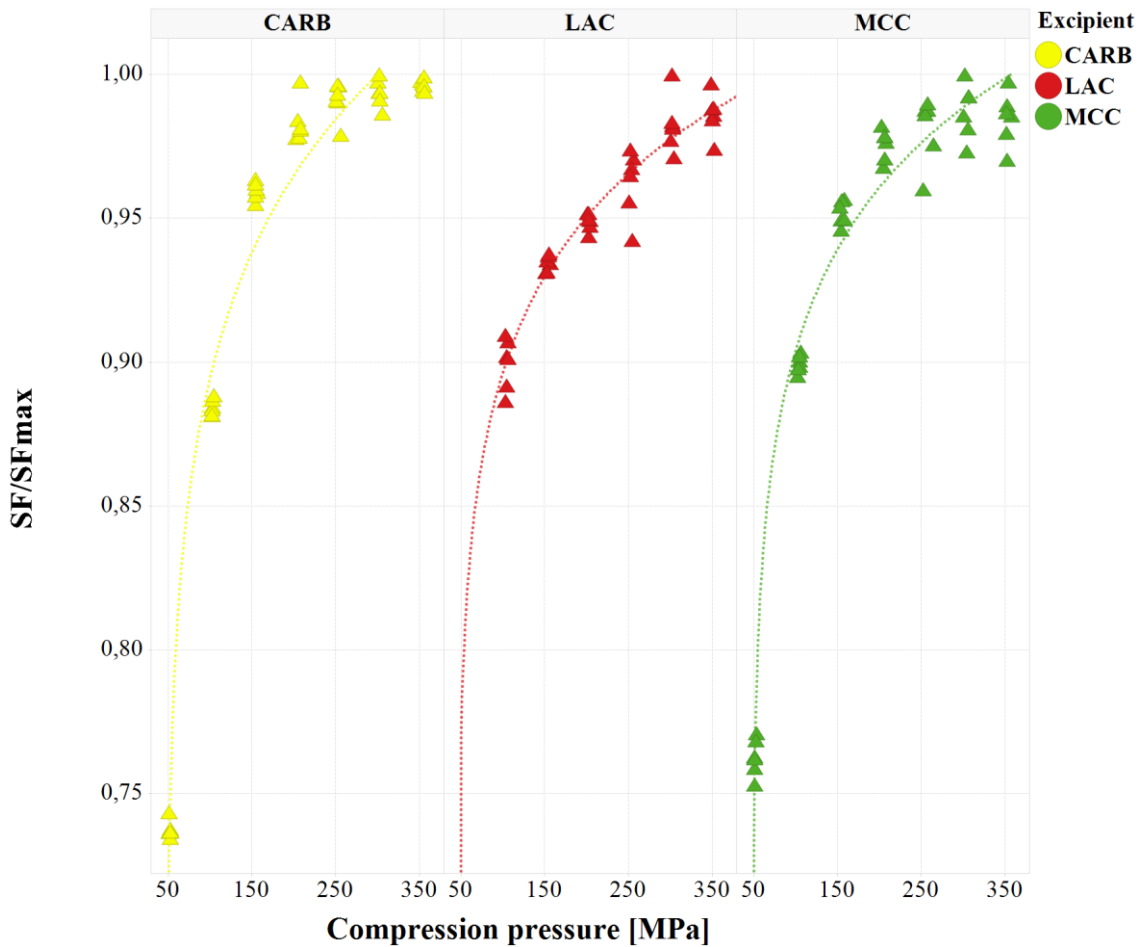
Figure 62   Excipients - Percolation SF/SF_{max} vs. compression pressure

SF_{max} of MCC and LAC had a similar value which caused a similar value of S [128] although they had a different course of their compressibility graph. In contrast to the plastic deformable materials MCC and CARB, LAC reached a plateau of SF exceeding a compression pressure of 300 MPa, while MCC and CARB reached that plateau at pressure values of about 200 MPa. This behaviour is due to the brittle deformation characteristics of LAC [129] which resulted in lower compressibility compared to plastic deformation, the course seemed to be steadily increasing which could be a consequence of the pre-agglomerated LAC and induces a brittle fracture (see Figure 61).

All excipients showed similar percolation thresholds, where the percolation threshold of LAC was lower than the threshold of MCC. As the percolation threshold is defined as the pressure limit above which particle rearrangement has completed and an infinite cluster formed (see 3.3.1.1), excipients of higher bulk or working density will need less pressure to settle, i.e. rearrange. The working density (bulk density) can be derived from V_0-values at 1-2 MPa (see 3.3.1.2 & 4.5.1.3) and were 0.9376 g/cm³ ($V_0 = 0.2117$ cm³) for LAC and 0.4996 g/cm³ ($V_0 = 0.3990$ cm³) for MCC which explains the lower percolation threshold for the spherically shaped Tablettose 80® (LAC) particles in contrast to the fibrous Avicel PH 102® (MCC) particles.

Table 11   Estimated parameters for the Percolation model

Modell Parameter	MCC	LAC	CARB
$\dfrac{SF}{SF_{max}} = S * (x_p - p_c)^q$ or $SF = S * (x_p - p_c)^q * SF_{max}$			
SF_{max} (measured)	0.9264	0.9242	0.8338
	Estimate	Estimate	Estimate
S	0.7248	0.7183	0.6778
p_c	48.7851	46.4764	48.3177
q	0.05615	0.05565	0.07033
R²	0.9753	0.9306	0.9715

MCC = Microcrystalline cellulose; LAC = α − Lactosemonohydrate; CARB = Sodium carboxymethylcellulose; SF = Solid fraction; SF_{max} = Maximal solid fraction; S = Proportional constant; x_p = Compression pressure [MPa]; p_c = Percolation threshold; q = compressibility exponent; R^2 = correlation coefficient

The compressibility exponent q provided a reasonable interpretation of the course of the graphs (see Figure 62) and relates to the steepness of the compressibility plot approximating SF_{max} (maximal densification) over the whole range of the applied compression pressure. CARB showed the highest value and achieved the maximal densification already at 200 MPa, whereas MCC and LAC exhibited similar values of q, which was driven by the behaviour discussed earlier (particle shape) and can also be explained by considering Eq. (6), which caused normalisation through maximum measured solid fraction (SF_{max}). The coefficient of correlation was ≥ 0.9306 and showed good fitting results for the model (see Table 11).

4.5.1.3   Kawakita

According to the modification of Kawakita C (see 3.3.1.2), a proof for the new definition of C is exemplarily shown for microcrystalline cellulose in Figure 63 where $C = V_0 - V_P/ V_0$ is correlated to solid fraction (SF). V_0 was determined in-die for microcrystalline cellulose (n = 3) to be in a typical range of 1-2 MPa. The linear correlation between both definitions throughout the range of interest (for tableting & roller compaction) for solid fraction from 0.72 - 0.91 was confirmed by the high coefficient of correlation ($R^2 \geq 0.9951$) (see Figure 63). LAC and CARB showed similar behaviour resulting in correlation coefficients of 0.9954 and 0.9928 respectively (see APPENDIX 8.1.4).
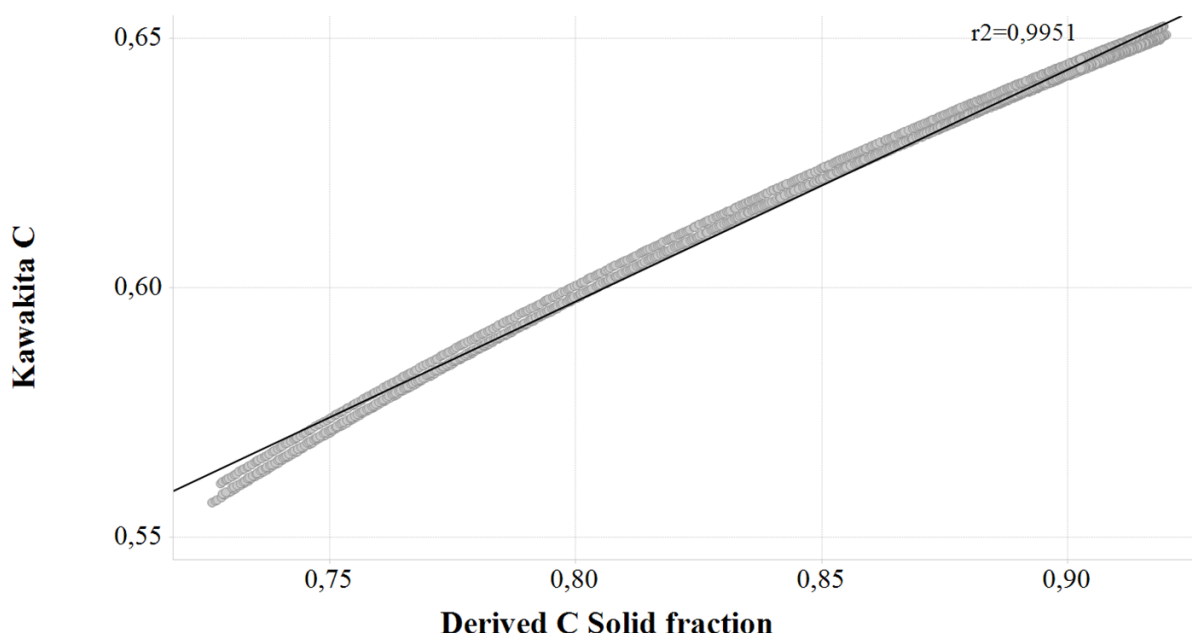
Figure 63   "In-die" data MCC- Kawakita C vs. derived C equal to solid fraction

Considering the applicability of the Kawakita model, the linearity of the plot P/SF vs compression pressure is a specified condition. For all excipients, good linearity was

demonstrated and therefore a high coefficient of correlation could be achieved ($R^2 \geq 0.9992$) over the whole range of compression pressure (see Table 12, Figure 64).
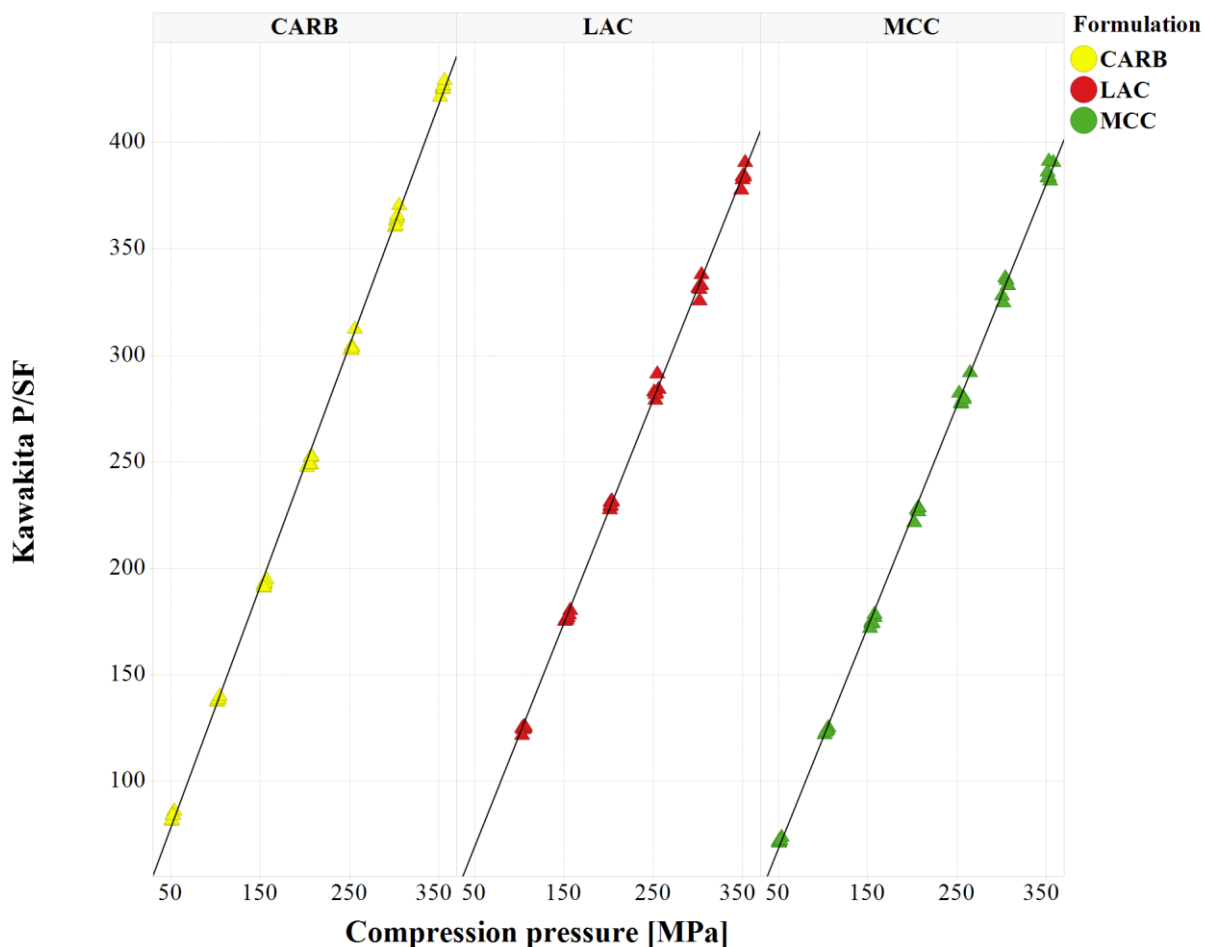
Figure 64   Kawakita - Excipients P/SF vs. compression pressure [MPa]

This proves that it was possible to determine V_{min} by a Helium-Pycnometer and to consequently use solid fraction as C. Thus, the Kawakita parameter a can be seen as maximum strain or by the definition of Eq. (8) as maximum achievable solid fraction. Kawakita a decreased in the order of MCC > LAC > CARB, which was consistent with the observed values of SF_{max} determined for the Percolation model shown above (see Table 11), and emphasised that MCC was the most compressible excipient. Considering b^{-1}, MCC showed the highest deformation capacity (low value), followed by LAC and CARB.

Table 12   Estimated parameters for the Kawakita model

Modell Parameter	MCC	LAC	CARB
Kawakita a	0.9614	0.9522	0.8836
Kawakita b^{-1}	17.0257	17.7252	24.7369
Fitted Parameter	**MCC** Estimate	**LAC** Estimate	**CARB** Estimate
Slope	1.0401	1.0502	1.1317
Intercept	16.3693	16.8779	21.8582
R^2	0.9992	0.9992	0.9992

MCC = Microcrystalline cellulose; LAC = α − Lactose monohydrate; CARB = Sodium carboxymethylcellulose; R^2 = correlation coefficient

4.5.1.4   Exponential

Results of parameter estimation of the exponential model showed a good coefficient of correlation $R^2 \geq 0.9282$. For LAC the R^2 was quite low because LAC had a more linear course of the graph, as mentioned above (see Table 13).

Table 13   Estimated parameters for the Exponential model

Modell Parameter	Estimate		
	MCC	**LAC**	**CARB**
d	0.9153	0.9342	0.8335
f	-0.5257	-0.1928	-0.5345
g	-0.0179	-0.0062	-0.0172
R^2	0.9916	0.9282	0.9960

MCC = Microcrystalline cellulose; LAC = α − Lactosemonohydrate; CARB = Sodium carboxymethylcellulose; d, f, g = Exponential constants; R^2 = correlation coefficient

4.5.2 Prediction of solid fraction – Mixtures

All three models were applied to the excipients and then multiplied by their mass fraction according to the composition of the mixture to predict the solid fraction Eq. (16) (see 3.3.1.4). In order to compare the prediction with the observation, the mean value of six tablets was used. For MCC 1:3 LAC at 50 MPa no reasonable values could be determined because the tablets were too soft.
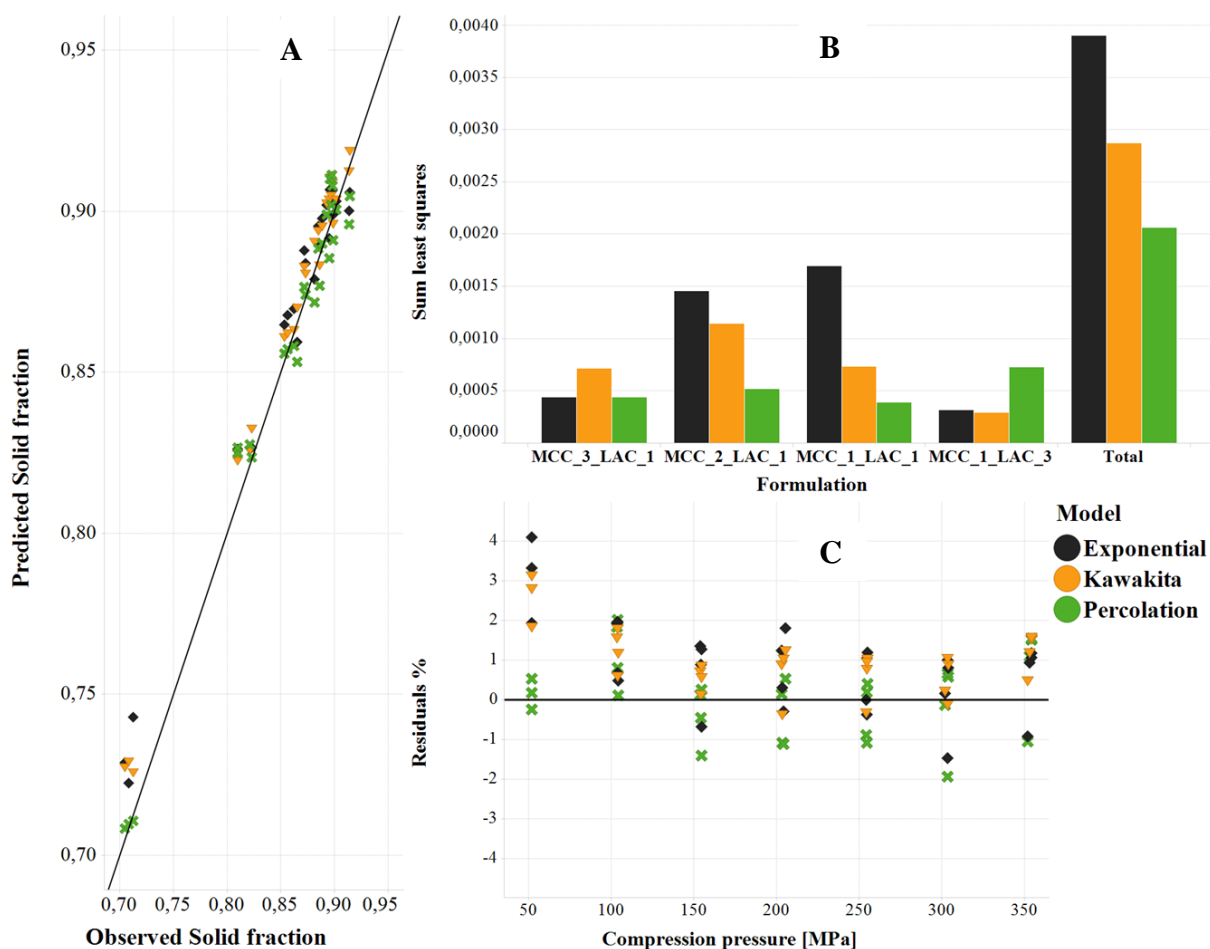
Figure 65   Results models – Plot A: Predicted vs. observed solid fraction – Plot B: Sum least squares of model for each formulation and total sum least squares of the models – Plot C: Residuals vs. compression pressure range [MPa]

For the exponential model a slight trend of overpredicting the solid fraction can be seen (see Figure 65A). However, according to this the results of the three models differ in terms of the observed values only in a range of -0.017 to 0.030, which is only a small difference for solid fraction. Considering the absolute residuals a relevant deviation over the compression pressure cannot be anticipated. The total sum of the least squares (see Figure 65B) follows the order Percolation < Kawakita < Exponential model, which demonstrates that the Percolation

model yields the best prediction of the solid fraction for all mixtures. The exponential model has a stronger overprediction of the solid fraction, whereby the Percolation leads to a moderate underprediction (see Figure 65C). Verifying the model's quality of prediction by subdividing the sum of least squares by mixtures, gives an enhanced ability for interpretation (see Figure 65B). For the mixtures #1 - #3, which had a higher fraction of MCC, the percolation model achieved a much more precise prediction than Kawakita or the Exponential model. A reason for the good prediction of the solid fraction by the percolation model can be that it also takes into account the maximum achievable solid fraction (SF_{max}), which provides a limit for the system. The poor prediction by the percolation model for the mixture #4 MCC 1:3 LAC can be caused by the lower correlation coefficient 0.9306 for LAC (see Table 11), whereas Kawakita has a correlation coefficient of 0.9992 (see Table 12). Nevertheless Mixture #4 has a rather untypical high load of LAC (72.37 %) for a tablet formulation. This could be an interesting point for further investigations to verify if the percolation model is also in good agreement for formulations, which have similar brittle compression behaviour like LAC. Despite this the Kawakita model gives the best coefficient of correlation (see Table 12) for all excipients, it resulted in valuable predictions of all mixtures. Comparing predictions of solid fraction by Kawakita to recent papers, which focus on the prediction of porosity by Kawakita [75,79,81], residuals in a similar range from -0.39 % to 3.12 % compared to Busignies et al. (2012) were found , lower than 2.5 % [79], which is in a good agreement. Also Frenning et al. (2009) have shown that it is possible to predict the effective Kawakita parameters a and b^{-1} of spherical pellets out of single compression analyses. However, this reflects that it is possible to derive C as solid fraction (see 3.3.1.2), which is defined by measured V_{min} and V_p, to get reasonable results for the prediction of solid fraction by Kawakita and to obtain a possible comparison between various research laboratories.

4.5.3 Summary

A modified Kawakita model and the Percolation theory were successfully adapted for the compressibility plot to predict the solid fraction of four compositions using single compression analysis of the excipients. These two mechanistic models, were both compared with a statistical model based on a simple exponential function. Both theoretical models showed very good prediction of solid fraction. The Percolation model seems to be more suitable for a common composition of tablets in pharmaceutical industry, whereas Kawakita showed better results for mixtures which deform predominantly by brittle fragmentation. The limited input data set (tablet geometry/mass, true density) and common software for regression analysis, makes it easy to establish a more complex dataset for different excipients providing systematic guidance for the formulator. Further investigations are needed to consider mixtures with different active pharmaceutical ingredients and excipients with brittle fracture.

In respect to roller compaction process, Percolation and Kawakita can provide an opportunity to predict the solid fraction of ribbons if an correlation between compression pressure at the tablet press and specific compaction force of the roller compactor will be established, which will reduce the number experiments at a roller compactor to find the right process settings for a specified formulation.

5.   MATERIALS

5.1   MATERIALS

Table 14   Materials

Name	Trade name	Supplier	Batch #
α−Lactosemonohydrate (LAC)	Tablettose 80®	Meggle Wasserburg GmbH & Co. KG, Megglestraße 6-12, 83512 Wasserburg am Inn, Germany	203403 200292 203403
Microcrystalline cellulose (MCC)	Avicel® PH102	FMC Biopolymer Co, 1735 Market St., Philadelphia, PA 19103, USA	400994 905814 903926
Sodium carboxymethylcellulose (CARB)	AcDiSol®	FMC Biopolymer Co, 1735 Market St., Philadelphia, PA 19103, USA	401433 408157 802637
Magnesium stearate (MGST)	LIGAMED®	Peter Greven GmbH & Co. KG, Peter-Greven-Straße 20-30, 53902 Bad Münstereifel, Germany	304668 308990-1
Metformin hydrochloride (MET)	Metformin hydrochloride	Weifa AS, Gruvevn. 1, P.O. Box 98, NO-3791 Kragera, Norway	401889
Graphite powder	DryFlo®	Micromeritics Instrument Corporation, 4356 Communications Dr, Norcross, GA 30093, USA	-

α−Lactosemonohydrate (LAC) is a commonly diluent in tablets. α−Lactosemonohydrate occurs by a crystallisation of a supersaturated solution of lactose below 93°C [91]. A processed product is Tablettose 80®, whereby fine milled lactose particles agglomerate during a continous spray drying processs by water. The resulting agglomerates show increased flowability and increased tabletability, due to eased fracturing into smaller particles compared to single crystals of the size of the agglomerates. LAC is an excipient, which shows a typical brittle compression behaviour [90,91].

Microcrystalline cellulose (MCC) is a partially depolymerized cellulose derived from α−cellulose wood pulps using sulfuric acid, followed by a washing step and a spray drying

process, which results in fibrous MCC particles [130]. MCC is one of the frequently used excipients as diluent and binder, because of its good plastic deformation under pressure [60]. Sodium carboxymethylcellulose (CARB) is a cross-linked polymer of carboxymethylcellulose sodium used as disintegrant as it has a high water uptake ability combined with an high swelling property to provide a fast disintegration of the tablet.

Magnesium stearate (MGST) is a lubricant to reduce the sticking or friction between stainless steel (e.g. rolls, punches) and powder. Metformin hydrochloride (MET) is an oral antihyperglycemic drug, used for type 2 diabetes. The API belongs to the biguanide class. Metformin has been used as model API in chapter 4.4. Different fractions of LAC and MCC were employed in this thesis. CARB and MGST were on constant levels (see 5.2).

5.2 FORMULATIONS

5.2.1 Placebo composition - Chapter 4.1, 4.2 and 4.3

Table 15   Placebo composition – Chapter 4.1, 4.2 and 4.3

	MCC 2:1 LAC	**MCC 1:1 LAC**
Component	Content % (w/w)	Content % (w/w)
Microcrystalline cellulose	64.0	48.0
α−Lactosemonohydrate	32.0	48.0
Sodium carboxymethylcellulose	3.0	3.0
Magnesium stearate	1.0	1.0

MCC = Microcrystalline cellulose; LAC = α − Lactosemonohydrate

5.2.2 API composition - Chapter 4.4

Table 16   API composition (Metformin) – Chapter 4.4

	DL 21 % **(Target DL)**	**DL 27 %**	**DL 15 %**
Component	Content % (w/w)	Content % (w/w)	Content % (w/w)
Metformin hydrochloride	21.0	27.0	15.0
Microcrystalline cellulose	50.0	46.0	54.0
α−Lactosemonohydrate	25.0	23.0	27.0
Sodium carboxymethylcellulose	3.0	3.0	3.0
Magnesium stearate	1.0	1.0	1.0

DL = Drug load

5.2.3 Placebo composition- Chapter 4.5

Table 17   Placebo composition – Chapter 4.5

Mixture	#1 MCC 3:1 LAC	#2 MCC 2:1 LAC	#3 MCC 1:1 LAC	#4 MCC 1:3 LAC
Component	Content % (w/w)	Content % (w/w)	Content % (w/w)	Content % (w/w)
Microcrystalline cellulose	72.36	64.32	48.24	24.13
α–Lactosemonohydrate	24.12	32.16	48.24	72.37
Sodium carboxymethylcellulose	3.02	3.01	3.02	3.00
Magnesium stearate	0.50	0.50	0.50	0.50

MCC = Microcrystalline cellulose; LAC = α − Lactosemonohydrate

6. MANUFACTURING & ANALYTICAL METHODS

6.1 MANUFACTURING AND TECHNOLOGIES

Table 18   Overview experimental methods

Chapter	Equipment	Parameter	Material attribute
4.1	Material characterisation	-	True density, Particle size distribution, Bulk/Tapped density, Tabletability, Compressibility, Compactibility
4.1	MacroPactor	2, 4, 6, 8 kN/cm	Solid fraction ribbon: Throughput method, Mercury porosimetry, GeoPycnometer (GeoPyc)
4.2	MacroPactor / MiniPactor	2, 4, 6, 8 kN/cm	Particle size distribution, Solid fraction ribbon, Tabletability, Compressibility
4.3	MiniPactor	4.1, 7.0, 9.6, 11.4 kN/cm	Solid fraction ribbon, Particle size distribution, Particle appearance, Porosity granules, Tabletability, Compressibility
4.4	MacroPactor / MiniPactor	4, 5.1, 6, 8, 10 kN/cm	Solid fraction, Solid fraction distribution along roll width/ribbon length with near infrared reflectance
0	FlexiTab	50 – 350 MPa	Solid fraction tablet

Table 19   Manufacturing equipment

Name	Process	Manufacturer
Comil 196 U	Pre-Screening	Quadro Engineering Corp., Canada
Handscreen	Screening	Kressner, Germany
Tumbling blender	Blending	Servolift GmbH, Germany
Turbula blender	Blending	Turbula type 2A, Willy A. Bachofen AG Maschinenfabrik, Germany
MiniPactor	Dry granulation	Gerteis Maschinen + Process-engineering, Switzerland
M1075-GMP-Polygran® Walzenpresse	Dry granulation	Gerteis Maschinen + Process-engineering, Switzerland
Fette 1200	Tableting	Fette Compacting GmbH, Germany
Fette 1200i	Tableting	Fette Compacting GmbH, Germany
FlexiTab	Tableting	Röltgen GmbH & Co. KG, Germany

6.1.1 PREPARATION OF MIXTURES AND PROCESS FLOW CHARTS

6.1.1.1 Mixture for roller compaction

Table 20 Manufacturing flow chart: Mixture

Step	Equipment	Materials	Operation	In-process controls
1.0	Screening mill	Microcrystalline cellulose α – Lactose monohydrate Sodium carboxymethylcellulose Metformin hydrochloride	→ Pre-screening	Bulk/tapped density, PSD
			↓	
2.0	Freefall blender		Pre-blending	
			↓	
			Pre-blend	
3.0	Handscreen	Magnesium stearate	→ Screening	
			↓	
	Handmix	Equal weight parts of Pre-blend (Step 2.0)	→ Hand mix	
			↓	
			Hand screen-mix 0	
4.0	Freefall blender	Pre-blend (Step 2.0) Handscreen-mix 0 (Step 3.0)	→ Blending	
			↓	
			Dry-mix	Bulk/tapped density, Hausner ratio, PSD

117

Table 21   Process parameters: Mixture

Step	Process step	Description of manufacturing process	Process parameter
1.0	Pre-screening	Microcrystalline cellulose, α–Lactose monohydrate, Sodium carboxymethylcellulose and Metformin are prescreened with Comil 196U	Mesh size : 1.016 [mm] Rotations: 630 [rpm] Sieve: rasp
2.0	Pre-blending	Pre-screened is blended in freefall container blender	Time: 20:00 [min] Rotations: 10 [rpm] Bin: 1000L (190L Metformin)
3.0	Screening	Magnesium stearate is screened with a handscreen and then manually mixed with equal weight parts of Pre-blend	Mesh size: 1.000 [mm]
4.0	Blending	Pre-blend and Handscreen-mix is blended in freefall container blender	Time: 10:00 [min] Rotations: 10 [rpm] Bin: 1000L (190L Metformin)

Table 22   Batch size: Mixture

Composition	Name	Batch size [kg]	Total [kg]
Placebo	MCC 2:1 LAC	248.75	497.5
	MCC 1:1 LAC	248.75	
Metformin	MET 21	67.66	73.66
	27 % DL	3	
	15 % DL	3	

6.1.1.2   Chapter 4.2 and 4.3

Table 23   Manufacturing flow chart: Chapter 4.2 and 4.3

Step	Equipment	Materials	Operation	In-process controls
6.A	Roller compactor	Dry-mix (Step 4.0)	→ Dry compacting	Solid fraction ribbon
			↓ Milling	
			↓ *Granules*	Bulk/tapped density, PSD
7.A	Handscreen	Magnesium stearate	→ Screening	
	Handmix	Magnesium stearate with equal weight parts of granules (Step 6.A)	↓ → Hand mix	
			↓ *Hand screen-mix A*	
8.A	Freefall blender	Granules (Step 6.A) / Handscreen-mix A (Step 7.A)	→ Final blending	
			↓ *Final blend*	
9.A	Rotary tablet press	Final blend (Step 8.A)	→ Tableting	
			↓ *Tablet cores*	Tensile strength, solid fraction

Table 24   Process parameters: Chapter 4.2 and 4.3

Step	Process step	Description of manufacturing process	Process parameter
6.A	Dry compacting & milling	Dry-mix is compacted and the ribbons are directly milled by the roller compactor M1075-GMP-Polygran® and MiniPactor®	Ratio tamping auger/feeding auger: 160 [%] Roll speed: 2 [rpm] Automatic gap control: ON Gap size: 3 [mm] Granulator speed: 70 [rpm] Granulator angle: 360°/360° [cw/ccw] Sieve: 0.8 [mm], square Milling: Star rotor **Chapter 4.2:** Compaction force: 2, 4, 6, 8 [kN/cm] **Chapter 4.3 (Scale Model):** Compaction force: 4.1, 7.0, 9.6, 11.4 [kN/cm]
7.A	Screening	Magnesium stearate is screened with a handscreen and then manually mixed with equal weight parts of granules	Mesh size: 1.000 [mm]
8.A	Final blending	Granules and handscreen-mix A are blended in freefall container blender	Time: 10:00 [min] Rotations: 10 [rpm] Bin: 40L
9.A	Tableting	Final blend is compressed into tablet cores with a rotary press	Compression force: 3, 5, 7, 9, 11, 13, 15 [kN], RSD ≈5 % Pre-compression force: 0 [kN] Compression speed: 80.000 [tbl/h] Punch size: 8 [mm], round convex punches, bevelled edges Target weight: 220 [mg]

Table 25   Batch size: Chapter 4.2 and 4.3

Composition	Name	Batch size [kg]	Total [kg]
Placebo	MCC 2:1 LAC	10 (each kN/cm)	240
	MCC 1:1 LAC	10 (each kN/cm)	
	Scale Model	10 (each kN/cm)	

Table 26   Manufacturing flow chart: Chapter 4.2: Comparison milling process

Step	Equipment	Materials		Operation	In-process controls
6.B	Single punch press	Dry-mix (Step 4.0)	→	Tableting	
				↓	
				Tablet cores	Solid fraction
7.B	Roller compactor	Tablet cores (Step 6.B)	→	Milling	
				↓	
				Granules	PSD
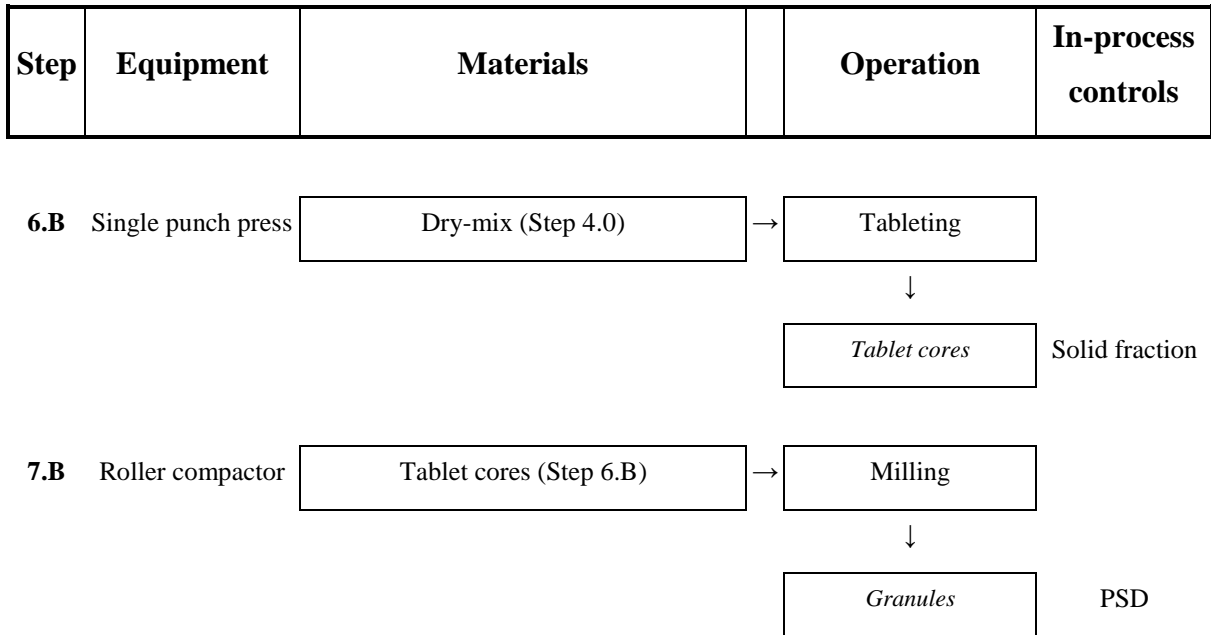
Table 27   Process parameters: Chapter 4.2: Comparison milling process

Step	Process step	Description of manufacturing process	Process parameter
6.B	Tableting	Dry-mix is compressed into tablet cores with a single punch press	Compression force: is defined by target SF Target SF : MCC 2:1 LAC : 0.62 (6.5 kN), 0.77 (16.0 kN) MCC 1:1 LAC: 0.64 (6.7 kN), 0.79 (18.0 kN) Punch size: 16 [mm], round and biplane Target weight: 600 [mg] Feeder: ON Automatic lubrication: press chamber coating system ON, every ten tablets
7.B	Milling	Tablets are milled within one hour by roller compactor´s granulator M1075-GMP-Polygran® and MiniPactor®	Granulator angle: 360°/360° [cw/ccw] Sieve: 0.8 [mm], square Milling: Star rotor

Table 28   Batch size: Comparison milling process

Composition	Name	Batch size [kg]	Total [kg]
Placebo	MCC 2:1 LAC	1.2 (each SF, 2000 tablets)	4.8
	MCC 1:1 LAC	1.2 (each SF, 2000 tablets)	

Table 29   Manufacturing flow chart: Chapter 4.3: Porosity granules

Step	Equipment	Materials		Operation	In-process controls
6.C	Sieving	Granules (Step 6.A)	→	Sieving	
				↓	
				Sieve fractions granules (90µm, 180µm, 250µm)	Mercury porosimetry

Table 30   Process parameters: Chapter 4.3: Porosity granules

Step	Process step	Description of manufacturing process	Process parameter
6.C	Sieving	Granules are separated by sieve analysis	Time: 10 min Amplitude: 2 mm Interval time: 10 s Sieve fraction of 90µm, 180µm, 250µm

6.1.1.3 Chapter 4.4

Table 31 Manufacturing flow chart: Chapter 4.4

Step	Equipment	Materials		Operation	In-process controls
6.D	Roller compactor	Dry-mix (Step 4.0) (Metformin composition)	→	Dry compacting	Solid fraction ribbon (GeoPyc, NIR)
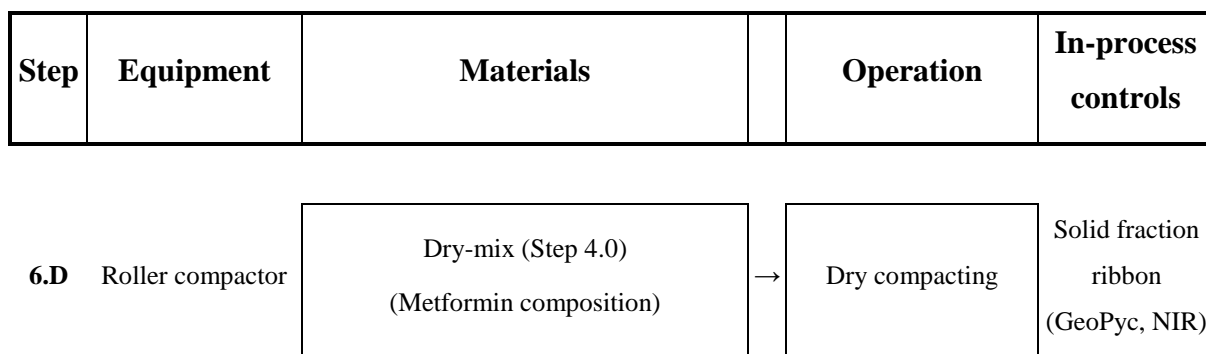
Table 32 Process Parameters Chapter 4.4

Step	Process step	Description of manufacturing process	Process parameter
6.D	Dry compacting & milling	Dry-mix is dry compacted and the ribbons directly milled by the roller compactor M1075-GMP-Polygran® and MiniPactor®	Ratio tamping auger/fedding auger: 160 [%] Roll speed: 2 [rpm] Automatic gap control: ON Gap size: 3 [mm] Granulator speed: 70 [rpm] Granulator angle: 360°/360° [cw/ccw] Sieve: 0.8 [mm], square Milling: Star rotor **Specific compaction force:** 4, 6, 8, 10 [kN/cm] **Scale up:** Large scale: 5.1 [kN/cm]

Table 33 Batch size: Chapter 4.4

Composition	Name	Batch size [kg]	Total [kg]
Placebo	MET 21	5 (each kN/cm)	51
	27 % DL	3	
	15 % DL	3	

6.1.1.4   Chapter 4.5

Table 34   Manufacturing flow chart: Chapter 4.5

Step	Equipment	Materials		Operation	In-process controls
I	Turbula blender	Microcrystalline cellulose α − Lactose monohydrate Sodium carboxymethylcellulose	→	Blending	
				↓	
				Pre-blend	
II	Handscreen	Magnesium stearate	→	Screening	
				↓	
	Handmix	Equal weight parts of Pre-blend (Step I)	→	Hand mix	
				↓	
				Hand screen-mix	
III	Freefall blender	Pre-blend (Step I) Handscreen-mix (Step II)	→	Blending	
				↓	
				Dry-mix	
IV	Single punch press	Dry-mix (Step III)	→	Tableting	
				↓	
				Tablet cores	Solid fraction

Table 35   Process parameters: Chapter 4.5

Step	Process step	Description of manufacturing process	Process parameter
I	Pre-blending	Material is blended in turbula blender	Time: 03:00 [min] Rotations: 50 [rpm] Bin: 2L
II	Screening	Magnesium stearate is screened with a handscreen and then manually mixed with equal weight parts of Pre-blend	Mesh size: 1.000 [mm]
III	Blending	Pre-blend and handscreen-mix is blended in a turbula blender	Time: 05:00 [min] Rotations: 50 [rpm] Bin: 2L
IV	Tableting	Dry-mix is compressed into tablet cores with a single punch press	Compression force: 4, 8, 12, 16, 20, 24, 28 [kN] Punch size: 10 [mm], round and biplane Target weight: 200 [mg]

Table 36   Batch size: Chapter 4.5

Composition	Name	Batch size [kg]	Total [kg]
Placebo	MCC 3:1 LAC	0.5	2
	MCC 2:1 LAC	0.5	
	MCC 1:1 LAC	0.5	
	MCC 1:3 LAC	0.5	

6.2   ANALYTICAL METHODS

Table 37   Analytical equipment

Name	Sample	Attribute	Manufacturer
AccuPyc II	Raw material, Unprocessed blends	True density	Micromeritics Instrument Corporation, USA
Stampf-Volumeter PT-TD1 + Engelsmann STAV II	Raw material, granules	Bulk/Tapped density	Stampf-Volumeter PT-TD1, Pharma Test Apparatebau GmbH, Germany
Retsch AS 200 control	Raw material, granules	Particle size distribution	Retsch GmbH, Germany
Pascal 140-240/440	Granules, ribbons	Porosity (mercury), Solid fraction	Thermo Fisher Scientific, USA
Keyence VHX 5000 (VH-Z20R/Z20T)	Granules	Mircroscopy	Keyence Deutschland GmbH, Germany
GeoPycnometer (GeoPyc1360)	Ribbons	Solid fraction	Micromeritics Instrument Corporation, USA
Bruker Multi-Purpose Analyzer (MPA), Fourier Transform, Detector RT-InGaAs	Ribbons	Near infrared spectroscopy	Bruker Optics, Germany
Micrometer screw	Ribbons	Micrometer screw	MIB – Messzeuge GmbH, Germany
AT400	Tablets	Weight	Mettler-Toledo GmbH, Germany
Erweka TBH 310 MD	Tablets	Geometry tablets, weight, breaking force	Erweka GmbH, Germany
FlexiTab	Raw material, Unprocessed blends, granules	Compression analysis	Röltgen GmbH & Co. KG, Germany
Erweka TBH 310 MD	Tablets	Geometry tablets, breaking force	Erweka GmbH, Germany
Kraemer UTS 12 F	Tablets	Geometry tablets, weight, breaking force	Kraemer Elektronik GmbH, Germany

Table 38   Software and data processing

Data	Name
In die data (Compressibility)	Data Acquisition System DAQ4, Dr. M. Hucke
General data evaluation and figures	Spotfire Version 7.5.1.8, Tibco® Software Inc., USA
Polynom fitting	Excel, Microsoft® Office Professional Plus 2010
Power calculation	G*Power Statistical Power Analyses Version 3.1.9.2
Contour plots and figures	Statistica Version 12®, StatSoft GmbH, Germany
T-Test, ANOVA	Statistica Version 12®, StatSoft GmbH, Germany
Spectra and near infrared reflectance method development	OPUS version 7.2®, Bruker Optik GmbH, Germany
Data fitting Chapter 4.5	OriginPro 8G®, OriginLab Corporation, USA

6.2.1 Raw material and granules

6.2.1.1 True density

True density of all excipients and blends was measured by a helium gas pycnometer (AccuPyc II, Micromeritics Instrument Corporation, USA), the helium penetrated into the voids between particles or intragranular voids. The displaced volume determined solids' volume. A blank measurement of the chamber was previously performed ($\approx$9.2 cm³). Afterwards metal spheres calibrated the amount of displaced helium. Temperature was controlled to guarantee same analysis conditions. Fill pressure was set to 19.5 psig with an equilibration rate of 0.005 psig/min. 10 fill purges resulted in one mean value for the true density.

6.2.1.2 Bulk/Tapped density

Bulk and tapped density of powders and granules measured in a 250 ml cylinder (Engelsmann STAV II). A mass of 100 g was filled into the cylinder. The volume for the bulk density was determined. Afterwards taps of 10, 500, 1250, 2500 were used (Stampf-Volumeter PT-TD1) to determine the tapped volume. Bulk, tapped density and Hausner ratio were calculated according to United States Pharmacopeia (USP) [16].

6.2.1.3 Particle size distribution

Particle size distribution of powders and granules were performed in triplicate by sieve analysis. Sieve analyses was performed with a sieve tower, which comprised sieves of 63, 90, 125, 180, 250, 355, 500, 630, 710 and 1000 µm mesh size. Analysis time was 10 min with an amplitude of 2 mm and an interval time of 10 seconds (Retsch AS 200 control). Retained mass on each sieve was determined by an analytical mass balance. Sample size was 100 g (n = 3). The total amount passed [%] of the sample was calculated for each sieve and plotted versus the mesh size for a detailed analyses. d_{50} represents the cumulative mean particle size calculated by Retsch AS 200 according to USP [16].

6.2.1.4 Mercury porosimetry

Mercury intrusion-porosimetry is the method of choice to measure the porosity of solids. Mercury is a non-wetting-liquid for the most solids because it has a high surface tension and a high contact angle of over 90° on solids [131]. Without an external pressure mercury cannot intrude into pores. Washburn (1921) [132] derived an equation, where he stated that a capillary has a cylindrical pore. The force of the capillary which prevents the intrusion of the liquid is dependent of the surface tension of the liquid, the angle of contact with the solid and the length of the area of contact between liquid and the surface of solid, which can be defined by 2*π*radius of the pore.

$$Counteracting\ force\ capillary = 2 * \pi * r * y * cos\ (\theta) \qquad \text{Eq. (18)}$$

The force required to enter the pore can be defined as:

$$External\ P = \frac{F}{area} \qquad \text{Eq. (19)}$$

$$External\ F = \pi * r2 * P \qquad \text{Eq. (20)}$$

If are both in equilibrium Eq. (19) and Eq. (20)

$$2 * \pi * r * y * cos\ (\theta) = \pi * r^2 * P \qquad \text{Eq. (21)}$$

This shows that pore radius is inversely proportional to the applied pressure

$$r = \frac{-2*y*cos(\theta)}{P} \qquad \text{Eq. (22)}$$

r = radius, y = surface tension (liquid), $cos\ (\theta)$ = angle [°] of contact, F = Force, P = Pressure

A capacitive sensor measured the intruded volume of mercury during increasing pressure, whereby the intruded volume of mercury per sample (relative volume mm³/g) correlates with pore size distribution.

$$Relative\ volume\ (mm^3/g)\ =\ \frac{Intruded\ mercury\ volume\ at\ radius\ (mm^3)}{Sample\ mass\ (g)}\qquad\text{Eq. (23)}$$

Calculations were performed using Win-Pascal Software Vers. 1.05 with a contact angle of 140° and a surface tension of 0.48 N/m. Low pressure porosimetry was performed with a Pascal 140 (0 – 400 kPa) and high pressure porosimetry with a Pascal 400 (max. 400 MPa). Pressure increased after the intruded mercury achieved an equilibration (0.08 – 0.32 kPa/sec). The dilatometer was first evacuated to 0.01 kPa (≈ 73540 µm) and then filled by mercury. Afterwards the pressure was increased to 400 MPa (≈ 1.8 nm).
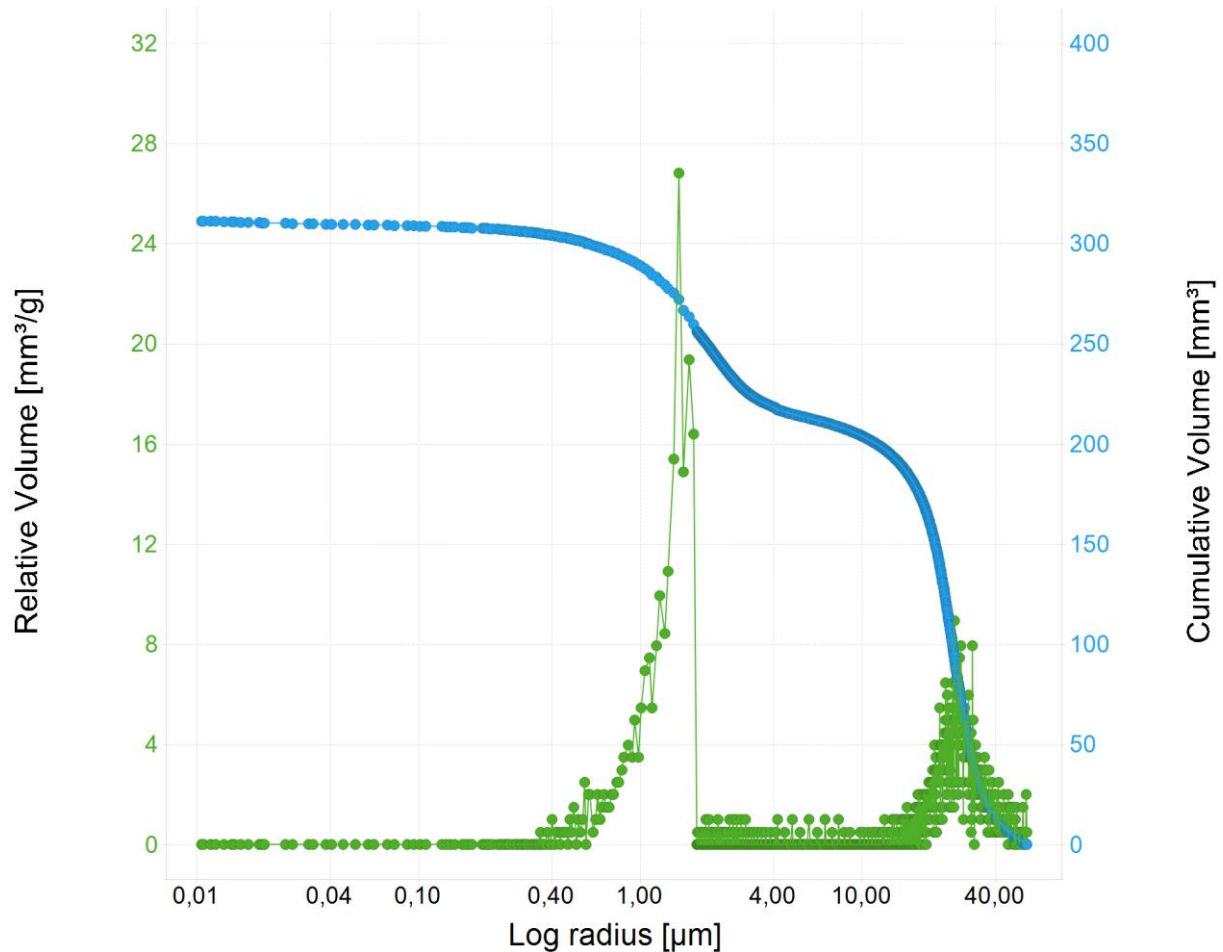
Figure 66   Mercury porosimetry of granule sieve fraction – Example 90 µm

The granules were divided into sieve fraction of 90, 180 and 250 µm by sieve analyses. Sample size of the granules was about 0.2 g (n = 1). Two different pore size distributions could be observed over the whole range of radius (pressure range) for all sieve fraction, which can be attributed to intergranular pores between particles and intragranular pores of particles (Figure 66) [110,111]. Intergranular pores have been found at a higher radius and intragranular pores in the region of 0.4 µm – 1.8 µm. Thus cumulative sum of the relative volume (mm³/g) of the intruded mercury in low radius region was used to compare the porosity between the granules.

6.2.1.5   Compression analysis

Excipients, blends and granules were tableted by a single punch press (FlexiTab). FlexiTab provides the possibility to adjust the dwell time, punch velocity and compression pressure independent of tablet height or mass. Bi-plan punches with a 10 mm diameter were used. Die filling was done manually with 300 mg of mass for "in-die" compressibility plots (n = 3) and 200 mg for tabletability and compactibility plots. For "in-die" measurements, FlexiTab was equipped with a force displacement system containing an incremental position sensor and strain gauges. The force displacement system was corrected to account for an elastic deformation of the punch with 0.0033 mm/kN and an offset of 0.0148 mm. For details the reader is referred to Verena Maria Gläßer (2008). Data acquisition was done by DAQ4 (Hucke Software, Solingen, Germany) and data transformation by Tibco Spotfire (Tibco Software Inc.). The switching threshold from pneumatic to hydraulic pressure was set to 1.2 kN ($\approx$ 15 MPa). Pressure range for "in-die" measurement was 0 – 235 MPa and for "out-of-die" 50 – 350 MPa. Filling depth was constant at 8.5 mm. Tablets were weighed directly after ejection by analytical balance. "Out-of-die" tablets were determined directly after ejection by an automatic tablet tester to calculate the solid fraction (n = 6) and the tensile strength (n = 3). Compression settings are depicted in Table 39.

Table 39   Process parameter – FlexiTab – Tableting profile

Upper Punch (downwards) % of maximal Pressure		Upper punch (upwards) % of maximal Pressure	
20 %	Dwell time 50ms		80 %
20 %			
90 %	16,2 KN		80 %
15 %	7,13 KN		100 %
Switching threshold from pneumatic to hydraulic pressure 1.2 kN			

6.2.1.5.1   Heckel equation determination

Heckel equation is often used to classify materials by compression behaviour [56]. It is assumed that the densification process follows a first-order law. The course of the densification process is divided in three phases (Phase1: particle rearrangement, fragmentation; Phase 2: plastic deformation; Phase 3: elastic recovery, decompression) [63]. The Yield pressure is determined in phase 2 (plastic deformation) and indicates if a material undergoes plastic deformation (low Yield pressure equal to high compressibility). Calculating the Yield pressure is done by applying a linear regression model at a predefined pressure range to determine it by 1/slope. Resulting intercept *A* of the linear regression can be seen as index for particle rearrangement.
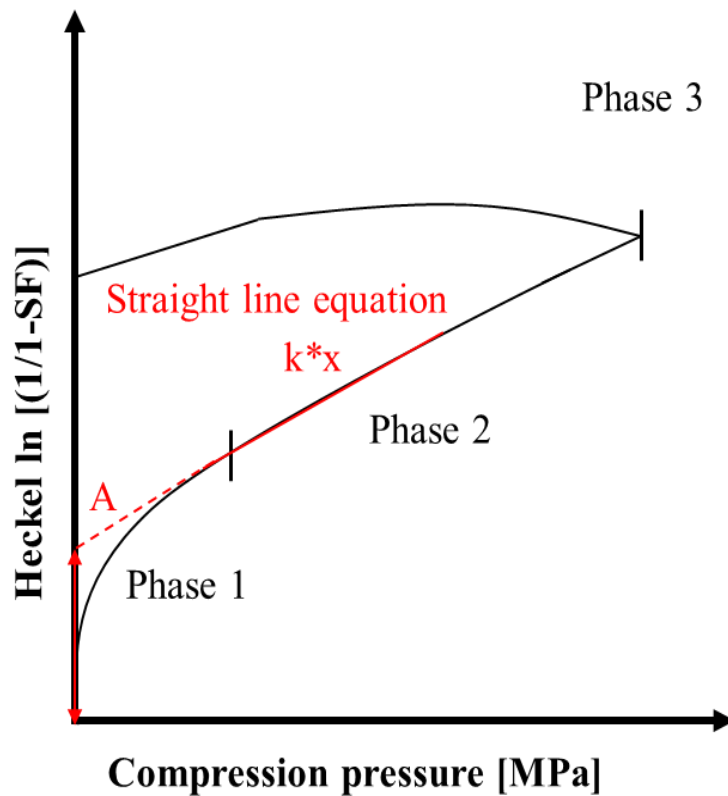
Figure 67   Schematic Heckel plot [63]

$$\text{Heckel} = \ln\left(\frac{1}{1 - Solid\ fraction}\ or\ \frac{1}{\varepsilon}\right) = k * P + A \ [61] \qquad \text{Eq. (24)}$$

$$\text{Yield pressure}\ (P_y) = \frac{1}{k} \qquad \text{Eq. (25)}$$

For linear regression a defined pressure range was chosen depending on a normal operating pressure (unprocessed materials 20 MPa – 120 MPa, granules 120 MPa – 160 MPa).

6.2.2   Ribbon – Solid fraction

6.2.2.1   Throughput method

Different authors have described the calculation of the solid fraction of ribbons by weighing the throughput of the granules [5,26] or the weight of ribbons [27,34]. For comparison all described formulas were adapted by replacement of ribbon´s weight with granule´s weight (Peter (2010) [27], Nkansah et al. (2008) [34]).

For this purpose, the complete granule throughput was collected five times for 5 min over different time intervals after reaching constant gap (steady state).

Herting et al. (2007) [26]:

$$Volume_{ribbon} = \pi * d_{rolls} * w_{rolls} * v_{rolls} * gap * t \qquad \text{Eq. (26)}$$

d_{rolls} = diameter rolls [cm], w_{rolls} = width rolls [cm], v_{rolls} = velocity rolls [rpm], gap= gap [cm], t = production time [min]

Nkansah et al. (2008) [34] modified this formula by adding the surface of the rolls and substituted the gap by height measurements of the ribbons with a micrometer screw:

$$Volume_{ribbon} = \pi * d_{rolls} * w_{rolls} * v_{rolls} * height_{ribbon} * t \pm void_{surface} \quad \text{Eq. (27)}$$

voids$_{surface}$ = knurled Gerteis®: 50 mm width 2.946 cm³, 25 mm width 1.473 cm³

Gamble et al. (2010) modified the formula of Herting for collecting the weight of granules:

$$Volume_{ribbon} \pm (void_{surface} * (\pi * d_{rolls} * v_{rolls} * \frac{t}{gap})) \qquad \text{Eq. (28)}$$

Peter (2010) [27]:

$$Volume_{ribbon} = (\pi * (d_{rolls} + \frac{gap}{2})) * v_{rolls} * (gap * w_{rolls}) \qquad \text{Eq. (29)}$$

Solid fraction was calculated according to Eq. (30):

$$Solid\ fraction_{ribbon=} \frac{(mass_{granules}\ [g] * \frac{t}{volume_{ribbon}[cm^3]})}{true\ density\ [\frac{g}{cm^3}]} \qquad \text{Eq. (30)}$$

6.2.2.2 Mercury porosimetry

Win-Pascal Software Vers. 1.05 was applied to calculate the volume of a ribbon with an contact angle of 140° and a surface tension of 0.48 N/m (see 6.2.1.4). Pressure increased till an equilibration of the intruded mercury was achieved (0.08 – 0.32 kPa/sec). The dilatometer was first evacuated to 0.01 kPa ($\approx$ 73540 µm) and then filled by mercury. Afterwards the pressure increased to 0.150 MPa (pore radius $\approx$ 4.90µm), as a result only the cracks of the surface of the ribbons were filled and the mercury surrounded the surface of the ribbon. Differences between chamber volume and filled dilatometer with mercury and ribbon allowed to calculate the solid fraction of the ribbon (see Eq. (1)). Ribbons were cut into two pieces of 25 mm width and 10 mm length to fit into the dilatometer (n = 3).

6.2.2.3   GeoPycnometer

Solid fraction measurements were carried out using a GeoPycnometer 1360 which is based on the principle of volume displacement [17]. The principle, is that the irregularly shaped sample is surrounded by a graphite powder (Dry Flo) with good flowability. The result is the displaced volume by the sample ribbon, which allows calculating the solid fraction.

Figure 68   GeoPyc1360® – Micromeritics Instrument Corporation

Ribbons were measured in a rotating cylindrical vessel, whereby a plunger is pushed through the vessel and a densification takes place until a specified force is gained. The GeoPynometer calculated the volume increase by a comparison of step 2 and step 3 (see Figure 69).
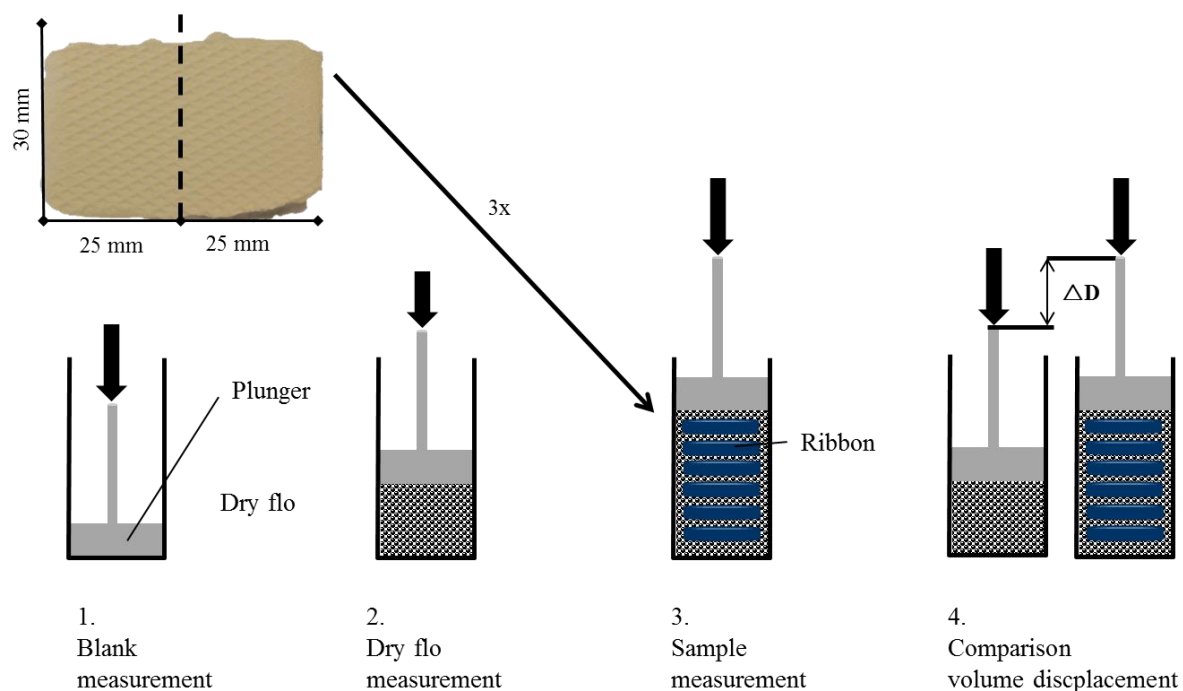
Figure 69   GeoPycnometry – Process of measurement

Afterwards the solid fraction of the ribbons is calculated by dividing the weight by the corresponding volume, which represents $\rho_{Aparent\ density}$ (see Eq. (1)). Ribbons were cut into 6 rectangular pieces of 25 mm* 30 mm (width / length) in order to fit into the sample cup (diameter 38.1 mm). Five samples, each containing 6 pieces, for each specific compaction force, were analysed in a measurement cycle of 6 with a plunger force of 38 N. This method was used throughout this thesis, except stated otherwise.

6.2.2.4   Near infrared spectroscopy

Infrared spectroscopy can be classified into near infrared, mid infrared and far infrared spectroscopy. Near infrared (NIR) spectroscopy is a nondestructive spectroscopic analytical technique. In a wavelength range of 800 nm to 2500 nm, corresponding to a wavenumber of about 4000 – 12500 cm^{-1}, absorption of the electromagnetic radiation by molecules occurs. This absorption results in uptake of specific energy, which results to vibrations of chemical bonds due to overtones and combination vibrations of C-H, O-H and N-H functional groups [134–136]. Therefore, NIR spectroscopy is also called vibrational spectroscopy. Overtones vibrations can be described by the anharmonic oscillator model as a transition over multiple energy levels e.g. from ground stage to a second level occurs. Therefore, these vibrations are called overtones. In contrast to that, the harmonic oscillator model for fundamental vibrations is described as transition from one level to the next level [134–136]. Combination vibrations represent these sums of multiple fundamental vibrations in a NIR spectrum, which are more intense compared to overtones. The induced overtone and combination vibrations can overlap resulting in broad peaks in a NIR spectrum. Mathematical techniques (chemometrics) like multivariate data analysis, principal component analysis (PCA) and partial least square analysis (PLS) [137–139] are used to investigate chemical information or physical information. For both properties quantative models can be developed based on a correlation between concentration of the sample and proportional change of the NIR spectra. Various authors demonstrated a correlation between NIR spectra to an upcoming physical property change like particle size distribution of granules [20,38], hardness/porosity of tablets [119–121] or solid fraction of ribbons [32,38,122,140]. Thus, NIR can be used to investigate the solid fraction distribution along the roll width between different scales. Process flow of NIR method development is depicted in Figure 70.
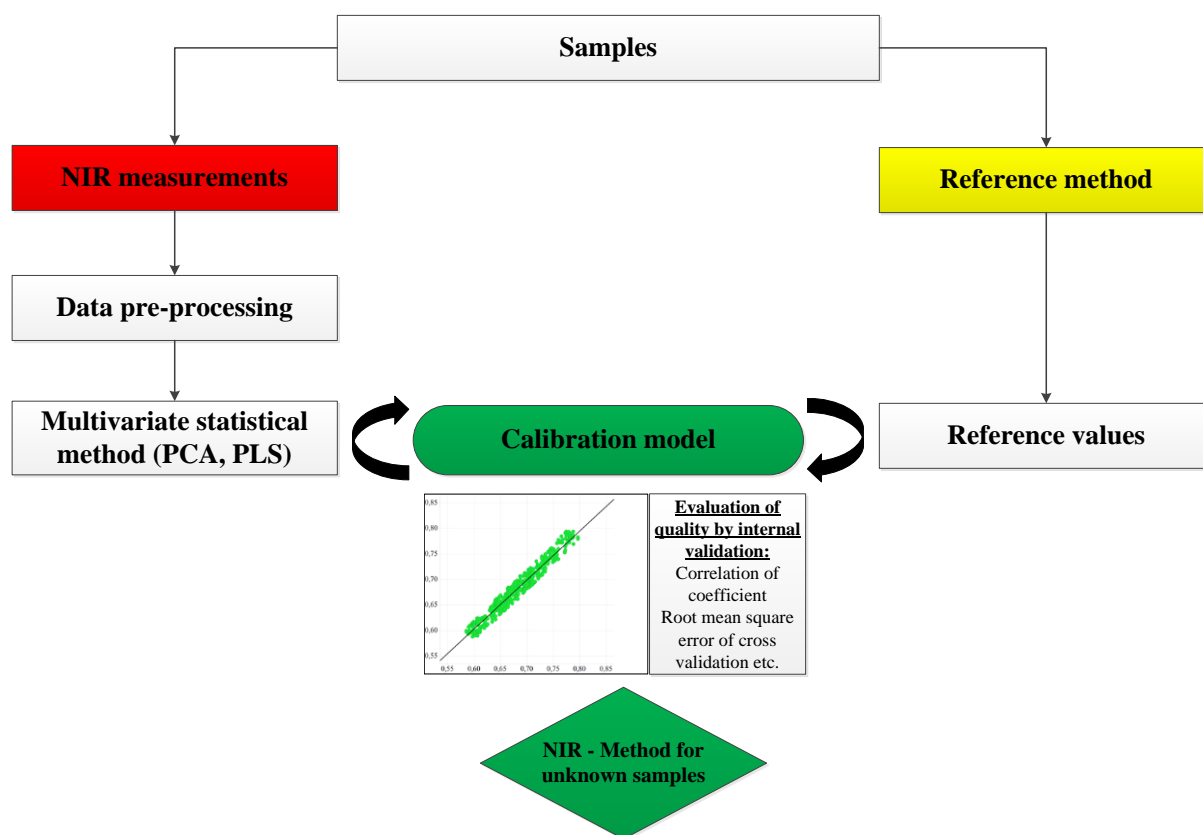
Figure 70   Process flow – NIR method development

A Fourier-transform NIR spectrometer (Bruker Multi-Purpose Analyzer MPA) equipped with a fibre optic probe for measurements in diffuse reflection mode was used, which provides a high precision, accuracy of wavelength measurements and a high scan speed [135,136]. Treatment of acquired spectra was done with OPUS version 7.2.

Diffuse reflection is defined as the ratio of the radiation reflected (*I*) by the sample compared to the reflection of a reference surface (*I₀*) (Reflection = I/I_0, Absorption = -log (Reflection)) [134,141]. Reflection of the radiation decreases due to fewer boundaries between air and solids (high solid fraction). Thus, if the solid fraction is high the absorption will increase and less diffuse reflection is detected [142]. A schematic representation of the NIR radiation and corresponding reflection of the ribbons, characterised by a different solid fraction, is depicted in Figure 71.

Low solid fraction

High solid fraction
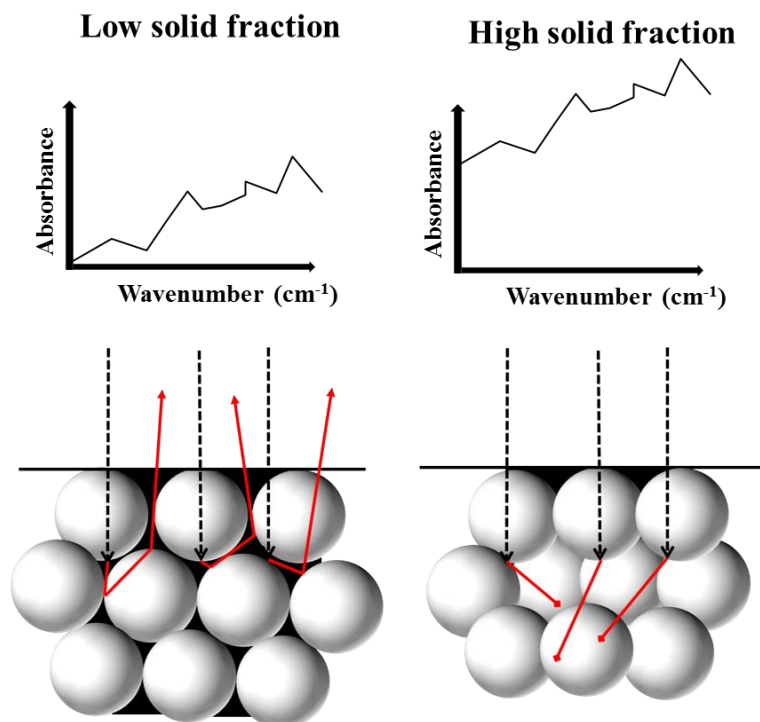
Figure 71   Schematic drawing - NIR and solid fraction

6.2.2.4.1   Principal component analysis (PCA) and Partial least square analysis (PLS)

Principal component analysis (PCA) allows extracting the relevant information out of the spectra and gives the opportunity to develop a broader overview of the spectra. Thus, plenty amount of data can be condensed [139,141]. Observed variables (original data) are converted to a three-dimensional space [139]. A linear regression is performed to describe the transformed data, which results into principal components or factors. The main effect, which explains the highest variance of the data, is defined as the first factor. Higher ranked factors explain less variance of the data. These factors are described in multi-dimensional factor space, which leads to a score system of coordinates and enables an interpretation of the observed variance of the spectra [134]. Partial least square (PLS) analysis allows quantifying the correlation between observed variance of spectra and the provided properties (reference

values) [134]. Thus, PCA represents an investigation of factors determining the variance between various spectra, whereby PLS allows correlating the variance of the different spectra to the observed reference values (e.g., the solid fraction).

6.2.2.4.2   Data transformation

Data pre-processing techniques for NIR spectra are applied for solid samples to minimize systematic variations caused by interfering light scattering (noisy signal), impact of measuring setups or sample conditions (see 4.4.1.2.1) [124]. A first derivation was used and calculated by Savitzky-Golay algorithm by using polynomial fitting over 9 smoothing steps (smoothing filter) [141].

6.2.3   Tablet

The properties of tablets were measured 48h after production unless stated otherwise. Geometry and mass of the tablets were obtained by using an automatic tablet tester (Kraemer UTS 12 F) and an analytic balance (± 1 mg), respectively.

6.2.3.1   Tensile strength

Tensile strength considers the tablet dimensions and is the normalized breaking force independent of tablet shape. Calculations were done according to USP [16].

$$Tensile\ strength\ (TS) = \frac{10*F}{\pi*D^2} * \left[\frac{2.84*h}{D} - \frac{0.126*h}{W} + \frac{3.15*W}{D} + 0.01\right]^{-1} \qquad \text{Eq. (31)}$$

F = breaking force [N]; D = diameter [cm]; h = height [cm]; W = central cylinder thickness [cm]

6.2.3.1.1   Reworkability index

An adapted reworkability index was used, which was first introduced by Herting et al. (2007), to illustrate the loss of tensile strength after roller compaction:

$$Tensile\ strength_{ratio} = \frac{TS_{granule}}{TS_{powder(0\ kN/cm)}}[26] \qquad \text{Eq. (32)}$$

Adaption for seven compression pressures:

$$TS_{ratio}\% = \frac{1}{n}\sum_{i=1}^{n} = \left(\frac{TS_{ratio\ 60MPa} + TS_{ratio\ 100\ MPa}\ldots + TS_{ratio\ 300\ MPa}}{n}\right) * 100 \qquad \text{Eq. (33)}$$

6.2.3.2   Solid fraction

Solid fraction of tablets was calculated according to Eq. (34):

$$Solid\ fraction = \frac{\rho_{APP}}{\rho_{TRUE}} = \frac{\frac{m\,[g]}{V_P[cm^3]}}{\rho_{TRUE}\left[\frac{g}{cm^3}\right]} \qquad \text{Eq. (34)}$$

Volume round biplane tablet:

$$V_P = \pi * \left(\frac{D}{4}\right)^2 * h \qquad \text{Eq. (35)}$$

Volume round convex tablet:

$$V_P = 2 * \left[\frac{1}{3} * \pi * (h_c)^2 * (3 * c_r) - h_c\right] + \left(\pi * \left(\frac{D}{4}\right)^2 * W\right) \qquad \text{Eq. (36)}$$

ρ_{APP} = apparent density [g/cm³]; ρ_{TRUE} = true density [g/cm³]

V_P = volume at applied pressure [cm³]; D = diameter [cm]; h = height [cm]; m = mass [g]; h_c = height calotte [cm]; c_r = curvature radius; W = central cylinder thickness [cm]
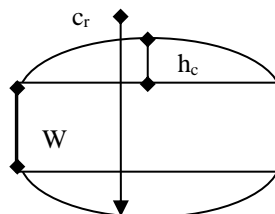
7.   SUMMARY

Granulation processes for solid oral dosage forms are commonly used in the pharmaceutical industry to enhance the quality of the final product, i.e. tablets. Today, roller compaction is one of the most common granulation techniques for solid oral dosage forms as it provides advantages like simple operation, due to integrated process control mechanisms, suitability for water- or heat-sensitive APIs and opportunity for an implementation in a continuous manufacturing process. Although roller compaction was intensively investigated, the impact of upscaling from a small to a larger roller compactor or vice versa is not fully understood.

To account for this knowledge gap, in this thesis the effect of a scale up on the quality attributes of intermediate- and final products, was investigated. Therefore, the controversially discussed topic of reduced tabletability of roller compacted granules caused by work hardening phenomena, particle size enlargement effect, porosity of granules and lubricant sensitivity was investigated. Two formulations, one predominantly plastic deforming and the other predominantly brittle deforming, were used. Both had been previously characterised in respect to their compressibility, tabletability and compactibility and processed at both scales to differentiate between material and scale dependent effects on the intermediate- and final product. Finally, a successful scale up strategy was developed to achieve the same product quality for all scales.

Solid fraction of the ribbons is well known as key intermediate critical quality attribute for downstream processing of a roller compaction process. Different established analytical methods were compared for the measurement of the solid fraction of ribbons. The GeoPycnometer method (volume displacement) turned out as the most reliable and most robust method.

Subsequently, both formulations were dry granulated at both scales with equal process settings. A higher solid fraction of the ribbons was obtained for both formulations at the larger scale. For the predominantly plastic deforming formulation the particle size distribution of the granules was similar for both scales, resulting in a lower tensile strength of the tablets of the large scale, which was mainly impacted by the work hardening effect and sensitivity towards lubricant. The increased solid fraction of the ribbon produced by the large scale compared to the small scale correlated with a lower tensile strength of the tablets. In contrast, negligible differences of the tensile strength of the tablets between both scales were observed for the predominantly brittle deforming formulation, although the particle size distribution of the

granules differed at higher specific compaction forces of the large scale. This was driven by the impact of the brittle deforming component, which enhances the fracturing behaviour of the granules and resulted in a negligible susceptibility towards work hardening, lubricant and particle size enlargement effect. In conclusion, even though differences existed between ribbons produced at both scales, these could be balanced if the formulation contains a high proportion of a brittle component. This strategy will allow enhancing the robustness of the scalability of the process and the final product quality.

Previously it was demonstrated that a different solid fraction of the ribbon resulted in a different tensile strength of the tablets between scales for the predominantly plastic formulation. This formulation however, is commonly used to counteract the main disadvantage of the roller compaction; the reduced tabletability of granules of tablets (loss of tensile strength). To account for this, a new approach (Scale Model) was developed for the predominantly plastic formulation to achieve the same solid fraction of the ribbon at both scales. Same solid fraction at both scales resulted in a same porosity of the granules, compressibility and tensile strength of the tablets, although a different particle size distribution of the granules was obtained. This demonstrated that the particle size distribution of granules should not to be considered as the main intermediate quality attribute to achieve a successful scale up for a roller compaction process, because the porosity and the compressibility of the granules defining the microstructure of a tablet during tableting and subsequently the resulting tensile strength of the tablets. The Scale Model approach demonstrated a practicable solution for the pharmaceutical industry to scale the process from small development batches to commercial batches and still achieve equal quality of the tablets.

In order to investigate the observed higher solid fraction at the large scale at equal process settings for both scales a new analytical method via NIR was developed to measure the solid fraction distribution along the roll width. It was possible to predict the solid fraction of unknown samples by acquiring the NIR spectra comprising reduction of analysis time compared to the GeoPycnometer method, which measured the "total" solid fraction of the ribbon. The effect of the cheek plates (lower solid fraction at the edges) decreased with increased distance to the cheek plates, which was especially the case for the larger scale with a broader roll width. This led to a higher "total" solid fraction of the ribbons produced by the large scale compared to the small scale at equal process settings. These results explained the previously observed different quality attributes of intermediate- and final products. The proposed scale up approach showed that the differences of resulting granules and tablets

between scales can be balanced for a predominantly plastic deforming formulation through the adaption of the specific compaction force. Thus, adapting the specific compaction force by measurements of the "total" solid fraction (GeoPycnometer) is a suitable scale up strategy for a roller compaction process.

Moreover, the solid fraction of a tablet (compressibility) was an important impact factor, which reinforced the development of theoretical models to predict the solid fraction for unknown powder mixtures based on single component compression analysis. A new theoretical developed Percolation and a modified Kawakita model were evaluated for model application. An exponential model was added to elucidate whether the two-parametrised models with theoretical background are superior in terms of predictability of solid fraction compared to a model without parametrised variables. Four mixtures were compressed over a wide pressure range at various fractions of a plastic and brittle deforming component. Based on single compression analysis of the pure excipients and application of these models, it was possible to predict the solid fraction of all mixtures. The Kawakita model showed overall superior prediction accuracy, whereas the Percolation model resulted in the best fit for mixtures containing the plastic deforming component in a range of 72%–48%. Both models were in good agreement at residuals below 3%. The prediction could serve as a systematic guidance for the formulator to select appropriate excipients depending on the active pharmaceutical ingredient to build quality into the drug product according to the Quality by Design approach.

In summary, this thesis provides a new profound knowledge and an appropriate guidance for the scale up of a roller compaction process. An effect of a scale up of a roller compaction process on the quality attributes of intermediate- and final products was demonstrated. This effect can be balanced by applying the proposed scale up strategy or by diminishing the formulation susceptibility to scale dependent effects with an increased proportion of a predominantly brittle deforming component in the formulation.

8. APPENDIX

8.1 ANALYTIC DATA

8.1.1 CHAPTER 4.1 MATERIAL ATTRIBUTES AND METHOD COMPARISON FOR SOLID FRACTION MEASUREMENTS OF RIBBONS

4.1.2 Formulation impact on the solid fraction within one scale

Mean height ribbon (Nkansah et al. (2008), micrometer screw):

Specific compaction force [kN/cm]	Gap [mm]	Mean height ribbon [mm] ± SD
2	3	3.585 ± 0.027
4	3	3.798 ± 0.047
6	3	3.790 ± 0.047
8	3	3.806 ± 0.022

SD = Standard deviation of mean

8.1.2 CHAPTER 4.2 COMPARISON OF TWO ROLLER COMPACTORS OF DIFFERENT SCALE AT SAME PROCESS

4.2.3 Particle size distribution of granules

Granule attributes (MacroPactor):

Specific compaction force [kN/cm]	MCC 2:1 LAC			MCC 1:1 LAC		
	d_{50} [µm] $\pm$ SD n = 3	Hausner ratio*US P n = 1	Bulk density [g/cm³] n = 1	d_{50} [µm] $\pm$ SD n = 3	Hausner ratio*US P n = 1	Bulk density [g/cm³] n = 1
0	103.00 ± 0.00	1.23	0.48	110.00 ± 2.05	1.23	0.52
2	83.17 ± 1.41	1.29	0.51	78.76 ± 3.56	1.27	0.53
4	97.80 ± 0.82	1.35	0.53	81.51 ± 2.95	1.33	0.56
6	138.13 ± 13.36	1.32	0.54	139.13 ± 2.94	1.31	0.58
8	132.75 ± 11.95	1.26	0.56	210.17 ± 2.45	1.31	0.59

MCC = Microcrystalline cellulose; LAC = α − Lactosemonohydrate; SD = Standard deviation of mean

Granule attributes (MiniPactor):

Specific compaction force [kN/cm]	MCC 2:1 LAC			MCC 1:1 LAC		
	d_{50} [µm] ± SD n = 3	Hausner ratio*USP n = 1	Bulk density [g/cm³] n = 1	d_{50} [µm] ± SD n = 3	Hausner ratio*USP n = 1	Bulk density [g/cm³]
0	103.00 ± 0.00	1.23	0.48	110.00 ± 2.05	1.23	0.52
2	87.56 ± 0.47	1.27	0.47	70.35 ± 0.47	1.37	0.50
4	98.25 ± 0.00	1.33	0.50	73.04 ± 0.82	1.37	0.55
6	112.60 ± 1.24	1.31	0.54	88.80 ± 3.68	1.35	0.59
8	136.38 ± 2.45	1.31	0.56	105.35 ± 0.00	1.33	0.60

MCC = Microcrystalline cellulose; LAC = α − Lactosemonohydrate; SD = Standard deviation of mean

Tablets comparison milling process at two scale: Solid fraction tablets

Formulation	SF	MacroPactor SF ± SD n = 20	MiniPactor SF ± SD n = 20
MCC 2:1 LAC	0.62	0.6239 ± 0.0032	0.6253 ± 0.0042
	0.77	0.7748 ± 0.0036	0.7759 ± 0.0028
MCC 1:1 LAC	0.64	0.6370 ± 0.0033	0.6367 ± 0.0037
	0.79	0.7921 ± 0.0016	0.7889 ± 0.0030

MCC = Microcrystalline cellulose; LAC = α − Lactosemonohydrate; SF = Solid fraction; SD = Standard deviation of mean

4.2.4 Influence of granules on tablet attributes

Reworkability index tablets – MiniPactor – MCC 2:1 LAC/ MCC 1:1 LAC
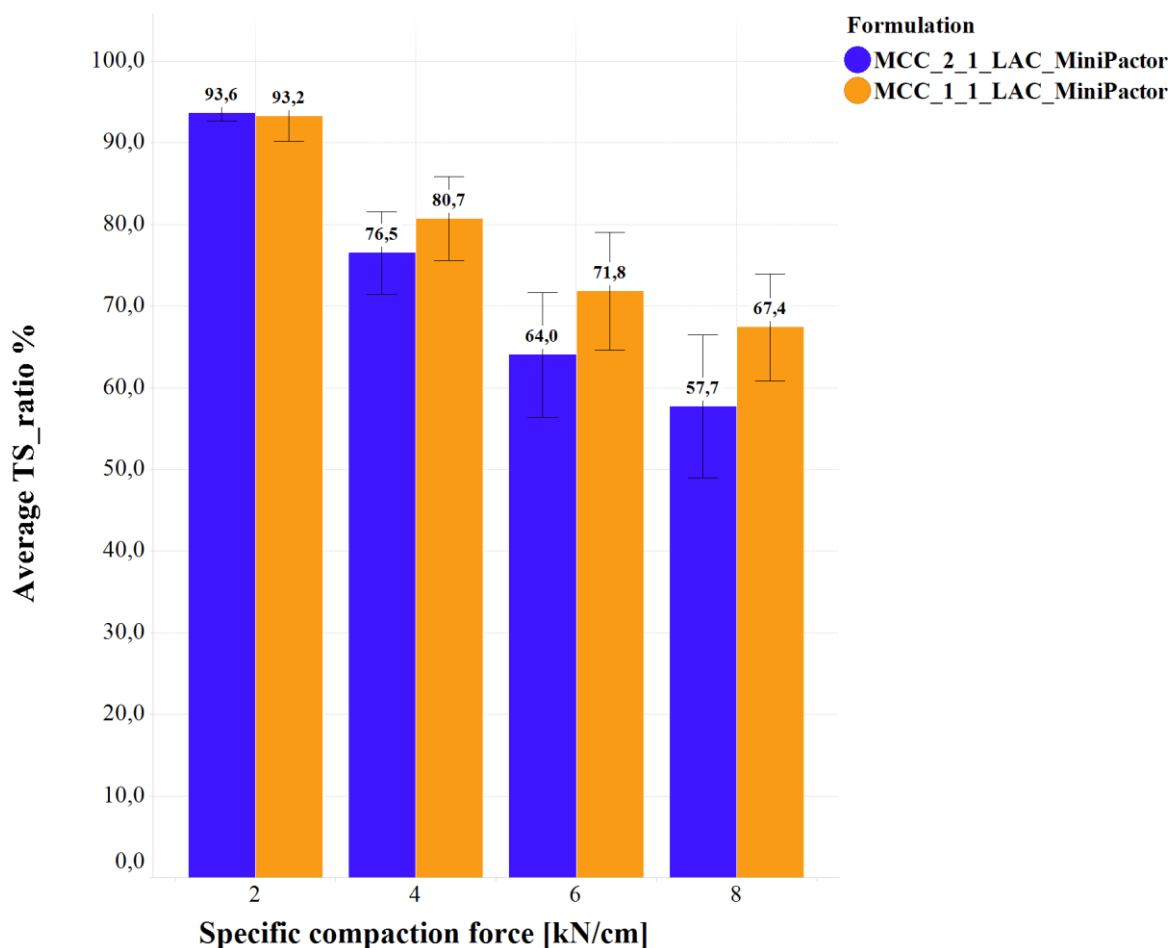
Reworkability index tablets –MiniPactor – MCC 2:1 LAC/MCC 1:1 LAC, TS_{ratio} = tensile strength of tablets of compacted blend in proportion to unprocessed blend Eq. (33), mean (n = 350), error bars (standard deviation of mean)

Results Heckel -Yield pressure granules – MacroPactor/MiniPactor – MCC 1:1 LAC

Yield pressure P_y (1/slope)		0 kN/cm	2 kN/cm	4 kN/cm	6 kN/cm	8 kN/cm
	MacroPactor	189.68	197.90	201.12	208.36	211.87
	MiniPactor	189.68	197.18	200.73	206.72	212.57
	Difference	0	0.72	0.39	1.64	-0.70

P_y = Yield pressure Heckel

8.1.3   CHAPTER 4.4 INVESTIGATION OF SOLID FRACTION DISTRIBUTION ALONG THE ROLL WIDTH BETWEEN DIFFERENT SCALES VIA NIR AT-LINE

4.4.1 Method evaluation to determine solid fraction along the roll width by GeoPycnometer and NIR

Spectral bands NIR spectra:

Content	Chemical group	Specified range
Metformin[125]	Primary amine NH2 - Combination bands	$5000 – 4762$ cm^{-1}, ($2000 – 2100$ nm)
	Secondary amine NH - Overtone bands	6570 cm^{-1} (1522 nm), 9597 cm^{-1}, (1042 nm)
	Imid group C=NH – Overtone band	5924 cm^{-1}, (1688 nm)
Water[126]	Hydroxyl O–H – Combination bands	5208 cm^{-1}, (1920 nm)
	Hydroxyl O–H – Overtone band	7040 cm^{-1} (1420 nm)

8.1.4 MODEL DEVELOPMENT – PREDICTING SOLID FRACTION OF A TABLET

4.5.1 Application of models – Excipients

Correlation Kawakita C and new derived C solid fraction

Material	V_0 [cm³] at 1-2 MPa	Correlation Kawakita C vs. Derived C solid fraction	R^2
MCC	0.398955	0.4647 x + 0.2255	0.9951
LAC	0.211695	0.9113 x + 0.4904	0.9954
CARB	0.267273	0.7789 x + 0.2133	0.9928

MCC = Microcrystalline cellulose; LAC = α − Lactosemonohydrate; CARB = Sodium carboxymethylcellulose;

V_0 = Initial volume [cm³]; C = Degree of volume reduction; R^2 = Correlation coefficient

8.2   STATISTICAL TESTS

8.2.1   CHAPTER 4.1 MATERIAL ATTRIBUTES AND METHOD COMPARISON FOR SOLID FRACTION MEASUREMENTS OF RIBBONS

4.1.2 Comparison of throughput, mercury porosimetry and GeoPycnometry

Comparison mercury porosimetry and GeoPycnometry – T-Test

Specific compaction force [kN/cm]	Mercury porosimetry (n = 3) vs. Geopycnometry (n = 5) T- Test $\alpha = 0.05$ p
2	0.1471
4	0.8437
6	0.7130
8	0.1614

8.2.2   CHAPTER 4.2 COMPARISON OF TWO ROLLER COMPACTORS OF DIFFERENT SCALE AT SAME PROCESS

4.2.1 Formulation impact on the solid fraction within one scale

Solid fraction comparison between formulations within one scale – T-Test

Specific compaction force [kN/cm]	MCC 2:1 LAC vs. MCC 1:1 LAC MacroPactor T- Test α = 0.05 p	MCC 2:1 LAC vs. MCC 1:1 LAC MiniPactor T- Test α = 0.05 p
2	0.000000	0.000075
4	0.000000	0.000000
6	0.000001	0.000000
8	0.000001	0.000034

MCC = Microcrystalline cellulose; LAC = α − Lactosemonohydrate

4.2.3 Particle size distribution of granules

d_{50} granules – MacroPactor/MiniPactor- MCC 2:1 LAC/MCC 1:1 LAC- T-Test

Formulation	Specific compaction force [kN/cm]	d_{50} [μm] ± SD n = 3		T-test α = 0.05 p
		MacroPactor	MiniPactor	
MCC 2:1 LAC	0	103.00 ± 0.00		-
	2	83.17 ± 1.41	87.56 ± 0.47	0.0147
	4	97.80 ± 0.82	98.25 ± 0.00	1.0000
	6	138.13 ± 13.36	112.60 ± 1.25	0.0501
	8	132.75 ± 11.95	136.38 ± 2.45	0.7189
MCC 1:1 LAC	0	110.00 ± 2.05		-
	2	78.76 ± 3.56	70.35 ± 0.47	0.0269
	4	81.51 ± 2.95	73.04 ± 0.82	0.0111
	6	139.13± 2.94	88.80 ± 3.68	0.0001
	8	210.17± 2.45	105.35 ± 0.00	0.0000

MCC = Microcrystalline cellulose; LAC = α − Lactosemonohydrate; d_{50} = Median particle dimension; SD = Standard deviation of mean

d_{50} granules of milled tablets – MacroPactor/MiniPactor- MCC 2:1 LAC/MCC 1:1 LAC- T-Test

Formulation	Milled tablets (SF)	MacroPactor d_{50} [μm] ± SD n = 3	MiniPactor d_{50} [μm] ± SD n = 3	T-Test α = 0.05 p
MCC 2:1 LAC	0.62	99.16 ± 4.96	99.55 ± 1.89	0.9336
	0.77	163.16 ± 7.41	163.98 ± 10.27	0.9721
MCC 1:1 LAC	0.64	86.41 ± 0.47	88.45 ± 1.70	0.1347
	0.79	138.76 ± 6.94	145.80 ± 3.40	0.2696

MCC = Microcrystalline cellulose; LAC = α − Lactosemonohydrate; d_{50} = Median particle dimension; SD = Standard deviation of mean

4.2.4 Influence of granules on tablet

Pre-validation sample size tablets (tensile strength)

A Pre-validation of the tensile strength showed a relative standard deviation of maximum 10 % within one compression pressure. Thus, differences of over 10 % of tensile strength were defined as relevant for scale up. Target was to detect these differences with a power of 0.95 over the whole compression pressure range. Sample size 50 tablets for each compression pressure. (Pre-validation setup: MCC 2:1 LAC, 4 kN/cm)

Compression pressure [MPa]	59.68	99.47	139.26	179.05	218.84	258.63	298.42
Tensile strength [N/mm²]	0.39	0.94	1.53	2.03	2.47	2.88	3.02
Standard deviation of mean	0.0392	0.087	0.1389	0.1448	0.1482	0.1752	0.2033
Relative standard-deviation %	10	9.3	9.09	7.14	6	6.09	6.72
Detect differences if value = (+10 %)	0.43	1.03	1.68	2.23	2.72	3.17	3.33
Detect differences if value = (-10 %)	0.35	0.84	1.37	1.82	2.22	2.59	2.72
Calculated sample size to detect difference ±10 % with a Power of 0.95 (1-beta) alpha = 0.05	52	52	48	30	22	22	26
Determined sample size of 50 resulting Power for 10 % deviation	0.94	0.95	0.96	1	1	1	1

One Way ANOVA within scale and compression pressure (equal to five means comparison with each other)

All tests were passed (see column comment)

    A. Levenes's test for homogeneity ($\alpha = 0.05$)

    B. ANOVA univariate test of significance ($\alpha = 0.05$)

    C. Post Hoc ANOVA Bonferroni ($\alpha = 0.05$)

MacroPactor	Compression Pressure	Comment	0 kN/cm	2 kN/cm	4 kN/cm	6 kN/cm	8 kN/cm
MCC 2:1 LAC	59.68		*	*	X	X	*
	99.47		*	*	*	*	*
	139.26		*	*	*	*	*
	179.05		*	*	*	*	*
	218.84		*	*	*	X	X
	258.63		*	*	*	*	*
	298.42		*	*	X	X	*
MCC 1:1 LAC	59.68		*	*	X	*	X
	99.47		*	*	*	*	*
	139.26		*	*	*	*	*
	179.05		*	*	*	*	*
	218.84	+	*	*	*	X	X
	258.63	+	*	*	*	*	*
	298.42		*	*	*	X	X

MCC = Microcrystalline cellulose; LAC = α − Lactosemonohydrate

* indicates significanct differences (p ≤ 0.05)

X = no significant difference between values

+ Levene's test showed significance (eq. heteroscedasticity)

MiniPactor	Compression Pressure	Comment	0 kN/cm	2 kN/cm	4 kN/cm	6 kN/cm	8 kN/cm
MCC 2:1 LAC	59.68		*	*	*	*	*
	99.47	+	*	*	*	*	*
	139.26		*	*	*	*	*
	179.05		*	*	*	*	*
	218.84		*	*	*	*	*
	258.63		*	*	*	*	*
	298.42		*	*	*	*	*
MCC 1:1 LAC	59.68		*	*	*	X	X
	99.47		*	*	*	*	*
	139.26		*	*	*	*	*
	179.05	+	*	*	*	*	*
	218.84	+	*	*	*	*	*
	258.63	+	*	*	*	*	*
	298.42		*	*	*	*	*

MCC = Microcrystalline cellulose; LAC = α − Lactosemonohydrate

* indicates significant differences ($p \leq 0.05$)

X = no significant difference between values

+ Levene's test showed significance (eq. heteroscedasticity)

Tensile strength tablets - Impact scale - MacroPactor vs. MiniPactor – MCC 2:1 LAC/MCC 1:1 LAC - T-Test

Formulation	Compression pressure [MPa]	Tensile strength [N/mm²] n = 50 T-test α = 0.05 MacroPactor vs. MiniPactor				
		Comment	2 kN/cm	4 kN/cm	6 kN/cm	8 kN/cm
MCC 2:1 LAC	59.68		*	*	X	X
	99.47		*	*	*	* <10 %
	139.26		*	*	*	*
	179.05		*	*	*	*
	218.84		*	*	*	* <10 %
	258.63		*	*	* <10 %	*
	298.42		*	*	*+	* <10 %
MCC 1:1 LAC	59.68		* <10 %	X <10 %	* <10 %	+* <10 %
	99.47		* <10 %	*	X <10 %	X <10 %
	139.26		+*	* <10 %	X <10 %	* <10 %
	179.05		* <10 %	* <10 %	* <10 %	+* <10 %
	218.84		X <10 %	* <10 %	X <10 %	* <10 %
	258.63		X <10 %	* <10 %	X <10 %	+* <10 %
	298.42		X <10 %	X <10 %	X <10 %	X <10 %

MCC = Microcrystalline cellulose; LAC = α − Lactosemonohydrate

* = indicates significant differences (p ≤ 0.05)

X = no significant difference between values

+ = Levene's test showed significance (eq. heteroscedasticity)

<10 % = mean values difference smaller than 10 %

8.2.3   CHAPTER 4.3 ADAPTED PROCESS SETTINGS OF DIFFERENT SCALES TO ACHIEVE SIMILAR PRODUCT QUALITY

4.3.1 Achieving the same solid fraction of ribbon by using adapted process parameter

Solid fraction ribbons – MacroPactor/Scale Model – MCC 2:1 LAC – T-Test

Specific compaction force [kN/cm]	Target SF vs. MCC 2:1 LAC Scale Model T- Test $\alpha = 0.05$ p
2	0.000000
4	0.636793
6	0.000000
8	0.000000

SF = Solid fraction; MCC = Microcrystalline cellulose; LAC = α − Lactosemonohydrate

4.3.2 Particle size distribution and porosity of granules

d_{50} granules – MacroPactor/Scale Model- MCC 2:1 LAC - T-Test

MacroPactor		Scale Model		T-Test $\alpha = 0.05$ p
Specific compaction force kN/cm	d_{50} [µm] ± SD n = 3	Specific compaction force [kN/cm]	d_{50} [µm] ± SD n = 3	
2	83 ± 1	4.1	105 ± 0	0.000033
4	98 ± 1	7.0	137 ± 1	0.000005
6	138 ± 13	9.6	179 ± 2	0.013335
8	133 ± 12	11.4	245 ± 6	0.000294

d_{50} = Median particle dimension; SD = Standard deviation of mean

4.3.3 Tabletability and compressibility influenced by material attributes of granules and ribbons

Example calculation of detecting a ±5 % difference with a sample size of n = 50

Compression pressure [MPa]	59.68	99.47	139.26	179.05	218.84	258.63	298.42
Tensile strength [N/mm²]	0.39	0.94	1.53	2.03	2.47	2.88	3.02
Standard deviation of mean	0.0392	0.087	0.1389	0.1448	0.1482	0.1752	0.2033
Relative standard deviation %	10	9.3	9.09	7.14	6	6.09	6.72
Detect differences if value = (+5 %)	0.41	0.98	1.6	2.13	2.59	3.02	3.18
Detect differences if value = (-5 %)	0.37	0.89	1.45	1.93	2.35	2.73	2.87
Determined sample size of 50 resulting Power for ±5 % deviation	0.21	0.62	0.7	0.93	0.98	0.93	0.97

Tensile strength tablets - MacroPactor vs. Scale Model – MCC 2:1 LAC/MCC 1:1 LAC - T-Test

Formulation	Compression pressure [MPa]	Tensile strength [N/mm²] n = 50 T-test α = 0.05 MacroPactor vs. Scale Model				
		Comment	2 kN/cm	4 kN/cm	6 kN/cm	8 kN/cm
MCC 2:1 LAC	59.68		*	*<10 %	*	*
	99.47		*<10 %	*<10 %	*	*
	139.26		*<10 %	*<10 %	*	*
	179.05	+	X<10 %	*<10 %	*	*
	218.84		X<10 %	*<10 %	X<10 %	*
	258.63		X<10 %	*<10 %	*	*
	298.42		*<10 %	*<10 %	*<10 %	*

MCC = Microcrystalline cellulose; LAC = α − Lactosemonohydrate

* = indicates significant differences (p ≤ 0.05)

X = no significant difference between values

+ = Levene's test showed significance (eq. heteroscedasticity)

<10 % = mean values difference smaller than 10 %

8.2.4   CHAPTER 4.4 INVESTIGATION OF SOLID FRACTION DISTRIBUTION ALONG THE ROLL WIDTH BETWEEN DIFFERENT SCALES VIA NIR

4.4.3 Scale up approach – Comparison of solid fractions of ribbons of a Metformin formulation at two

Solid fraction ribbons – MacroPactor/MiniPactor – T-Test

Specific compaction force [kN/cm]	MacroPactor MET 21 vs. MiniPactor MET 21 T- Test $\alpha = 0.05$ p
2	0.000014
4	0.001711
6	0.000041
8	0.000046

MET 21 = Metformin drug load 21 %

8.3   LIST OF TABLES

REFERENCES

[1]   Dilip M. Parikh (Ed.), Handbook of Pharmaceutical Granulation Technology, Second Edition ed., Taylor & Friends, 2005.

[2]   P. Kleinebudde, Roll compaction/dry granulation: pharmaceutical applications, European Journal of Pharmaceutics and Biopharmaceutics 58 (2004) 317–326.

[3]   Y. Teng, Z. Qiu, H. Wen, Systematical approach of formulation and process development using roller compaction, European Journal of Pharmaceutics and Biopharmaceutics 73 (2009) 219–229.

[4]   R.M. Iyer, S. Hegde, J. DiNunzio, D. Singhal, W. Malick, The impact of roller compaction and tablet compression on physicomechanical properties of pharmaceutical excipients, Pharmaceutical Development and Technology 19 (2014) 583–592.

[5]   J.F. Gamble, M. Tobyn, A.B. Dennis, T. Shah, Roller compaction: application of an in-gap ribbon porosity calculation for the optimization of downstream granule flow and compactability characteristics, Pharmaceutical Development and Technology 15 (2010) 223–229.

[6]   B. Rambali, L. Baert, E. Jans, D. Massart, Influence of the roll compactor parameter settings and the compression pressure on the buccal bio-adhesive tablet properties, International Journal of Pharmaceutics 220 (2001) 129–140.

[7]   S.K. Kochhar, M.H. Rubinstein, D. Barnes, The effects of slugging and recompression on pharmaceutical excipients, International Journal of Pharmaceutics 115 (1995) 35–43.

[8]   Hancock, B.C., Colvin, J.T., Mullarney, M.P., Zinchuk, A.V., The relative densities of pharmaceutical powders, blends, dry granulations, and immediate-release tablets, Pharmaceutical Technology (2003) 1543–2521.

[9]   J. Bultmann, Multiple compaction of microcrystalline cellulose in a roller compactor, European Journal of Pharmaceutics and Biopharmaceutics 54 (2002) 59–64.

[10]   J. Mosig, P. Kleinebudde, Critical evaluation of root causes of the reduced compactability after roll compaction/dry granulation, Journal of Pharmaceutical Sciences 104 (2015) 1108–1118.

[11]   G. Bindhumadhavan, J. Seville, M.J. Adams, R.W. Greenwood, S. Fitzpatrick, Roll compaction of a pharmaceutical excipient: Experimental validation of rolling theory for granular solids, Chemical Engineering Science 60 (2005) 3891–3897.

[12]   M. Bi, F. Alvarez-Nunez, F. Alvarez, Evaluating and modifying Johanson's rolling model to improve its predictability, Journal of Pharmaceutical Sciences 103 (2014) 2062–2071.

[13]   Arthi D. Rajkumar, Gavin K. Reynolds, David Wilson, Stephen Wren, Michael J. Hounslow, Agba D. Salman, Investigating the effect of processing parameters on pharmaceutical tablet disintegration using a real-time particle imaging approach, European Journal of Pharmaceutics and Biopharmaceutics 106 (2016) 88–96.

[14]   Julian Quodbach & Peter Kleinebudde, A critical review on tablet disintegration, Pharmaceutical Development and Technology 21 (2016) 763–774.

[15]   L.X. Yu, G. Amidon, M.A. Khan, S.W. Hoag, J. Polli, G.K. Raju, J. Woodcock, Understanding pharmaceutical quality by design, The AAPS journal 16 (2014) 771–783.

[16]   United States Pharmacopeial Convention Inc., United States Pharmacopeia - National Formulary, USP 39–NF 34 ed.

[17]   A.V. Zinchuk, M.P. Mullarney, B.C. Hancock, Simulation of roller compaction using a laboratory scale compaction simulator, International Journal of Pharmaceutics 269 (2004) 403–415.

[18]   ICH, Q8: Pharmaceutical development: Part I: pharmaceuticaldevelopment; Part II: annex to pharmaceutical development., 2009, http://www.ich.org/fileadmin/Public_Web_Site/ICH_Products/Guidelines/Quality/Q8_R1/Step4/Q8_R2_Guideline.pdf, accessed 4 June 2017.

[19]   C.S. Omar, R.M. Dhenge, J.D. Osborne, T.O. Althaus, S. Palzer, M.J. Hounslow, A.D. Salman, Roller compaction: Effect of morphology and amorphous content of lactose powder on product quality, International Journal of Pharmaceutics 496 (2015) 63–74.

[20]   R. Kona, R.M. Fahmy, G. Claycamp, J.E. Polli, M. Martinez, S.W. Hoag, Quality-by-design III: application of near-infrared spectroscopy to monitor roller compaction in-process and product quality attributes of immediate release tablets, AAPS PharmSciTech 16 (2015) 202–216.

[21]   H. Lim, V.S. Dave, L. Kidder, E. Neil Lewis, R. Fahmy, S.W. Hoag, Assessment of the critical factors affecting the porosity of roller compacted ribbons and the feasibility of using NIR chemical imaging to evaluate the porosity distribution, International Journal of Pharmaceutics 410 (2011) 1–8.

[22]   M. Khorasani, J.M. Amigo, J. Sonnergaard, P. Olsen, P. Bertelsen, J. Rantanen, Visualization and prediction of porosity in roller compacted ribbons with near-infrared

chemical imaging (NIR-CI), Journal of Pharmaceutical and Biomedical Analysis 109 (2015) 11–17.

[23]   M.K. Ghorab, R. Chatlapalli, S. Hasan, A. Nagi, Application of thermal effusivity as a process analytical technology tool for monitoring and control of the roller compaction process, AAPS PharmSciTech 8 (2007) 23.

[24]   J. Sakwanichol, S. Puttipipatkhachorn, G. Ingenerf, P. Kleinebudde, Roll compaction/dry granulation: comparison between roll mill and oscillating granulator in dry granulation, Pharmaceutical Development and Technology 17 (2012) 30–39.

[25]   J. Nordstrom, G. Alderborn, The granule porosity controls the loss of compactibility for both dry- and wet-processed cellulose granules but at different rate, Journal of Pharmaceutical Sciences 104 (2015) 2029–2039.

[26]   M.G. Herting, P. Kleinebudde, Roll compaction/dry granulation: effect of raw material particle size on granule and tablet properties, International Journal of Pharmaceutics 338 (2007) 110–118.

[27]   S. Peter, Untersuchungen zur Homogenisierung der Schülpendichte und Entwicklung eines Vorhersagemodells auf der Basis von Tablettierversuchen. PhD thesis, University of Bonn, 2010.

[28]   R.F. Mansa, Roll compaction of pharmaceutical excipients and prediction using intelligent software. PhD thesis, University of Birmingham, 2006.

[29]   T. Feng, F. Wang, R. Pinal, C. Wassgren, M.T. Carvajal, Investigation of the variability of NIR in-line monitoring of roller compaction process by using Fast Fourier Transform (FFT) analysis, AAPS PharmSciTech 9 (2008) 419–424.

[30]   A.M. Miguelez-Moran, C.-Y. Wu, H. Dong, J.P.K. Seville, Characterisation of density distributions in roller-compacted ribbons using micro-indentation and X-ray micro-computed tomography, European Journal of Pharmaceutics and Biopharmaceutics 72 (2009) 173–182.

[31]   I. Akseli, S. Iyer, H.P. Lee, A.M. Cuitino, A quantitative correlation of the effect of density distributions in roller-compacted ribbons on the mechanical properties of tablets using ultrasonics and X-ray tomography, AAPS PharmSciTech 12 (2011) 834–853.

[32]   D. Acevedo, A. Muliadi, A. Giridhar, J.D. Litster, R.J. Romanach, Evaluation of three approaches for real-time monitoring of roller compaction with near-infrared spectroscopy, AAPS PharmSciTech 13 (2012) 1005–1012.

[33]   F. Wöll, Entwicklung von Methoden zur Charakterisierung von Schülpen. PhD thesis, University of Halle-Wittenberg, 2003.

[34]   P. Nkansah, S.-J. Wu, S. Sobotka, K. Yamamoto, Z.J. Shao, A novel method for estimating solid fraction of roller-compacted ribbons, Drug Development and Industrial Pharmacy 34 (2008) 142–148.

[35]   J. Brudy, Systematische Rezepturentwicklung für die Walzenkompaktierung: Anhand binärer und ternärer Mischungen ausgewählter Komponenten. PhD thesis, University of Heidelberg, 2007.

[36]   A. Michrafy, H. Diarra, J.A. Dodds, M. Michrafy, Experimental and numerical analyses of homogeneity over strip width in roll compaction, Powder Technology 206 (2011) 154–160.

[37]   M. Alleso, R. Holm, P. Holm, Roller compaction scale-up using roll width as scale factor and laser-based determined ribbon porosity as critical material attribute, European journal of pharmaceutical sciences official journal of the European Federation for Pharmaceutical Sciences 87 (2016) 69–78.

[38]   Abhay Gupta, Garnet E. Peck, Ronald W. Miller, Kenneth R. Morris, Nondestructive measurements of the compact strength and the particle-size distribution after milling of roller compacted powders by near-infrared spectroscopy, Journal of Pharmaceutical Sciences 93 (2004) 1047–1053.

[39]   P. Guigon, O. Simon, Roll press design—influence of force feed systems on compaction, Powder Technology 130 (2003) 41–48.

[40]   Y. Funakoshi, T. Asogawa, E. Satake, The use of a Novel Roller Compactor with a Concavo-Convex Roller pair to Obtain Uniform Compacting Pressure, Drug Development and Industrial Pharmacy 3 (2008) 555–573.

[41]   A.M. Miguelez-Moran, C.-Y. Wu, J.P.K. Seville, The effect of lubrication on density distributions of roller compacted ribbons, International Journal of Pharmaceutics 362 (2008) 52–59.

[42]   W. Shi, O.L. Sprockel, A practical approach for the scale-up of roller compaction process, European Journal of Pharmaceutics and Biopharmaceutics 106 (2016) 15–19.

[43]   Ana Pérez Gago, Gavin Reynolds, Peter Kleinebudde, Impact of roll compactor scale on ribbon density. In Press, Corrected Proof, Powder Technology (2017).

[44]   S. Malkowska, K.A. Khan, Effect of Re-Conpression on the Properties of Tablets Prepared by Dry Granulation, Drug Development and Industrial Pharmacy 9 (1983) 331–347.

[45] Christer Nyström, Göran Alderborn, Margareta Duberg & Per-Gunnar Karehill, Bonding Surface area and Bonding Mechanism -Two Important Factors fir the Understanding of Powder Comparability, Drug Development and Industrial Pharmacy 19 (1993) 2143–2196.

[46] C.C. Sun, M.W. Himmelspach, Reduced tabletability of roller compacted granules as a result of granule size enlargement, Journal of Pharmaceutical Sciences 95 (2006) 200–206.

[47] M.G. Herting, P. Kleinebudde, Studies on the reduction of tensile strength of tablets after roll compaction/dry granulation, European Journal of Pharmaceutics and Biopharmaceutics 70 (2008) 372–379.

[48] S.-J. Wu, C.C. Sun, Insensitivity of compaction properties of brittle granules to size enlargement by roller compaction, Journal of Pharmaceutical Sciences 96 (2007) 1445–1450.

[49] X. He, P.J. Secreast, G.E. Amidon, Mechanistic study of the effect of roller compaction and lubricant on tablet mechanical strength, Journal of Pharmaceutical Sciences 96 (2007) 1342–1355.

[50] C.C. Sun, P. Kleinebudde, Mini review: Mechanisms to the loss of tabletability by dry granulation, European Journal of Pharmaceutics and Biopharmaceutics 106 (2016) 9–14.

[51] Narang, Ajit S, Boddu, Sai H S. (Ed.), Excipient Applications in Formulation Design and Drug Delivery, Springer International Publishing AG Switzerland, 2015.

[52] Saurabh M. Mishra & Bhagwan D. Rohera, An integrated, quality by design (QbD) approach for design, development and optimization of orally disintegrating tablet formulation of carbamazepine, Pharmaceutical Development and Technology 22 (2017) 889–903.

[53] C.K. Tye, C.C. Sun, G.E. Amidon, Evaluation of the effects of tableting speed on the relationships between compaction pressure, tablet tensile strength, and tablet solid fraction, Journal of Pharmaceutical Sciences 94 (2005) 465–472.

[54] J.M. Sonnergaard, A critical evaluation of the Heckel equation (1999) 63–71.

[55] C. Sun, D.J. Grant, Influence of Elastic Deformation of Particles on Heckel Analysis, Pharmaceutical Development and Technology 6 (2001) 193–200.

[56] Jukka Ilkka and Petteri Paronen, Prediction of the compression behaviour of powder mixtures by the Heckel equation, International Journal of Pharmaceutics 94 (1993) 181–187.

[57]   Fredrik Nicklasson, Göran Alderborn, Analysis of the Compression Mechanics of Pharmaceutical Agglomerates of Different Porosity and Composition Using the Adams and Kawakita Equations, Pharmaceutical Research 17 (2000).

[58]   G. Frenning, J. Nordström, G. Alderborn, Effective Kawakita parameters for binary mixtures, Powder Technology 189 (2009) 270–275.

[59]   J. Nordström, K. Welch, G. Frenning, G. Alderborn, On the physical interpretation of the Kawakita and Adams parameters derived from confined compression of granular solids, Powder Technology 182 (2008) 424–435.

[60]   S. Patel, A.M. Kaushal, A.K. Bansal, Compression Physics in the Formulation Development of Tablets, Crit Rev Ther Drug Carrier Syst 23 (2006) 1–66.

[61]   Heckel RW., Density–pressure relationship in powder compaction, Transactions of the Metallurgical Society Of Aime (1961) 671–675.

[62]   K. Kawakita, K.-H. Lüdde, Some considerations on powder compression equations, Powder Technology 4 (1971) 61–68.

[63]   M. Duberg, C. Nyström, Studies on direct compression of tablets XVII. Porosity—pressure curves for the characterization of volume reduction mechanisms in powder compression, Powder Technology 46 (1986) 67–75.

[64]   V. Mazel, V. Busignies, S. Duca, B. Leclerc, P. Tchoreloff, Original predictive approach to the compressibility of pharmaceutical powder mixtures based on the Kawakita equation, International Journal of Pharmaceutics 410 (2011) 92–98.

[65]   V. Busignies, V. Mazel, H. Diarra, P. Tchoreloff, Prediction of the compressibility of complex mixtures of pharmaceutical powders, International Journal of Pharmaceutics 436 (2012) 862–868.

[66]   H. Leuenberger, R. Leu, Formation of a Tablet: A Site and Bond Percolation Phenomenon, Journal of Pharmaceutical Sciences 81 (1992) 976–982.

[67]   H.L. Martin Kuentz, A new theoretical approach to tablet strength of a binary mixture consisting of a well and a poorly compactable substance, European Journal of Pharmaceutics and Biopharmaceutics 49 (2000) 151–159.

[68]   V. Busignies, B. Leclerc, P. Porion, P. Evesque, G. Couarraze, P. Tchoreloff, Application of percolation model to the tensile strength and the reduced modulus of elasticity of three compacted pharmaceutical excipients, European Journal of Pharmaceutics and Biopharmaceutics 67 (2007) 507–514.

REFERENCES

[69] Martin Kuentz, Hans Leuenberger, M. Kolb, Fracture in disordered media and tensile strength of microcrystalline cellulose tablets at low relative densities, International Journal of Pharmaceutics 182 (1999) 243–255.

[70] N. Ramirez, L.M. Melgoza, M. Kuentz, H. Sandoval, I. Caraballo, Comparison of different mathematical models for the tensile strength-relative density profiles of binary tablets, European journal of pharmaceutical sciences official journal of the European Federation for Pharmaceutical Sciences 22 (2004) 19–23.

[71] M. Kuentz, H. Leuenberger, Modified Young's modulus of microcrystalline cellulose tablets and the directed continuum percolation model, Pharmaceutical Development and Technology 1 (1998) 13–19.

[72] K. Kawakita, K.-H. Lüdde, Some considerations on powder compression equations, Powder Technology 4 (1971) 61–68.

[73] Fredrik Nicklasson, Göran Alderborn, Analysis of the Compression Mechanics of Pharmaceutical Agglomerates of Different Porosity and Composition Using the Adams and Kawakita Equations, Pharmaceutical Research (2000).

[74] J. Nordström, K. Welch, G. Frenning, G. Alderborn, On the physical interpretation of the Kawakita and Adams parameters derived from confined compression of granular solids, Powder Technology 182 (2008) 424–435.

[75] G. Frenning, J. Nordström, G. Alderborn, Effective Kawakita parameters for binary mixtures, Powder Technology 189 (2009) 270–275.

[76] J.M. Sonnergaard, Impact of particle density and initial volume on mathematical compression models, European Journal of Pharmaceutical Sciences (2000) 307–315.

[77] J. Sonnergaard, Investigation of a new mathematical model for compression of pharmaceutical powders, European Journal of Pharmaceutical Sciences 14 (2001) 149–157.

[78] J. Nordstrom, I. Klevan, G. Alderborn, A particle rearrangement index based on the Kawakita powder compression equation, Journal of Pharmaceutical Sciences 98 (2009) 1053–1063.

[79] V. Busignies, V. Mazel, H. Diarra, P. Tchoreloff, Prediction of the compressibility of complex mixtures of pharmaceutical powders, International Journal of Pharmaceutics 436 (2012) 862–868.

[80] C.M. Ramaswamy, Y. Varma, D. Venkateswarlu, Compaction of mixtures of materials, The Chemical Engineering Journal 1 (1970) 168–171.

[81] V. Mazel, V. Busignies, S. Duca, B. Leclerc, P. Tchoreloff, Original predictive approach to the compressibility of pharmaceutical powder mixtures based on the Kawakita equation, International Journal of Pharmaceutics 410 (2011) 92–98.

[82] C.-Y. Wu, S.M. Best, A.C. Bentham, B.C. Hancock, W. Bonfield, A simple predictive model for the tensile strength of binary tablets, European Journal of Pharmaceutical Sciences 25 (2005) 331–336.

[83] A. Michrafy, M. Michrafy, M.S. Kadiri, J.A. Dodds, Predictions of tensile strength of binary tablets using linear and power law mixing rules, International Journal of Pharmaceutics 333 (2007) 118–126.

[84] A. Gupta, G.E. Peck, R.W. Miller, K.R. Morris, Real-time near-infrared monitoring of content uniformity, moisture content, compact density, tensile strength, and Young's modulus of roller compacted powder blends, Journal of Pharmaceutical Sciences 94 (2005) 1589–1597.

[85] I. Klevan, Compression Analysis of Pharmaceutical Powders Assessment of Mechanical Properties. PhD Thesis, University of Tromsø, 2011.

[86] S. Patel, A.M. Kaushal, A. Bansal, Kumar, Effect of particle size and compression force on compaction behavior and derived mathematical parameters of compressibility, Pharmaceutical Research 24 (2007) 111–124.

[87] J. Sonnergaard, Investigation of a new mathematical model for compression of pharmaceutical powders, European Journal of Pharmaceutical Sciences 14 (2001) 149–157.

[88] J.M. Sonnergaard, Quantification of the compactibility of pharmaceutical powders, European Journal of Pharmaceutics and Biopharmaceutics 63 (2006) 270–277.

[89] J. Dressler, Vergleichende Untersuchungen pharmazeutischer Hilfsstoffe unter Einsatz eines inkrementalen Weggebers zur präzisen Wegmessung an einer Exzenter-Tablettenpresse. PhD thesis, University of Tübingen, 2002.

[90] H. Vromans, A.H. De Boer, G.K. Bolhuis, C.F. Lerk, K.D. Kussendrager and H. Bosch, Studies on tableting properties of lactose, Pharmaceutisch Weekblad Scientific Edition 7 (1985) 186–193.

[91] Coenraad F. Lerk, Consolidation and Compaction of Lactose, Drug Development and Industrial Pharmacy 19 (1993) 2359–2398.

[92] A. Michrafy, M. Michrafy, M.S. Kadiri, J.A. Dodds, Predictions of tensile strength of binary tablets using linear and power law mixing rules, International Journal of Pharmaceutics 333 (2007) 118–126.

[93]   Busignies V., Leclerc B., Porion P., Evesque P., Couarraze G., Tchoreloff P., Compaction behaviour and new predictive approach to the compressibility of binary mixtures of pharmaceutical excipients, European Journal of Pharmaceutics and Biopharmaceutics 64 (2006) 66–74.

[94]   J.M. Sonnergaard, Impact of particle density and initial volume on mathematical compression models, European Journal of Pharmaceutical Sciences 11 (2000) 307–315.

[95]   M. Whiteman, Yarwood J. R., The Evaluation of Six Lactose-Based Materials as Direct Compression Tablet Excipients, Drug Development and Industrial Pharmacy 8 (1988) 1023–1040.

[96]   Busignies V., Leclerc B., Porion P., Evesque P., Couarraze G., Tchoreloff P., Investigation and modelling approach of the mechanical properties of compacts made with binary mixtures of pharmaceutical excipients, European Journal of Pharmaceutics and Biopharmaceutics 64 (2006) 51–65.

[97]   N. Müller, Untersuchungen zur Prozessüberwachung und -regulierung bei der Walzenkompaktierung mittels Drehmomenterfassung an der Granuliereinheit. PhD thesis, University of Bonn, 2012.

[98]   P.K. Haress Mangal, Experimental determination of residence time distribution in continuous dry granulation, International Journal of Pharmaceutics (2017) 91–100.

[99]   J. Sakwanichol, S. Puttipipatkhachorn, G. Ingenerf, P. Kleinebudde, Roll compaction/dry granulation: comparison between roll mill and oscillating granulator in dry granulation, Pharmaceutical Development and Technology 17 (2012) 30–39.

[100]   J. Hilden, G. Earle, E. Lilly, Prediction of roller compacted ribbon solid fraction for quality by design development, Powder Technology 213 (2011) 1–13.

[101]   H. Vromans, F.C. Lerk, Densification properties and compactibility of mixtures of pharmaceutical excipients with and without magnesium stearate 46 (1988) 183–192.

[102]   G. Alderborn, K. Pasanen, C. Nystrom, Studies on direct compression of tablets. XL Characterization of particle fragmentation during compaction by permeametry measurements of tablets☆, International Journal of Pharmaceutics 23 (1985) 79–86.

[103]   T. Jahn, K.-J. Steffens, Press chamber coating as external lubrication for high speed rotary presses: lubricant spray rate optimization, Drug Development and Industrial Pharmacy 31 (2005) 951–957.

[104] I. Sinka, J. Cunningham, A. Zavaliangos, The effect of wall friction in the compaction of pharmaceutical tablets with curved faces: A validation study of the Drucker–Prager Cap model, Powder Technology 133 (2003) 33–43.

[105] F. Freitag, K. Reincke, J. Runge, W. Grellmann, P. Kleinebudde, How do roll compaction/dry granulation affect the tableting behaviour of inorganic materials? Microhardness of ribbons and mercury porosimetry measurements of tablets, European journal of pharmaceutical sciences official journal of the European Federation for Pharmaceutical Sciences 22 (2004) 325–333.

[106] N. Huber, Veränderung der Tablettiereigenschaften von Trockengranulaten aus Mikrokristalliner Cellulose durch Zusatz verschiedener Hilfsstoffe. PhD thesis, 2011.

[107] L. Perez-Gandarillas, A. Mazor, D. Souriou, O. Lecoq, A. Michrafy, Compaction behaviour of dry granulated binary mixtures, Powder Technology 285 (2015) 62–67.

[108] S. Hein, K.M. Picker-Freyer, J. Langridge, Simulation of roller compaction with subsequent tableting and characterization of lactose and microcrystalline cellulose, Pharmaceutical Development and Technology 13 (2008) 523–532.

[109] K.A. Riepma, H. Vromans, K. Zuurman and CF. Lerk, The effect of dry granulation on the consolidation and compaction of crystalline lactose, International Journal of Pharmaceutics 97 (1993) 29–38.

[110] Sari Westermarck, Anne Mari Juppo, Lasse Kervinena, Jouko Yliruusib, Pore structure and surface area of mannitol powder, granules and tablets determined with mercury porosimetry and nitrogen adsorption, European Journal of Pharmaceutics and Biopharmaceutics 46 (1997) 61–68.

[111] Juppo, A.M. and Yliruusi, J, Effect of Amount of Granulation Liquid on Total Volume and Pore Size Distribution of Lactose, Glucose and Mannitol Granules, European Journal of Pharmaceutics and Biopharmaceutics 40 (1994) 299–309.

[112] A.K. Samanta, K.Y. Ng, P.W.S. Heng, Cone milling of compacted flakes: Process parameter selection by adopting the minimal fines approach, International Journal of Pharmaceutics 422 (2012) 17–23.

[113] S. Yu, C.-Y. Wu, M.J. Adams, G. Reynolds, B. Gururajan, J. Gargiuli, T. Leadbeater, R. Roberts, D.J. Parker, The use of positron emission particle tracking (PEPT) to study milling of roll-compacted microcystalline cellulose ribbons, Powder Technology 285 (2015) 74–79.

[114] O. Simon, P. Guigon, Correlation between powder-packing properties and roll press compact heterogeneity, Powder Technology 130 (2003) 257–264.

REFERENCES

[115] H. Busies, Dichteverteilung in Schülpen. PhD thesis, University of Bonn, 2006.

[116] A.R. Muliadi, J.D. Litster, C.R. Wassgren, Modeling the powder roll compaction process: Comparison of 2-D finite element method and the rolling theory for granular solids (Johanson's model), Powder Technology 221 (2012) 90–100.

[117] A.M. Miguélez-Morán, Roller compaction of pharmaceutical ingredients: On the understanding of the compaction and the use of knowledge based Applications in the formulation of tablets. PhD thesis, University of Heidelberg, 2009.

[118] A. Mazor, L. Perez-Gandarillas, A. de Ryck, A. Michrafy, Effect of roll compactor sealing system designs: A finite element analysis, Powder Technology 289 (2016) 21–30.

[119] J.D. Kirsch, J.K. Drennen, Nondestructive tablet hardness testing by near-infrared spectroscopy: A new and robust spectral best-fit algorithm, Journal of Pharmaceutical and Biomedical Analysis 19 (1999) 351–362.

[120] Marcelo Blanco, Manel Alcala, Josep M. Gonzalez, Ester Torras, A Process Analytical Technology Approach Basedon Near Infrared Spectroscopy: Tablet Hardness,Content Uniformity, and Dissolution Test Measurements of Intact Tablets 95 (2006) 2137–2144.

[121] P.S. Jeckel, Bestimmung wesentlicher Tablettenparameter mit hilfe der Nahinfrarot-spektroskopie. PhD thesis, University of Bonn, 2008.

[122] J. Austin, A. Gupta, R. Mcdonnell, G.V. Reklaitis, M.T. Harris, The use of near-infrared and microwave resonance sensing to monitor a continuous roller compaction process, Journal of Pharmaceutical Sciences 102 (2013) 1895–1904.

[123] A. Candolfi, D.L. Massarta, S. Heuerdingb, Investigation of sources of variance which contribute toa proper measuring setup or data pre-process techniques NIR-spectroscopic measurement of pharmaceutical formulations, Analytica Chimica Acta 345 (1997) 185–196.

[124] Asmund Rinnan, Frans van den Berg, Sören Balling Engelsen", Review of the most common pre-processing techniques for near-infrared spectra.

[125] I. Habib, Near infra-red reflectance spectroscopic determination of metformin in tablets, Talanta 60 (2003) 185–190.

[126] Xiangji Zhou, Patricia Hines, Matthew W. Borer, Moisture determination in hygroscopic drug substances by near infrared spectroscopy, Journal of Pharmaceutical and Biomedical Analysis 17 (1997) 219–225.

[127] Soh, Josephine L. P., F. Wang, N. Boersen, R. Pinal, G.E. Peck, M.T. Carvajal, J. Cheney, H. Valthorsson, J. Pazdan, Utility of multivariate analysis in modeling the effects of raw material properties and operating parameters on granule and ribbon properties prepared in roller compaction, Drug Development and Industrial Pharmacy 34 (2008) 1022–1035.

[128] Martin Kuentz, Hans Leuenberger, M. Kolb, Fracture in disordered media and tensile strength ofmicrocrystalline cellulose tablets at low relative densities, International Journal of Pharmaceutics (1999) 243–255.

[129] S. Patel, A.M. Kaushal, A.K. Bansal, Compression Physics in the Formulation Development of Tablets, Critical Reviews in Therapeutic Drug Carrier Systems 23 (2006) 1–66.

[130] G. Thoorens, F. Krier, B. Leclercq, B. Carlin, B. Evrard, Microcrystalline cellulose, a direct compression binder in a quality by design environment--a review, International Journal of Pharmaceutics 473 (2014) 64–72.

[131] A.P. Webb, An Introduction To The Physical Characterization of Materials by Mercury Intrusion Porosimetry with Emphasis On Reduction And Presentation of Experimental Data, 2001, http://www.particletesting.com/Repository/Files/An_Introduction_to_the_Physical_Ch aracterization_of_Materials_by_Mercury_Intrusion_Porosimetry.pdf, accessed 14 December 2016.

[132] E.W. Washburn, Note on a method of determining the distribution of pore sizes in a porousmaterial, Proc.Nat.Acad.Sci. (1921) 115–116.

[133] Verena Maria Gläßer, Kompressionsanalyse im Vergleich zwischen hydraulischer und Rundlauftablettenpresse. Diploma thesis, University of Tübingen, 2008.

[134] Gabriele Reich, Near-infrared spectroscopy and imaging: Basic principles and pharmaceutical applications, Advanced Drug Delivery Reviews 57 (2005) 1109–1143.

[135] Celio Pasquini, Near Infrared Spectroscopy: Fundamentals, Practical Aspects and Analytical Applications, Journal of the brazilian chemical society 14 (2003) 198–219.

[136] H.W. Siesler, Y.Ozaki, S. Kawata, H.M. Heise (Ed.), Near-infrared Spectroscopy - Principles, Instruments, Applications, Wiley-Vch, 2002.

[137] Alexey L. Pomerantseva and Oxana Ye. Rodionova, Process analytical technology: a critical view ofthe chemometricians, Journal of Chemometrics 26 (2012) 299–310.

[138] Sanni Matero, Frans van den Berg, Sami Poutiainen, Jukka Rantanen, Jari Pajander, Towards Better Process Understanding: Chemometrics and Multivariate Measurements

in Manufacturing of Solid Dosage Forms, Journal of Pharmaceutical Sciences 102 (2013) 1385–1403.

[139] Theodora Kourti, Application of latent variable methods to process control and multivariate statistical process control in industry, International Journal of Adaptive Control and Signal Processing 19 (2005) 213–246.

[140] A.K. Samanta, A.D. Karande, K.Y. Ng, Heng, Paul Wan Sia, Application of near-infrared spectroscopy in real-time monitoring of product attributes of ribbed roller compacted flakes, AAPS PharmSciTech 14 (2013) 86–100.

[141] Waltraud Kessler, Multivariate Datenanalyse für Pharma-, Bio- und Prozessanalytik, 1 ed., Wiley-Vch, 2007.

[142] S.M. Short, R.P. Cogdill, P.L.D. Wildfong, J.K.3. Drennen, C.A. Anderson, A near-infrared spectroscopic investigation of relative density and crushing strength in four-component compacts, Journal of Pharmaceutical Sciences 98 (2009) 1095–1109.